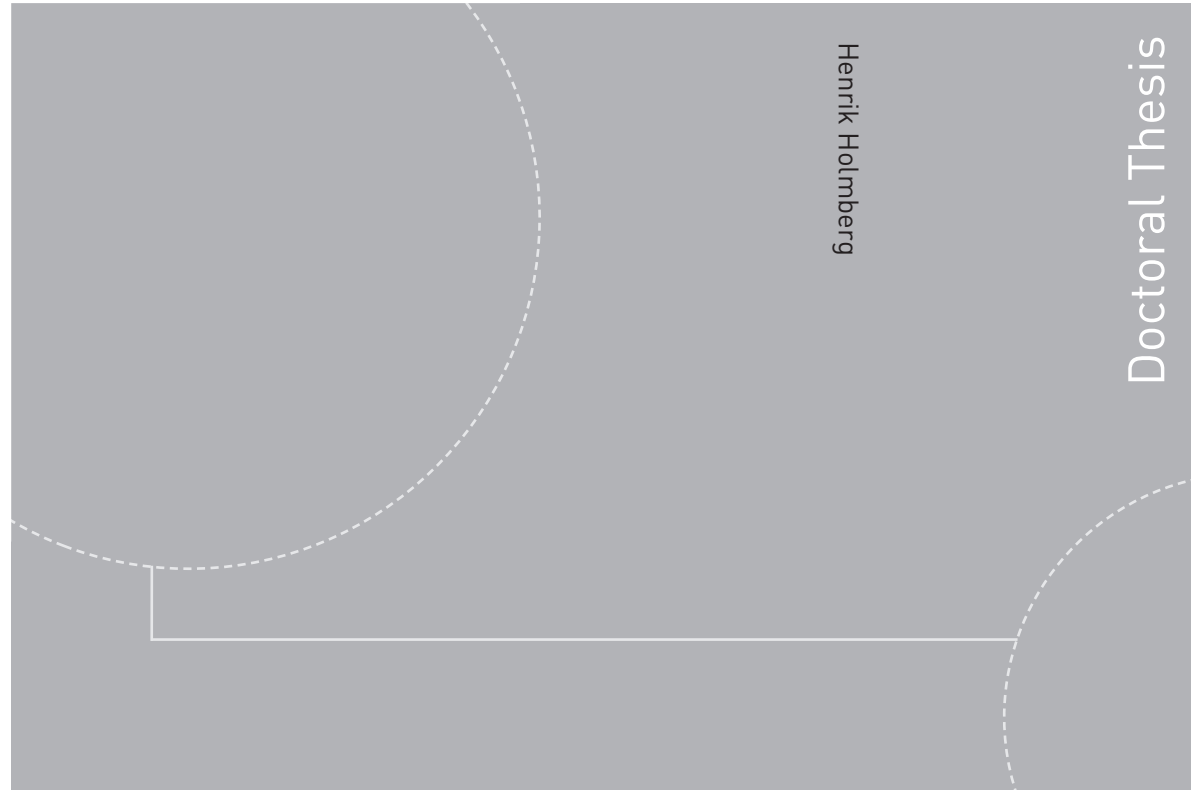


ISBN 978-82-326-1490-5 (printed version)
ISBN 978-82-326-1491-2 (electronic version)
ISSN 1503-8181



Doctoral theses at NTNU, 2016:76

Henrik Holmberg
**Transient Heat Transfer in Boreholes
with Application to
Non-Grouted Borehole Heat
Exchangers and Closed Loop
Engineered Geothermal Systems**

Doctoral theses at NTNU, 2016:76

NTNU
Norwegian University of
Science and Technology
Faculty of Engineering
Science and Technology
Department of Energy and Process Engineering

 **NTNU**
Norwegian University of
Science and Technology

 NTNU

 **NTNU**
Norwegian University of
Science and Technology

Henrik Holmberg

Transient Heat Transfer in Boreholes with Application to Non-Grouted Borehole Heat Exchangers and Closed Loop Engineered Geothermal Systems

Thesis for the degree of Philosophiae Doctor

Trondheim, April 2016

Norwegian University of Science and Technology
Faculty of Engineering
Science and Technology
Department of Energy and Process Engineering



Norwegian University of
Science and Technology

NTNU

Norwegian University of Science and Technology

Thesis for the degree of Philosophiae Doctor

Faculty of Engineering

Science and Technology

Department of Energy and Process Engineering

© Henrik Holmberg

ISBN 978-82-326-1490-5 (printed version)

ISBN 978-82-326-1491-2 (electronic version)

ISSN 1503-8181

Doctoral theses at NTNU, 2016:76



Printed by Skipnes Kommunikasjon as

PREFACE

This thesis is presented as the partial fulfillment of the requirements for the degree of Doctor of Philosophy (Ph.D) at the Norwegian University of Science and Technology (NTNU), Trondheim, Norway.

The work was carried out at the Department of Energy and Process Engineering (EPT) at the faculty of Engineering Science and Technology under the supervision of Professor Erling Næss as the main supervisor and Professor Emeritus Otto K. Sønju as co-supervisor.

ABSTRACT

This thesis concerns heat transfer processes in single boreholes and systems of boreholes. The thesis is divided in two parts of which the first considers borehole heat exchangers (shallow geothermal energy), and the second part deals with heat transfer in an engineered geothermal system, made up of boreholes forming a closed loop system (deep geothermal energy). The essence of the thesis is described hereunder, starting with the borehole heat exchangers.

The borehole heat exchangers (BHEs) are used in ground source heat pump (GSHP) systems as a source and sink for thermal energy, the U-tube configuration of BHEs is the most common. In this thesis the heat transfer processes in U-tube BHEs are studied with the use of both numerical and analytical models.

A novel numerical model for the heat transfer in non-grouted BHEs (which is common in Norway and Sweden) has been developed. The model includes a correlation that accounts for the occurrence of natural convection in the water surrounding the collector. The model is compared with experimental data from distributed temperature measurements obtained during both a distributed thermal response test (heat injection) and during heat pump operation (heat extraction). The model is found to accurately replicate the experimental data. The model is used to analyze the experimental data and to gain further understanding for the heat transfer processes in non-grouted BHEs.

A borehole thermal energy storage (BTES) using a given solar collector as the means of thermal recharge is studied. The BTES is operated with two individually, but thermally interacting circuits with different thermal loads, were only one of the circuits is thermally recharged during the warm season. The system is studied using an analytical model which allows for individual thermal loads in the different boreholes of the BTES. The system is found to have a marginally better performance as compared to the alternative of applying thermal recharge to all BHEs. With access to more energy for thermal recharge it would be better to recharge both circuits.

The coaxial BHE is an alternative to the conventional U-tube BHE, and it has in general a lower internal thermal resistance, which improves the performance of the GSHP system. In addition, it is more suitable for deep boreholes since for a given borehole dimension it can allow for a larger flow area, and thus for a larger mass flow and / or a lower pressure drop.

A numerical model is developed for the coaxial BHE. The model assumes the geometry of a pipe-in-pipe coaxial BHE, and it is compared with distributed temperature measurements from a thermal response test. The model is found to accurately predict the experimental data. The model is used to analyze the experimental data and to gain further understanding of the heat transfer processes in coaxial BHEs. The model is also used to study the influence of borehole depth on the performance of the BHE. It is found that for the case of heat extraction the performance of the BHE increases with borehole depth, even when accounting for the additional pressure losses and pump work needed. Further, it is found that when used in GSHP installations, the highest thermal performance for a deep borehole is a coaxial BHE with a thin-

walled center pipe, which is operated with a high mass flow rate. This allows for larger thermal extraction rates while the costs involved with the coaxial BHE is kept at a minimum.

In the second part of the thesis, a closed loop engineered geothermal system (EGS) is studied. The system studied is based on the US Patent US6247313B1 (Plant for exploiting geothermal energy). It is a novel EGS concept for heat extraction from depths in the range of 3- 6 km. In essence, the system consists of an injection and a production well that are interconnected by a series of parallel boreholes, which forms a subsurface heat exchanger.

In the present work the EGS is studied primarily with the objective to provide hot water in the temperature range of district heating (DH) networks. The thermal performance of the system and the operation characteristics of the system have been the main focus of the study.

The system is studied using a numerical model developed within the present work. The model can be used to study the transient behavior and the performance of the EGS concept on both short time scales (minutes to hours) and on longer time scales, in order of the life time of the system. To perform a more detailed study of the EGS as a provider of hot water to a DH-network the model is applied in conjunction with DH data. It is predicted that the system can sustain heat production for a significant time while requiring little or no use of high value energy for fluid circulation. It also found that the system can be operated dynamically to cover periods with higher or lower heat demands.

Since the primary and dominant heat transport is thermal conduction, the temperature difference between the fluid temperature and the rock temperature, together with the effective thermal conductivity of the rock are the most important parameters determining the amount of energy that can be extracted from the system.

In absence of direct measurements the temperature and the thermal conductivity of the rock at the target depth have to be estimated. This can be done using measurements from shallower boreholes in combination with thermal modeling and by applying geophysical models.

In the present work a section of the Oslo rift is modelled by combining regional measurements of thermal conductivity and radiogenic heat production with heat flow data from boreholes (< 1000 m) and with the results from a geophysical model. The thermal model have a relatively large uncertainty primarily related to the temperature regime in the bedrock.

Since thermal output of the system is dependent on the temperature level of the heat consumer and the temperature of the bedrock. It is better to focus on the presence of a suitable heat consumer that guarantees a high operation time at a low temperature range than pinpointing the areas with the highest heat flow when finding suitable locations for an EGS.

The EGS is scalable both in temperature and in thermal output, the results presented in this thesis are for a small system (1- 3 MW_{th}) suitable for a smaller district heating grid, larger systems in the range of 50 MW_{th} have been dimensioned.

ACKNOWLEDGMENTS

I would like to acknowledge that this PhD was financed from the Norwegian center for renewable energy (SFRE). I also want to express my thanks to Professor Erling Næss and Professor emeritus Otto K Sønju, firstly for initiating this PhD project, and secondly for supporting and guiding me along this journey.

I also want to thank José Acuña at KTH in Sweden for sharing his valuable work and measurement data with me, and I want to thank Randi Kalskin Ramstand at NTNU/ Asplan Viak AS for her guidance, support and openness.

I am grateful for the friends I've made in the colleagues at NTNU and for the good problem solving lunch discussions we've had.

Julia, my life companion has supported and pushed me along, and has as well been joined by our two sons, August and Anton. In a world craving for renewable energy resources it has been a privilege to study geothermal energy, but for spending weekends and late evenings in the office I am sincerely in debt.

NOMENCLATURE

Abbreviations

BHE	Borehole heat exchanger
BTES	Borehole thermal energy storage
DTRT	Distributed thermal response test
EGS	Engineered geothermal system
FLS	Finite line source solution
GSHP	Ground source heat pump
HDR	Hot dry rock
ICS	Infinite cylindrical source solution
ILS	Infinite line source solution
TRT	Thermal response test
TRCM	Thermal resistance and capacity model

Symbols

c	Concentration [%]
C	Specific heat capacity [J/kg·K]
d	Diameter [m]
H	Heat production rate [μ W/m ³]
k	Thermal conductivity [W/ m·K]
\dot{m}	Mass flow rate [kg / s]
q''	Heat flux [W /m ²]
q'	Specific heat load [W /m]
Q	Heat load [W]
r	Radius [m]
R_b	Local borehole thermal resistance [K·m/ W]
R_b^*	Effective borehole thermal resistance [K·m/ W]
s	Center pipe wall thickness [m]
t	Time [s]
T	Temperature [K]
W	Electric power [W]
z	Axial coordinate [m]

Dimensionless numbers & ratios

θ	Dimensionless temperature, $= \frac{T-T_\infty}{T_s-T_\infty}$ [-]
Nu	Nusselt number, hL/k [-]
γ	Aspect ratio of spheroids [-]
i	Thermal conductivity ratio, $i = \frac{k_f}{k_g}$ [-]
K	Radius ratio r_b / r_i [-]
COP_{total}	Total COP, $\frac{Q+W_{hp}}{W_{hp}+W_p}$ [-]
COP	Coefficient of performance, $\frac{Q+W_{hp}}{W_{hp}}$ [-]
Ra^*	Modified Rayleigh number [-]

Subscripts

g	Ground
b	Borehole
f	Fluid
m	Mean value
local	Local value
0	Initial value
th	Thermal
∞	Infinite / undisturbed
s	Surface
p	Pump
hp	Heat pump
in	Inlet
i	Inner
out	Outlet

Greek symbols

α	Thermal diffusivity, $\frac{k}{\rho C}$ [m ² /s]
v	Specific volume [m ³ / kg]
ρ	Density [kg/m ³]
ϕ	Porosity [%]
μ	Dynamic viscosity [Pa· s]
φ	Circumferential coordinate [°]
η	Pump Efficiency [%]

STRUCTURE OF THE THESIS

This thesis is essentially made up by 6 papers and a report which are introduced separately by individual introductions. The thesis is divided in two parts, the first part deals with heat transfer in borehole heat exchangers and the second part considers heat transfer in a closed loop geothermal system intended for heat extraction from crystalline rock at several kilometers depth. The two parts are preceded by a general introduction clarifying the general objectives and the scope of work. Heat transfer through thermal conduction and thermal transport properties of rocks are essential and common for several parts of the thesis, this is, therefore, summarized in a separate section of the thesis.

PUBLICATION LIST:

The papers appended to this thesis are the following

Paper 1: Holmberg. H., Næss. E., Sønju. K. O., Numerical model for non-grouted borehole heat exchanges, part 1- Development. (2016) Submitted to Geothermics

Paper 2: Holmberg. H., Acuña. J., Næss. E., Sønju. K. O., Numerical model for non-grouted borehole heat exchanges, part 2-Evaluation. (2016) Accepted for publication, Geothermics

Paper 3: Holmberg. H., Ramstad. K. R., Næss. E., Sønju. K. O., Solar Assisted Borehole Thermal Energy Storage for Ground Source Heat Pump System. (2016) Submitted to Energy and Buildings

Paper 4: Holmberg. H., Acuña. J., Næss. E., Sønju. K. O., Thermal Evaluation of Deep Coaxial Borehole Heat Exchangers. (2016) Submitted to Renewable Energy

Paper 5: Holmberg. H., Sønju. K. O., Næss. E., A novel concept to Engineered geothermal systems, PROCEEDINGS, Thirty-Seventh Workshop on Geothermal Reservoir Engineering Stanford University, Stanford, California, January 30 - February 1, 2012.

Paper 6: Holmberg. H., Næss. E., Evensen. J. E., Thermal modeling in the Oslo rift, Norway, PROCEEDINGS, Thirty-Seventh Workshop on Geothermal Reservoir Engineering Stanford University, Stanford, California, January 30 - February 1, 2012.

Additional publication included in appendix:

Holmberg. H., Acuña. J., Næss. E., Sønju. K. O., Deep borehole heat exchangers, application to ground source heat pump systems, Proceedings World Geothermal Congress 2015, Melbourne, Australia. 19 -25 April 2015.

CONTENTS

PREFACE	i
ABSTRACT	iii
ACKNOWLEDGMENTS	v
NOMENCLATURE	vi
STRUCTURE OF THE THESIS	vii
PUBLICATION LIST:	vii
CONTENTS	ix
1. Introduction	1
1.1. General objectives.....	1
1.2. Scope of the research.....	2
1.2.1. Non- grouted borehole heat exchangers	2
1.2.2. Closed loop engineered geothermal system.....	4
2. Conductive heat transfer in rock and thermal properties of rock	7
2.1. Heat transfer	7
2.1.1. Analytical methods.....	8
2.1.1.1. Infinite line source.....	8
2.1.1.2. Finite line source	9
2.1.1.3. Infinite cylindrical source	9
2.1.2. Superposition methods	9
2.1.2.1. Temporal superposition	10
2.1.2.2. Superposition of mean and peak loads.....	10
2.1.2.3. Spatial superposition.....	10
2.1.3. Numerical methods.....	11
2.1.4. Temperature profiles	11
2.1.4.1. Constant wall temperature	12
2.1.4.2. Constant heat load	13
2.2. Thermal properties of rock	18

2.2.1.	Thermal conductivity.....	18
2.2.1.1.	Porosity.....	19
2.2.1.2.	Anisotropy	21
2.2.1.3.	Temperature dependencies	22
2.2.1.4.	Pressure dependencies	24
2.2.1.5.	Influence of scale.....	24
2.2.2.	Specific heat capacity	25
2.2.3.	Thermal diffusivity.....	27
2.2.4.	Radiogenic heat production	27
2.2.5.	Summary	28
PART I	29
I	Non-grouted borehole heat exchangers.....	29
I-1	Introduction	29
I-2	Section structure	30
I-3	Previous works	31
I-3.1	Shallow geothermal energy – borehole heat exchangers.....	31
I-3.1.1	Conductive heat transfer around the borehole – Analytical.....	31
I-3.1.2	Conductive heat transfer around the borehole – Numerical.....	32
I-3.1.3	Natural convection	33
I-3.2	Coaxial borehole heat exchanger	34
I-3.3	Borehole thermal energy storage (BTES)	35
I-4	Numerical model for non-grouted borehole heat exchangers	36
I-4.1	Introduction.....	36
I-4.2	Objectives	36
I-4.3	Methodology	36
I-4.3.1	Numerical model	36
I-4.3.2	Natural convection	37
I-4.4	PAPER 1 : Numerical Model for Non-Grouted Borehole Heat Exchanges, Part 1- Development.....	39

I-4.5	PAPER 2: Numerical Model For Non-Grouted Borehole Heat Exchanges, Part 2- evaluation.....	63
I-4.6	Additional Results and Discussion.....	77
I-4.6.1	Distributed Thermal response test.....	77
I-4.6.2	Heat pump operation.....	80
I-4.7	Conclusions.....	85
I-5	Solar assisted borehole thermal energy storage	86
I-5.1	Introduction.....	86
I-5.2	Objectives.....	86
I-5.3	Background.....	86
I-5.4	Methodology	90
I-5.5	Discussion	91
I-5.6	PAPER 3: Solar Assisted Borehole Thermal Energy Storage for Ground Source Heat Pump System.....	93
I-6	Deep coaxial borehole heat exchangers	119
I-6.1	Introduction.....	119
I-6.2	Objectives.....	119
I-6.3	Background.....	119
I-6.4	PAPER 4: Thermal Evaluation of Coaxial Deep Borehole Heat Exchangers	123
I-6.5	Additional results and discussion	145
I-6.5.1	Simulation of 190 m coaxial BHE.....	146
I-6.5.1.1	Heat Injection to 190 m coaxial BHE	147
I-6.5.1.2	Heat extraction from 190 m coaxial BHE	151
I-6.5.1.3	Summary	153
I-6.5.2	Simulation of 800 m coaxial BHE.....	153
I-6.5.2.1	Heat extraction from 800 m coaxial BHE	154
I-6.5.2.2	Heat injection to 800 m coaxial BHE	158
I-6.5.2.3	Summary	160
I-6.5.3	Parametric study of coaxial BHE	160

I-6.5.3.1	Heat pump and system performance	160
I-6.5.3.2	Results from parametric study	161
I-6.6	Conclusions.....	167
PART II	169
II	Closed loop engineered geothermal systems	169
II-1	Introduction	169
II-2	Section structure	170
II-3	Previous works	170
II-3.1.	Engineered geothermal systems (EGS)	170
II-3.2.	EGS- concepts.....	172
II-3.3.	Numerical simulation	174
II-4	A novel concept to engineered geothermal systems.....	177
II-4.1.	Introduction.....	177
II-4.2.	Objectives.....	177
II-4.3.	Background.....	177
II-4.4.	PAPER 5 : A Novel Concept to Engineered Geothermal Systems	179
II-5	Thermal modeling in the Oslo rift	189
II-5.1.	Introduction.....	189
II-5.2.	Objectives.....	189
II-5.3.	Background.....	189
II-5.4.	PAPER 6: Thermal Modeling in The Oslo Rift, Norway.....	191
II-6	Numerical model for simulation of the novel closed loop engineered geothermal system- as applied to district heating systems.	203
II-6.1.	Introduction.....	203
II-6.2.	The EGS concept.....	204
II-6.3.	Heat transfer and thermal properties.....	205
II-6.4.	Numerical model	206

II-6.4.1.	Heat conduction in the rock.....	206
II-6.4.2.	Momentum equation for the heat carrier fluid	207
II-6.4.3.	Energy equation for the heat carrier fluid	207
II-6.4.4.	Coupling between the conduction and convection models.....	209
II-6.5.	Results and discussion.....	210
II-6.5.1.	Validation of the numerical model.....	210
II-6.5.1.1.	Conductive model	210
II-6.5.1.2.	Convective model.....	211
II-6.5.2.	Simulation of closed loop EGS.....	213
II-6.5.2.1.	Thermal interference between wells.	218
II-6.5.3.	EGS system coupled with district heating.....	219
II-6.6.	Conclusions.....	221
	References.....	223
	Appendix	229
A.	Analytical solutions	229
	Infinite line source (ILS).....	229
	Finite line source (FLS)	229
	Infinite cylindrical source (ICS).....	229
	ICS with heat flux boundary	229
	ICS with temperature boundary.....	230
	Multipool method	230
B.	Deep coaxial borehole heat exchangers	231
	Constant inlet temperature	231
	Thermal recharge with inlet through the annular space	232
C.	Closed loop engineered geothermal system.....	235
	EGS coupled with distric heating.....	235
D.	Deep Borehole Heat Exchangers, Application to Ground Source Heat Pump Systems – Proceedings presented at World Geothermal Congress 2015.....	239

1. INTRODUCTION

Geothermal energy is an abundant energy resource, which can be utilized to provide clean energy for heating and cooling purposes and /or electricity production. Low temperature geothermal resources can as well be utilized either direct in low temperature applications, or be upgraded with the use of a heat pump.

The use of borehole heat exchangers in ground source heat pump systems is a mature technology; there are, however, room for improvements, primarily related to the design of the ground-coupling, i.e. the borehole heat exchanger.

At present, the use of deep geothermal energy as an energy resource is primary confined to areas with hydrothermal systems which in turn are geographically constricted to volcanic active areas. In addition there are some geothermal installations exploiting water reservoirs in sedimentary basins outside the active areas. However, it is Engineered Geothermal Systems (EGS) that have been pointed out as the way for geothermal energy to grow outside it constrains and to reach a significant share of its global potential. These have, however, not been fully developed and proven commercially viable at the present time.

1.1. General objectives

The aim of this thesis is to provide insight and methods for calculation of the heat transfer in boreholes, primary for the purpose of heat extraction. The thesis is divided into two parts of which the first deals with shallow geothermal energy and heat transfer in borehole heat exchangers. The second part is about the heat transfer in a closed loop geothermal system intended for heat extraction from crystalline rock at several kilometers depth. The objectives of the thesis can be summarized as:

- Study the local and global heat transfer processes in borehole heat exchangers with the aim to provide possible improvements to the technology.
- Develop methods to calculate the thermal performance of a closed loop geothermal system with the aim to provide energy in the range applicable to district and residential heating.

1.2. Scope of the research

1.2.1. NON- GROUTED BOREHOLE HEAT EXCHANGERS

The borehole heat exchanger (BHE) forms the ground-coupling for a ground source heat pump system (GSHP). A primary objective with the heat pump is to reduce the use of electricity for heating purposes, this is measured by the coefficient of performance (COP) of the heat pump, which is directly related to the temperature of energy source, i.e the temperature provided by the BHE.

The use of BHEs is widespread and established. In Lund (2010) it is estimated that 49 % of the worlds use of geothermal energy comes from the use of GSHP systems.

In Sweden it is estimated that approximately 400 000 GSHP plants were in operation by the end of 2011, extracting about 12 TWh of heat and 500 GWh of cooling. About 300 000 of the installations utilize vertical BHEs as the heat source and sink (Andersson and Bjelm (2013)). While the market for smaller GSHP installations (single house installations) have stagnated due to market saturation, there is a steady growth in the market for larger systems (smaller district heating networks). In addition, there is a trend to use deeper boreholes.

Ramstad (2011) concluded that the entire heat and cooling demand in Norway can be covered by GSHP installations. About 5000 new GSHP installations are built in Norway each year (Midtømme et al. (2013)). There is a trend to deeper boreholes for BHEs, and there are some few installations operating with BHEs with a depth in range of 500 m. Due to new building regulations, which demands that the 60 % of the energy used for heating (and hot water) in buildings ($> 500 \text{ m}^2$) must be supplied by an energy carrier other than electricity and/ or fossil fuels; there is the potential for a large number of medium sized GSHP installations.

The BHE usually consists of a borehole in which a heat carrier is circulated through a polyethylene pipe (collector). The most common collector has the shape of a U-tube and forms a barrier between the heat carrier and the borehole. The heat carrier which in this case is in indirect contact with the ground, usually consists of a mixture of water and an anti-freeze solution (e.g alcohol).

When in operation, there is a temperature difference between the heat carrier in the BHE and the ground caused by the thermal resistance in the BHE. During heat extraction and injection, this temperature difference can constitute a relatively large share of the total temperature difference between the heat carrier in the borehole heat exchanger and the undisturbed temperature of the ground. By reducing the thermal resistance in the BHE the source temperature for the heat pump can be increased during heat extraction and the temperature during heat injection can be reduced. Alternatively the amount of energy that can be extracted or injected can be increased.

The two major parts of the internal resistance in the BHE are the resistance through the collector material, and the resistance in the medium surrounding the collector. In Norway and Sweden

the BHEs are usually non-grouted; that is, the space surrounding the U-tube collector is filled with ground water. In these BHEs the internal resistance is significantly affected by natural convection in the water which enhances the heat transfer. Although it is well known that natural convection occurs, there is a lack of detailed studies into the subject. In addition, there have up to the present not been any BHE -models that include the effects of the presence of natural convection.

The thermal resistance in the BHE can as well be reduced using an alternative collector design, such as the coaxial collector. This has been shown experimentally by Kjellson and Hellström (1999) and by Acuna (2013).

Borehole heat exchanger systems can be upscaled either by increasing the number of boreholes, or by increasing the borehole depth. With several interacting boreholes, BHE systems can be tailored to cover specific heating and cooling demands; this does, however, increase the need for flexible simulation programs that can be used to determine the performance of borehole field using arbitrary BHE configurations. There exists good dimensioning tools for BHEs using predefined and fixed borehole patterns; the designer wanting to use configurations other than the predefined choices are, however, forced to make qualified guesses. There is a need for more flexible tools for BHE dimensioning, such tools can be developed using both analytical and numerical methods.

In areas where there is a limited available construction area, the borehole system can be made compact by placing the boreholes with a small separation distance. This favors thermal interaction and, therefore, the thermal load must be balanced over the year. It is, therefore, required that the boreholes are thermally recharged. In cases where there are little possibilities for thermal recharge, the number of boreholes (and thermal interaction) can be reduced by increasing the borehole depth and thereby creating a BHE system which requires less thermal recharge. There is little experience with deep BHEs at the present time, although, there are some deep BHEs operating in abandoned oil and gas wells in Germany with open loop coaxial collectors and with depths of about 1200 m to 2300 m.

In deeper boreholes, it is more favourable to use a coaxial collector than a U-tube collector since it reduces the borehole thermal resistance and the pressure losses, alternatively, allows for higher mass flow rates.

It is primarily the heat transfer processes in the BHEs that are studied within this thesis, and this has been done through the use of numerical models. The models provide insight and understanding for the acting local heat transfer processes in BHEs which can be used to develop improved collector designs. The thesis also focuses on the possibility to increase the borehole depth and thereby, creating larger BHE installations with a smaller surface footprint.

1.2.2. CLOSED LOOP ENGINEERED GEOTHERMAL SYSTEM

Geothermal energy is ideal as a base load resource for direct usage of heat. Through history, geothermal energy has been used to cover direct heating purposes such as heating, bathing and agricultural demands. In the development of Engineered Geothermal Systems (EGS) mainly electricity production has been in focus and thus areas with the highest geothermal potential (highest temperatures) have been targeted. While low temperature resources that can be exploited for direct heat-purpose has been given less attention. This was pointed out in the IEA-roadmap for geothermal energy (IEA 2011), which urges countries to assess their potential also for low temperature applications.

The global geothermal resources suitable for direct utilization have been estimated in Stefansson (2005) and in Krewitt et al. (2009). Stefansson characterized resources with a temperature lower than 130 °C as applicable for direct usage and concluded that this amounts to 68 % of the total geothermal resource. The study by Stefansson, Krewitt et al. (2009) estimated the global geothermal resources suitable for direct use applications, to be 289 000 TWh_{th} / year, which is 6.5 times larger than the worldwide use of energy for heating in 2008 (IEA 2011). Most of the accessible geothermal resources are to be found outside the geographical boundaries of the conventional hydrothermal resources. These resources can be accessed and mined through Engineered Geothermal Systems (EGS).

The worldwide use of geothermal energy for direct purposes in 2010 was 62 GWh_{th} /year (excluding heat pumps) Lund et al. (2010). The Blue Hi-REN scenario in the IEA energy technology perspectives 2010 (IEA 2010) projects the direct use of geothermal energy to increase to 1.6 TWh_{th} in 2050 (excluding heat pumps).

This puts the projected use as an almost negligible fraction of the estimated accessible resource. Even for this target, it is crucial that EGS (which is currently in the stage of research, development and demonstration) becomes a viable commercial technology within the next decades.

The projected use of geothermal energy does, therefore, show the amount of energy that is believed to be technically and economically viable, given the current state of technology, and the projected advancements.

Low temperature resources can as well be used to produce electricity with binary cycles at temperatures lower than 100 °C. This has much in common with heat recovery from low grade waste and the efficiency for such a process is bounded to be low as given by the laws of thermodynamics. Thus electricity production would only be considered if there were no other way of disposing the heat, or in remote locations outside the electricity grid. Through direct use of geothermal energy a high efficiency is ensured, while the resource can be used to displace, for example, electric resistance heating or other high grade fuels that could be used for electricity production.

District heating provides an ideal way to distribute low grade thermal energy, and it accounts for 85 % of the direct use of geothermal energy worldwide Lund et al. (2010). The stable nature

of geothermal energy makes it a suitable base load candidate in a district heating grid. However, at present district heating grids often operate at an excessively high temperature. In Scandinavia it is common with production temperatures around 80-90 °C and return temperatures around 65 °C. In some systems even higher temperatures can be found. High temperatures are often related to requirements from industrial processes while domestic consumers in general have a significantly lower temperature demand (< 60 °C). Future district heating nets are likely to be operated at lower temperatures as the heating demand of buildings decrease, this also reduces transmission losses and promotes renewable energy resources such as solar and geothermal.

While the most common approach to EGS is a system where wellbores for injection and production of fluid are connected by artificially created fractures, there exist also alternative approaches. The primary focus of the second part of this thesis is an EGS concept in which the heat transfer is based primarily on thermal conduction. The system has been presented by the Norwegian company, Rock Energy AS, and it consists of an injection well and a production well that are interconnected by a subsurface heat exchanger consisting of several directionally drilled wellbores in parallel.

In theory this gives a reliable system with a predictable long term performance. The amount of energy extracted from the system is, however, in direct proportion to the difference between the temperature of the inlet fluid and the targeted reservoir temperature. Thus a shift towards lower temperatures in district heating can have a tremendous impact on the accessible geothermal potential.

This type of system has not been extensively studied prior to the work presented in this thesis, and as pointed out in IEA geothermal roadmap (IEA 2011), theoretical studies of this particular type of concept are needed.

The geological conditions in Norway are less favorable compared to many other places where EGS projects have been initiated. Heat flow studies have, however, showed that the expected geothermal gradients are in the range of 20 °C to 30 °C, which means that an EGS could be built based on what is considered accessible depths (4- 6 km) to provide hot water in the temperature range of district heating.

2. CONDUCTIVE HEAT TRANSFER IN ROCK AND THERMAL PROPERTIES OF ROCK.

This thesis focuses primarily on the extraction and injection of thermal energy in boreholes and on the heat transfer in the rock domain surrounding the boreholes. Inside the borehole, convective processes transfer the energy between the rock and the heat carrier fluid. The thermal transport surrounding the boreholes is in this thesis assumed to be by pure thermal conduction. Due to the low thermal diffusivity of the rock, this is a relatively slow process.

Convective heat transfer is, for the applications and range of parameters studied here, a well known phenomenon that can be readily quantified by empirical correlations from the literature. For most of the cases studied in this thesis, the fluid flow is either fully turbulent or in the transitional stage. Although the convective heat transfer is important as it provides the boundaries for the conductive heat transport, it is the conductive heat transfer that will be governing the heat transfer process. This is because the thermal resistance between the wall of the borehole and the heat carrier fluid is small and often negligible compared to the higher thermal resistance in the surrounding conductive domain.

It is, therefore, important both to have a calculation method that can handle the conductive heat transfer with a suitable flexibility and accuracy, and to have a good estimate, or knowledge of the thermal properties (i.e. the effective thermal conductivity and the specific heat capacity) of the rock domain.

2.1. Heat transfer

The conductive heat transport can be treated using either numerical methods or analytical solutions, some of which will be summarized hereunder. The choice of method depends on the specific problem at hand, the required transient accuracy and in some cases the computational load required.

For conductive heat transfer around boreholes it is suitable to consider the heat conduction equation in cylindrical coordinates as given in Equation 2-1.

$$\frac{\partial T}{\partial t} = \frac{1}{r} \frac{\partial}{\partial r} \left(\alpha r \frac{\partial T}{\partial r} \right) + \frac{1}{r^2} \frac{\partial}{\partial \varphi} \frac{\partial}{\partial r} \left(\alpha r \frac{\partial T}{\partial r} \right) + \frac{\partial}{\partial z} \left(k \frac{\partial T}{\partial z} \right), \quad 2-1$$

where r is the radial coordinate, φ is the circumferential coordinate and z is the axial coordinate as seen in Figure 2-1. A common assumption is that of symmetric heat transfer around the borehole; hence, circumferential variations are not present. This assumption has been applied consistently throughout this thesis. Further simplifications can be made by neglecting axial heat conduction and by assuming constant thermal properties. These assumptions are implicitly made when using the analytical solutions described hereunder. Numerical solutions are in general more flexible than the analytical, but might also require assumptions (simplifications) in order to reduce the computational load.

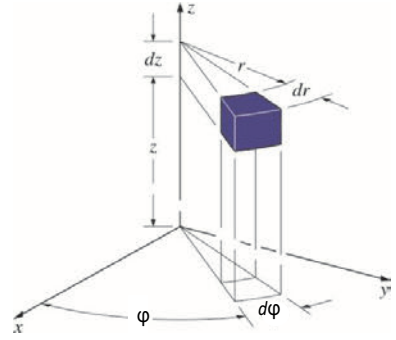


Figure 2-1. Radial coordinate system

Numerical and analytical solutions both have their respective strengths and weaknesses, and there is no direct answer to which type of solution that is the preferable. By combining the respective strengths of analytical and numerical models, hybrid solutions can be derived. An good example of this is the hybrid EWS – model of borehole heat exchangers (Wetter and Huberg (1997)), where a numerical solution is used to account for the transient heat transfer of a single borehole while the thermal interaction between several nearby boreholes is superimposed using analytical solutions.

2.1.1. ANALYTICAL METHODS

Analytical solutions applicable to shallow and deep geothermal energy are described in the following subsections. The equations corresponding to each solution can be found in Appendix A.

2.1.1.1. INFINITE LINE SOURCE

The infinite line source (ILS), commonly referred to as the line source, is commonly used both for shallow borehole heat exchangers (to evaluate thermal response tests) (Ghelin (2002)) and to determine the temperature changes in deep boreholes (Ramey (1962)).

The infinite line source does not account for the finite length of the borehole: it is, thereby, assumed that it can be represented by an infinite series of point sources. In the description of the heat transfer inside and around a borehole, the solution is limited by two primary factors:

- The geometry of the borehole is described by a point source, the borehole is, thereby, assumed to have the thermal properties of the surrounding conductive domain. This limits the solution for early transients (times less than around 12 hours).

- The assumption of an infinite line source limits the solution as it is not applicable for large time periods (up to several years), during which the heat transfer becomes 2-dimensional (radial and axial directions).

The analytical solution for the infinite line source can be found in Appendix A - Equation A-1.

2.1.1.2. FINITE LINE SOURCE

In the finite line source solution (FLS), the finite length of the borehole is accounted for by applying a mirroring technique to the infinite line source solution. The finite line source solution is still not accurate for short time periods by the point source description of the borehole. It accounts for the finite length of the borehole and gives the correct solution for large time periods. The FLS solution is considered as the most appropriate analytical solution for BHEs.

The analytical solution for the finite line source can be found in Appendix A - Equations A-2 to A-4 with reference to Lamarche and Beauchamp (2007).

2.1.1.3. INFINITE CYLINDRICAL SOURCE

The infinite cylindrical source solution (ICS) is the analytical solution to heat transfer in an infinite solid medium bounded internally by a cylindrical surface. It is presented in Carslaw and Jaeger (1959) for a constant heat flux boundary and for a constant temperature boundary.

The analytical solution for the infinite cylindrical source can be found in Appendix A – Equations A-5 to A-6 with reference to Carslaw and Jaeger (1959).

In the description of the heat transfer in and around a borehole, the solution is limited by two primary factors.

- The solution considers the heat transfer to be located on the surface of a cylindrical hole, the internal thermal capacity of the borehole is, thereby, neglected, This limits the solution for early transients.
- The finite length of the borehole is neglected. This limits the solution as it is not applicable for large time periods, during which the heat transfer becomes 2-dimensional.

2.1.2. SUPERPOSITION METHODS

The flexibility of the analytical solutions can be greatly improved by using spatial and temporal superposition. Thereby complex solutions can be derived with superposition of several spatially distributed heat sources/ sinks and time-varying thermal loads.

2.1.2.1. TEMPORAL SUPERPOSITION

Transient numerical models use time-discretization, whereby a continuous time-varying boundary condition, i.e. thermal load, is divided into discrete loads with a corresponding time-interval. The response, in form of a temperature change, is then the sum of the response for each discrete load. For certain cases (i.e. isotropic thermal domains) the thermal response can as well be determined by superposition of time-discrete analytical solutions, i.e. one solution for each time step is required.

For long time-series (e.g. yearly simulations using hourly load values) this can become a computationally demanding problem; it can, therefore, be beneficial to use an aggregation scheme where historical loads are lumped together to averaged heat loads with a longer duration, see e.g. Bernier (2004) and Javed (2012).

2.1.2.2. SUPERPOSITION OF MEAN AND PEAK LOADS.

A time varying thermal load can be considered as composed of a mean value and a fluctuating component. Thereby, a solution can first be determined based on the mean value (which is constant in time), and the thermal response from the fluctuating (time- varying) component can then be added to the mean value solution. This is a method to get a characteristic solution, without necessarily solving the entire problem. The procedure is beneficial since the mean value solution requires less computational effort (either numerical or analytical) as compared to solving the entire time-varying problem. This methodology is strictly not conservative, since the energy in the peak loads are already included in the average value. The error involved is, however, negligible, given that the time-duration of the peak load is small compared to the larger time-duration of the mean load.

The methodology with superposition of mean and peak-loads is applied in Paper 3 where hourly peak load values are superpositioned to monthly average values, in this case, it is assumed that the heat transfer is uniform along the length of the boreholes. This methodology is also described in more detail in Section 2.1.4

It should be noted that the method cannot always be applied, e.g. for deep borehole heat exchangers (BHEs) the vertical distribution of the thermal load varies with the applied thermal load. If the mean value differs from the actual thermal load, this will result in a different distribution of the thermal load in the borehole.

2.1.2.3. SPATIAL SUPERPOSITION.

Given that the thermal domain is isotropic, the spatial linearity of the conduction equation allows for superposition of the thermal response from spatially distributed heat sources or sinks. Thereby, superposition can be used to determine the thermal influence from several boreholes at any given location. This is beneficial, since it allows for simulation of rather complex systems based on the analytical solutions.

2.1.3. NUMERICAL METHODS.

Although a lot of information can be gained from studying the analytical solutions presented, numerical methods offers transparency and are in general more flexible. Numerical methods have been used extensively in this thesis. It is primarily the finite difference method that has been applied. The finite element method has been sparsely used by the commercial simulation software, Comsol Multiphysics. The Matlab environment has been used as the platform for implementation of numerical codes.

Numerical methods can be used at different levels of resolution. Since the computational load increases with the level of resolution, it is usually desirable to simplify the problem at hand. In this thesis, heat transfer is studied for objects having a considerable aspect ratio; therefore, fully discretized models are infeasible since they require very large numerical grids and therefore a large computational effort. Still, models with a high resolution can be used to study parts of a problem.

Throughout this thesis, the boreholes are considered as axisymmetric objects, consistent with the assumptions involved when using analytical solutions. Nevertheless, some objects studied, e.g. borehole heat exchangers, have been shown to have a circumferential variation depending on the positioning of the collector Acuna (2010). The error involved by assuming axisymmetric heat transfer is believed to be negligible in most cases.

It is primarily implicit numerical models that have been used in this work, although explicit models have been used to verify the accuracy of the implicit models and for simulations using short time steps (in the range where the explicit model is faster than the implicit model), e.g. when studying the transient behavior of the non-grouted U-tube BHE (Paper 2).

2.1.4. TEMPERATURE PROFILES

When extracting heat from a borehole by convective transport (fluid flow), the main thermal resistance will usually be in the ground. Therefore, the fluid will obtain a temperature near that of the borehole wall. A good estimate of the expected fluid temperatures during heat extraction can, therefore, be based on the borehole wall temperature determined from the analytical solutions. In this section, the analytical solutions (Equation A-5 and Equation A-6) are used to study the radial heat transfer around a section of a borehole.

In Equation A-5 it is assumed that a constant heat load is imposed on the wall of the borehole, and in Equation A-6 the borehole wall is maintained at a constant temperature differing from the undisturbed temperature of the ground.

2.1.4.1. CONSTANT WALL TEMPERATURE

The profiles in Figure 2-2 show how the temperature profiles develop with time. The profiles are determined using Equation A-6. The temperature difference between the borehole wall (T_s) and the undisturbed temperature (T_∞) is, in this case, kept constant at 80 K. T_∞ is assumed as 140 °C.

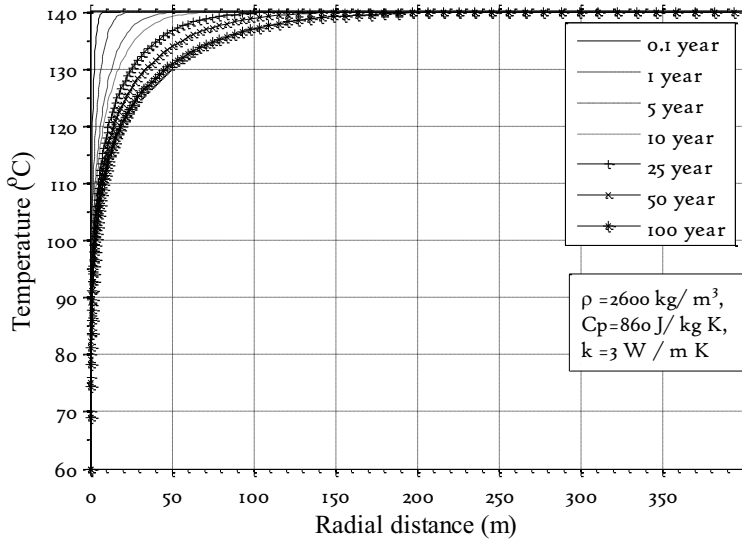


Figure 2-2. Radial temperature profiles surrounding a cylindrical cavity with a constant wall temperature.

The profiles are shown for times ranging between 0.1 year and 100 years. The profiles show the extent of the temperature decline in the ground. It is seen that after 100 years the thermal influence reach about 200 meters in radial direction. To better show the influence during the earlier times, the same profiles are presented based on a logarithmic radial distance in Figure 2-3. In order to show the relative thermal influence the temperature is made dimensionless by Equation 2-2.

$$\theta = \frac{T - T_\infty}{T_s - T_\infty} \quad 2-2$$

Thereby, the “thermal domain” influenced by the borehole can be determined.

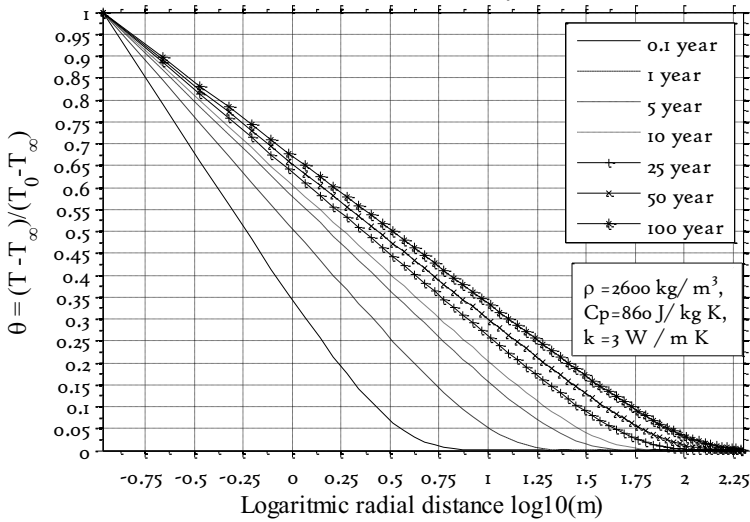


Figure 2-3. Dimensionless temperature profiles surrounding a cylindrical cavity with a constant wall temperature. The figure is shown with the radial distance represented on a logarithmic scale.

It is seen that after 0.1 year the change in temperature difference at 1 m radial distance is 35 % and that after 1 year the change at 10 meters is about 5 %. The thermal influence is important when the interaction between several heat sinks (e.g. boreholes) are studied. Using spatial superposition, the interaction between multiple heat sinks can be determined based on the profiles in Figure 2-3.

2.1.4.2. CONSTANT HEAT LOAD

Equation A-5 is used to study the result of a constant imposed heat load. In Figure 2-4 the heat load is constant at 150 W / m. Note that the temperature change for the smaller radiuses is largest between the earliest profiles, while the temperature change is small between 10 and 100 years (on the order of 9 K), and (on the order of 5.5 K) between 25 and 100 years. The non-dimensional temperature profiles in Figure 2-3 can be replicated by applying Equation 2-2 to the profiles in Figure 2-4.

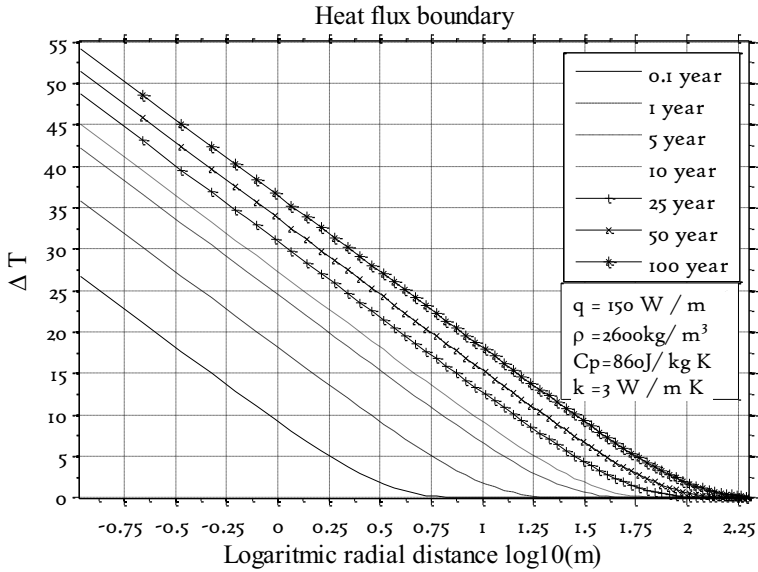


Figure 2-4. Radial temperature profiles surrounding a cylindrical cavity with a constant wall heat load (W/m). The figure is shown with radial distance on a logarithmic scale. $\Delta T = T_{\infty} - T$

Figure 2-4 is illustrative for the long term performance of a conduction based heat extraction process. It is shown that, given the specific heat extraction rate of 150 W/m, a system sized for the thermal performance during year 25 will have a rather small decrease in temperature when extending the operation time to 100 years. This is further described in the following figures.

The temperature profiles for different heat loads can be determined after specific operation times. In Figure 2-5 and Figure 2-6 the temperature profiles are shown for given heat loads after 10 years, 25 years and 50 years.

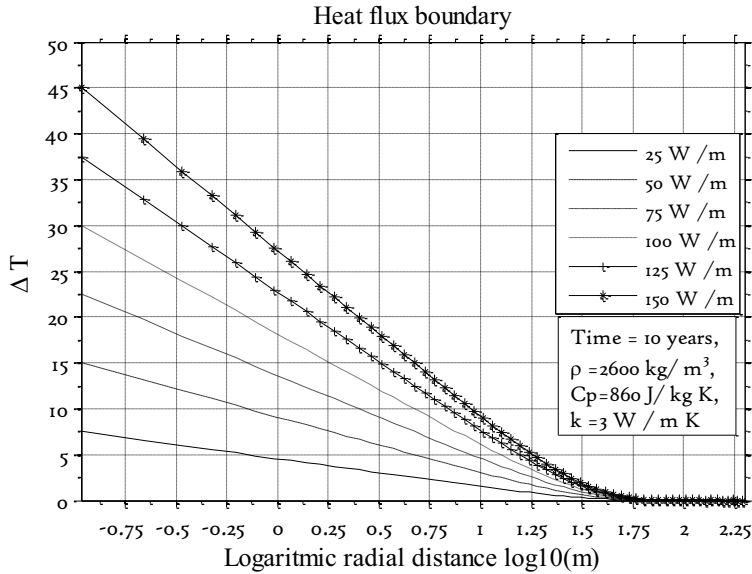
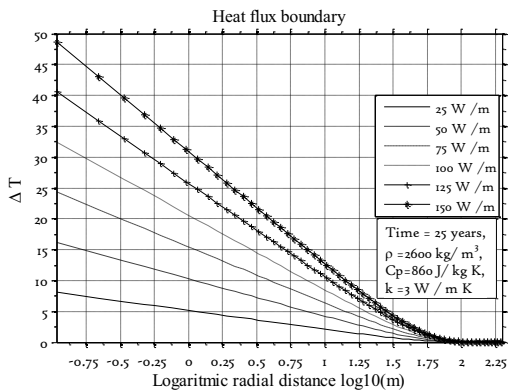
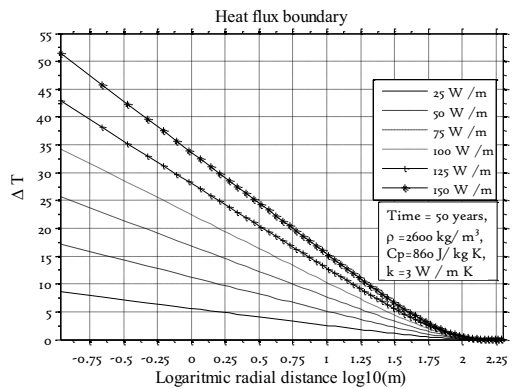


Figure 2-5. Radial temperature profiles (temperature difference) surrounding a cylindrical cavity with a constant wall heat load (W / m) at 10 years. The figure is shown with radial distance on a logarithmic scale. $\Delta T = T_{\infty} - T$

It is seen from Figure 2-5 that the change in borehole wall temperature after 10 years of operation varies between 7 K for 25 W / m to 45 K for 150 W / m. As the operation time increases from 10 to 25, respective 50 years, a temperature change on the order of 6 K is seen for the highest heat extraction rate, while for the lowest heat extraction rate, the change is on the order of 1 K.



a



b

Figure 2-6. a) 25 years, b) 50 years, radial temperature profiles (temperature difference) surrounding a cylindrical cavity with a constant wall heat flux (W / m) at 50 years. The figures are shown with radial distance on a logarithmic scale. $\Delta T = T_{\infty} - T$

In Figure 2-7, the temperature change on the borehole wall is shown as a function of the imposed heat load and the duration of the heat load.

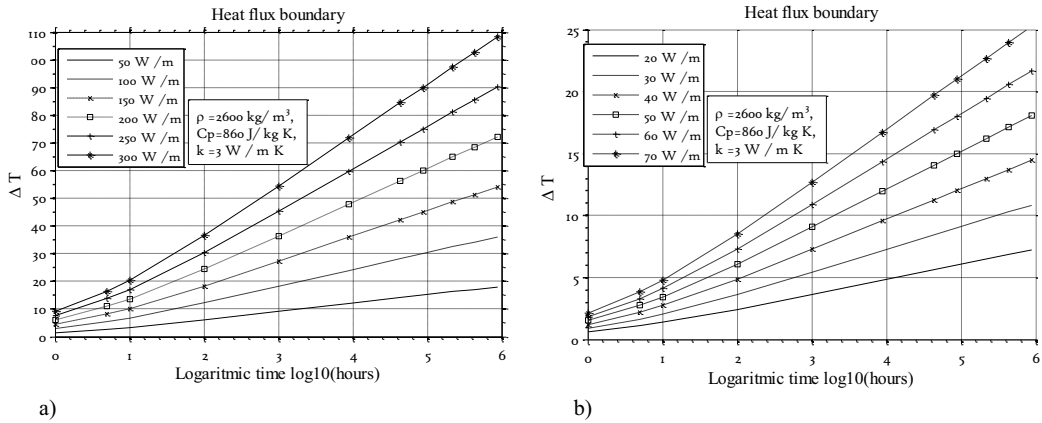


Figure 2-7. Temperature change of the borehole wall for various heat loads and duration. The graphs are shown with a logarithmic time scale. $\Delta T = T_{\infty} - T_{r_b}$

As shown in Figure 2-7, a heat load of 150 W / m with a duration of 10 hours results in a temperature change of 10 K, and the change increases linearly with the heat load and is 20 K for a heat load of 300 W/m. The figure can be used to illustrate the superposition of mean and peak loads(see Section 2.1.2.2) as shown by the following example.

Assuming an EGS system based on the conductive heat transfer from boreholes, the average specific heat supply from the system is 150 W/m of the borehole, and the peak thermal load is 250 W/m. Such a system could, thereby, supply a peak thermal load of 1 MW_{th} using the equivalence of 4 km length of borehole (e.g. parallel boreholes placed at the same conditions).The yearly energy supply from such a system would then be 5,26 GWh. The operating temperatures of the system can be determined using Figure 2-7.

Assuming that heat has been extracted for 25 years with an average extraction rate of 150 W / m, the resulting temperature change of the borehole wall is about 48 K. The peak load of 250 W / m, with an assumed duration of 10 hours can then be superpositioned to the average value. This results in a further temperature change of 6. 8 K (first subtracting the mean value from the peak and then read in the figure) the total temperature change is then about 55 K. With an undisturbed rock temperature of 140 °C it can, therefore, be determined that after 25 years the borehole will have a surface temperature of 85 °C while heat is being extracted. Extending the heat extraction period from 25 to 100 years reduces the borehole wall temperature with further 5.5 K.

It is, therefore, apparent that from a thermal perspective the heat extraction from such a system can be operated for a significant time.

The influence of the borehole diameter and the ground thermal conductivity on the temperature change of the borehole wall during a constant heat extraction rate is shown in Figure 2-8 and

Figure 2-9. In Figure 2-8 the diameter is varied from 0.1142 m (4.5 “) to 0.2540 m (10 “). It is seen that the temperature change declines with increasing borehole diameter. Two profiles are shown, one for the relative response after 25 years and one for the relative response after 10 hours. It is seen that after 25 years, doubling the diameter gives about 10 % decrease in temperature change. The influence of diameter is larger for shorter time periods and for a 10 h period, which is equivalent to e.g. the duration of a daily peak load, the borehole diameter only has to be increased from 0.1142 m (4.5 “) to 0.1397 m (5.5”) to reduce the temperature change of the borehole wall with 10 %.

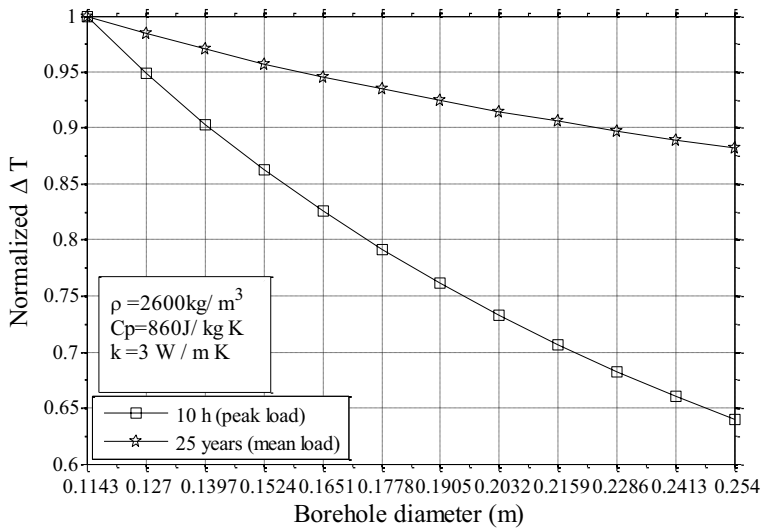


Figure 2-8. Normalized change in borehole wall temperature, constant heat load. $\Delta T = T_{\infty} - T_{r_b}$

Rock thermal conductivity has a significant influence on the temperature change of the borehole wall as seen in Figure 2-9. The temperature change of the borehole wall is almost inversely proportional to the change in thermal conductivity, that is, the temperature change is about 3 times higher when decreasing the conductivity from 4.5 W/m·K to 1.5 W/m·K. This shows that it is crucial to have a good estimate of the effective thermal conductivity of the ground when sizing a system based on conductive heat transfer.

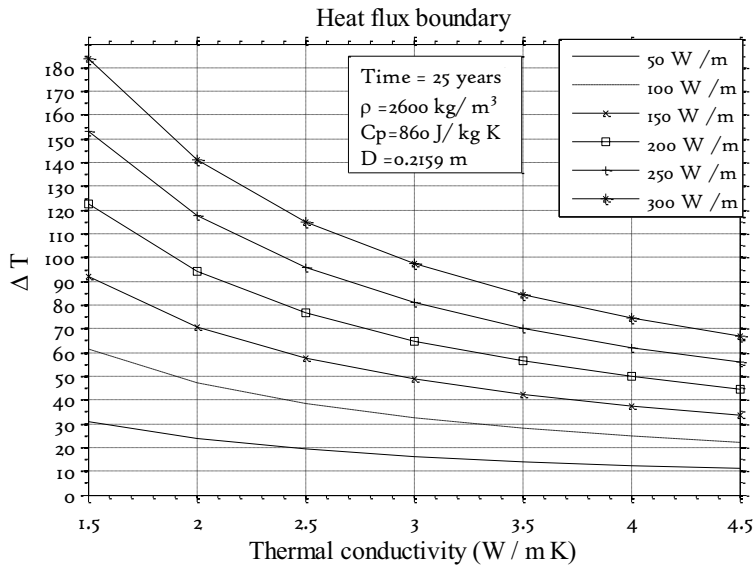


Figure 2-9. Change in borehole wall temperature with thermal conductivity. Profiles are taken at 25 years. $\Delta T = T_{\infty} - T_{r_b}$

The figures presented in this subsection show some of the fundamental characteristics of conductive heat transfer around boreholes. Using the figures it is relatively simple to get an overall picture of the limitations for heat extraction from boreholes, either in form of borehole heat exchangers as discussed in Part 1 of this thesis or in form of a closed loop engineered geothermal system as presented in Part 2. The transient heat transfer, especially with varying load conditions in both time and space, is, however, easier to study using numerical methods, and to some extent also superposition of analytical solutions.

2.2. Thermal properties of rock

This section focuses on the thermal properties of rock, namely the thermal conductivity, specific heat capacity, and radiogenic heat production. The section is a supplement to the papers in the thesis.

2.2.1. THERMAL CONDUCTIVITY

Thermal conductivity is a thermal transport property of a material. In relation to rocks, the thermal conductivity is a somewhat abstract property to link to a certain rock type or lithology.

The effective thermal conductivity refers to the actual, or measurable value for a rock type. It is important to have a good estimate of the effective thermal conductivity, since it has a large

influence on the performance of both borehole heat exchangers and engineered geothermal systems.

In-situ values refers to the actual effective thermal conductivity of the rock surrounding the borehole at a certain depth. In the case of crystalline rocks, the effective thermal conductivity depends on a number of factors such as temperature, pressure, minerals, porosity, fluid saturation and scale. These factors are for most cases interconnected, e.g. the effect of fluid saturation is related to the porosity, which can be affected by the specific minerals in the rock and their respective thermal properties. For certain rock types, such as metamorphic rocks, the thermal conductivity can also be highly anisotropic.

Measurements of thermal conductivity are often performed at ambient temperature and pressure and then corrected to predict the in-situ, or effective, thermal conductivity values at both higher temperature and pressure. It is, therefore, worthwhile to have a sound understanding for thermal conduction and the different factors that influences the thermal conductivity.

In solid non-conducting materials, heat is carried by vibrations of the crystalline lattice. These vibrations, or waves, can be thought of as discrete energy packets (phonons). The thermal conductivity of the material is related to the scattering of phonons. In the case of a pure crystal this occurs by Umklapp scattering which is proportional to the mean free path length (that the phonon can travel), which in turn is inversely proportional to the absolute temperature. Therefore, the thermal conductivity of non-conducting materials decrease with increasing temperature ($k \propto T^{-1}$) (Eckert and Drake 1978).

For crystalline rocks, the temperature dependency of thermal conductivity is less pronounced than for the pure crystal, since other factors such as impurities, grain boundaries and fractures also contribute to phonon scattering (Seipold 1998). For temperatures higher than 500 to 600 °C, heat may also transported by thermal radiation (which increases proportional to T^4); this contribution can, however, be neglected for the temperature range of interest here (≤ 200 °C).

2.2.1.1. POROSITY

The porosity (ϕ) is defined as the ratio between void-volume and total volume of the rock. Even for rock with a low porosity ($\phi < 1$ %) the influence on effective thermal conductivity can be significant. This is because the porosity can be distributed in the form of thin fractures. If these are water saturated, the effect is small since water has a relatively high thermal conductivity (≈ 0.6 W /m·K) as compared to air (≈ 0.02 W /m·K) which usually fills the fractures in the case of dry rock samples. The difference in effective thermal conductivity between dry and water saturated low porosity rocks can be on the order of 30% (Schärli and Rybach (1984)).

There are several methods to calculate the effect of porosity, the most fundamental and simple method would be to consider the porosity as thermal resistances either normal (series) to the heat flow, or in parallel with the heat flow. For simplicity, it is assumed that the thermal properties of the rock are isotropic and that the void-volume is occupied with a single medium.

The normal and parallel cases are expressed by Equation 2-3 and Equation 2-4, respectively, and constitute limiting cases for the influence of porosity on the thermal conductivity.

$$\text{Normal: } k = \frac{1}{\frac{\phi}{k_f} + \frac{1-\phi}{k_g}}, \quad 2-3$$

$$\text{Parallel: } k = \phi k_f + (1 - \phi)k_g, \quad 2-4$$

where k_f and k_g are the thermal conductivities of the fluid respective the rock.

A more restrictive approach was derived by Hashin and Strikeman (1962). The method was originally intended to be used to determine magnetic permeability of two-phase materials, but has been frequently cited and used for thermal conductivity (Zimmerman, 1989).

$$k^- = k_f + \frac{3k_f(k_g - k_f)(1-\phi)}{3k_f + (k_g - k_f)\phi}, \quad 2-5$$

$$k^+ = k_g + \frac{3k_g(k_f - k_g)\phi}{3k_g + (k_f - k_g)(1-\phi)}, \quad 2-6$$

where the k^+ and k^- refers to an upper respective lower limit to the influence of porosity.

Another method proposed in the literature (Zimmerman, 1989) considers the cracks or porosity of the rock as spheroids in a homogenous matrix. The basic idea was proposed by Maxwell (1892):

$$k = k_g \frac{(1-\phi)(1-i) + r\beta\phi}{(1-\phi)(1-i) + \beta\phi} \quad 2-7$$

where $i = \frac{k_f}{k_g}$. β is given by:

$$\beta = \frac{1-i}{3} \left(\frac{4}{2+(i-1)M} + \frac{1}{1+(i-1)(1-M)} \right), \quad 2-8$$

$$\text{where } M = \frac{2\theta - \sin(2\theta)}{2\tan(\theta)\sin^2(\theta)}, \quad 2-9$$

and $\theta = \arccos(\gamma)$.

γ is defined by Zimmerman (1989) as the aspect ratio of the spheroids; some limiting cases are:

$$\text{a) Thin cracks: } \beta \rightarrow \frac{(1-i)(1+2i)}{3i} \quad \gamma \rightarrow 0, \quad 2-10$$

$$\text{b) Spherical pores: } \beta = \frac{3(1-i)}{2+i}, \quad 2-11$$

$$\text{c) Needle-like pores: } \beta \rightarrow \frac{(1-i)(5+i)}{3(1+i)} \quad \gamma \rightarrow \infty, \quad 2-12$$

Case a) corresponds to the lower limit of Hashin and Strikeman (1962) while case b) and c) are closer to the the upper limit.

In Figure 2-10, the normalized thermal conductivity is shown as a function of porosity as determined by the correlations listed above. It is assumed that the porous voids are filled with water ($k_f=0.6$ W/m·K), and that the rock has a thermal conductivity $k_g=3$ W/m·K.

As shown, there is a clear difference between the parallel and series cases, while the respective limits by Hashin and Strikeman (1962) and (Zimmerman, 1989) essentially gives the same results.

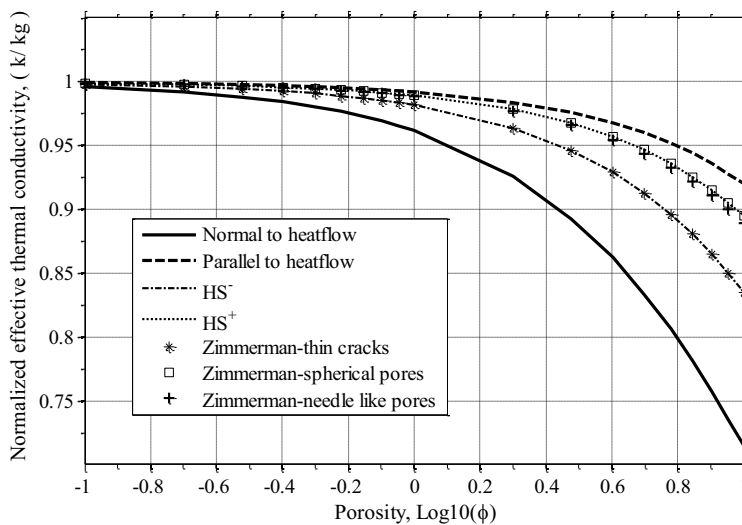


Figure 2-10. Normalized thermal conductivity as function of porosity ($\phi = 0 - 10\%$), $k_f/k_g=0.2$

The porosity of crystalline rocks is in general in the order of 1 % (Walsh and Brace (1984)). The upper and lower bounds provided by the limiting cases (normal and parallel) give for this case a reduction between 0.08 % and 3.8 % in effective thermal conductivity, and the more restrictive methods gives a reduction between 1 % and 1.8 %. The effect of porosity is, in general limited for fluid saturated rocks and is believed to be counteracted by static pressure in the crystalline basement. Nevertheless, there can be fractures and fracture zones having a significant porosity.

2.2.1.2. ANISOTROPY

While the effective thermal conductivity of plutonic rocks, e.g granites, varies little with direction, a significant anisotropy can be observed for metamorphic rocks, e.g gneiss. These rocks are formed by layers of different minerals, and the effective thermal conductivities measured perpendicular and parallel with the foliation can be significantly different. On a sample of gneiss, Clauser and Huenges (1995) observed a reduction of the effective thermal conductivity of 40 % when measured perpendicular to the foliation as compared to parallel with the foliation.

The anisotropic effective thermal conductivity can be explained by a layered structure consisting of minerals having high, respective low intrinsic thermal conductivities. The minerals with a lower thermal conductivity acts as thermal resistances in the perpendicular direction, while not having a large influence on effective thermal conductivity parallel with the foliation.

Clauser and Huenges (1995) also observed that for a rock with a porosity on the order of 1 % the anisotropy was independent of the degree of fluid saturation. This is because anisotropy is being caused mostly by the distribution of minerals having different properties. It is, however, likely that fractures that contribute to the porosity are aligned with the layered structure and for larger porosity values, a change in the anisotropy would be expected as a function of the saturation degree.

The anisotropy of thermal conductivity is found to decrease with increasing temperature. This is because minerals with a high thermal conductivity at ambient temperature in general have a stronger temperature dependency than those with a lower thermal conductivity. Therefore, the differences in thermal conductivity between the minerals in the rock decreases with increasing temperature and thereby also the anisotropy.

2.2.1.3. TEMPERATURE DEPENDENCIES

The temperature dependency of thermal conductivity is mineral-specific and therefore, dependent on the constituents of the rock. For the rock types of interest, igneous rock and metamorphic rock, the dependency is in general linked to the content of feldspar respective quartz.

Pure quartz has an orderly crystalline structure which gives a high thermal conductivity ($k \approx 7 \text{ W} / \text{m} \cdot \text{K}$ at ambient temperature) (Clauser (2006)) and a strong temperature dependency. Therefore, rocks with a high content of quartz in general have a high value of thermal conductivity at ambient temperature, which then decreases relatively fast with increasing temperature.

Feldspar has a lower thermal conductivity at ambient temperature, and because of its metallic constituents, the thermal conductivity of some feldspars increases with temperature (since in metals, heat is also being transported by electrons). This can offset the reduction in thermal conductivity of other minerals, leading to a reduced temperature dependency for rocks with a high content of feldspar.

Measurements of temperature dependency are in general performed on dry samples, and at ambient pressure, therefore, measured values must be corrected for the effect of fluid saturation and pressure. Since rocks in general are anisotropic conglomerates of different minerals (having different properties and thermal expansion coefficients), heating the rock samples during measurements can cause thermal cracking due to differential expansion which in turn increases the porosity, and reduces the effective thermal conductivity. This effect is most pronounced in dry samples (Pridnow et al. 1996, Clauser 2006). In Abdulagatov et al. (2006) the temperature dependency was measured on dry rock samples at elevated hydrostatic pressures. It was seen that with increasing pressure, the temperature dependency decreased. It can, therefore, be

assumed that some of the reduction in measured thermal conductivity with increasing temperature can be attributed to thermal cracking, an effect which would be counteracted by the increased pressure for in-situ conditions.

Several authors have published empirical correlations for the temperature dependency of thermal conductivity. A summary of these correlations can be found in Lee and Deming (1998), Vosteen and Schellschmidt (2003) and in (Clauser 2006). The probably most commonly used correlation was first published by Sass et al. 1992 based on data from Birch and Clark (1940) and is presented here as adapted by Vosteen and Schellschmidt (2003) for magmatic and metamorphic rocks:

$$k(T \text{ (}^\circ\text{C)}) = \frac{k(0)}{0.99 + T(^{\circ}\text{C})(a - b/k(0))}, \quad 2-13$$

where $a = 0.003 \pm 0.0015$ and $b = 0.0042 \pm 0.0006$, and $k(0)$ is given by :

$$k(0) = 0.53k(25 \text{ }^\circ\text{C}) + \frac{1}{2}\sqrt{1.13(k(25 \text{ }^\circ\text{C}))^2 - 0.42k(25 \text{ }^\circ\text{C})} \quad 2-14$$

Equation 2-13 has been cited and used in several publications e.g. (Clauser and Huenges, 1995), (Vosteen and Schellschmidt, 2003) and (Clauser, 2006), (Hartman, 2008).

Seipold (1998) also derived a general equation for the temperature dependency of thermal conductivity based on measurements on magmatic and metamorphic rocks:

$$k(T(\text{K})) = 1/(B(T(\text{K}) - 532 \pm 45) + 0.448 \pm 0.014), \quad 2-15$$

where the parameter B can be determined using the thermal conductivity of a rock at any temperature.

It is important to note that correlations such as Equation 2-13 cannot replace actual site specific measurements. Because of the high variability in properties within specific rock types, large errors can be introduced if measurements are replaced by generally published values for a specific rock or lithology.

The correlations do, however, show the general temperature dependency for the thermal conductivity of crystalline rocks. The temperature dependency as described by Equation 2-13 and Equation 2-15 is shown in Figure 2-11.

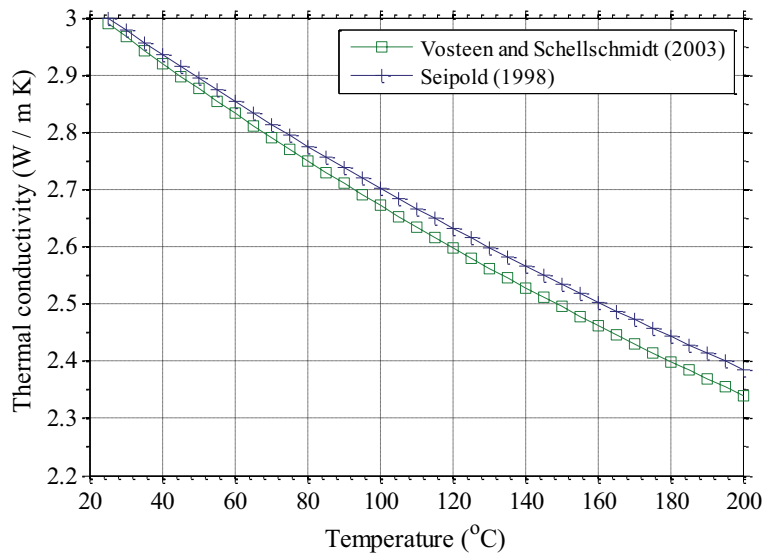


Figure 2-11. Temperature variation of thermal conductivity as determined by Equation 2-13 (Vosteen and Schellschmidt (2003)) and by Equation 2-15 Seipold (1998).

In Figure 2-11 it is assumed that the thermal conductivity is $3 \text{ W / m} \cdot \text{K}$ at $25 \text{ }^\circ\text{C}$. With this starting value, the two equations give similar values, A larger difference is, however, seen for lower values of thermal conductivity.

2.2.1.4. PRESSURE DEPENDENCIES

The influence of pressure on the effective thermal conductivity of crystalline rocks depends on porosity, as well as fluid saturation. With increasing pressure, fractures that occur in-between grain boundaries in the rock closes. Walsh and Decker (1966) performed measurements on crystalline rocks with low porosity ($\approx 1 \%$), and with a pressure up to 930 bar. They found that for fluid saturated samples, the increase in thermal conductivity is much less pronounced than for dry samples. This is to be expected since water has a higher thermal conductivity than air, the effective thermal conductivity of the fluid saturated samples is, therefore, close to the intrinsic thermal conductivity also at ambient pressure.

Horai and Susaki (1989) measured thermal conductivity of dry rock samples (igneous and metamorphic) during elevated quasi-hydrostatic pressure in the range up to 12 000 bar. From the results it was seen that thermal conductivity increased as the pressure rose to around 2000 bar; this was explained by the reduction in porosity and contact resistance. The effect of an increased pressure is somewhat limited as the closed fractures still acts as structural defects which contribute to phonon scattering. As the pressure increases further, the internal crystalline structure of the rock starts to change, leading to further increase in thermal conductivity.

2.2.1.5. INFLUENCE OF SCALE

The thermal conductivity can vary strongly within the same lithology and laboratory measurements of thermal conductivity are usually conducted on small samples (core samples), which might not be representative of the in situ effective thermal conductivity on a larger scale. It is, therefore, important to be careful when extrapolating measured values.

In geothermal installations based primarily on heat transfer by thermal conduction, the thermal performance depends on the value of the effective thermal conductivity of the rock volume that is accessed by the system. For a normally sized GSHP system, e.g. for a school building, the accessed rock volume can be more than 10^6 m^3 .

Larger GSHP systems are usually dimensioned based on a thermal response test (TRT) performed in one of the boreholes, this test provides a measurement of the effective thermal conductivity for the rock volume directly surrounding the borehole.

In general, TRTs yield a higher value of thermal conductivity than laboratory measurements. The difference with application to dimensioning of GSHP system has been studied by Leibel (2012). Leibel concluded that the effective thermal conductivity cannot be predicted from laboratory measurements due to large local variations. In addition, the effective thermal conductivity as measured from the TRT can be affected by other factors such as fluid circulation in the ground.

2.2.2. SPECIFIC HEAT CAPACITY

The specific heat capacity is defined as the energy required to raise the temperature of a unit of mass by one degree. In general, the specific heat capacity of rocks varies with temperature, pressure, porosity and fluid saturation.

The specific heat capacity of a rock can be determined from the volume fractions of its respective mineral constituents and their respective specific heat capacities. Since specific heat capacity is a scalar unit it does not have any variation with direction, i.e. anisotropy.

The effect of pressure and fluid saturation are interconnected with the porosity and can be neglected for low porosity ($\phi \leq 1\%$) crystalline rocks. According to (Waples 2004) the effect of pressure is in the order of 0.1 % per km of rock column and can safely be neglected. This leaves temperature as the only dependent variable for specific heat capacity.

The specific heat capacity of solid non-porous rocks increases with temperature. The increase is relatively large, e.g. for quartzite the increase between ambient temperature (20 °C) and 200 °C is about 30 % (Waples 2004).

The temperature dependency of a rock can be measured using calorimetric methods or it can be calculated based on the respective mass fraction of the minerals in the rock and their respective temperature dependencies. Clauser (2006) provided coefficients for a wide range of minerals which can be used to determine the specific heat capacity as a function of the temperature using Equation 2-16 as derived by Kelly (1960):

$$C = A_1 + 2A_2 - \frac{A_3}{T(K)^2} \quad 2-16$$

A number of empirical equations (on the form of Equation 2-16) exist that describe the temperature dependency of specific heat capacity. Some of those have been summarized by Waples (2004) who also derived a universal correlation for minerals and rocks. The correlation was derived based on heat capacity values for rock and minerals, normalized by their respective values at 200 °C and is given by:

$$C_{nT} = 8.95 * 10^{-10}T(^{\circ}C)^3 - 2.13 * 10^{-6}T(^{\circ}C)^2 + 0.00172T(^{\circ}C) + 0.716 \quad 2-17$$

$$C_{T2} = C_{T1} * C_{nT2}/C_{nT1} \quad 2-18$$

The procedure involved when using Equation 2-17 and Equation 2-18 is described in Waples (2004). The advantage with Equation 2-17 and Equation 2-18 is that the correlation is universal and only requires a measured value of the specific heat capacity of a rock or mineral at a defined temperature, while correlations on the form of Equation 2-16 require that either coefficients or measurements of the temperature dependency are available. Correlations derived for a specific mineral are, however, likely to be more accurate than the universal correlations.

Using Equation 2-17 and Equation 2-18 the variation of specific heat capacity of a typical granite, having a specific heat capacity of 860 J /kg·K at 20 °C was calculated for the range 20 °C to 200 °C. The result is shown in Figure 2-12.

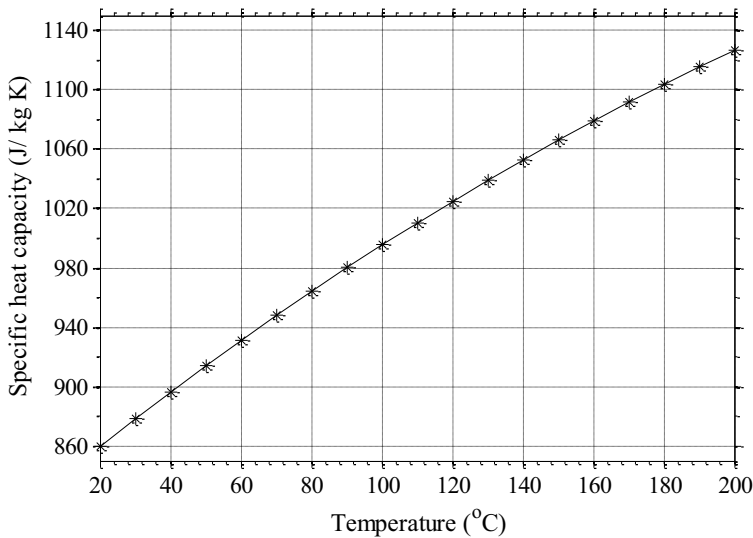


Figure 2-12. Specific heat capacity as function of the temperature.

As shown, the specific heat capacity increases from 860 J / kg·K to almost 1060 J / kg·K as the temperature increases from 20 °C to 140 °C, an increase of 22 % . Between 20 °C and 200 °C the increase is 31 % . This means that the rocks ability to store thermal energy has increased.

2.2.3. THERMAL DIFFUSIVITY

The thermal diffusivity is a measure of how much energy the rock can conduct relative to its storage capacity. It is defined as the ratio between the thermal conductivity and the product of the heat capacity and the density ($\alpha = k/(C \cdot \rho)$). As the thermal conductivity decreases with increasing temperature while the specific heat capacity increases with increasing temperature, the thermal diffusivity experiences a decrease with increasing temperature.

Using Equation 2-17, Equation 2-18 and Equation 2-13 the change in thermal diffusivity of a rock can be estimated, assuming initial values of: $k = 3 \text{ W / m} \cdot \text{K}$ (25 °C) and $C=860 \text{ (J / kg} \cdot \text{K)}$ (20 °C), $\rho = 2600 \text{ kg/ m}^2$, the density of the rock is assumed constant. The variation with temperature in the range 25 °C to 200 °C is seen in Figure 2-13.

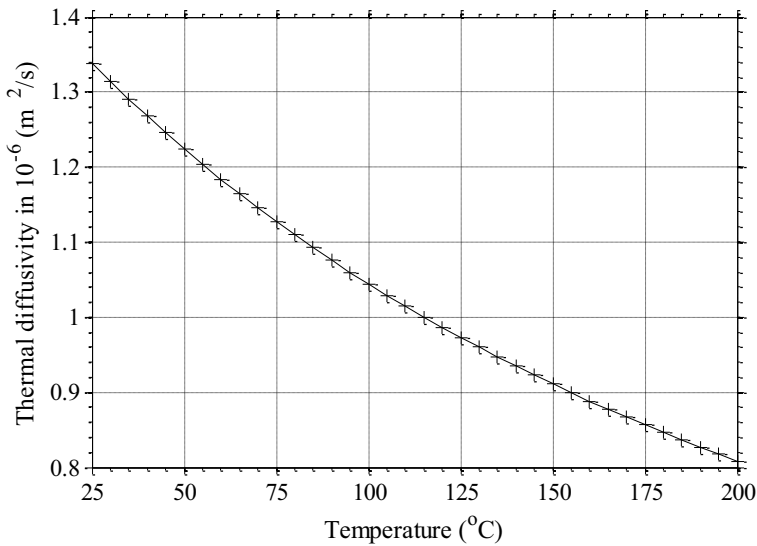


Figure 2-13. Thermal diffusivity determined as a function of temperature. The values are based on Equations 2-13 and 2-17.

2.2.4. RADIOGENIC HEAT PRODUCTION

About half of the continental heat flow originates from the decay of radioactive isotopes in the crust, mainly from uranium (^{238}U), thorium (^{232}Th) and potassium (^{40}K) (Turcotte and Schubert, (2002)). In stable continental regions, variations in crustal heat flow is, therefore, tightly connected to variations in radiogenic heat production. High isotope concentrations are

associated with enriched felsic rocks like granite, while depleted mafic rocks have the lowest concentration and thus a lower heat production.

The total heat production (H ($\mu\text{W}/\text{m}^3$)) can be estimated based the concentration of the respective elements using Equation 2-19 as given by Rybach (1988):

$$H = \rho(9.52c_U + 2.56c_{Th} + 3.48c_K)10^{-5}, \quad 2-19$$

where ρ is the density of the rock and c is the mass concentration of the respective isotopes.

Radiogenic heat production is closely related to lithological variations which can be significant, and is difficult to generalize and correlate with parameters such as geological age, crustal depth and metamorphic grade (Slagstad 2008).

2.2.5. SUMMARY

The main characteristics of rock thermal properties has been discussed. Correlations for temperature and pressure dependencies of thermal properties give an indication, but are no replacement for actual measurements. Considering fluid saturated rock with low porosity, it is the temperature dependency of rock thermal conductivity that can have the largest influence on conductive heat transfer processes. For the temperature range considered for deep geothermal installations in Part 2 of this thesis (around 140 °C), the reduction in thermal conductivity is around 15 % (from Figure 2-11) compared with ambient conditions. As seen from Figure 2-9 a reduction in rock thermal conductivity is proportional to a reduction in borehole wall temperature during heat extraction.

The temperature dependencies of thermal conductivity as described by Equations 2-13 and 2-14 is implemented in Paper 5: *A novel concept to Engineered geothermal systems*, Paper 6: *Thermal modeling in the Oslo rift*, and in the report presented in Section 0: *Numerical model for simulation of novel closed loop engineered geothermal system- as applied to district heating systems*. Also the temperature dependencies for specific heat capacity as described by Equations 2-16 and 2-17 are implemented in Paper 5 and Equation 2-19 is used when determining the radiogenic heat production in Paper 6.

PART I

I NON-GROUTED BOREHOLE HEAT EXCHANGERS

I-1 Introduction

This section concerns primarily the heat transfer in borehole heat exchangers (BHE). Conventionally the BHE consists of a borehole with a depth ranging between 50- 300 m and with a polyethylene collector, forming a U-tube in the borehole. A heat carrier fluid circulates through the collector and exchanges energy with the medium filling the borehole (grout or water), and with the ground surrounding the borehole. Alternatively, coaxial BHEs can be used, as will be explored later in this section.

The BHE can have a dual purpose as it can serve both as a thermal energy source for a heat pump and as a sink for excess thermal energy. Larger installations are usually constructed by placing multiple BHEs in parallel. The BHEs interact through heat transfer in the ground and the thermal characteristics of a BHE installation can be tailored and predetermined, i.e. the number of BHEs, individual distances and depths, can be determined to cover a specified heating and cooling demand.

A GSHP system, where on a yearly basis the same energy quantities are transferred to the boreholes as are extracted can be said to be balanced, while a system where more energy is being extracted is negatively unbalanced.

The origin of the energy transferred in these systems is largely dependent on both the system design and the way the system is operated, e.g. in a balanced system, the boreholes provide the means for thermal exchange with a large thermal mass. The sum of the energy exchange can over time, however, be zero. Therefore, the energy transferred in the system cannot be said to be of geothermal origin; the same applies to positively balanced system where the ground surrounding the boreholes is being heated up.

In a negatively balanced system, the ground surrounding the borehole is cooled down as energy is being extracted. In a shallow borehole, the energy can be said to originate partly from the surface, i.e. the ground is heated up by the ambient temperature at the surface, which in turn, largely is dependent on solar energy. As the borehole depth is increased, the temperature in the ground increases; therefore, the potential for heat extraction increases whereas the potential for heat injection (cooling) decreases. In addition, the distribution of the heat transfer along the borehole during heat extraction is proportional to the temperature gradient in the borehole (which usually is positive); therefore, most of the energy will be extracted from the lower part of the borehole and can clearly be said to be of geothermal origin.

The purpose of the BHE is to provide a stable, and (in case of heating) a higher source temperature level for the heat pump than alternative thermal energy sources, such as air or water resources e.g. lakes or rivers. The internal thermal resistance of the BHE is, therefore,

important as it reflects the temperature difference required between the heat carrier fluid and the borehole wall. E.g. with an effective (overall) thermal resistance of 0.1 K m/W the temperature difference required for a specific thermal load of 30 W / m is 3 K. However, if the thermal resistance could be decreased, the evaporator temperature, and therefore, also the COP of the heat pump would increase. Reducing the required temperature difference with 2 K, can mean an improvement of the heat pump COP on the order of 5 %.

I-2 Section structure

Part I of the thesis is divided into four main subsections, where the first subsection (Section I-3) presents previous work and the second subsection (Section I-4) concerns the heat transfer in non-grouted boreholes, i.e. water -filled U-tube BHEs. The heat transfer is studied on a local scale. A numerical model is developed and complemented with a heat transfer correlation for the influence of natural convection in the water surrounding the collector. The model is compared with experimental data and is found to accurately predict the measurements. The model is further used to study the heat transfer in the U-tube BHE. The essence of this subsection is presented in Papers 1 and 2.

In the third subsection (Section I-5), a system is studied, where a matrix of borehole heat exchangers is used together with a solar collector. The boreholes provide energy to a heat pump system used in a school building. The boreholes are recharged with a solar collector in the summer season. The system is nearly balanced and the boreholes are placed with a relatively small separation distance. The system is studied with an analytical model that accounts for the thermal interaction between the boreholes. The results from the model are compared with temperature measurements from the system during the first year of operation. The model is then used to study the long term performance of the system including the effect of a negatively or positively balanced load. The essence of this subsection is presented in Paper 3.

In the fourth subsection (Section 0), the primary objective is to study the thermal performance of coaxial BHEs as a function of borehole depth. With increasing borehole depth, the mass flow has to be increased in the BHE to ensure that the thermal performance is high. To allow for high flow rates without causing excessive pressure drops, the borehole heat exchanger has to have a large flow area. This is accomplished using a coaxial pipe-in-pipe BHE. The thermal performance of a coaxial pipe-in-pipe BHE is studied using a numerical model which is developed in the present work and validated against experimental data. The essence of this subsection is presented in Paper 4.

I-3 Previous works

I-3.1 SHALLOW GEOTHERMAL ENERGY – BOREHOLE HEAT EXCHANGERS.

In this subsection a brief summary of previous works related to the aspects of borehole heat exchangers studied within the scope of the thesis is presented. That is, the use of analytical and numerical models to simulate the performance of BHEs (U-tube and coaxial) including the influence of natural convection in non-grouted (water filled) boreholes.

I-3.1.1 CONDUCTIVE HEAT TRANSFER AROUND THE BOREHOLE – ANALYTICAL

The thermal response of the BHE can usually be divided into two parts: (1) the heat transfer in the surrounding ground and (2) the internal heat transfer in the BHE and its constituents. Analytical solutions used for the heat transport in the ground are in general related to the Infinite Line Source (ILS) (Ingersoll and Plass (1948)) or the Infinite Cylindrical Source (ICS) solutions presented in Carslaw and Jaeger (1959). In using either of these two solutions, it is assumed that the ground is isotropic and that the heat transfer surrounding the borehole can be represented as a 1-dimensional problem. The internal heat capacity of the borehole is in the case of the ICS solution neglected while for ILS solution it is implicitly assumed to have the same thermal capacitance as the surrounding rock (as the ILS assumes a point source). This limits the accuracy of the analytical models for time steps shorter than 10 - 15 hours (depending on the dimensions of the borehole). In addition, the assumption of a 1-dimensional heat transfer problem limits the applicability for longer operation times because the heat transfer problem then becomes 2-dimensional.

Further, the Finite Line Source (FLS) solution is an improvement to the ILS, and it uses mirroring techniques to consider the ground's surface and is, therefore, accurate for longer time scales. The FLS was presented first in Eskilson (1987). The structure of the solution was further improved by Zeng et al. (2002) and by Lamarche and Beauchamp (2007). The FLS is considered as the most appropriate analytical solution for BHEs (Fossa et al. 2011).

The accuracy for short time scales of the analytical models has been addressed by Yavuzturk and Spitler (1999) and by (Javed (2012), who developed short time response factors based on a numerical scheme.

The analytical solutions can be used with spatial and temporal superposition to create flexible solutions. The evaluation of the analytical solutions does, however, require numerical integration which in the case of the large time series of loads (e.g. with short time steps) can become computationally heavy. The responses for a fixed borehole pattern and time series of thermal loads can be precalculated and stored as response factors for more rapid calculation. This approach was first used by Eskilson (1987) who introduced the response factors as g -functions, although, in this case, a two-dimensional finite difference code was used.

Compiled collections of g-functions form the basis for the most widely used method to dimensioning BHEs. The method is fast, but limited to the precalculated borehole patterns. Authors such as Bernier (2004), Lamarche and Beauchamp (2007), and Javed (2013) have provide ways to accurately determine the performance of BHEs using the analytical solutions while keeping the computational load down, thereby, making it easier to calculate the thermal response from arbitrary borehole patterns.

Recently, also spectral methods have been applied to evaluate the analytical solutions for temporal superposition, and thus, reducing the computational load (Lazzarotto (2104) and Marcotte and Pasquier (2014)).

It should be mentioned that in using the analytical models, the internal resistance of the borehole is usually assumed constant. In addition, due to the simplifications, the models does not account for the transient behaviour of the heat carrier in the borehole.

I-3.1.2 CONDUCTIVE HEAT TRANSFER AROUND THE BOREHOLE – NUMERICAL.

The analytical models can be computationally cost effective, but they are not capable of describing all the involved phenomena in the BHE, and therefore, lack some of the accuracy, flexibility and transparency that can be gained from numerical models.

There has been a lot of work done with numerical models on BHEs, and the progress is somewhat coupled with the development in numerical methods generally. It can be seen that the level of detail has continuously increased. Earlier works focused on describing the thermal interaction between boreholes, often using a simplified representation of the boreholes, such as a cartesian grid (Lund and Östman 1985) or neglecting the early transients in the system (Eskilson and Claesson 1988). The advancement in numerical methods and the accessibility of multipurpose numerical simulation tools with built in grid generation made it easier to build more complex models. An example of a 3- dimensional model with a higher level of detail is that of He (2012). The very large aspect ratio of the BHE does, however, make it impractical to use a fully discretised model for the entire BHE. Therefore, models are often constructed for a limited part of the BHE for more detailed studies.

Efficient numerical models have been presented amongst others by Al- Khoury et al. (2005) and by Bauer et al. (2011^a) using the analogy with electric networks when describing the thermal resistances within the borehole, these models are referred to as thermal resistance and capacity models (TRCM). In such a model the entire length of the borehole is discretized while the different parts in the borehole are described using single nodes. Further works on TRCM-models are presented by Diersch et al. (2011^a) and Diersch et al. (2011^b) and Mottaghy and Dijkshoorn (2012).

In all the above publications, the simulated BHEs were grouted and therefore, the internal heat transfer between the collectors and the wall of the borehole is treated as thermal conduction. In non-grouted boreholes, the heat transfer between the collector and the wall of the borehole is dependent on the possible presence of buoyancy-driven flow (natural convection).

I-3.1.3 NATURAL CONVECTION

In Sweden and Norway it is common practice that the boreholes are non-grouted, the boreholes are, therefore, filled with ground water. When the BHE is in operation a temperature gradient is established between the collector pipes and the wall of the borehole. This establishes a convective movement due to the density differences with temperature in the water in the borehole. Natural convection in BHEs has been pointed out by Nordell (1994), by Gehlin (2002) and by Kjellsson (2009). The influence of natural convection was studied in more detail by Gustafsson et al. (2010) using numerical simulation on a 3 m borehole section.

Although detailed studies of natural convection in BHEs are scarce, the water filled BHE resembles an enclosure with a high aspect ratio for which theoretical and experimental studies of natural convection are presented in the literature. Seki et al. (1978) presented visualizations of natural convection in a fluid filled vertical slot with an aspect ratio (height /width) of 15 and Wright et al. (2006) visualized natural convection in an air-filled vertical cavity with an aspect ratio of 40. In both studies the flow transits from a conductive regime to a secondary flow regime before becoming turbulent. Natural convection in vertical annulus with high aspect ratio has been studied by (Choi and Korpela (1980), Lee and Korpela (1983), Keyhani et al. (1983) and Littlefield and Desai (1986).

In water filled enclosures, the effect of natural convection is tightly connected to the coefficient of thermal expansion of water, for which the minimum coincides with the maximum density at 4°C. Using a thermal extraction response test, Gustafsson and Westerlund (2011) showed that the thermal resistance in a water filled borehole is highest when the temperature of the borehole water is in the range of 4°C.

In essence, the effect of natural convection depends on the temperature level in the borehole and the thermal load; therefore, the effect is usually larger during a heat injection than during heat extraction. As a result, the internal resistance in the BHE as determined from a thermal response test (TRT) with heat injection can differ significantly from the value experienced during heat pump operation.

The present work as presented in Papers 1 and 2 is an extension of the numerical TRCM concept (which has been presented for grouted BHEs by e.g. Al- Khoury et al. (2005), Bauer et al. (2011^a) and Diersch et al. (2011^a)) for non-grouted BHEs. An extensive literature review regarding natural convection in high aspect ratios enclosures (not directly related to BHEs) is used to derive a correlation for natural convection in non-grouted BHEs. Although using a different approach, the model presented in the present work extend the work by Gustafsson et al. (2010) and Gustafsson and Westerlund (2011). The developed model which is compared with measurement data from Acuña (2013), is used to study the transient heat transfer in U-tube BHEs in detail.

I-3.2 COAXIAL BOREHOLE HEAT EXCHANGER

The coaxial BHE can be used either as an open loop, where the circulated heat carrier (water) is in direct contact with the borehole rock, or it can be used as closed system with a secondary heat carrier fluid.

There are two main reasons why the coaxial borehole heat exchanger might be favorable as compared to the U-tube borehole heat exchanger. Firstly, it has the potential of reducing the internal thermal resistance in the BHE, and thereby increase the temperature of the heat carrier. Secondly, it can utilize a relative large fraction of the borehole as flow area, and therefore, allow larger mass flow rates without causing excessively large pressure losses.

In this thesis it is primarily the second reason that is exploited as the behavior of the coaxial BHE is studied for deeper boreholes where the mass flow rate has to be increased.

Deep coaxial BHEs have been studied by Kohl et al. (2000) (1213 m deep open loop coaxial BHE with a steel centerpipe) and by Kohl et al. (2002) (2302 m deep open loop coaxial BHE with a vacuum insulated central pipe). In both cases a numerical model was used to simulate and evaluate the performance of the BHEs. The conclusion was that the performance of the installations would be improved (in case one) by using an insulated central pipe, and (in case two) by using a higher mass flow rate. Dijkshoorn et al. (2013) studied the feasibility of using a 2500 m deep coaxial BHE for heating purposes and for cooling purposes through an absorption heat pump. Dijkshoorn concluded that the concept would require a prohibitively expensive center pipe.

If the coaxial BHE is applied as an open loop system, the freezing point of water becomes a natural lower limit for the possible inlet temperature of the water to the BHE. In addition, contaminations in the water might cause fouling in the top side heat exchangers. Acuña (2013) studied experimentally a coaxial BHE in which the heat carrier was separated from the borehole wall by a thinwalled flexible pipe. The pipe was not entirely sealed and can, therefore, not be considered as a closed BHE, the circulation of water between the BHE and the rock were, however, restricted which reduces the risk for contaminations. It was seen that the collector performed satisfactory and with a better thermal performance than a conventional U-tube collector.

Closed loop BHEs can be used either with water or with an antifreeze solution as the heat carrier. For coaxial BHEs in deeper boreholes this requires, however, significant volumes of heat carrier fluid. In addition, the temperature in the borehole increases with borehole depth due to the geothermal temperature gradient, and therefore, the need for antifreeze solution decreases.

In the present work, as presented in Paper 4 and in Section 0 of this thesis, the coaxial BHE is studied using a TRCM model, the work focuses on the use of coaxial BHEs for boreholes in the depth range (200 - 1000) m depth with the application to heat pump operation. The model which is compared with measurement data from Acuña(2013) is used for detailed study of the transient heat transfer in coaxial BHEs and to evaluate the thermal performance as function of primarily the borehole depth.

I-3.3 BOREHOLE THERMAL ENERGY STORAGE (BTES)

Kjellsson (2009) has shown that it is not viable to store thermal energy using a single borehole. However, the thermal interaction between several closely packed boreholes (placed with only a few meter spacing) can be used to store energy. In such configuration, heat losses from the inner boreholes are reduced by the outer boreholes, as a consequence, the temperature level increases for the center boreholes. In the warm season the boreholes can be used for cooling purposes, (provided that they are cool enough) and thereby, be thermally charged. Alternatively, they can be thermally charged with a high temperature source, e.g. solar energy from collectors or either waste, or surplus heat from industry or from district heating. Provided that the yearly thermal load is positively balanced (i.e. more energy is being transported to the boreholes than extracted) the temperature level will increase.

The increase in the temperature level in these storages are in general rather modest, with variation between (2 °C to 8 °C) (Anderson and Bjelm (2013)). There also exists high temperature BTES, two examples of existing BTES are the Drake landing solar community in Canada and Anneberg in Sweden, which both provide heating to residential buildings using solar energy as the thermal source and. A high temperature thermal energy storage is also studied experimentally and theoretically in Nordell (1994).

In the present work (Paper 3) the use of an BTES working in a complete system with a solar collector is described and studied. The BTES is studied using an analytical model. The model uses the analytical FLS solution as presented in Lamarche and Beauchamp (2007). It is applied in an iterative scheme capable of balancing the thermal load between several thermally interacting but separated borehole circuits with different loads, such that two circuits with different loads, positive or negative can be simulated. While not drawing on the benefits from using spectral solution methods to the FLS solution, as applied in Lazzarotto (2104) and in Marcotte and Pasquier (2014), this work contributes by increasing the flexibility of BHE field simulation. In Paper 3, the developed model is used to study a solar charged BTES at a public school in Norway. Other possible applications for the model can be e.g. simulation of thermal interaction between existing and new borehole fields, e.g. in urban areas.

I-4 Numerical model for non-grouted borehole heat exchangers

I-4.1 INTRODUCTION

In the present work, a numerical model of a non-grouted U-tube BHE has been developed. The model is implemented in Matlab and is based on a finite difference numerical scheme using a thermal resistance and capacity model for the borehole. The model is developed specifically for non-grouted BHEs where the heat transfer by natural convection in the borehole is essential. The effect of natural convection is accounted for through a heat transfer correlation which is developed and described in Paper 1: *Numerical model for non-grouted borehole heat exchanges, part 1-Development*. The model is verified through comparison with experimental data in Paper 2: *Numerical model for non-grouted borehole heat exchanges, part 2-Evaluation*. The transient behavior of the non-grouted BHEs is studied in detail. It is seen that natural convection has a large influence on the heat transfer in the BHEs, and that it affects the transient behavior of the BHE. Additional results are presented after the papers in this subsection.

I-4.2 OBJECTIVES

The main objectives are:

- to develop a numerical model for a non-grouted U-tube borehole heat exchanger that accounts for natural convection in the fluid surrounding the collector,
- to compare the model with experimental results,
- to study the transient heat transfer in non-grouted U-tube borehole heat exchangers, and
- to provide basis for improved collector designs.

I-4.3 METODOLOGY

I-4.3.1 NUMERICAL MODEL

There are several possible ways to model a borehole heat exchanger, both analytical and numerical. In the present study, a simplified numerical model is used, the model can be categorized as a thermal resistance and capacity model (TRCM). The model considers the constituents of the BHE as one-dimensional objects while the surrounding ground is resolved with an axisymmetric grid. This enables transient simulation of the BHE with a high level of accuracy. TRCM – models have been presented earlier, see for example (Al- Khoury et al. (2005) and Bauer et al. (2011^a). The present study does, however, differ from the previous studies in that it considers non-grouted boreholes where the heat transfer in the borehole includes natural convection.

The model is developed and implemented in Matlab, which was chosen due to the high degree of flexibility and transparency.

I-4.3.2 NATURAL CONVECTION

In a non-grouted U-tube BHE, the heat transfer through the water surrounding the collector is enhanced by natural convection. This has been noted by several authors, and has a rather large influence on the thermal performance of the BHE. The increase in heat transfer due to natural convection is expressed by a Nusselt number (Nu) which relates the convective heat transfer to the conductive heat transfer. In the case of enclosures, Nu is usually expressed as a function of the Rayleigh number (Ra) and a relation for the physical dimensions of the enclosure, e.g. aspect ratio (height / width). For annular objects, Nu is often expressed as a function of the radius ratio (K). In the case of a large K, the annulus behaves as a single pipe in an infinite domain. For small values of K, the annulus approaches the case for a vertical 2-dimensional slot at $K=1$. In this limiting case, the average Nusselt number for the inner and outer pipes are essentially the same. The flow regimes of natural convection in a vertical slot has been visualized experimentally by Seki et al. (1978) for various fluids using polystyrene particles as tracer. Streak photographs were presented in Figure I-1 for oil with a Prandtl number of 480.



The width of the vertical slot is 20 mm, and the aspect ratio is 15. It is seen in Figure I-1 that a primary laminar flow circulates clockwise in (a), as the Rayleigh number (Ra) increases secondary flow patterns arise, (b), but still the flow is laminar. When Ra is further increased, the secondary flow pattern breaks down and turbulent flow is established in the upper part of the figure. With water, the convection was shown to be fully turbulent at $Ra=1.78 \cdot 10^5$.

It is seen that as the secondary flow arises, the flow transits from a pattern which is 2-dimensional (depend on the height and width of the cavity) to a flow which is essentially 1-dimensional, and only dependent on the width of the cavity.

Figure I-1. Streak photographs from Seki et al. (1978), $A = 15$, a) $Ra=1.33 \cdot 10^5$, b) $Ra=2.9 \cdot 10^5$, c) $Ra=1.4 \cdot 10^8$.

In the present study, the influence of natural convection is accounted for through a Nusselt correlation which was derived in Paper 1, based on a literature review regarding natural convection in enclosures (annulars and cavities) with high aspect ratios (height / width). The derived correlation is based on the modified Rayleigh number (Ra^*) and the radius ratio (K) as follows:

$$Nu = 0.1743Ra^{*(0.233-0.009K)}K^{0.442}$$

I-1

There is no dependency on the aspect ratio in the correlation; it is thus, implicit, that its validity is limited to the range where the convective heat transfer is 1-dimensional.

In Papers 1 and 2 , the Nusselt correlation is applied to the numerical model as a correction to the local borehole thermal resistance as determined based on conduction through water. As an alternative the Nusselt number can be used to determine the effective thermal conductivity of the water as follows:

$$k_{f_effective} = k_f * Nu ,$$

I-2

where k_f is the thermal conductivity of the fluid in the borehole, i.e. water.

The effective value can then be used to determine the local borehole resistance (R_b) with the multipool method. Equations describing the multipool method can be found in Appendix A Equation A-7 to A-10 with reference to Lamarche et al. (2010)

R_b is then used to determine the individual thermal resistances between the water in the borehole and the collector and between the water in the borehole and the borehole wall. In essence, this gives the same result as the approach shown in Papers 1 and 2. This approach is used in the additional results presented after the papers in this subsection.

I-4.4 PAPER 1 : NUMERICAL MODEL FOR NON-GROUTED BOREHOLE HEAT
EXCHANGES, PART 1-DEVELOPMENT

Holmberg H., E. Næss., Sønju. O. K. (2016)

Submitted to Geothermics

A numerical model of non-grouted borehole heat exchangers, Part1-Development

Henrik Holmberg^{a*}, Erling Næss^a, Otto K. Sønju^b

^a Dept Energy and Process Engineering, Norwegian University of Science and Technology, Kolbjørn hejes vei 1 B, 7491 Trondheim, Norway

^b Rock Energy AS, Lysaker torg 25, 1366 Lysaker, Norway

*Corresponding author. Tel.: +47 95749363

E-mail address: henrik.holmberg@ntnu.no

Keywords: Ground source heat pump Borehole heat exchanger, Natural convection, Simulation, Numerical.

Abstract

A numerical finite difference model for a non-grouted (water filled) borehole heat exchanger (BHE) is presented. The model uses the concept of thermal resistances and thermal capacities (TRCM), which has proven to be an efficient method for a fast and accurate numerical BHE model.

In non-grouted BHEs the heat transfer is largely affected by the presence of natural convection in the borehole water. In the present paper, a novel approach is presented where the numerical model is combined with a convective heat transfer model to form the first TRCM model accounting for the effect of natural convection. In an accompanying paper, the results from the numerical model are compared with an extensive set of experimental data.

In the present paper, the model is used to study the transient performance of non-grouted U-tube BHEs operated with shorter and longer operation intervals and to study the performance of these heat exchangers for boreholes in the depth range of 200 – 800 m.

The effect of natural convection is dependent on the water temperature and the specific heat load. A larger effect is observed with warmer water (heat injection) than for colder water (heat extraction). In deeper BHEs, the effect during heat extraction is largest in the lower part of the borehole and in case of the 800 m BHE, the resistance between the collector and the borehole wall is reduced by 82 % compared to conductive heat transfer.

It is found that the performance of the BHE decreases with increasing operation interval, meaning that a higher heat load can be sustained when operating with shorter intervals. Provided that the collector size and the borehole diameter can be increased, the heat extraction rate for deeper boreholes can be significantly higher than for the common 200- 300 m boreholes. It is also shown that one 800 m deep BHE can supply more heat than eight 200 m BHEs.

1.Introduction

Ground source heat pump systems (GSHP) that utilize boreholes as a heat source and sink have proven to have good characteristics and can be operated in such way that the bedrock keeps a near stable temperature throughout the year. Such systems can also be made space effective and have a small or negligible visual footprint. However, larger systems require a certain amount of space which might not be available in densely populated urban areas, such as city centers. An attractive solution is then to

drill the boreholes down to greater depths. In areas with thick layers of soil, this can also be economically motivated as it reduces the number of casings. Installations based 500 m deep boreholes are now being constructed on a commercial basis in Norway.

The borehole heat exchanger consists of a borehole in which a heat carrier fluid is circulated. This can be in either an open loop system where the heat carrier is in direct contact with the rock, or in a closed loop system where the heat carrier fluid is separated from the rock. The most common configuration is the closed loop, using a polyethylene U-tube (collector) inserted into the borehole. Depending on the diameter and depth of the borehole, different dimensions of the collector are used. While this might be considered as a crude heat exchanger, the U-tube BHE does have an acceptable performance.

Possibly the easiest way to design a deep BHE is by extrapolation of the existing concept, i.e. using a U-tube collector in a deeper borehole. There arises, however, some questions regarding the feasibility of such an installation, since it is known that also for BHEs in the range of 200 to 300 m, thermal shunting has been observed between the collector legs (Acuna 2013), which reduces the thermal effectiveness of the BHE. With increasing borehole depth and heat extraction rate the mass flow rate has to be increased in order to maintain a low temperature difference between the collector pipes. The mass flow rates that can be used are, however, limited by the size of the available flow area in the BHE, which in the case of the convectional U-tube collector is rather restricted. As a consequence, the borehole depth that can be utilized is limited by the mass flow rate that can be allowed without causing excessively high pressure losses. Therefore, either larger collector and borehole dimensions are required or alternative collector geometries such as the coaxial collector, which is suitable for deeper boreholes since it can utilize a larger fraction of the borehole as flow area, and therefore, allows for higher mass flow rates.

To evaluate and further improve the performance of a U-tube BHE with a deeper borehole it is important to understand the physical mechanisms acting in the borehole. In Norway and Sweden it is common that the borehole for the BHE is non-grouted and thus filled with water. In this case the performance of the BHE is affected by natural convection triggered by the temperature differences during extraction or injection of heat.

In the present paper, a numerical model suitable for U-tube BHEs based on non-grouted boreholes is developed. The model is used to study the transient behavior of BHEs and to evaluate the performance of U-tube BHEs with depths of 200 to 800 m.

The framework used in this study is based on the finite difference method. The numerical scheme is implemented in the commercial software package Matlab version (2012b). The paper starts with a review of related BHE literature before presenting the new model. In order to develop a correlation describing the influence of natural convection a survey of related literature has been carried out.

Nomenclature

Symbol

A	Aspect ratio $L / (r_0 - r_i)$ [-]
C	Specific heat capacity [J/kg K]
d	Diameter [m]
D_h	Hydraulic diameter [m]
f	Friction factor [-]
h	Heat transfer coefficient [W / m ² K]
GG	Geothermal gradient [K / m]
k	Thermal conductivity [W / m K]
K	Radius ratio r_0 / r_i [-]
\dot{m}	Mass flow rate [kg / s]
n	Index , temporal discretization
j	Index , spatial discretization
\dot{q}	specific heat load [W / m]
\dot{q}''	Heat flux [W / m ²]
r_1	Collector inner radius [m]
r_2	Collector outer radius [m]
r	Radius [m]
R	Thermal resistance [K m / W]
R _b	Local borehole thermal resistance [K m / W]
R_b^*	Effective borehole thermal resistance [K m / W]
S	Source term [W / m]
T	Temperature [K]
T_{inlet}	Inlet temperature [K]
t	Time [s]
u	Internal energy [J / kg]
V	Velocity [m/s]
H	Height of vertical enclosure [m]
L	Characteristic length scale [m]
Z	Vertical coordinate [m]

Greek symbols

α	Thermal diffusivity $\frac{k}{\rho C}$ [m ² /s]
β	Coefficient of thermal expansion [1/K]
Δ	finite increment in a variable
ρ	Density [kg /m ³]
ν	Kinematic viscosity [m ² /s]

Dimensionless numbers

Ra	Rayleigh number $g\beta L^3 \Delta T / \alpha \nu$ [-]
Ra*	Modified Rayleigh number $g\beta L^A \dot{q}'' / \alpha \nu k$ [-]
Pr	Prandtl number ν / α [-]
Gr	Grashof number Ra / Pr [-]
Nu	Nusselt number hL / k [-]

Index

b	borehole
bw	borehole wall
c	collector
f	heat carrier
g	ground
i	inner
local	local value
m	mean value
o	outer
w	water

2. BHE modeling

2.1 Introduction

Several methods, both numerical and analytical have previously been developed to calculate the thermal performance of borehole heat exchangers. The borehole constitutes a quite simple geometry, but is also a challenging thermal problem. Analytical methods are mostly used, and they have a long history of being used for the dimensioning of BHE installations.

Analytical methods are in general based on either the infinite line source or the infinite cylindrical source, as described by Ingersoll (1954) and Carslaw and Jaeger (1959). These methods can be computationally cost effective, but they are not capable of describing all the involved phenomena, and therefore, lack some of the accuracy, flexibility and transparency gained from numerical methods. These analytical solutions are based on average values, reflecting the one-dimensionality of the methods. Important research in the field can be attributed to Eskilsson (1987) and Hellström (1991). Improvements in the analytical methods have been presented by Zeng et al. (2003), and Lamarche and Beauchamp (2007), using the finite line source.

Numerical models of BHE with different levels of complexity have been published and can be used to gain more knowledge regarding the heat transfer in the BHE. Due to the very large aspect ratio of the BHE, fully discretized numerical models tend to become computationally demanding, and therefore, models are often constructed for a limited part of the BHE for more detailed studies.

Numerical models can be made more efficient by applying the analogy to electric networks when describing the thermal resistances within the borehole, thus reflecting a geometrical simplification where the different parts in the borehole are described by single nodes. A numerical grid is then used to describe the bedrock around the borehole in two or three dimensions, while the borehole, the collector and the heat carrier are simulated as one-dimensional features. These simplifications have earlier been referred to as thermal resistance and capacity models (TRCM), Bauer et al. (2011^a). A more detailed review of TRCM models is given in the following section.

2.2. Review of studies related to TRCM

Al-Khoury et al. (2005) addressed the comprehensive computational requirements involved with fully discretized numerical models for BHE and developed a finite element model using line elements to describe the BHE. The model was compared with experimental data and with analytical calculations for a double U-tube configuration in Al-Khoury (2006). De Carli et al. (2010) constructed a computational model based on discretized balance equations; however, simplifications on the heat capacities in the model reduced the accuracy for short time steps. Zarrella et al. (2011) elaborated on the model by De Carli et al. (2010) and improved the short time step accuracy by introducing thermal capacities for the grout in the borehole and the heat carrier fluid. In this approach the grout in the borehole was divided into two regions, an inner core and an outer shell with respective thermal capacities. The model was compared to a two-dimensional numerical model using Comsol Multiphysics (2008) and with measurements from a thermal response test (TRT).

Bauer et al. (2011^a) developed new thermal resistance and capacity models (TRCM) for coaxial, single and double U-tube BHEs, based on the models by Al-Khoury (2006). The internal grouted area of the borehole was divided into sections corresponding to each pipe in the borehole, increasing the level of detail as compared to previous models. The model was implemented in an axisymmetric finite difference scheme and compared with a fully discretized finite element model using ANSYS (2005). In Bauer et al. (2011^b) the TRCM model was implemented in a three-dimensional grid. The model was again verified with a fully discretized model (ANSYS) and also compared to measured data from a TRT. It was noted that the evaluation time for a TRT could be reduced if accurate transient numerical models were used instead of the analytical line source models, since the numerical models are more accurate for shorter time intervals.

Diersch et al. (2011^a and 2011^b) evaluated and compared the numerical finite element method by Al-Khoury et al. (2005) and Al-Khoury (2006) to the analytical solution of Eskilson and Claesson (1988). These methods were also compared using a fully discretized two-dimensional axisymmetric finite difference model of a coaxial BHE. It was found that the numerical model by Al-Khoury was a better match to the fully discretized model than the analytical model. The numerical model was implemented in FEFLOW (2010) and coupled with the transient system simulation code TRNSYS (2004).

Mottaghy and Dijkshoorn (2012) coupled transport equations for the heat and mass transport in a coaxial BHE and solved the equations using a finite difference code. Numerical simulations were

compared to measured data from the 2302 m deep coaxial borehole heat exchanger in Weggis, Switzerland. The coaxial heat exchanger as well as the double U-tube collector was treated, using the thermal resistances as derived by Hellström (1991). The coaxial BHE in Weggis has also been analyzed earlier by Kohl et al. (2002) using a fully numerical axisymmetric model based on the finite element method.

Pasquier and Marcotte (2012) added further refinement to the model by Bauer et al. (2011^a) by adding additional nodes (heat capacities and thermal resistances), and a strategy to determine the individual resistances. The U-tube collector was treated, and the model was compared to a two-dimensional finite element models in Comsol Multiphysics (2008).

The approaches presented in most of the cited literature are rather similar, i.e. the BHE geometry is represented by a number of nodes with associated thermal capacities and resistances constituting a local problem which is then coupled to a grid representing the surrounding rock domain. It is important to point out that in all of the presented models for U-tube BHEs, the boreholes have been assumed to be grouted, and the transport of heat between the collectors is treated as thermal conduction. Thus, the discretization of the grouted domain into sections having a specific position and an associated thermal capacity increased the transient accuracy of the models. There exists, however, no models that are applicable to non-grouted BHEs where natural convection has a major influence on the thermal performance.

In the present work, a numerical model has been developed exclusively for non-grouted, water filled boreholes. This poses a different problem than grouted boreholes, as the heat transfer between the collector and the wall of the borehole is dependent on the possible presence of buoyancy-driven flow (natural convection), discussed in further detail in the next section. The model uses the TRCM concept and it is based on the finite difference method. The model considers conventional U-tube collectors, but is, equally applicable to other collector types.

3. Natural convection

During operation of the non-grouted BHE, the existence of a temperature difference in the borehole triggers natural convection which reduces the internal thermal resistance of the BHE. The influence of natural convection during TRT has previously been noted by several authors including Gehlin (2002) and Kjellsson (2009) and was also studied by Gustafsson et al. (2010) for a borehole having diameter 0.1036 m equipped with a PEM40 collector. Gustafsson et al. (2010) came to the conclusion that for the specific BHE –configuration studied, natural convection resulted in a reduction of the thermal resistance in the water by a factor of around 3-4, which is very significant.

Thus, for a TRCM model for water filled BHEs, heat transfer by natural convection must be considered rather than pure conductive heat transfer. Consequentially, the borehole resistance (R_b) will not be a constant for a certain flow rate, but a function of the local temperature differences and the local temperature of the borehole water.

From the perspective of natural convection, the BHE constitutes an enclosure with a high aspect ratio, where the aspect ratio is defined as the length of the borehole divided by the internal characteristic length scale. In order to establish a correlation for the specific case of a BHE to be used in the present

paper, some of the literature related to natural convection in enclosures with high aspect ratio is reviewed and described below.

Natural convection in enclosures having high aspect ratios is usually characterized by a Rayleigh number (Ra) based on the width of the enclosure. For small values of Ra , the heat transfer is dominated by a conduction regime, while for larger values secondary multicellular laminar flow is induced, which increase the heat transfer. With further increase in Ra , the secondary flow structures become unstable and transits into turbulence. The establishment of secondary flows in a tall vertical annulus has been studied by Choi and Korpela (1980) for different radius ratios (K) and Prandtl numbers (Pr). Lee and Korpela (1983) determined numerically the Nusselt number for an infinitely tall two-dimensional cavity having secondary flows using the average values for the centre part of a tall cavity. The results were compared to cavities having aspect ratios (A) between 5 and 40 and points to a limiting case for the influence of aspect ratio when the Rayleigh number is sufficiently high.

The transition from the conduction regime to the secondary flow regime is characterized by a critical Rayleigh number (Ra_c). Wright et al. (2006) visualized natural convection in an air-filled vertical cavity, and for a cavity having $A \approx 40$, the secondary flow became unstable at approximately $Ra/Ra_c = 1.4$, and the transition to full turbulence started at $2 \leq Ra/Ra_c \leq 8$.

An implicit consequence of the onset of turbulent flow is the lack of applicability of existing numerical models; these have in general been developed for laminar flow and might be valid through the conduction regime and the laminar part of the secondary flow regime. In the turbulent regime, however, the problem becomes significantly more complex. Several authors have reported lower heat transfer rates from numerical studies than obtained from experimental results, see Wright et al. (2006).

Keyhani et al. (1983) presented a correlation for the dependence of the average Nu of the Rayleigh number for a vertical annulus having $A = 27.6$ and $K = 4.33$, for $10^3 \leq Ra \leq 2.3 \times 10^6$, based on experiments with air and helium. Through the results from a numerical study by Vahl Davis and Thomas (1969) the correlation (Equation 1) was extended to the range $1 \leq K \leq 10$, $1 \leq A \leq 33$

$$Nu = 0.188Ra^{0.322} A^{-0.238} K^{0.442} \quad 1$$

An alternative formulation of Equation 1 based on the modified Rayleigh number, $Ra^* = RaNu$ is shown in Equation 2.

$$Nu = 0.291Ra^{*0.244} A^{-0.238} K^{0.442} \quad 2$$

Keyhani et al. (1985) extended the work from Keyhani et al. (1983) to vertical tube bundles in an enclosure through experiments with 3×3 , and 5×5 vertical rod bundles. Air, helium and water were used in the experiments. Lafortune and Menely (1990) performed experiments with 7 vertical heating rods in a water filled vertical circular enclosure, and found the results to agree well with the results from Keyhani et al. (1985). The general Nu -correlations from Keyhani et al. (1985) were, however, presented explicitly for air and helium and overpredict the heat transfer rate for water.

Littlefield and Desai (1986) performed a numerical study on a vertical annulus containing a fluid having $Pr=10$, and derived correlations that were essentially similar to the results from Keyhani (1983) for the range $1.5 \leq K \leq 5$ and $10 \leq A \leq 50$, see Equation 3. Gustafsson (2010) performed numerical

simulations on an annulus with water and found the results to be consistent with the correlation of Littlefield and Desai (1986).

$$Nu = 0.443Ra^{*(0.233-0.009K)}A^{-0.245}K^{0.442} \quad 3$$

The definition of the Nusselt and Rayleigh numbers requires a characteristic length scale (L). For a vertical annular pipe with high aspect ratio, the width of the radial gap between the cylinders is usually used as the length scale; this dimension is equivalent to half the hydraulic diameter and has been used as the characteristic length scale in a BHE as follows

$$L = D_h/2 \quad 4$$

$$D_h = 2(r_0 - r_i) \quad 5$$

$$K = r_0/(r_0 - D_h/2) \quad 6$$

The position of the collectors in the borehole is arbitrary; however, Sparrow and Charmchi (1983) studied the influence of eccentric and concentric positions of the inner pipe in an annulus, and found that the position had little influence on the average Nusselt number. They used a radius ratio of $K=5$; it is likely that the position will have a larger influence for smaller radius ratios.

According to Choi and Korpela (1980) the critical Rayleigh number is $Ra_c = 28590$ for a fluid with $Pr = 15$, in a tall annulus with $K=2.5$. Ra_c increases with increasing Pr , so this can be considered as a restrictive higher limit for boreholes since Pr for water varies between 13.4 and 9.4 in the range $0 - 10^\circ C$. For a borehole with a diameter of 14 cm equipped with a single PEM40 collector, the hydraulic diameter approach would yield a radius ratio of 2.14. With the presence of natural convection, the temperature difference between the surface of the collector and the wall of the borehole would vary somewhere between 1- 6 K at a heat transfer rate of 30 W/ m. With this heat transfer rate, it is only in the immediate vicinity of the density maximum of water where Ra is less than Ra_c . This means that for most conditions, secondary flows will be present in the borehole. Since the Rayleigh number increases rapidly when moving away from the density maximum, the flow is likely to be turbulent.

The aspect ratio and radius ratio dependencies from Vahl Davis and Thomas (1969) were used by both Keyhani et al. (1983) and Keyhani et al. (1985). The aspect ratio dependency ($A^{-0.238}$) was derived for $A \leq 33$ and is not suitable for tall enclosures having high Ra , as evident in comparison with the results from Lee and Korpela (1983). Littlefield and Desai (1986) reported a similar dependency ($A^{-0.245}$) for $10 \leq A \leq 50$. Lee and Korpela (1983) presented an approximate expression for the average Nusselt number (Nu) as a function of aspect ratio for a vertical slot, Equation 7.

$$Nu = \frac{10}{A}Nu_{10} + \left(1 - \frac{10}{A}\right)Nu_c \quad 7$$

Nu_{10} and Nu_c are the average Nusselt numbers for a cavity having $A=10$, and the average Nusselt number for the center part of a tall cavity. Comparing the aspect ratio dependency in Equation 3 with Equation 7 reveals that the asymptotic value Nu_c is reached already at $A \approx 45$. With $K = 1$, and $A = 45$, Equation 3 can be compared with the correlation from Wright (1996) for a two-dimensional enclosure with large aspect ratio, and the average deviation between the two correlations is less than 2 % over the range ($10^4 \leq Ra \leq 10^6$). Based on the above it is reasonable to neglect the aspect ratio dependency in Equation 1, 2 and 3 by setting $A = 45$ as a maximum value given that $Ra > Ra_c$.

This then reduces Equation 3 to:

$$Nu = 0.1743Ra^{*(0.233-0.009K)}K^{0.442}$$

8

In a non-grouted BHE, the Nusselt number can be used to relate the reduced thermal resistance between the collector and the wall of the borehole to the larger conductive resistance ($R_{b_{cond}}$), which can be determined based on the multipole method from Bennet et al. (1987) as presented in Lamarche (2010). In Figure 1 Equation 8 is compared to experimental data from (Kjellsson and Hellström, 1999), as published in Gustafsson (2010), where R_b has been determined from Equation 9.

$$R_b = \frac{R_{b_{cond}}}{Nu} + R_{b_{collector}}$$

9

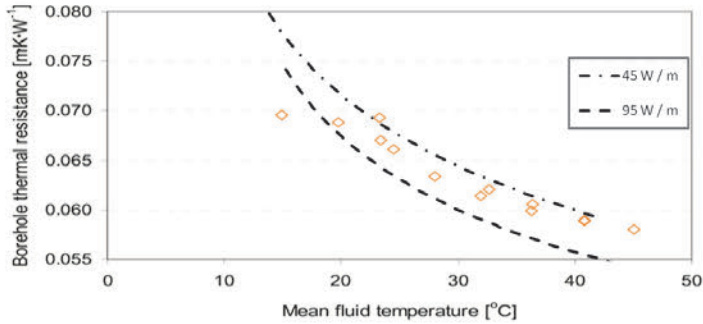


Figure 1. Borehole thermal resistance as determined from Equation 9 as a function of mean fluid temperature in the borehole. Experimental data from (Kjellsson and Hellström, 1999) as published in Gustafsson (2010).

In Figure 1 the dotted lines correspond to the borehole resistance calculated by Equation 9 while the experimental data is represented by the markers. The mean fluid temperature in the graph is the arithmetic average of the inlet and outlet temperatures of the collector. The actual water temperature in the borehole should consequently be a few Kelvin lower (Gustafsson 2010), and this has been accounted for in the use of Equation 8. The heat transfer rates in the experiments were in the range between 45 and 95 W/m, hence, two calculated curves are shown in the figure. As observed, the results from Equation 9 show a similar trend and are in reasonable agreement with the experimental data. The water properties were evaluated using NIST (2013). $R_{b_{cond}}$ was determined to be about 0.2 K m/ W and the internal thermal resistance in the collector was calculated assuming a heat carrier mass flow rate of 1 kg / s and a thermal conductivity of 0.42 W/ m K for the collector material. For turbulent flow conditions it is mainly the resistance of the collector walls that matters.

While the thermal resistance is usually determined from thermal response tests (TRT) where the thermal response from an injection test is analyzed, Gustafsson (2011) has experimentally shown that during heat extraction the borehole resistance differs from the values determined from heat injection tests. The highest resistance was found when the water temperature in the borehole was around 4 °C. This corresponds to the temperature where water has its maximum density, and therefore, induced natural convection reverses when the water temperature passes this point.

The heat transfer can also be improved by forced circulation of the borehole fluid. This can be achieved by a submersible pump as described by Liebel et al. (2012). Based on the results from Gustafsson (2011) and the discussion above it would be expected that inducing forced convection is most profitable during heat extraction, during small heat loads or when the average water temperature is around 4 °C. Likewise, other methods to improve the heat transfer would have highest impact at

these conditions; for example, Kumar (1997) reported on significant improvements in heat transfer by placing longitudinal fins on the outside of the inner pipe of an annulus.

In the following section, Equation 8 is used to account for the influence of natural convection

4. Heat transfer in the BHE and in the ground surrounding the borehole

4.1 Introduction

The model of the U-tube BHE is setup as a Y-circuit, where two nodes represent the heat carrier streams and one node represent the water in the borehole, see Figure 2. In comparison with other TRCM – models used for grouted BHEs; this is a simpler representation of the BHE geometry which is motivated by the presence of natural convection. The Y-circuit implies that there is no direct contact between the collector pipes, or between the collector and the wall of the borehole. The model does not contain any explicit information on the position of the collectors in the borehole, in each segment of the discretized borehole the heat transfer is expressed as a resistance between the mixing cup temperatures of the heat carrier and water in the borehole. The thermal capacity of the collector walls is neglected. This may affect the transient behavior of the model; however, for a typical installation the thermal capacity of the collector walls is on the order of 1-2 % of the heat capacity of the water and heat carrier in the borehole; hence this assumption will not introduce any significant error.

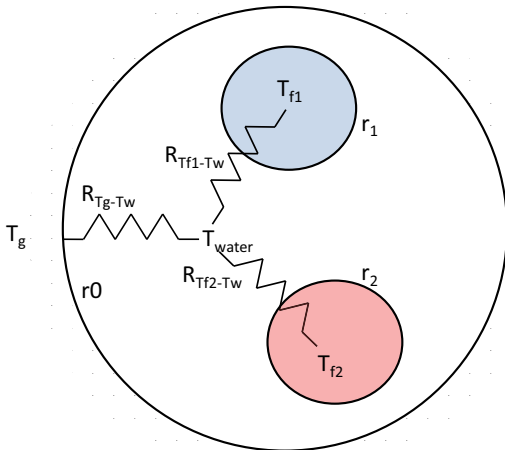


Figure 2. Y circuit employed in the numerical scheme.

Based on the Y-circuit in Figure 2. the local borehole resistance R_b can be expressed as:

$$R_b = R_{T_g-T_w} + \frac{1}{\frac{1}{R_{T_{f1}-T_w}} + \frac{1}{R_{T_{f2}-T_w}}}, \quad 10$$

where

$$R_{T_{f1}-T_w} = \frac{1}{2\pi r_{11} h_{c11}} + \frac{\ln(r_{12}/r_{11})}{2\pi k_c} + \frac{1}{2\pi r_{12} h_{c21}}, \quad 11$$

$$R_{T_{f2}-T_w} = \frac{1}{2\pi r_{21} h_{c12}} + \frac{\ln(r_{22}/r_{21})}{2\pi k_c} + \frac{1}{2\pi r_{22} h_{c22}}, \quad 12$$

$$\text{and } R_{T_g-T_w} = \frac{1}{2\pi r_0 h_0} \quad 13$$

The influence of natural convection is represented by the heat transfer coefficients, (h_0 , h_{c21} and h_{c22}) which are determined from the derived Nusselt correlation (Equation 8) together with $R_{b_{\text{cond}}}$ as determined from the multipole method. The first two parts of $R_{T_{f1}-T_w}$ and $R_{T_{f2}-T_w}$ represent the internal thermal resistance of the collector, hereafter called $R_{b_{\text{collector}}}$.

In the following, the set of equations describing the heat and mass transfer in the BHE are discretized and coupled with the heat transfer in the surrounding ground. This forms the numerical model which has been implemented and solved in Matlab (version 2012b).

The BHE creates a heat source or sink in the ground which gives the potential for heat transport by thermal conduction through the ground. This is the main heat transfer mechanism in the ground although heat can also be transported through advection.

Within the collector there is a heat carrier fluid, usually brine or an alcohol / water mixture. The heat transfer between the fluid and the collector wall depends primarily on the flow conditions. If the flow is laminar, the heat transfer coefficient is less than for turbulent conditions; therefore, it is desirable that the flow is slightly turbulent. In any flow condition the heat transfer coefficient can be readily determined by analytical or empirical equations.

For the turbulent case, the convective heat transfer coefficient is calculated from the second Petukhov equation as modified by Gnielinski (1976), shown in Equation 14.

$$Nu = \frac{(f/8)(Re-1000) Pr}{1+12.7(f/8)^{0.5}(Pr^{2/3}-1)}, \quad 14$$

where f is the friction factor determined from Equation 15.

$$f = (0.790 \ln(Re) - 1.64)^{-2} \quad 15$$

Assuming that the heat carrier is an incompressible fluid, the momentum equation can be neglected and the heat transfer in the BHE can be accurately represented using only the energy equation.

For fluid flow in a pipe the one-dimensional energy equation can be expressed as:

$$\pi r^2 \rho \frac{\partial u}{\partial t} + \pi r^2 \rho V \frac{\partial u}{\partial z} = S, \quad 16$$

where u is the fluid internal energy, r is the inner radius of the pipe, V is the bulk velocity and S is a source term for the convective heat transfer.

The equation can be rewritten as:

$$\pi r^2 \rho C \frac{\partial T}{\partial t} + \pi r^2 \rho V C \frac{\partial T}{\partial z} = S = \frac{\Delta T}{R} \quad 17$$

It is thus assumed that the change in internal energy only depends on the change in temperature of the fluid. C is the specific heat capacity of the fluid and ΔT represents the temperature difference between the mixing –cup fluid temperature in the pipe and the source (i.e. the borehole water or the borehole wall), R is the thermal resistance as calculated by Equation 11 to 13.

The ground surrounding the borehole is in the present work discretized with an axisymmetric cylindrical grid. In order to couple the thermal conduction in the rock with the thermal processes in the borehole, a flux boundary on the wall of the borehole is introduced. In the conduction equation this is achieved through central finite difference and the use of a ghost node (T_0) as shown in Figure 3. This method gives a 2nd order accurate implementation of the heat flux boundary condition.

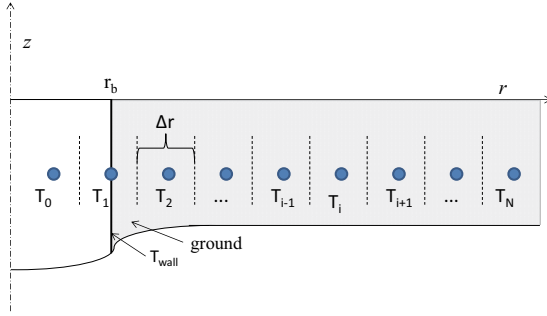


Figure 3. Illustration for coupling of conductive and convective model. T_0 is a ghost node, used in the implementation of the boundary condition.

Hence:

$$q'' = -k \frac{dT}{dx} \approx -k \frac{T_2 - T_0}{\frac{1}{2}\Delta r_0 + \Delta r_1 + \frac{1}{2}\Delta r_2}, \quad 18$$

$$T_0 = T_2 - \frac{q''}{k} \left(\frac{1}{2}\Delta r_0 + \Delta r_1 + \frac{1}{2}\Delta r_2 \right), \quad 19$$

T_0 is then used in the discretization of the first element of the conductive domain. The heat flux can also be expressed as:

$$q'' = \frac{T_1 - T_{water}}{2\pi r_0 R_{\Gamma_g - \Gamma_w}}, \quad 20$$

Where the T_1 is the borehole wall temperature and T_{water} is the bulk temperature of the water in the borehole.

The complete equation system representing the heat transfer in the BHE is summarized as:

Convection in the borehole water:

$$\pi r_0^2 \rho_w C_w \frac{\partial T_w}{\partial t} + \pi r_0^2 \rho_w V_w C_w \frac{\partial T_w}{\partial z} = \frac{\Delta T_{T_g - T_w}}{R_{T_g - T_w}} + \frac{\Delta T_{T_{f1} - T_w}}{R_{T_{f1} - T_w}} + \frac{\Delta T_{T_{f2} - T_w}}{R_{T_{f2} - T_w}} \quad 21$$

Convection in collector pipe 1 and 2:

$$\pi r_1^2 \rho_f C_f \frac{\partial T_{f1}}{\partial t} + \pi r_1^2 \rho_f V_{f1} C_f \frac{\partial T_{f1}}{\partial z} = \frac{\Delta T_{T_{f1} - T_w}}{R_{T_{f1} - T_w}} \quad 22$$

$$\pi r_2^2 \rho_f C_f \frac{\partial T_{f2}}{\partial t} + \pi r_2^2 \rho_f V_{f2} C_f \frac{\partial T_{f2}}{\partial z} = \frac{\Delta T_{T_{f2} - T_w}}{R_{T_{f2} - T_w}} \quad 23$$

Equations 21 to 23 are discretized together with the conductive domain using an implicit finite difference scheme, this is then solved through matrix division in Matlab. The parameters used for the spatial and temporal discretization are summarized in Table 1.

Table 1. Discretization parameters

Parameters	min	max
Δr [m]	0.002	1
Δz [m]	1	4
Δt [s]	10	200

In the interpretation of the numerical results in the following section, R_b^* is determined from Equation 24 using mean values of temperatures and specific heat load, while R_b is determined from Equation 25 using local values.

$$R_b^* = \frac{T_{f m} - T_{b w m}}{q'_m} \quad 24$$

$T_{f m}$ is the heat carrier mean fluid temperature, defined as the arithmetic average of the inlet and outlet fluid temperatures of the collector.

$$R_b = \frac{T_{f local} - T_{b w local}}{q'_{local}} \quad 25$$

5. Results and discussion

An advantage with the presented model is that it is accurate on a timescale of minutes (as shown in the accompanying paper) while being fast enough to allow parameter studies of the transient behavior of the BHE. In the following, the model is used to study the transient behavior of the BHEs and the performance as a function of borehole depth.

To illustrate the capability of the developed model, simulations in three main areas are carried out as follows:

- Transient heat transfer in a 200 m deep BHE during upstart, heat injection and extraction.

- The influence of the length of the operation intervals on the performance of BHEs with depths 200 m and 800 m
- The influence of the borehole depth (in the range 200 m to 800 m) on the thermal performance of the BHE

The results are presented in the following subsections.

In Figure 4 the transient temperature profiles are shown for a 200 m deep BHE with a PEM40 x 2.4 mm collector. With a coolant mass flow rate (\dot{m}) of 0.5 kg /s the time constant of the BHE is about 13 minutes (the time it takes for the fluid to circulate through the U-tube collector). Profiles are shown for heat injection (Figure 4.a) and heat extraction (Figure 4.b). The initial profile represents the undisturbed temperature in the borehole and is based on a geothermal gradient (GG) of 0.02 K /m.

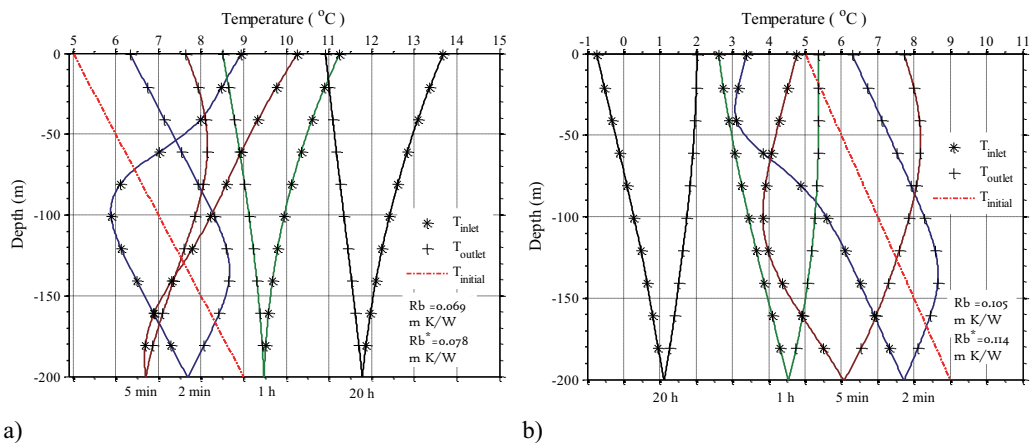


Figure 4. Transient evolution of the temperature profile in a 200 m deep borehole with a diameter of 140 mm. a) heat injection, 6 kW. b) heat extraction, 6 kW. Collector: PEM40 x 2.4, \dot{m} =0.5 kg /s, coolant: 20 volume-% ethyl alcohol,

It is seen that after 1 hour, the initial transients have diminished and the shape of the temperature profile is rather constant in both cases. The vertical average of R_b and R_b^* are evaluated after 20 hours and are shown for both cases in the figure. As shown, the resistances are higher during heat extraction than during heat injection.

Since GSHP systems are usually operated in an on- off manner, it is of interest to study the influence of the initial transients on the performance of the BHE. In the following, the results from a parametric study are presented. Heat extraction has been simulated using varying length of the operation period; each extraction period (with a constant heat extraction rate) is followed by a thermal recovery period of the same length during which the mass flow in the collector is zero. The simulations are over a sufficiently long time scale that the difference in total amount of extracted energy is less than 1 % between the simulations.

In Figure 5.a the BHE inlet temperature (T_{inlet}) is shown for a 200 m deep BHE which is simulated with three different periods of 0.2 h, 0.5 h respective 5 h, and the mass flow rate is shown for the 0.5 h period.

The simulations are compared based on the value of T_{inlet} during the last heat extraction period in each simulation; the temperature is evaluated both as a time average and in the end of the period. The results are shown in Figure 5.b as a function of the operation period length; the values are relative to the respective values at a period length of 10 h.

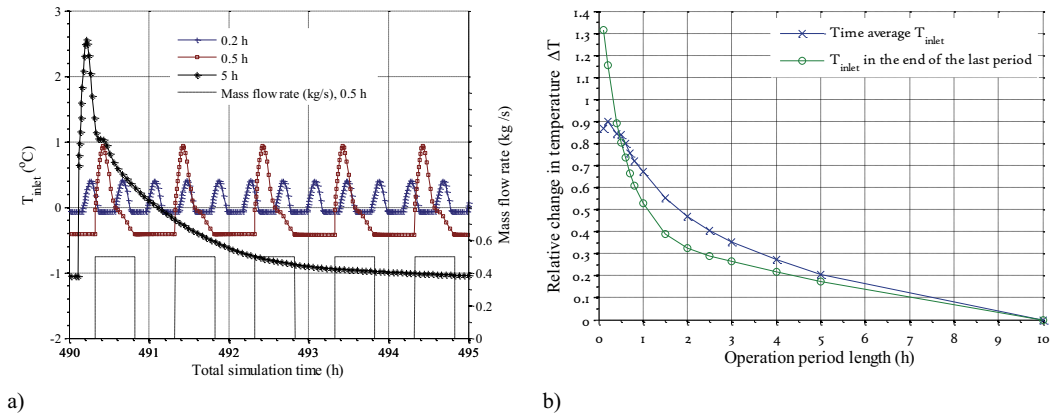


Figure 5. a) T_{inlet} determined for operation intervals: 0. 2 h, 0. 5 h and 5 h. b) influence on the average T_{inlet} and T_{inlet} in the end of the simulated period, simulation time 500 h. GG = 0.02 K /m, BHE depth 200 m, $d_b=140$ mm, collector: PEM40 x 2.4 mm, $\dot{m}=0.5$ kg / s. Q= 6 kW, Coolant: 20 volume-% ethyl alcohol.

In the case of the 200 m BHE, T_{inlet} in the end of the last heat extraction period corresponds to the minimum value. It is observed that T_{inlet} is largest for short operation cycles and that the difference between the shortest cycle and the largest is rather small, on the order of 0.9 K for the time average and 1.3 K for the minimum value. The differences can be explained by the transient dynamics of the borehole; whereas energy is only extracted from the borehole in the extraction periods, the conductive transfer of heat to the water in the borehole continues also in the heat recovery periods. For short operation periods, the heat transfer to the borehole in the recovery period can be as large as during the heat extraction period, while for longer periods, most of the heat transfer is during the heat extraction period; therefore, a higher specific heat load is required which reduces the temperature. The average of the specific heat load over the length of the borehole is shown in Figure 6.

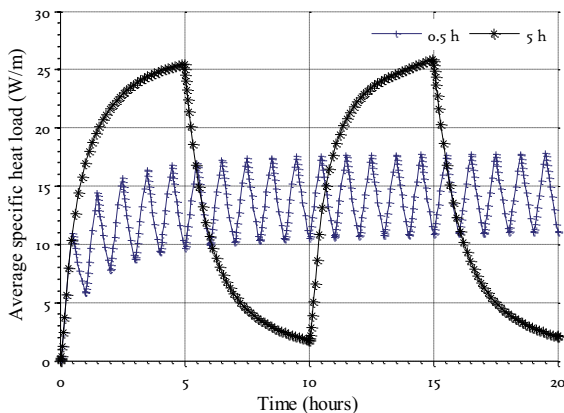


Figure 6. Vertical average of the specific heat load through the borehole wall during heat extraction and recovery periods, GG = 0.02 K /m, BHE depth 200 m, $d_b=140$ mm, collector: PEM40 x 2.4 mm, $\dot{m}=0.5$ kg / s, coolant: 20 volume-% ethyl alcohol

The results show that in theory there is a potential to increase the heat transfer rate using shorter operation intervals, e.g. a comparison between 0.5 h interval and 10 h interval reveals that the extraction rate can be about 16 % larger for the shorter interval while keeping the time-average of T_{inlet} at the level of the longer period.

The simulation presented in Figure 5 was repeated for an 800 m borehole, and the values of T_{inlet} are shown in Figure 7 as a function of the operation period length. The values are relative to the respective values at a period length of 10 h.

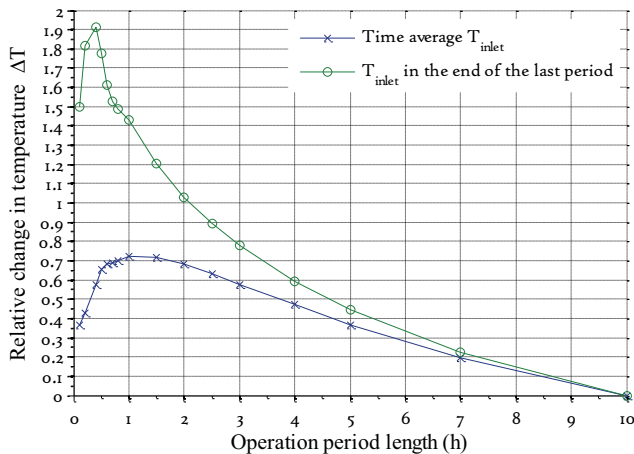


Figure 7. Influence on the average BHE inlet temperature of the operation period, simulation time 500 h. $GG = 0.02 \text{ K/m}$, BHE depth 800 m, $d_b=140 \text{ mm}$, collector: PEM50 x 2.4 mm, $\dot{m}=1.15 \text{ kg/s}$, $Q=32 \text{ kW}$, coolant: 20 volume-% ethyl alcohol.

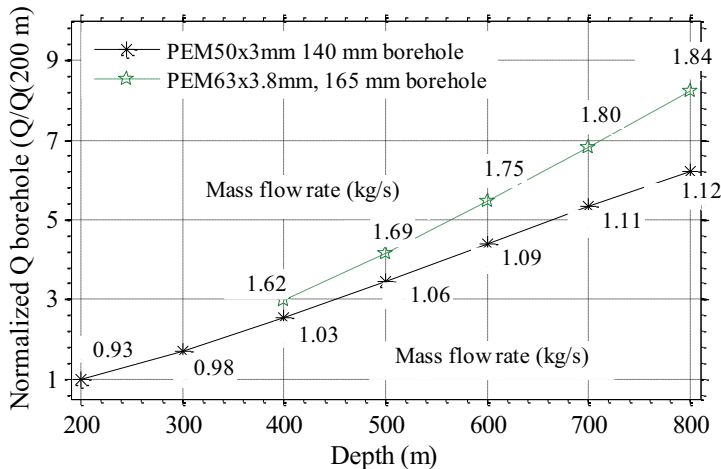
In this case, the minimum value of T_{inlet} is found at the start of each heat extraction period, as the colder fluid in the upper part of the borehole is being pumped up. It is seen that the highest temperature level is obtained for a slightly longer operation length (around 2 times the time constant of the BHE), while the initial transients during the startup of the circulation reduces the temperature for shorter periods.

To study the influence of borehole depth on the overall performance of the BHEs, it is assumed that the BHE supplies heat to a heat pump and that the total COP of the heat pump, including the circulation pump for the collector fluid, is constant. The performance is then measured by the amount of energy being provided by the BHE as a function of borehole depth. By assuming a constant total COP, it is implicit that the temperature lift by the heat pump, and the return temperature from the heat pump both are constant and invariant with borehole depth. Further, it is assumed that the ratio between the power used by the circulation pump (W_p) and the heat pump compressor (W_c) is constant. The parameters used in the simulation are presented in Table 2.

Table 2. Simulation parameters

Parameters	
d_b [mm]	140 / 165
Collector	PEM50 x 3 mm / PEM62 x 3.8 mm
η_{Pump} [%]	0.7
W_p / W_c [%]	5
COP [-]	4
T_{in} [°C]	1
Intervall [h]	5
GG [K / m]	0.02
k_g [W / m K]	3
k_c [W / m K]	0.42
coolant	20 volume-% ethyl alcohol
Simulation time (h)	500

The BHE is operated with a constant on/ off intervall of 5 hours as previously described. For each borehole depth the time-averaged extracted heat load (Q) is determined for the period at the end of the simulation. The mass flow rate is adjusted accordingly to the heat load and the requirement of a constant total COP. Results normalized to 200 m are presented for two collector and borehole dimensions in Figure 8.



The 800 m BHE is further studied using the larger borehole and collector and the corresponding mass flow rate from Figure 8. A constant heat extraction rate of 40 kW is applied for 20 hours. The temperature profiles and the distribution of specific heat load and local borehole resistance are shown in Figure 9.

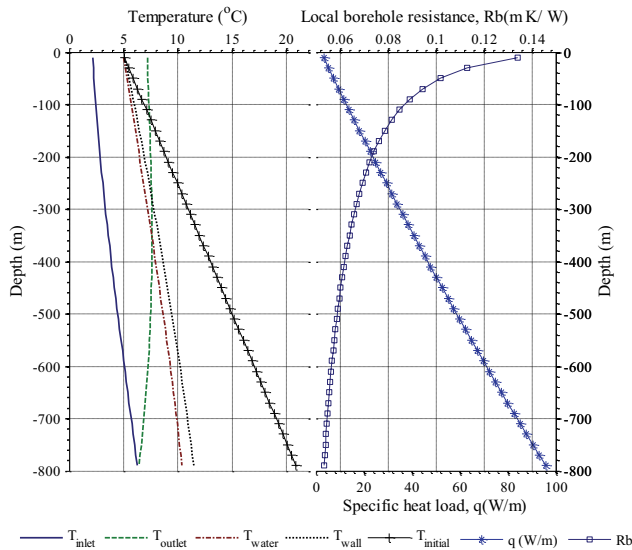


Figure 9. Temperature profiles and vertical distribution of specific heat load in the 800m borehole after 20 hours of continuous heat extraction ($Q=40$ kW). $GG = 0.02$ K/m, $d_b=165$ mm, collector: PEM63x 3.8, $\dot{m}=1.15$ kg/s, coolant: 20 volume-% ethyl alcohol.

For the case presented in Figure 9 the internal resistance of the collector is 0.026 m K /W. The effect of natural convection is, therefore, apparent in Figure 9 where the average of the local resistance varies between 0.054 m K /W for the deepest 100 m to ca 0.1 m K /W in the upper 100 m. If natural convection were neglected the local resistance would be about 0.185 m K /W. It is also noticeable that with natural convection, almost half of the total borehole resistance is in the material of the U-tube collector (since the convective resistance inside the collector is small). The reduction in resistance with depth is caused both by the increase in temperature and the increase in specific heat load. The vertical average of R_b is 0.068 m K /W and $R_b^* = 0.079$ m K /W.

The influence of natural convection is further illustrated using the radial temperature profile from the case above. In Figure 10, the temperature profile in the ground is shown together with the temperature of the borehole water and the mean fluid temperature. The profile is taken from the middle of the borehole, i.e. at 400 m depth. Also the corresponding profile for a case where natural convection is neglected is shown.

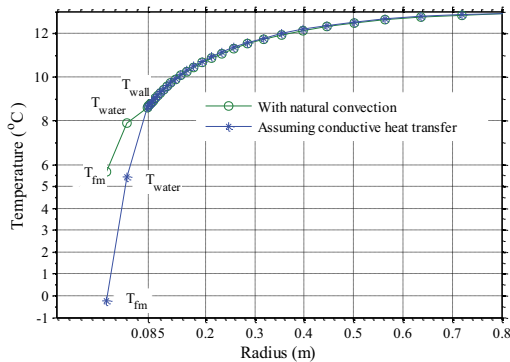


Figure 10. Radial temperature profiles with and without natural convection. Simulation parameters corresponding to the case shown in Figure 9.

The difference between the two cases clearly shows the large influence of natural convection. The mean fluid temperature is about 6 K lower for the conductive case where also most of the temperature change is in the borehole.

The results indicate that the U-tube borehole heat exchanger can be used successfully on a deeper borehole (800 m), provided that a large size collector is used. While the potential for heat extraction increases with borehole depth, the potential for cooling decreases (as well as the possibilities for thermal recharge). It is also shown that the specific heat load is higher in the lower part of the borehole. This might be a concern when placing several deep boreholes that can have thermal interaction, as the larger heat load implies larger thermal interference. Therefore, the boreholes require a larger undisturbed volume in the lower part, while less interference will be expected in the upper part. Several boreholes can, therefore, be placed closely together on the surface and then deviate outwards with increasing depth in order to create a sufficiently large space in between the lower parts of the boreholes.

6. Summary and conclusions

A numerical BHE model for non-grouted borehole has been presented based on the TRCM concept. The aim with the model is to simulate the transient performance of non-grouted BHEs based on boreholes with larger depths than the standard 200- 300 m.

To account for the thermal effects of natural convection in the water filled boreholes, a correlation for the influence of natural convection as a function of physical properties and the induced temperature difference has been developed. The correlation is validated by comparison to published experimental results. The validity of the numerical model, including the correlation for natural convection has been verified through comparison with an extensive set of field data presented in an accompanying paper (Holmberg et al. 2016).

To the knowledge of the authors, this is the first work which combines the TRCM approach with the effects of natural convection in non-grouted (water filled) boreholes.

The presented model is a strong tool for simulation of BHEs as it can simulate the performance rapidly and with high accuracy. As the entire length of the borehole is resolved, depth dependent effects such as thermal short circuiting are captured. The model is well suitable for simulation of early transients during the initial operation period of the BHE, e.g. during heat pump operation and it can also be used through parameter estimation to analyze operation data from BHE installations, and for optimization of BHE parameters.

In the present paper, the model is used to study the performance of non-grouted U-tube BHEs with depths in the range 200 m – 800 m. It is found that the thermal performance of non-grouted BHEs is largely affected by natural convection, e.g. the average local resistance in the simulated 200 m BHE is 52 % larger during heat extraction than during heat injection.

The results also indicate that the specific heat load can be increased with increased borehole depth. By using a larger collector and borehole diameter, it is possible to use a larger mass flow rate, and therefore, increase the effectiveness of the BHE. Using the assumption of a constant inlet temperature, and a constant total COP, it is seen that the heat extraction rate for a 800 m deep BHE can be on the order of eight times the extraction rate for a 200 m deep BHE. It is also seen that the specific heat load becomes unevenly distributed with most energy being extracted from the deeper parts of the borehole where also the internal resistance in the borehole becomes lowest due to the effect of natural convection.

Also the transient dynamics during heat pump operation are studied. It is found that the length of the operation interval has a rather small influence on the temperature level in the BHE. In the range studied (0.1 h – 10 h), it is seen that a slightly higher temperature can be found when using shorter operation intervals. This indicates that it is possible to have a higher heat extraction rate for shorter operation intervals than for longer intervals. For deep boreholes, this effect is more difficult to realize due to the larger time constant of the BHE.

References

- Acuña J, (2010). Improvements of U-pipe Borehole Heat Exchanger. Licentiate Thesis in Energy Technology. Stockholm: KTH.
- Al-Khoury, R., P.G. Bonnier., R.b.J. Brinkgreve, (2005) Efficient finite element formulation for geothermal heating systems. Part 1: Steady state, *International Journal of Numerical Methods in Engineering*, v 63, pp.988-1013
- Al-Khoury, R, (2006) Efficient finite element formulation for geothermal heating systems. Part 2: Transient, *International Journal of Numerical Methods in Engineering*, v 67, pp. 725-745
- ANSYS (2005) Multiphysics, Release 10.0, Dokumentation, ANSYS, inc, Canonsburg, PA.
- Bauer, D., Heidemann, W., H. Müller-Steinhagen., H.-J.G. Diersch (2011a) Thermal resistance and capacity models for borehole heat exchangers. *Int. J. Energy Res*, v 35, pp. 312-320
- Bauer, D., Heidemann, W., H.-J.G. Diersch (2011b) Transient 3D analysis of borehole heat exchanger modeling. *Geothermics*, v 40, pp. 250-260
- Carslaw, H.S., J.C. Jaeger (1959): *Conduction of heat in solids*, second ed, Oxford University press, Oxford.
- Choi I.G., S. A. Korpela, (1980) Stability of the conduction regime of natural convection in a tall vertical annulus, *Journal of fluid mechanics*, v 99, pp. 725-738
- Comsol Multiphysics (2008), Comsol multiphysics version 3.5, Stockholm: Sweden: 2008
- De Carli, M., M. Tonon., A. Zarrella., R. Zecchin, (2010) A computational capacity resistance model (CaRM) for vertical ground-coupled heat exchangers. *Renewable Energy*, v 35, pp. 1537-1550

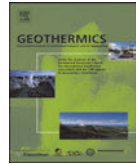
- De Vahl Davis, G., R.W. Thomas (1969) Natural convection between concentric vertical cylinder, High speed computing in fluid dynamics, physics of fluids, Supplement 2, pp. 198-207.
- Diersch, H.-J.G., D. Bauer., W. Heidemann., W. Rühaak., P Schätzl, (2011a) Finite element modeling of borehole heat exchanger systems Part 1. Fundamentals. Computers & Geosciences, v 37, pp. 1122-1135
- Diersch, H.-J.G., D. Bauer., W. Heidemann., W. Rühaak., P Schätzl, (2011b) Finite element modeling of borehole heat exchanger systems Part 1. Numerical simulation. Computers & Geosciences, v 37, pp. 1136-1147
- Eskilson, G. (1987) Thermal Analysis of Heat Extraction Boreholes. Doctoral Thesis, University of Lund, Department of Mathematical Physics. Lund, Sweden.
- Eskilson, P., J. Claesson, (1988) Simulation model for thermally interacting heat extraction boreholes. Numerical Heat Transfer, v 13, No 2 pp. 149- 165.
- FEFLOW, (2010) User's manual/reference manual/whitepapers. Recent release 6.0. Tech. rep., DHI-WASY GmbH, Berlin. <http://www.feflow.info>.
- Ghelin S. (2002) Thermal Response Test Method Development and Evaluation, Doctoral Thesis, Department of Environmental Engineering. Luleå University of Technology. Sweden.
- Gnielinski, V. (1976) New Equations for heat and Mass Transfer in Turbulent pipe and Channel Flow. International Chemical Engineering, v 16, pp. 359-368
- Gustafsson, A.-M., L. Westerlund., Hellström, G. (2010) CFD-modelling of natural convection in a groundwater-filled borehole heat exchanger. Applied thermal engineering, v 30, pp. 683-691
- Gustafsson, A.-M., L. Westerlund, (2011) Heat extraction thermal response test in groundwater-filled borehole heat exchanger Investigation of the borehole thermal resistance, Renewable energy, v 36 pp. 2388- 2394
- Gustafsson, A.-M, (2010) Thermal Response Test, influence of convective flow in groundwater filled borehole heat exchangers. Doctoral Thesis, Department of Civil, Mining and Environmental Engineering. Luleå University of Technology. Sweden.
- Hellström, G. (1991) Ground Heat Storage, Thermal analyses of Duct Storage Systems, Theory. Department of Mathematical physics, University of Lund, Sweden
- Ho, C. J., Y.H. Lin, (1990) Natural convection of cold water in a vertical annulus with constant heat flux on the inner wall., Journal of heat transfer, v 112, pp. 117- 123
- Holmberg, H., Acuña, J., Næss, E., Sønju, K. O, (2016) Numerical model for non- grouted borehole heat exchangers, Part 2-Evaluation. Geothermics (2016) <http://dx.doi.org/10.1016/j.geothermics.2014.11.002>
- L.R., Zobel, O.J., Ingersoll, A.C (1954) Heat Conduction with Engineering, Geological, And Other Applications, University Of Wisconsin Press.
- Keyhani, M., F.A. Kulacki, R.N. Christensen, (1983) Free convection in a vertical annulus with constant heat flux on the inner wall, Transactions of the ASME 105.
- Keyhani, M., F.A. Kulacki, R.N. Christensen, (1985) Experimental Investigation of free convection in a vertical rod bundle – A general correlation for Nusselt number, Journal of heat transfer, v 107, pp. 611-623
- Kjellsson, E. (2009) Solar Collectors Combined with Ground-Source Heat Pumps in Dwellings, Analyses of System Performance. Doctoral thesis, Building Physics. University of Lund, Sweden.
- Kjellsson E., Hellström G, (1999) Laboratory study of the heat transfer in a water-filled borehole with a c-pipe – Preliminary report. Lund University, Lund, Sweden.
- Kohl, T., R. Brenni., W. Eugster, (2002) System performance of a deep borehole heat exchanger. Geothermics, v 31, pp. 687-708
- Kumar R., M. A. Kalam, (1991) Laminar thermal convection between vertical coaxial isothermal cylinders, Int. J. Heat and Mass Transfer, v 34, No 2, pp. 513- 524
- Kumar, R, (1997) Three-dimensional natural convective flow in a vertical annulus with longitudinal fins, Int. J. Heat Mass Transfer, v 40 No 14. pp. 3323-3334.
- Lafortune J.F., D.A. Menely, (1990) Natural convection in a vertical cylinder: comparison of COMMIX-1A predictions with experiment. Int. J. Heat and Mass Transfer, v 33, pp. 435-445
- Lamarche, L., B. Beauchamp, (2007), A new contribution to the finite line-source model for geothermal boreholes, Energy and buildings, pp. 188-189
- Lamarche, L., S. Kajl., B. Beauchamp., (2010) A review of methods to evaluate borehole thermal resistance in geothermal heat-pump systems. Geothermics, v 39 pp. 187-200

- Lee. Y., S. Korpela, (1983) Multicellular natural convection in a vertical slot, *Journal of Fluid Mechanics*, v 126, pp. 91-121
- Lemmon. E.W., M.O. McLinden and D.G. Friend, (2012) "Thermophysical Properties of Fluid Systems" in NIST Chemistry WebBook, NIST Standard Reference Database Number 69, Eds. P.J. Linstrom and W.G. Mallard, National Institute of Standards and Technology, Gaithersburg MD, 20899, <http://webbook.nist.gov>, (retrieved December 4, 2012).
- Liebel. H.T., S. Javed., G. Vistnes, (2012) MIR-TRT with forced convection in a groundwater filled borehole in hard rock. *Renewable Energy*, v 48 pp. 263-268
- Littlefield. D., P. Desai, (1986) Buoyant Laminar convection in a vertical cylindrical annulus, *Journal of heat transfer*, v 108, pp. 815-821
- Matlab 2012b, The MathWorks Inc., Natick, Massachusetts, United States.
- Melinder. Å. (2007) Thermophysical Properties of Aqueous Solutions Used as Secondary Working Fluids. Doctoral Thesis, Dept. of Energy Technology, Royal Institute of Technology, KTH, Stockholm, Sweden
- Mottaghy D., L. Dijkshoorn, (2012) Implementing an effective finite difference formulation for borehole heat exchangers into a heat and mass transport code, *Renewable energy*, v 45, pp. 59-71
- Pasquier. P., D. Marcotte, (2012) Short-term simulation of ground heat exchanger with an improved TRCM *Renewable Energy*, v 46, pp. 92-99
- Pécheux. J., P. Le Quééré., F. Abcha, (1994) Curvature effects on axisymmetric instability of conduction regime in a tall air-filled annulus. *Physics of fluids*, v 6, pp. 3247- 3255
- Sparrow. E. M., M. Charmchi, (1983) Natural convection experiments in an enclosure between eccentric or concentric vertical cylinders of different height and diameter. *Int. J. Heat and Mass Transfer*, v 26, No 1, pp. 133- 143
- Thomas. R. W., De Vahl Davis. G., (1970) Natural Convection in annular and rectangular cavities, A Numerical study, Proceedings fourth international heat transfer conference. Paris, Vol. 4, NC.2.4, Elsevier, Amsterdam.
- Wetter. M., A. Huber, (1997) TRNSYS Type 451 Vertical borehole heat exchanger EWS model. Version 2.4 Model description and implementing into TRNSYS. Luzern, Zürich, Switzerland.
- Wright. J.L., H. Jin., K.G.T., Hollands., D. Naylor, (2006) Flow visualization of natural convection in a tall air-filled vertical cavity. *International Journal of Heat and Mass Transfer*, v 49, pp. 889-904
- Wright. J. (1996) A correlation to quantify convective heat transfer between vertical window glazings. *ASHRAE Trans*, v 102, No 1 pp. 940-946
- Yavuzturk. C, (1999) Modeling of vertical ground loop heat exchangers for ground source heat pump systems. Doctoral Thesis, Oklahoma State University
- Zarella. A., M. Scarpa., M. De Carli, (2011) Short time step analysis of vertical ground-coupled heat exchangers: The approach to CaRM, *Renewable Energy*, v 36, pp. 2357-2367
- Zeng. H., N. Diao., Z. Fang, (2003): A finite line-source model for boreholes in geothermal heat exchangers, *Heat Transfer Asian Research*, v 31, pp. 558–567.

I-4.5 PAPER 2: NUMERICAL MODEL FOR NON-GROUTED BOREHOLE HEAT
EXCHANGES, PART 2- EVALUATION

Holmberg. H, Acuña. J., E. Næss., Sønju. O. K. (2016)

Geothermics (2016) [doi:10.1016/j.geothermics.2014.11.002](https://doi.org/10.1016/j.geothermics.2014.11.002)



Numerical model for non-grouted borehole heat exchangers, Part 2—Evaluation



Henrik Holmberg^{a,*}, José Acuña^b, Erling Næss^a, Otto K. Sønju^c

^a Department of Energy and Process Engineering, Norwegian University of Science and Technology, Kolbjørn hejes vei 1 B, 7491 Trondheim, Norway

^b Department of Energy Technology, KTH Royal Institute of Technology, Brinellvägen 68, 100 44 Stockholm, Sweden

^c Rock Energy AS, Lysaker torg 25, 1366 Lysaker, Norway

ARTICLE INFO

Article history:

Received 29 January 2014

Accepted 18 November 2014

Available online 9 December 2014

Keywords:

Ground source heat pump

Borehole heat exchanger

Natural convection

Simulation

Numerical

ABSTRACT

In this paper a simplified and not fully discretized numerical model is used to simulate the performance of a non-grouted (water filled) borehole heat exchanger (BHE). The model enables simulation of the initial transient behavior of a BHE and gives transparent insight into the heat transfer mechanism acting during the startup and operation of the BHE installation. To account for the thermal effect of natural convection that arises in non-grouted BHEs, the model is complemented with a Nusselt-correlation. The model is presented in detail in Holmberg et al. (2014) and in the present paper it is evaluated based on distributed temperature measurements from Acuña (2010). The measurements were obtained during a distributed thermal response test (DTRT) and during heat pump operation, both on a 261 m deep borehole equipped with a U-tube collector and a distributed temperature sensing system. Despite the simplifications involved with the model, it agrees well with the measured data even on a time scale on the order of minutes. The Nusselt number related to natural convection in the borehole was found to be 6.4 during the DTRT and 3.68 during heat pump operation. This indicates the large differences in the borehole thermal resistance during heat injection and heat extraction.

© 2014 Elsevier Ltd. All rights reserved.

1. Introduction

A numerical model for a BHE has been developed and the model is evaluated in the present paper by comparing the results with distributed temperature measurements performed during a distributed thermal response test (DTRT) and during heat pump operation. The single U-tube collector is used in this study; however, the model is equally applicable to other collector configurations.

The model is based on the finite difference method and uses a simplified thermal resistance and capacity model (TRCM) as presented in Bauer et al. (2011) and Diersch et al. (2011a, 2011b) for the borehole. The ground surrounding the borehole is resolved through an axisymmetric cylindrical grid in two-dimensions, while the borehole, the collector and the heat carrier are treated as one-dimensional features. It is assumed that heat transfer in the ground is by thermal conduction; ground water advection has thus been

neglected in this study. For non-grouted BHEs the heat transfer within the borehole is enhanced by natural convection triggered by the temperature difference between the collector and the borehole wall. In the present model, this is accounted for through a Nusselt-correlation. Furthermore, the model is setup as a modified TRCM model based on a Y-circuit. For a detailed description, the reader is referred to the accompanying paper (Holmberg et al., 2014).

The developed model is used in the present paper to simulate the hydraulic and thermal response of a BHE that has been mapped thoroughly by Acuña (2010). Through a distributed temperature sensing system (DTS), the vertical temperature profiles in the borehole were measured during a thermal response test and during heat pump operation. These measurements are well suited for the evaluation of numerical models where the axial extent of the borehole is discretized.

A thermal response test (TRT) is commonly used to evaluate the effective thermal conductivity of the rock surrounding the borehole, and the internal thermal resistance in the borehole (Ghelin, 2002). This is usually referred to as the effective borehole thermal resistance (R_b^*) as defined by Hellström (1991).

$$R_b^* = \frac{T_{fm} - T_{bwm}}{q_m} \quad (1)$$

Abbreviations: BHE, borehole heat exchanger; TRT, thermal response test; DTRT, distributed thermal response test; DTS, distributed temperature sensing; TRCM, thermal resistance and capacity model.

* Corresponding author. Tel.: +47 95749363.

E-mail address: henrik.holmberg@ntnu.no (H. Holmberg).

<http://dx.doi.org/10.1016/j.geothermics.2014.11.002>

0375-6505/© 2014 Elsevier Ltd. All rights reserved.

Nomenclature

C_p	Specific heat capacity [J/kg K]
D_h	hydraulic diameter [m]
k	thermal conductivity [W/m K]
K	radius ratio $r_0/(r_0 - D_h/2)$
q''	heat flux [W/m ²]
q'	specific heat load [W/m]
Q	heat load [W]
r	radius [m]
R_b	local borehole thermal resistance [K·m/W]
R_b^*	effective borehole thermal resistance [K·m/W]
T	temperature [°C]
L	characteristic length scale $D_h/2$ [m]
g	gravitational acceleration [m/s ²]

Greek symbols

α	thermal diffusivity [m ² /s]
β	coefficient of thermal expansion [1/K]
ν	kinematic viscosity [m ² /s]

Dimensionless numbers

Ra^*	modified Rayleigh number $g\beta L^4 q'' / \alpha \nu k$
--------	--

Index

0	borehole dimensions
c	collector dimensions/properties
f	heat carrier fluid
in	inlet
out	outlet
$local$	local value
m	mean value
w	water
g	ground temperature/properties
bw	borehole wall

In Eq. (1), T_{fm} is the heat carrier mean fluid temperature, defined as the arithmetic average of the inlet and outlet fluid temperatures of the collector, T_{bwm} is the average temperature of the borehole wall, and q'_m is the average heat load per meter borehole length. The borehole resistance is thus defined as an average of the thermal resistance for the entire BHE which also reflects the one-dimensionality of the analytical methods often used for BHE modeling. These methods are typically based on either the infinite line source (Ingersoll et al., 1954), or the infinite cylindrical source (Carslaw and Jaeger, 1959). When discussing the borehole thermal resistance in relation to numerical models, it should be noted that there is a difference between the effective (R_b^*) and “local” (R_b) resistance (Eq. (2)) as evaluated from numerical models or from distributed measurements.

$$R_b = \frac{T_{f,local} - T_{bw,local}}{q'_{local}} \quad (2)$$

For the case of only conduction heat transfer, the local borehole resistance is primarily influenced by the positioning of the collector, the thermal conductivity of the borehole filling material, and the dimensions of the collector and borehole. In such cases, the conductive thermal resistance can be determined based on the multipole method from Bennet et al. (1987) as presented in Lamarche et al. (2010). The experimental results from Acuña (2010) are based on a borehole with 14 cm diameter equipped with a PEM40 U-tube collector having about 2 cm spacing between the pipes. With only conductive heat transfer and using the multipole method such a configuration would yield a thermal resistance of approximately

0.22–0.23 K·m/W, and the internal resistance of the collector is about 0.026 K·m/W, assuming turbulent flow conditions for the heat carrier. Thus the total borehole resistance is ca. 0.25 K·m/W assuming only conduction.

Acuña on the other hand measured R_b to be 0.062 (K·m/W) during the DTRT which is significantly lower (75%) than the pure conductive resistance. This implies that there must be convection present during the test. This is a common phenomenon during TRT of water filled boreholes and has been pointed out by several authors (Ghelin, 2002; Kjellson, 2009); the induced temperature difference triggers natural convection in the well which enhances the heat transfer and reduces R_b . This affects the overall performance of GSHP systems, leading to less required borehole length and/or more effective heat pump operation. Natural convection in non-grouted BHE has been analyzed both experimentally and numerically in recent years, Kjellson (2009) and Gustafsson et al. (2010).

Gustafsson et al. (2010) performed CFD-studies of natural convection in a section of a BHE during heat injection. The results showed a decreasing borehole thermal resistance with increasing thermal load. According to the study, the Nusselt number (Nu) for natural convection was around 3–4 for the investigated geometry (borehole diameter $d = 0.1036$ m, equipped with a PEM40 U-collector). In that case Nu was defined as the ratio between the borehole resistance for pure conduction heat transfer and the borehole resistance with natural convection.

In the present work the constituents of the BHE are treated as one-dimensional features in the model, implying that only the mixing-cup temperatures for each section of the borehole are used. It has been assumed that the fluid in the collector exchanges heat only with the water in the borehole, and that there is no direct (conductive) heat exchange between the collectors or between the collector and the wall of the borehole.

The influence of natural convection is accounted for by a Nusselt correlation (Eq. (3)) based on the modified Rayleigh number and the radius ratio (K). Eq. (3) is derived in Holmberg et al. (2014). Given the Nusselt number, the local borehole resistance is determined from Eq. (4).

$$Nu = 0.1743 Ra^{*(0.233 - 0.009K)} K^{0.442} \quad (3)$$

$$R_b = \frac{R_{b,cond}}{Nu} + R_{collector} \quad (4)$$

where $R_{collector}$ represents the internal thermal resistance of the collector (fluid to pipe and pipe wall resistances). $R_{b,cond}$ is the thermal resistance based on conductive heat transfer through the water in the borehole as determined from the multipole method.

2. Experimental setup and measurement data**2.1. Introduction**

Measurement data from two experimental setups (DTRT and heat pump operation) are used in this paper. The experiments were performed on a 261 m deep borehole with a single polyethylene U-tube collector, the borehole was equipped with a (DTS) system, to obtain measurements of the vertical temperature profiles. The experimental setup and the measurement data will be further presented hereunder.

2.2. Experimental setup

The borehole was filled with groundwater, which is common practice in Nordic countries. The total U-tube length was 257 m and the groundwater level was about 5.5 m below the surface. Thus, the active U-tube length was 251.5 m. Parameters for the tested borehole are listed in Table 1.

Table 1
BHE parameters.

Borehole diameter	140 mm (5.5")
Active depth	251.5 m
Collector	U-pipe (PE40 × 2.4 mm)
Thermal conductivity, collector (k_c)	0.42 W/m K
Heat carrier	20 vol.% ethyl alcohol
Rock thermal conductivity (k_g)	3.08 W/m K (average from Acuña, 2010)
Rock specific heat (C_p)	830 J/K kg

Through a fiber optic cable installed along the depth of the borehole, DTS provided the temperature profile without the need of many individual temperature sensors. The cable was installed as a loop inside both legs of the U-tube to measure the vertical fluid temperature profile of the circulating fluid. The same cable also provided the undisturbed ground temperature profile, measured before the test was carried out. Fig. 1 gives an overview of the borehole with installed sensor cables as seen from the top.

Short light pulses from a laser were directed through the optic cable. A nonlinear part of the back-scattered light had a different frequency from the input light and traveled back from the temperature measurement location to the input location. The light scattering process that produced the frequency shift is called Raman scattering. The temperature and the position of any measured section were determined by analyzing the ratio between the intensities of the up-shifted and down-shifted light over a time window corresponding to the delay time for the light to travel to the measured section and back.

2.3. DTRT measurements

The measurements during the DTRT were taken using an instrument of the type HALO from Sensornet, which, according to the manufacturer specifications, has a spatial resolution of 2 m and temperature accuracy depending on the averaging time and distance from the instrument. The instrument data sheet presents temperature uncertainties within the range 0.05–0.45 K corresponding to measurement times from 60 min to 15 s. It is important to keep in mind that this type of measurement depends on the integration time, the measuring length interval, the laser features, the distance between the measured section and the instrument (cable length) and the calibration procedure, among others. For the specific test, the optic cables provided temperature measurements at

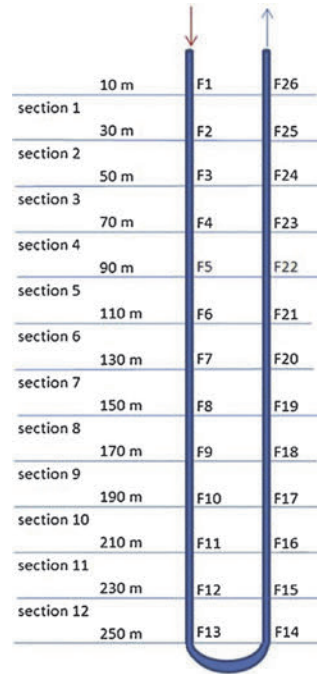


Fig. 2. Borehole sectioning.

52 segments (each 10 m long) that were later reduced to 26 locations, as can be seen in Fig. 2.

Temperature measurements were averaged over a segment of the cable for each numbered temperature location. The measurements are averaged over a time window of 5 min and the standard deviation during a 3 day period of measurements under undisturbed ground conditions was 0.03 K (the instrument data sheet gives a maximum deviation of 0.1 K for a 5 min integration time). Regarding systematic errors, the cable was carefully calibrated using an ice bath and the signal offset was corrected, allowing to adjust for accurate absolute temperature values along the entire cable length (± 0.1 K). Since most calculations were based on temperature differences, no significant errors were expected. Also, the influence of the unknown lateral position of the fiber optic cable inside the U-pipe was considered in the analysis of systematic errors. The flow pattern in the U-pipe was turbulent during the test (Reynolds number between 6500 and 8900), considering a two-layer model for the turbulent flow, the viscous boundary layer thickness is between 0.3 and 0.4 mm (where heat conduction is the only heat transfer mechanism). The temperature difference between the collector pipe wall and the fluid bulk temperature was calculated to be about 0.15 K for the conditions of this test, and the temperature drop in the viscous boundary layer was about 0.14 K, meaning it occurred mainly in this thin layer while the rest of the temperature profile was virtually flat. Given the diameter of the fiber optic cable of 3.8 mm, it can be concluded that the systematic error due to the cable position inside of the pipe was negligible. Details of these measurements have been reported earlier in Acuña (2010).

Additional equipment for the DTRT consisted of a circulation pump, an inductive flow and energy meter, a flow regulation valve and an electric heater with an adjustable power between 3 and 12 kW.

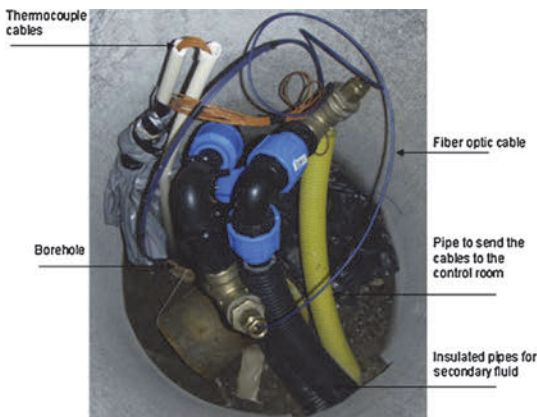


Fig. 1. Overview of the borehole components.

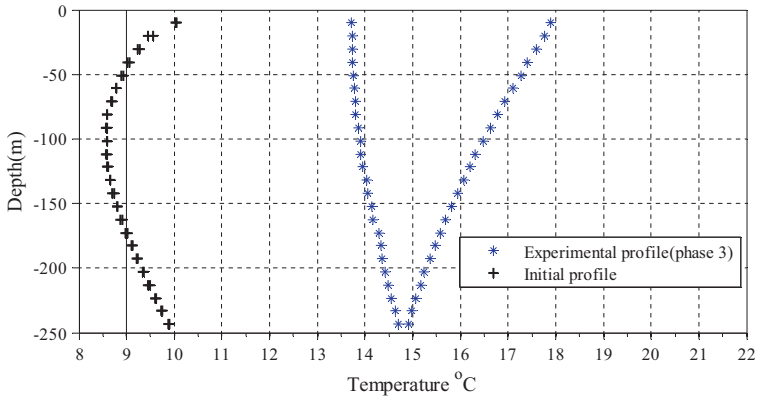


Fig. 3. Measured initial temperature profile and local time-averaged temperatures during Phase three of the DTRT.

The DTRT lasted approximately 160 h and consisted of four phases. Phase one of the DTRT focused on measuring the undisturbed ground temperature with no fluid circulation in the U-tube. This period lasted 65 h. During the Phase two, the fluid was circulated through the U-tube for 24 h without any heating. The temperatures along the entire borehole length became nearly uniform due to the circulation, with the mean value of (9.19 °C) which is slightly higher than the mean temperature of the undisturbed ground temperature profile (9.1 °C) this increase is caused by frictional heating inside the collector. During Phase three of 48 h, a nearly constant heat input rate of 9 kW to the circulating fluid was maintained. The rising temperature response of this period was used to estimate the borehole resistance. Finally, during the fourth phase, temperature measurements continued without any heating or circulation in order to observe the temperature recovery, and to determine the ground thermal conductivity, while taking advantage of the small temperature gradients inside the borehole during this period. The resulting average ground thermal conductivity value along the borehole depth was 3.08 W/m K. The present paper focuses on the heating phase (Phase three) of the DTRT for which the measurements will be presented and compared with the simulated results from the model. The time-averaged temperatures during the Phase three including the undisturbed temperature profile can be seen in Fig. 3.

2.4. Heat pump operation

The measurements during heat pump operation were obtained using an instrument of the type Sentinel-DTS from Sensornet with a spatial resolution of 1 m. The equipment was configured to measure every 1 m and therefore, approximately 257 measurement points were taken in each collector pipe. Temperatures were also measured at several depths with thermocouples, but these measurements have not been used in this study. The fiber optic cable was not fixed in the collector, therefore, the cable might be in contact with the wall of the collector at some parts. In order to measure and adjust the fluid mass flow rate, the borehole loop was also instrumented with an inductive flow meter of the type Brunata HGS9-R6 and a STA-D regulation valve, both located in the return line. In addition, closing and/or opening neighboring boreholes and a frequency controlled circulation pump were used for flow regulation purposes. The measurements were taken every 2 min for a period of 2 h during the 3rd operation day of the system. Measurements were taken at three different flow rates of approximately 0.34 l/s, 0.41/s and 0.5 l/s. In the current study, measurements from the lowest flow rate (≈ 0.34 l/s) have been used. The heat pump extracts approximately 6 kW during operation, and there is no fluid circulation in the collector when the heat pump is switched off.

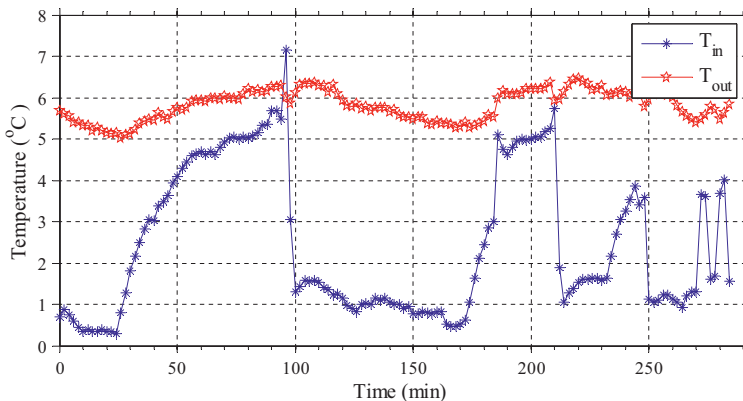


Fig. 4. Measured Inlet and outlet temperatures from the BHE during heat pump operation, $\dot{m} = 0.34$ l/s.

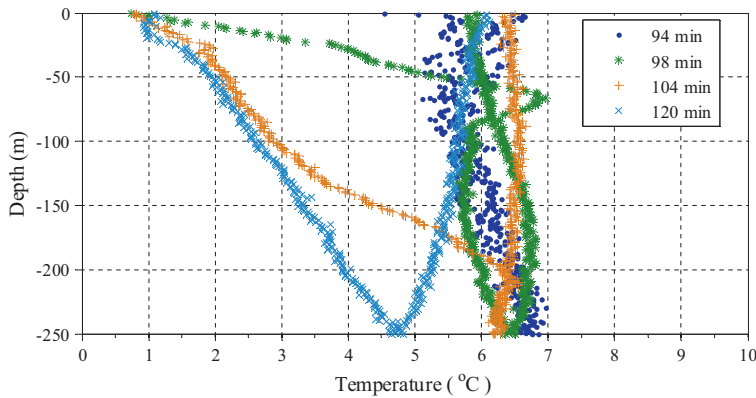


Fig. 5. Measured vertical temperature profiles at different times, $\dot{m} = 0.34$ l/s.

The inlet and outlet temperature from the BHE (measured in the upper part of the borehole) can be seen in Fig. 4, the inlet temperature drops rapidly when the heat pump starts (at 94.5 min) and recovers when the heat pump is switched off.

Measured vertical fluid temperature profiles at different times during the startup of the heat pump can be seen in Fig. 5.

3. Simulations

The simulations are performed in Matlab version R2012b on a standard PC having a 2.53 GHz dual core processor. The numerical model is based on finite difference and it uses a two-dimensional axisymmetric grid for the ground surrounding the borehole and TRCM-simplifications for the borehole and its constituents. The borehole is axially discretized using 0.5 m segments and the finest resolution of the radial grid is around 2.7 mm.

The DTRT is simulated using both an explicit model with a constant time step of 1 s and with an implicit model where the time step is varied between 2.5 s and 100 s. The aim of the explicit model is to give a detailed insight into the BHE operation during the first 10 h of Phase three. The implicit model is used to simulate the entire duration of the DTRT. With implicit time stepping, the entire simulation time is short, in the order of a few minutes, but the method is less accurate than the explicit method. The results show, however, that the implicit method is qualitatively accurate. The measured data had a time resolution of 5 min and were used to determine the heat load applied during Phase three of the DTRT, which has then been used in the simulation.

The heat pump operation is simulated using an explicit model having a constant time step of 1 s. The experimental data had a time-resolution of 2 min. The inlet and outlet temperatures are used to determine the amount of heat extracted when the heat pump is in operation. The total simulation time for the heat pump operation is approximately 6 min.

The simulation parameters are summarized in Table 2.

During the simulations the physical properties of the heat carrier and of the water in the borehole, such as thermal conductivity, specific heat capacity, viscosity etc. are evaluated based on the local

temperature using data of Melinder (2007) and NIST (2012), while the density is assumed constant. The thermal conductivity for the rock is set according to Table 1. The influence of natural convection is included via the Nusselt correlation (Eq. (3)).

4. Results and discussion

4.1. DTRT

The temperature measurements from Acuña (2010) are used as a reference to evaluate the model. The temperatures were measured along 10 m sections. The first measurements, which are at 10 m depth, are used together with the mass flow rate and the specific heat capacity of the heat carrier to determine the supplied heat load to the BHE. The undisturbed temperature profile is used as the starting value for the simulation.

The simulated temperatures in the collector at different depths throughout the DTRT are presented in Fig. 6.

The wiggles in the simulated profiles are caused by variations in the applied thermal load, these are also seen in Fig. 7 which shows the calculated axial arithmetic average of the R_b and R_b^* during Phase three.

It is seen that the local resistance decreases rapidly in the beginning (95–98 h), this is due to the definition in Eq. (2), where the local specific heat load to the borehole wall is used. Initially this heat load is low as the applied heat load to the BHE also is absorbed by the water in the borehole. As the heat uptake in the borehole water decreases, the local resistance still decreases slowly; this is then due to the increase in the temperature of the borehole water which increases the effect of natural convection. This decrease is, however, not seen in the effective resistance which keeps at a rather constant value for the entire Phase three.

Simulated and experimental mean fluid temperatures (T_{fm}) for Phase three are shown together in Fig. 8 and show excellent agreement.

In Figs. 9 and 10 the vertical temperature profiles are shown at 40 min, respective 5 h into Phase three (the position for these figures are marked in Fig. 8).

Table 2
Simulation parameters.

Data set	Duration	Mass flow	Heat load	Measurement resolution	Time discretization	Time-step
DTRT	(160 h)	≈ 0.52 l/s	Heat injection	5 min	Explicit Implicit	1 s 2.5–100 s
Heat pump operation	(284 min)	≈ 0.34 l/s	Heat extraction	2 min	Explicit	1 s

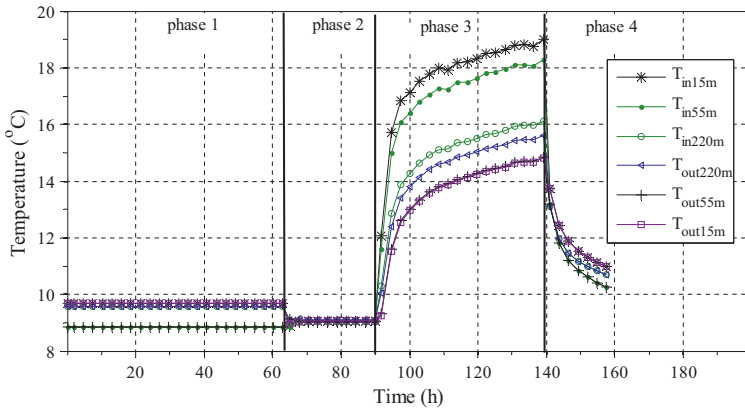


Fig. 6. Simulated temperatures in the collector at different depths during the DTRT. Phase one: no fluid circulation. Phase two: fluid circulation. Phase three: heat injection ($Q \approx 9 \text{ kW}$). Phase four: no fluid circulation.

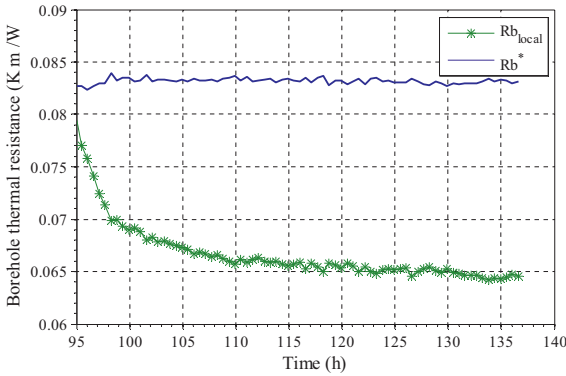


Fig. 7. Calculated local and effective borehole resistance (R_b) during simulation of heat injection TRT. The local value represents an axial arithmetic average.

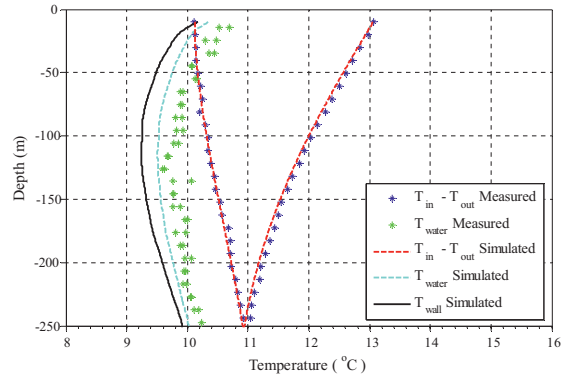


Fig. 9. Temperature profiles 40 min into Phase three of the DTRT.

The simulated temperature profiles in the collector ($T_{in} - T_{out}$) are in good agreement with the measured values. The simulated water temperatures are in general lower than the measured values. It is seen however, that the results correspond better to

the measurements after 5 h than after 40 min, which indicates a discrepancy in the starting conditions for the numerical simulation. With a measurement resolution of 5 min, this is to be expected.

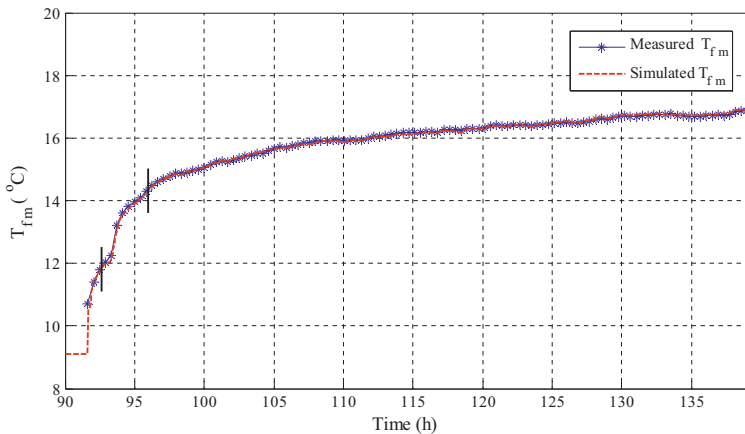


Fig. 8. Average fluid temperature (T_f) as calculated based on the simulated results and the experimental results.

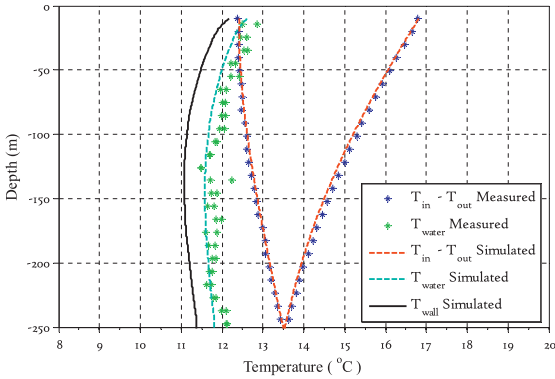


Fig. 10. Temperature profiles 5 h into Phase three of the DTRT.

The local time averaged temperatures in the collector along the borehole for Phase three of the DTRT are shown in Fig. 11; in addition, the initial temperature profile and the temperatures in the collector 3.2 h into Phase four are shown.

The initial profile in Fig. 11 represents the undisturbed vertical temperature profile in the borehole and it is used as the initial value in the simulation. The simulated profile is based on the time-averaged temperatures of the downward and upward fluid streams in the collector during Phase three. It is to be compared to the experimental profile that represents the measured temperatures for Phase three (also time averaged). As can be observed from Figs. 8–11 the model predictions agree well with the measurements, except for the initial startup, where the starting conditions are unknown.

In Fig. 12 calculations of the time-history of the mean collector fluid temperature using the analytical infinite cylindrical source solution of Carslaw and Jaeger (1959), the analytical finite line source solution (Lamarche and Beauchamp, 2007), the numerical calculations of the present work and the experimental data are shown. The analytical solutions are evaluated with a time step of 10 min. As can be seen, the numerical model approaches the measured data sooner than the analytical solutions. The analytical solutions uses the effective borehole resistance (R_b^*), while in case of the cylindrical source solution the thermal capacity of the borehole fluid is neglected, and in the finite line source solution it is

equal to the rock thermal capacity, this affects the transient behavior of the model. For further information on the implementation of the infinite cylindrical source solution and the finite line source solution for BHE simulation the reader is referred to Bernier et al. (2004) and Lamarche and Beauchamp (2007).

The results in Fig. 12 indicates that the test period for TRTs in non-grouted BHEs can be reduced using the developed model as compared to using conventional analytical solutions.

The local and effective borehole resistances are found to be slightly higher than the values determined by Acuña (2010) ($R_b = 0.062 \text{ K}\cdot\text{m}/\text{W}$) and from a standard TRT ($R_b^* = 0.079 \text{ K}\cdot\text{m}/\text{W}$). In the end of the simulation of Phase three, the axial average of the local resistance was determined to be $R_b = 0.064 \text{ K}\cdot\text{m}/\text{W}$ and the effective resistance as $R_b^* = 0.083 \text{ K}\cdot\text{m}/\text{W}$. It was found that the best fit to the experimental data was for a ground thermal conductivity of $3.05 \text{ W}/\text{m}\cdot\text{K}$ which is in good agreement with the in situ measurements. The average Nusselt number related to natural convection in the borehole was calculated to be 6.4 based on the simulation.

It is useful to distinguish between the effective borehole resistance R_b^* as determined by standard TRT and the local R_b which can be determined either through the result from distributed temperature measurements or, as in this study, by using the numerical results on a local scale. The latter gives, in general, a lower thermal resistance than R_b^* . In the case of the TRT performed by Acuña (2010) the difference is approximately 30%. However, since existing dimensioning tools are defined based on the effective value as evaluated from standard TRTs, using an averaged local value would lead to an under-dimensioning of the GSHP installation. The difference between the effective and local resistance increase with borehole depth and decrease with increased flow rate (Lamarche et al., 2010).

In the simulated case, an increase of the flow rate from $0.5 \text{ kg}/\text{s}$ to $1 \text{ kg}/\text{s}$ reduces the difference between the local and effective resistance to about 10%. This is connected to the vertical temperature profile of the heat carrier, which becomes straighter for a higher mass flow rate, thus bringing the two definitions (Eqs. (1) and (2)) of the resistances closer together.

Fig. 13 shows the temperature profiles from a thermal extraction TRT which is numerically simulated by simply extracting heat instead of injecting during Phase three, using the same parameters as in the described DTRT. It can be observed that the shape of the temperature curves has a wiggle at 117 h. This is the point where the average temperature in the borehole water corresponds with the density maximum at 4°C . The simulations are based on

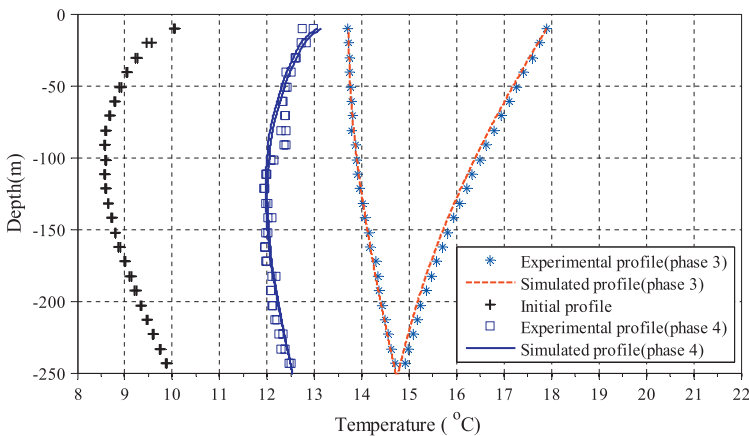


Fig. 11. Local temperatures in the collector during Phase one, Phase three (time averaged) and Phase four.

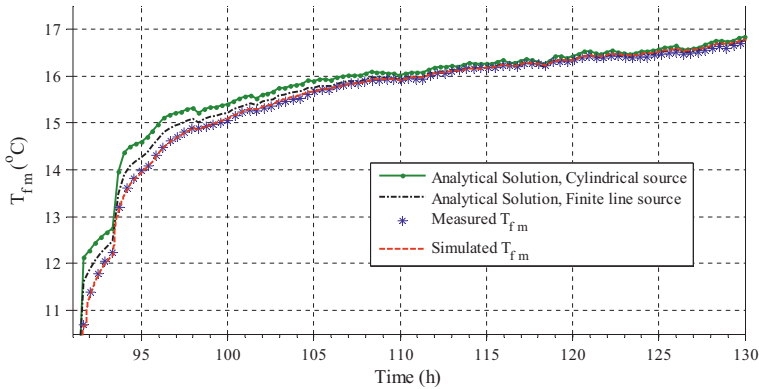


Fig. 12. T_{fm} calculated with the analytical infinite cylindrical source solution, the analytical finite line source solution, the numerical model and based on measurements.

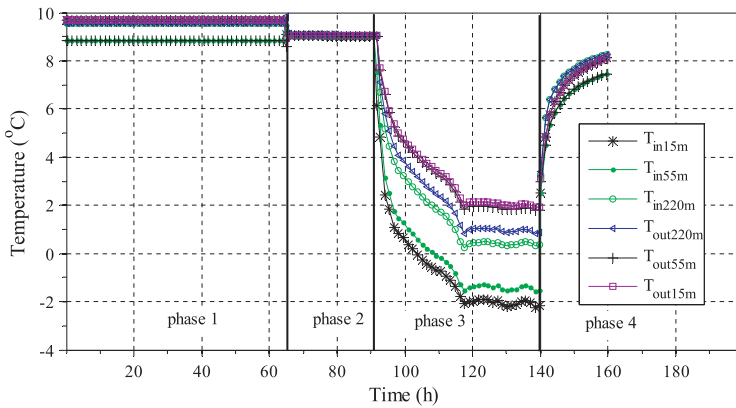


Fig. 13. Simulated temperatures in the collector at different depths during an extraction TRT.

the same conditions as the injection DTRT discussed above; however, in this case the effective borehole resistance varies between $R_b^* = 0.09 \text{ K} \cdot \text{m}/\text{W}$ and $R_b^* = 0.131 \text{ K} \cdot \text{m}/\text{W}$ as shown in Fig. 14.

It can be noted that when the local resistance increases the difference between the local and the effective values decreases, this

is because the heat transfer between the collector pipes (thermal shunting) is less pronounced for a higher local resistance.

4.2. Heat pump operation

The undisturbed vertical temperature profile measured prior to the DTRT is used as the starting point for the simulation. Since the measurements of the DTRT and heat pump operation were taken at different seasons, the top 20 m of the borehole is neglected in the simulation to avoid possible errors induced by the seasonal temperature difference in the ground. The measurements were performed on the 3rd day of heat pump operation. To account for the induced thermal transients prior to the measurements, the simulation is started with a constant heat extraction period during which the temperature of the borehole is decreased to the level of the measurements, i.e. the simulated recovery profile is a good fit to the measurement. Since the measurements were done on a 2 min basis the matching of startup and stop of the fluid flow did involve some initial assumptions. Further, the collector was equipped with a fiber optic cable that occupies some of the flow area in the collector. This is taken into account when calculating the internal cross sectional area of the collector pipe. Simulated mean fluid temperatures (T_{fm}) are shown in Fig. 15.

The heat pump is in operation between 94.5 and 172 min, and this period has been chosen for further study. In the start of the

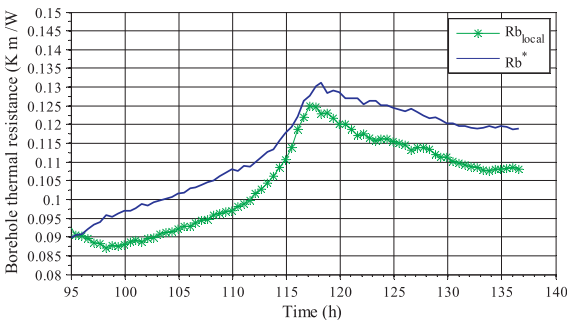


Fig. 14. Calculated local and effective borehole resistance (R_b^*) during simulation of heat extraction TRT. The maximum value is found when the average water temperature in the borehole passes 4°C. The local value represents an axial arithmetic average.

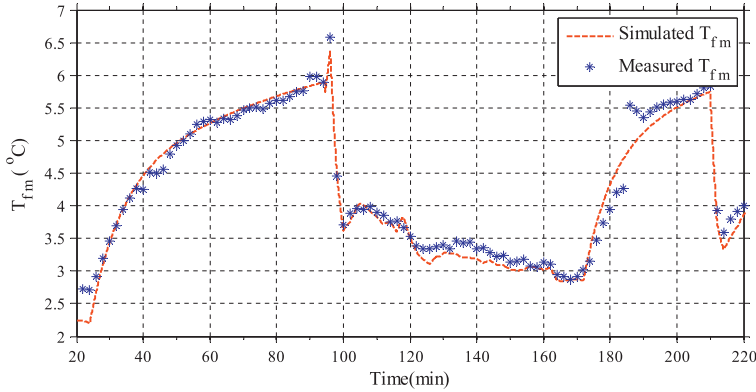


Fig. 15. T_{fm} calculated with the numerical model and from measurements during heat pump operation. Simulated with $\dot{m} = 0.34$ l/s when the heat pump is in operation.

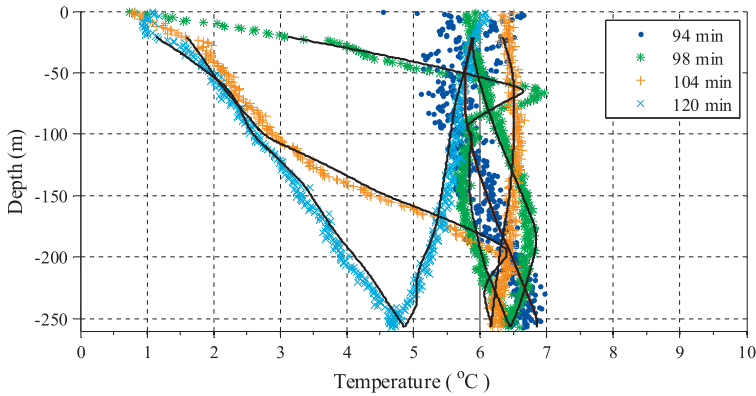


Fig. 16. Evolving temperature profiles at different times, simulated with $\dot{m} = 0.34$ l/s.

operation period, there is a peak caused by resident fluid in the connection between the borehole and the heat pump. As the fluid circulation starts, this fluid travels down in the collector. This is seen in Fig. 16 where the evolving vertical temperature profile in the BHE is shown.

The solid lines in Fig. 16 correspond to the simulated temperature profile while the measurements are shown by markers. The simulation begins a 20 borehole depth. The flow starts at 94.5 min; therefore, the first profile in the figure is the recovered profile from previous operation.

The simulated values are a close match to the measured profiles, which shows that the present model can be used as an accurate tool to simulate the performance of a BHE even on a time scale on the order of minutes.

Earlier works have reported transient accuracy after 15–20 min of operation for TRCM-models (Bauer et al., 2011) which then is related to grouted boreholes where the heat is transferred by thermal conduction. In the present case, the heat is transferred by natural convection which increases the heat transfer rate, and thus the transient error is less. This enables the study of the transient performance of water filled BHEs during startup and short operation intervals.

In Fig. 17 the model is used to study the transfer of heat (Q) in the BHE during the heat pump operation. The figure shows the heat recovery period (20–94 min) in which the mass flow in the collector is zero, and the heat extraction period (94–170 min).

In the heat recovery period the heat transferred at the borehole wall (Q_{bw}) decreases steadily through the period, the heat is used to heat up the water in the borehole and the fluid in the collector. The heat stored in the borehole water (Q_w) increases first rapidly, increasing the water temperature. As the borehole water temperature increases, some heat is transferred to the heat carrier

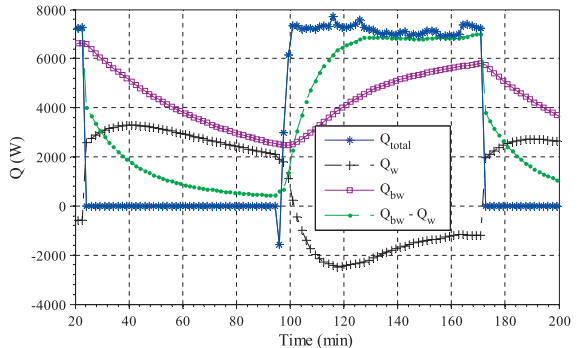


Fig. 17. Simulated energy flow, Q_{total} is the total amount of energy transferred from the BHE. Q_w is the change in energy of the water. Q_{bw} is the energy transferred from the surrounding rock.

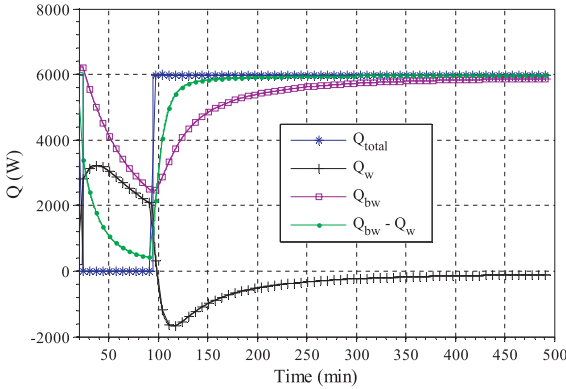


Fig. 18. Simulated energy flow, Q_{total} is the total amount of energy transferred from the BHE. Q_w is the change in energy of the water. Q_{bw} is the energy transferred from the surrounding rock.

in the collector, increasing its temperature as well. The net heat transferred to the collector is shown as $Q_{bw} - Q_w$ in Fig. 17.

During the heat extraction period, the heat is initially taken from the stored energy within the collector, thereafter the heat is taken from both the stored energy in the water and from the rock surrounding the borehole. Q_w becomes negative in this period which means that the water is being cooled down. The sum of Q_w and Q_{bw} is here the total amount of heat extracted from the water and the surrounding rock, after the initial part of the period this corresponds to the total amount of heat being extracted from the BHE. Asymptotically Q_w will then approach zero as the heat extraction process becomes semi-steady state, all energy is then taken from the rock. In the end of the heat extraction process, roughly 80% of the heat is taken from the surrounding rock while the rest comes from the water in the borehole. The average Nusselt number related to natural convection was determined to be 3.68 during the heat extraction period.

The change in internal energy of the water in the borehole represents 20% of the total energy transferred to the heat carrier in the heat extraction period. It should, however, be said that the combination of a large diameter borehole, 14 cm and a low collector flow rate of ≈ 0.34 l/s does enhance the influence of both the fluid in the collector and the water in the borehole.

To further explore the heat transfer in the BHE, the heat pump operation was simulated again, now with a heat extraction period of more than 6 h. The results are visualized in Fig. 18. The heat load Q_{bw} goes asymptotically to the value of Q_{total} .

It is seen in Fig. 18 that the net heat to the borehole water approaches zero while the amount of heat extracted from the rock increases and approaches the total amount of heat extracted from the BHE, thus, a steady state operation is reached in the end of the figure.

As seen in Figs. 17 and 18 there are transient effects during the initial part of the heat pump cycles. The main reason for this transient behavior is the heat capacitance of the borehole system; the effect is due to the water in the borehole (about 3.3 m^3) and the heat carrier in the collector (about 0.5 m^3).

During these transients R_b^* will vary, this is because the extracted energy is not directly related to the temperature difference between the heat carrier and the wall of the borehole. The overall influence of these transients depends on the duration of the heat pump cycle and the physical dimensions and properties of the borehole heat exchanger, also, the transient time is somewhat reduced by the presence of natural convection. The resulting R_b^* can be calculated from Eq. (1), as shown in Fig. 19.

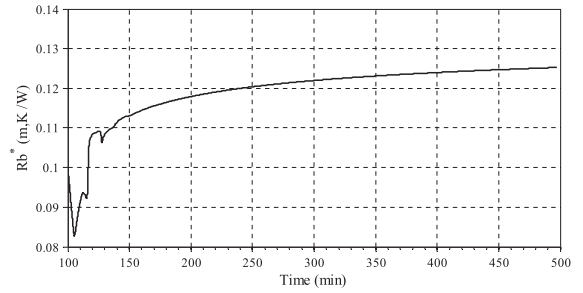


Fig. 19. Calculated effective borehole resistance (R_b^*) during simulation of heat pump operation.

It is seen that R_b^* increases during the initial startup period of the heat pump and approaches a semi-constant value, after 2 h the resistance deviates less than 5% of the value at the end of the simulation. This behavior means also that the resistance as determined from an extraction TRT would over predict the value for shorter operation intervals, such as for the heat pump operation shown in Fig. 17.

The main effect of the natural convection is that it reduces the borehole thermal resistance significantly.

The Nu -correlation has been used on a local scale in the presented results. It can as well be used on a global scale to determine an effective thermal conductivity of the water, thus accounting for natural convection. This can then be used practically together with the multipole method to determine R_b^* for non-grouted BHEs in quasi-steady state.

It is shown that for heat pump applications with relatively short cycle times one cannot predict the system performance accurately by assuming constant borehole resistance values. Variations in R_b^* of 30% are shown for the BHE system studied in this paper.

5. Summary and conclusions

A numerical model for non-grouted (water filled) borehole heat exchangers (BHEs) based on the thermal resistance and thermal capacity model (TRCM) approach has been evaluated in comparison with detailed measurements both from a distributed thermal response test (DTRT) and from heat pump operation. The evaluations were performed using different collector mass flow rates, time scales and for both heat extraction and heat injection scenarios. The numerical model includes a Nusselt correlation representing the effect of natural convection in the borehole. To the knowledge of the authors, this is the first work in which this type of model has been demonstrated and compared with data from distributed temperature measurements.

The Nusselt correlation can as well be used separately on a global scale using average values rather than local. It can, therefore, be used to account for natural convection also in other numerical or analytical models.

Local and time-averaged collector fluid temperatures in sections of the collector pipes have been used as a reference. The model replicates the results from the measurements both from the DTRT and the heat pump operation borehole. This shows that the numerical model is able to accurately capture the transient behavior of a non-grouted BHE even on time scales on the order of minutes. There is a significant difference in the thermal resistance in the borehole between thermal extraction and thermal injection. This is then directly related to natural convection, being the dominant heat transfer mechanism in the borehole.

The results presented have also shed light on the transient heat transfer processes that take place in a BHE during heat pump

operation and to the validity of the borehole resistance and the significance of water in the borehole during startup and short heat pump cycles.

References

- Acuña, J., (Licentiate thesis in Energy Technology 2010) 2010. Improvements of U-Pipe Borehole Heat Exchanger. KTH, Stockholm.
- Bauer, D., Heidemann, W., Diersch, H.-J.G., 2011. Transient 3D analysis of borehole heat exchanger modeling. *Geothermics* 40, 250–260.
- Bennet, J., Claesson, J., Hellstrom, G., 1987. Multipole method to compute the conductive heat transfer to and between pipes in a composite cylinder. Notes on Heat Transfer 3-1987. Department of Building Physics, Lund Institute of Technology, Lund, Sweden.
- Bernier, M.A., Pinel, P., Labib, R., Paillot, R., 2004. A multiple load aggregation algorithm for annual hourly simulations of GCHP systems. *HVAC&R Res.* 10 (4), 471–487.
- Carslaw, H.S., Jaeger, J.C., 1959. *Conduction of Heat in Solids*, second ed. Oxford University Press, Oxford.
- Diersch, H.-J.G., Bauer, D., Heidemann, W., Rühaak, W., Schätzl, P., 2011a. Finite element modeling of borehole heat exchanger systems. Part 1. Fundamentals. *Comput. Geosci.* 37, 1122–1135.
- Diersch, H.-J.G., Bauer, D., Heidemann, W., Rühaak, W., Schätzl, P., 2011b. Finite element modeling of borehole heat exchanger systems. Part 1. Numerical simulation. *Comput. Geosci.* 37, 1136–1147.
- Ghelin, S., (Doctoral thesis) 2002. Thermal Response Test Method Development and Evaluation. Department of Environmental Engineering, Luleå University of Technology, Sweden.
- Gustafsson, A.-M., Westerlund, L., Hellström, G., 2010. CFD-modelling of natural convection in a groundwater-filled borehole heat exchanger. *Appl. Therm. Eng.* 30, 683–691.
- Hellström, G., 1991. *Ground Heat Storage, Thermal Analyses of Duct Storage Systems, Theory*. Department of Mathematical Physics, University of Lund, Sweden.
- Holmberg, H., Næss, E., Sønju, K.O., 2014. Numerical model for non-grouted borehole heat exchangers, Part 1-Development. Submitted for publication.
- Ingersoll, L.R., Zobel, O.J., Ingersoll, A.C., 1954. *Heat Conduction with Engineering, Geological, and Other Applications*. University of Wisconsin Press, Madison.
- Kjellson, E., (Doctoral thesis) 2009. Solar Collectors Combined with Ground-Source Heat Pumps in Dwellings, Analyses of System Performance. Building Physics, University of Lund, Sweden.
- Lamarche, L., Beauchamp, B., 2007. A new contribution to the finite line-source model for geothermal boreholes. *Energy Build.*, 188–189.
- Lamarche, L., Kaji, S., Beauchamp, B., 2010. A review of methods to evaluate borehole thermal resistance in geothermal heat-pump systems. *Geothermics* 39, 187–200.

I-4.6 ADDITIONAL RESULTS AND DISCUSSION

Results from simulation with the numerical model are presented in Paper 2 where the model is compared with detailed experimental measurements from Acuna (2013). The measurements were taken during a distributed thermal response test (DTRT) and during heat pump operation.

In this subsection, complementary results are presented from simulation of the DTRT and the heat pump operation. The aim is to further explore the measurement data by use of the developed numerical model. The parameters for the BHE are summarized in Table I-1 and are applied both to the DTRT and the heat pump operation.

Table I-1 BHE parameters

Borehole diameter	140 mm (5.5 ")
Active depth	251.5 m
Collector:	U-pipe (PE 40x2.4mm)
Thermal conductivity, collector (k_c)	0.42 W / m·K
Heat carrier:	20 volume % ethyl alcohol
Rock thermal conductivity (k_g)	3.08 W / m K (average from Acuña (2010))
Rock specific heat capacity (C)	830 J / K kg
Mass flow rate	0.5 kg / s

I-4.6.1 DISTRIBUTED THERMAL RESPONSE TEST

The applied heat load during the DTRT (about 9 kW) is shown in Figure I-2. During the first 24 hours, the fluid in the collector is circulated without applying a heat load. A higher resolution of the measurement data was used during the first part of the simulation to study the transient behavior in more detail.

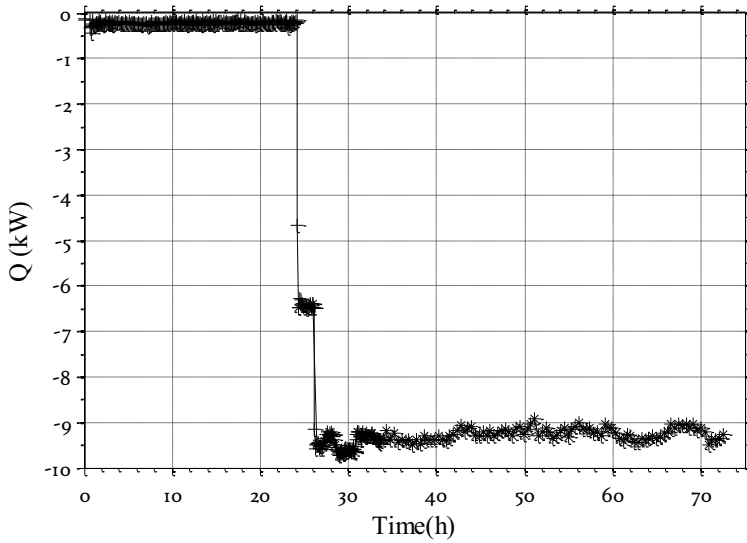


Figure I-2. Heat load applied during DTRT (the measured data is from the same test).

The simulated evolution of the vertical temperature distribution in the collector fluid during startup of the heating period of the response test is shown in Figure I-3. It is observed that the simulated temperature profiles are in close agreement with the measured temperatures.

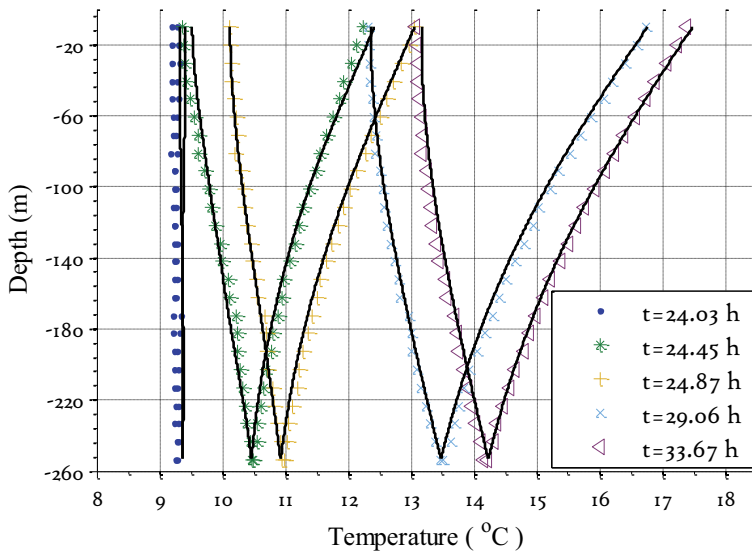


Figure I-3. Temperature profiles during DTRT, measured values from the experimental setup are denoted with markers, calculated values from simulation are shown as solid lines.

In Figure I-4 the water temperature profiles are shown. As seen the simulated water temperature is slightly lower than the measured temperature. This is due to frictional heat generation in the collector and heat losses in the circulation pump during the circulation phase (24 h) prior to the applied heat load. When the heat load is applied, the water temperature increases further in the borehole; it is seen that after some time, the simulated water temperature is in better agreement with the measured values.

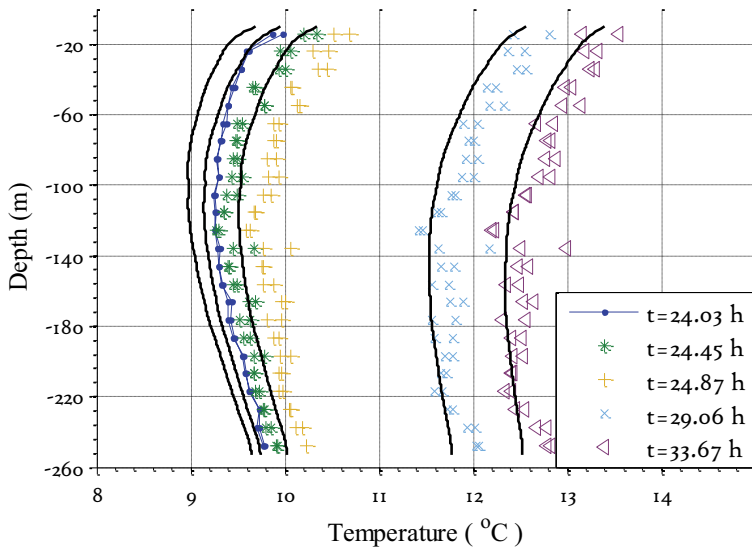


Figure I-4. Water temperature in the borehole during DTRT, profiles correspond to the times shown in Figure I-3. Measured values from the experimental setup are denoted with markers, calculated values from simulation are shown as solid lines.

The heat load through the borehole wall is shown in Figure I-5. The heat load is determined using Fourier's equation for heat conduction on the first numerical element in the model. It is seen that it takes some time for the heat load profile to develop. The first profile is taken before heat is being injected; at this point, the mass flow is already circulating in the collector and energy is being transported from the warmer parts (top and bottom) to the colder sections (middle) of the borehole. As the heat injection starts the profiles becomes negative, indicating that energy is being transported to the borehole. A rather constant profile is not established until about 6-7 hours after the beginning of the heat injection.

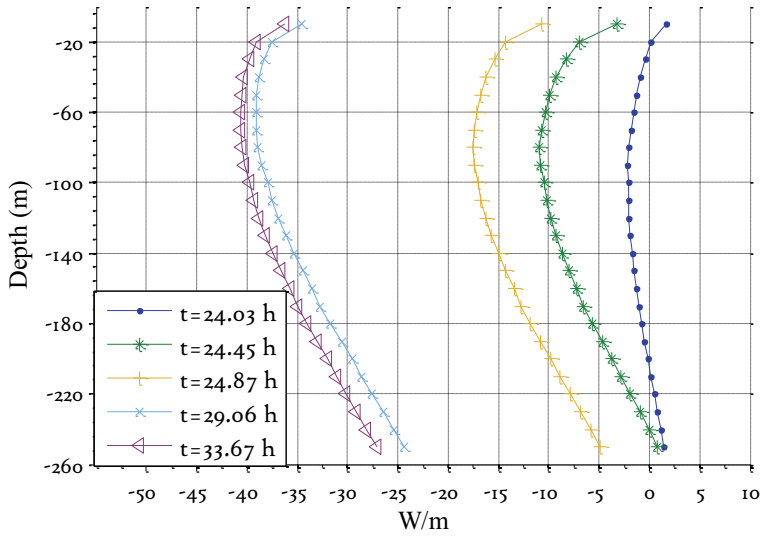


Figure I-5. Distribution of specific heat load in the borehole during the simulated DTRT. Profiles correspond to the times shown in Figure I-3. Only calculated values from simulation are shown.

The shape of the temperature curves in Figure I-4 as well as the distribution of the heat load in Figure I-5 reflects the undisturbed temperature profile in the borehole. It is seen that most of the heat load is taking place in the upper part of the borehole.

I-4.6.2 HEAT PUMP OPERATION

The generated thermal load during the heat pump operation is seen in Figure I-6. The mass flow is stopped in the intervals between the heat loads (shown as zero heat load). The following results focus on the time period 94- 172 minutes during which the heat pump is in operation, and on the time period 172- 210 minutes during which the heat pump is switched off and the borehole is recovering.

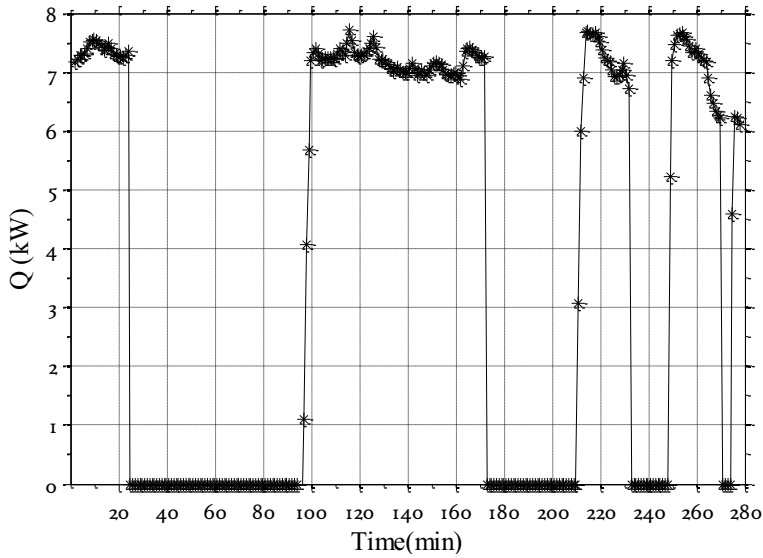


Figure I-6. Heat load generated during heat pump operation

The transient evolution of the vertical temperature profile in the collector fluid is shown in Figure I-7. This figure replicates the results show in Paper 2, the implementation used for the Nu-correlation which is described in Section I-4.3.2 is, however, somewhat different than the implementation used in Papers 1 and 2.

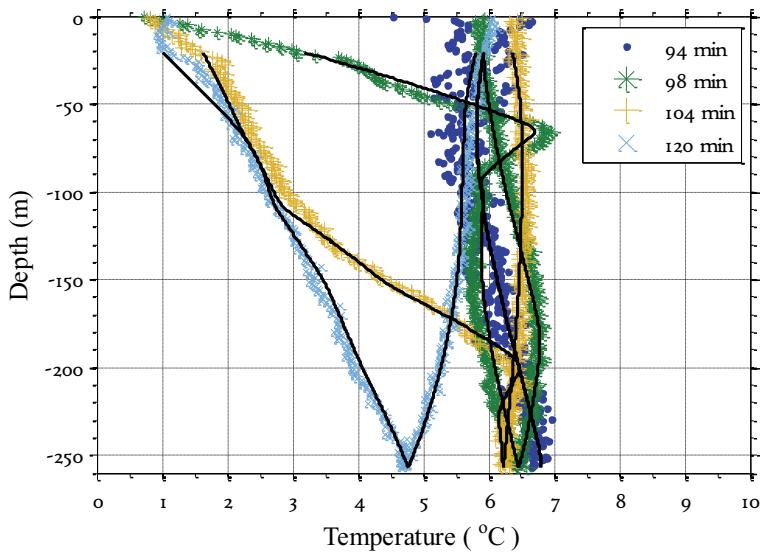
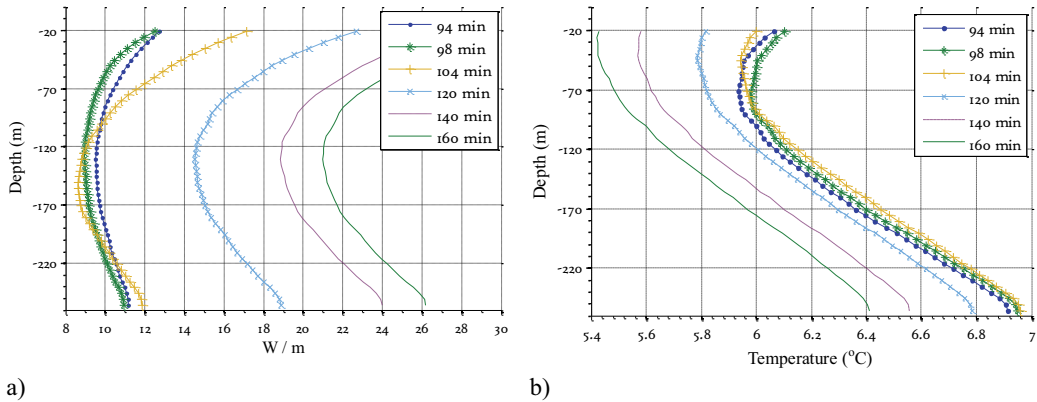


Figure I-7. Temperature profiles, experimental and simulated values, measured values from the experimental setup are denoted with markers, calculated values from simulation are shown as solid lines.

Note the wiggle on the second profile (98 min), this is caused by resident fluid in the top side piping which has a higher temperature than the fluid in the borehole.

The distribution of the specific heat load is determined for the profiles shown in Figure I-7, and the results are presented in Figure I-8 a. It should be noted that the generated average heat load of about 30 W/ m is rather constant in the heat extraction period. The water temperature distributions in the borehole are shown in Figure I-8 b.



a) Figure I-8. a) Calculated distribution of the specific heat load in the borehole, b) Calculated water temperature distributions in the borehole, the first four profiles correspond to the times shown in Figure I-7.

Initially, most of the energy is extracted from the water, as the water temperature decreases the heat load through the borehole wall increases. The vertical average of the water temperature distributions in the borehole are shown in Figure I-9 together with the vertical average distributions of the specific heat load through the borehole wall.

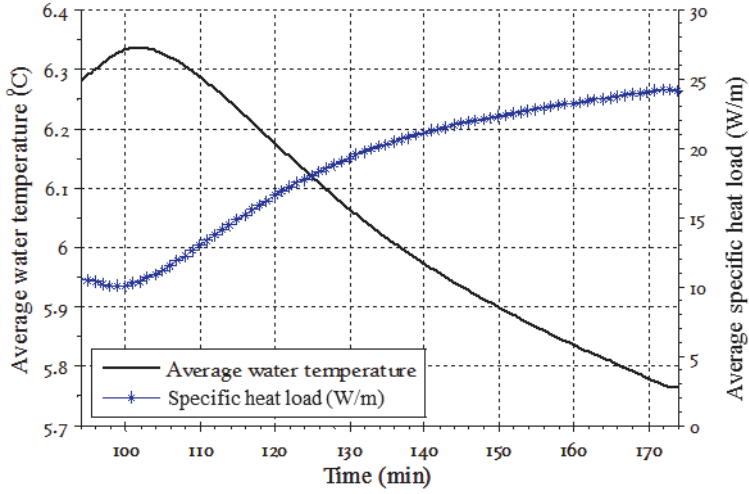


Figure I-9. Variation with time of the vertical average of the water temperature and the specific heat load in the borehole.

As the temperature of the borehole water decreases, the Rayleigh number also decreases. This would cause a reduction in the Nusselt number for natural convection; however, the increase in transfer has the counter effect and therefore, the Nusselt number increases during the entire heat extraction period. This is shown in Figure I-10.

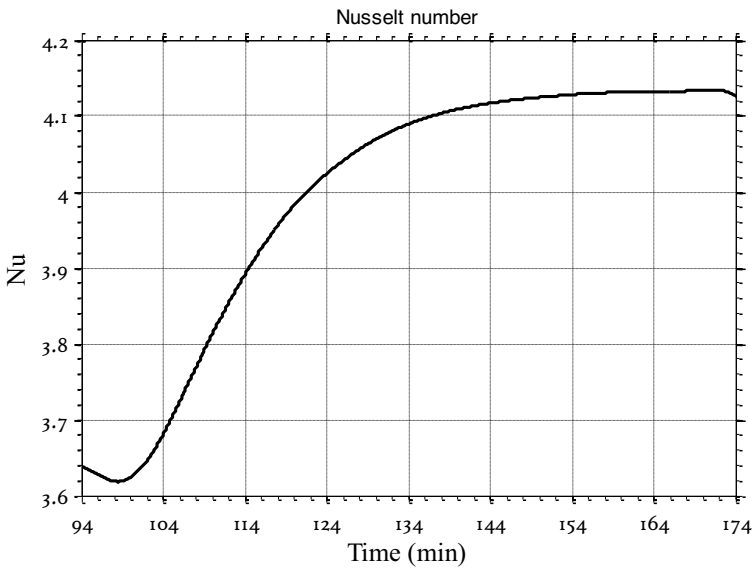


Figure I-10. Variation with time of the vertical average of the Nusselt number for natural convection.

The local and effective borehole resistances are calculated based on the simulation. The time variation of the vertical average is presented in Figure I-11 together with the effective value. The local resistance is determined based on the local heat load, the local borehole wall temperature and the local collector fluid temperatures as shown in Equation I-3:

$$R_b = \frac{T_{f\text{local}} - T_{bw\text{local}}}{q'_{\text{local}}} \quad (\text{m}\cdot\text{K}/\text{W}) \quad \text{I-3}$$

The effective resistance is determined based on the outlet and inlet temperatures from the collector, the applied heat load, and the vertical average of the borehole wall temperature as shown in Equation I-4:

$$R_b^* = \frac{T_{f\text{m}} - T_{bw\text{m}}}{q'_m} \quad (\text{m}\cdot\text{K}/\text{W}) \quad \text{I-4}$$

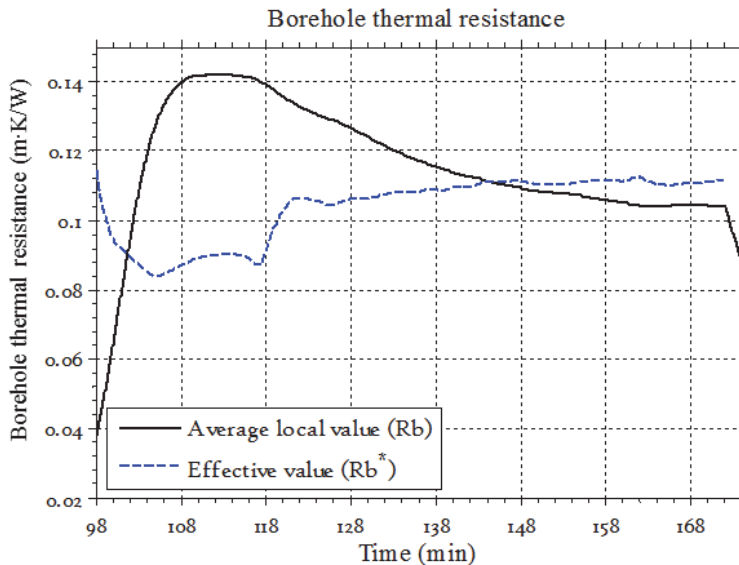


Figure I-11. Variation with time of the vertical average of the local resistance and the effective resistance.

The effective borehole resistance is in general higher than the local resistance as it reflects the sum of the local resistance and the interaction (heat transfer) between the collector pipes in the borehole. Figure I-11 has to be interpreted with Figure I-8 and Figure I-9 in mind; while energy is being extracted from the borehole, the temperature of the water in the borehole, and the heat carrier decreases. Therefore, there is initially not a direct connection between the energy extracted and the heat transfer in the borehole wall. This further elaborated on in Paper 2.

Once the heat pump is switched off, the temperature in the borehole recovers, this can be visualized in terms of the heat transfer to the borehole, i.e. the specific heat load. In Figure I-12,

the distribution of the specific heat load in the borehole is shown for the recovery period (172 – 210 minutes). The heat extraction with the heat pump stops at 172 minutes and the first profile is taken just as the mass flow stops.

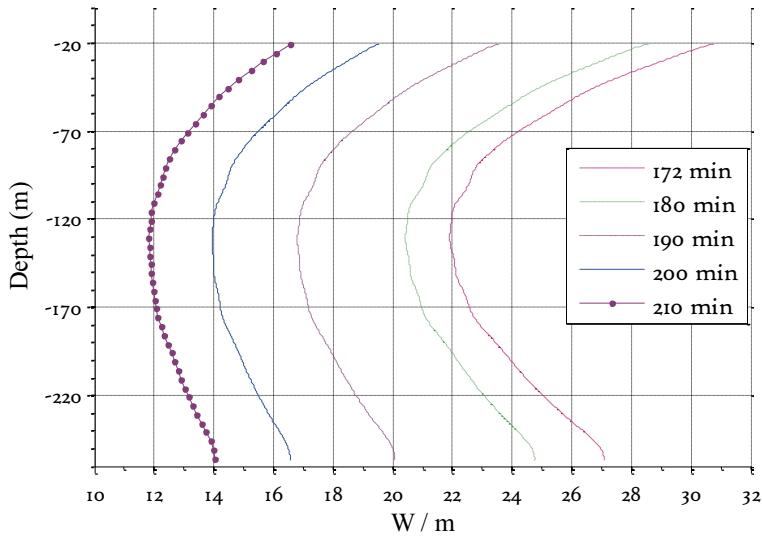


Figure I-12. Calculated distribution of the specific heat load in the borehole during thermal recovery. The mass flow in the U-tube collector is zero.

It is seen in the figure that the heat load is positive during the entire recovery period, that is, heat is being transferred from the surrounding rock to the fluid in the borehole.

I-4.7 CONCLUSIONS

The thermal performance of non-grouted BHEs has been studied using the developed transient numerical TRCM- model. The model uses a correlation to account for natural convection in a water filled BHE. The model is found to quite accurately predict the detailed experimental measurements even on a short time scale (order of minutes).

Transient effects during heat pump cycles and response test are analyzed. The importance of natural convection is studied, and it is seen that it dramatically reduces the internal resistance of the BHE.

The thermal capacitance of the water in the borehole is important primarily for the transient behavior of the BHE during shorter operation cycles as studied in Paper 1. As shown in Paper 2, the presence of natural convection enhances the heat transfer, and thus reduces the transient time period.

For longer operation periods (when a stable heat transfer is established between the collector and the borehole wall), it is primarily the rate of heat extraction or injection and the water temperature in the borehole that influences the internal resistance in the borehole.

Large differences related to natural convection are seen between heat injection (as in thermal response test) and heat extraction (heat pump operation).

The results presented in Paper 1 indicates that the specific heat load can be increased with increased borehole depth, it is also seen that the specific heat load becomes unevenly distributed with most of the energy being extracted from the deeper parts of the borehole where also the internal resistance in the borehole becomes lowest due to the effect of natural convection.

I-5 Solar assisted borehole thermal energy storage

I-5.1 INTRODUCTION

An analytical model for simulation of a solar assisted borehole thermal energy storage with separated and parallel borehole circuits is presented. The model is used to simulate and evaluate the performance of an installation at a public school in southern Norway. 24 boreholes 200 m deep are used together with a solar collector which is integrated in the school yard. The boreholes provide thermal energy to a heat pump in the cold season and are thermally recharged by heat from the solar collector in the warm season. The details of this study is presented in Paper 3 which is placed in the last part of this subsection.

I-5.2 OBJECTIVES

The main objectives for this study are:

- to study the performance of a solar assisted borehole thermal energy storage,
- to establish an analytical model that is able to simulate the thermal performance of a borehole thermal energy storage with separated and parallel borehole circuits, and
- to perform simulations to evaluate the performance of the studied system over time, including variations in operation strategies and magnitude of thermal recharge.

I-5.3 BACKGROUND

In this subsection, a system where a matrix of borehole heat exchangers is used together with a heat pump and a solar collector is studied. The focus of the study is on the local heat transfer processes in the borehole heat exchangers and on the interaction between the individual borehole heat exchangers.

An illustration of the system is shown in Figure I-13.

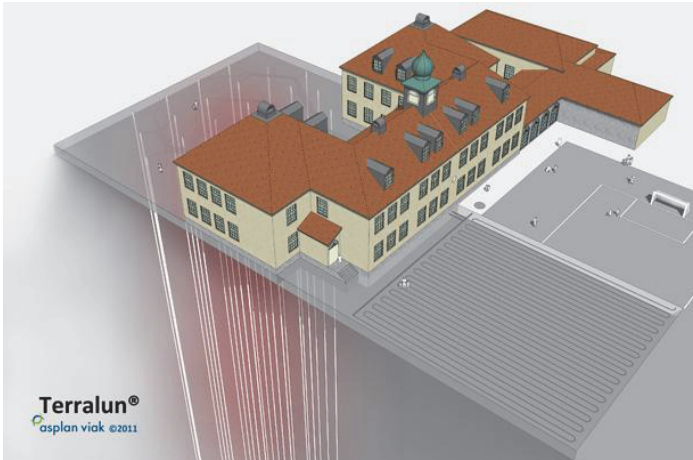


Figure I-13 System layout (Asplan viak (2014))

The system has been in operation since 2012, and the operational data (mass flow rates, temperatures, etc.) is continuously logged for every hour in a computer system.

The boreholes are closely spaced and are, thereby, able to provide a high thermal load relative to the size of the construction site. Since they are closely spaced, the performance of the individual BHEs is affected by thermal interaction with neighboring BHEs. The boreholes are connected in two parallel circuits and the layout of the boreholes is shown in Figure I-14. Both circuits are used for heat extraction in the cold season, while only the center circuit receives heat from the solar collector in the warm season.

During the first year of operation the boreholes supplied about 160 MWh of thermal energy to the heat pump and the boreholes in the center received a thermal load of about 124 MWh in the warm season.

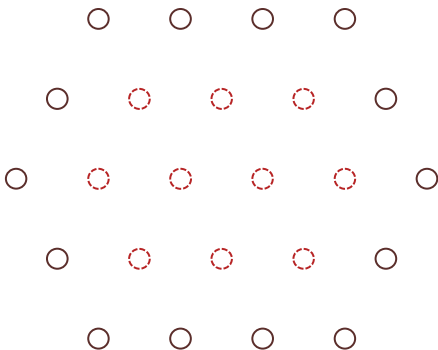


Figure I-14 Layout of the borehole installation. The boreholes are placed in equilateral triangles with 7 meter sides. The dashed boreholes represents the inner circuit.

The balance between the amount of thermal energy that is being extracted and recharged directly affects the temperature level in the boreholes. Often thermal recharge can be provided through the use of free cooling; that is, using the relatively cold heat carrier for cooling purposes without the use of the heat pump. This is an effective and economical method to thermally recharge the boreholes. Alternatively, other heat sources can be used. By injecting more heat than is being extracted, it is possible to increase the temperature level, and thereby improve the performance of the heat pump system. The temperature level can be further increased by placing the boreholes closely together with a short separation distance. The borehole system can then be categorized as a borehole thermal energy storage (BTES)

In the present study, the system delivers heat to a school building which is closed during the warm season and has, therefore, little or no need for cooling, which could have been used to thermally recharge the boreholes. To avoid a temperature decline in the system, the boreholes are instead thermally recharged with heat from the solar collector. The system layout including the solar collector is shown in Figure I-15. The figure shows the two borehole circuits in connection with the ground solar collector and the heat pump. Also the positions for temperature measurements are indicated.

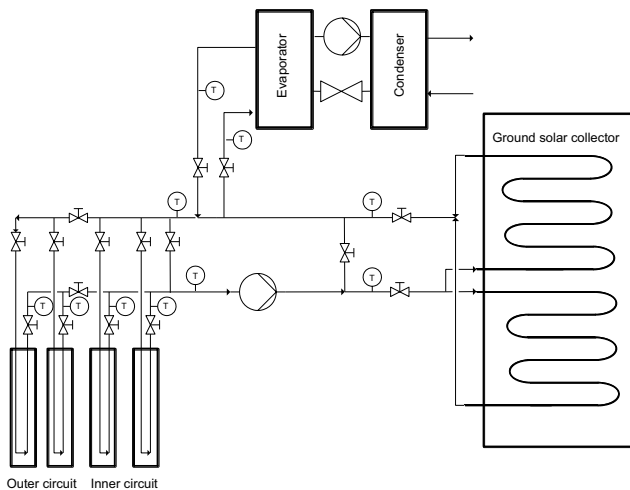


Figure I-15 System layout, the outlet temperatures from the BHEs are measured separately for each BHE, and the inlet temperature is measured before the heat carrier is distributed.

The solar collector covers about 1400 m² and consists of parallel coupled pipes that are covered by asphalt. Figure I-16 shows the installation during the construction phase.

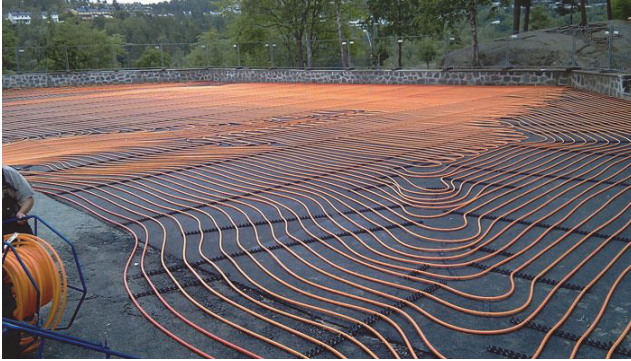


Figure I-16 Construction of solar collector (Asplan viak (2014))

The solar collector also provides heat to the heat pump in the intermediate season, while there still is a heating demand and the temperature from the solar collector is higher than the temperature from the BHEs.

In Figure I-17, the connections for the 10 BHEs in the inner circuit are shown. The return temperature is measured individually for each BHE.

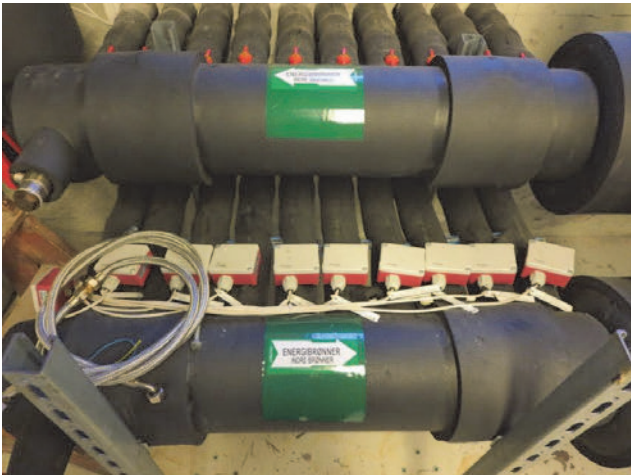


Figure I-17. Connections for inner circuit boreholes, temperature is being measured and logged on the return from the boreholes.

The logged data from the first year of operation is used as the input for this study. During the second year of operation the thermal recharge failed as the solar collector was disconnected from the system; therefore, the system was operated for 4 months without adding or extracting

thermal energy. Inlet and outlet temperatures from the BTES are shown in Figure I-18. The figure shows temperatures from January 2012 to September 2013.

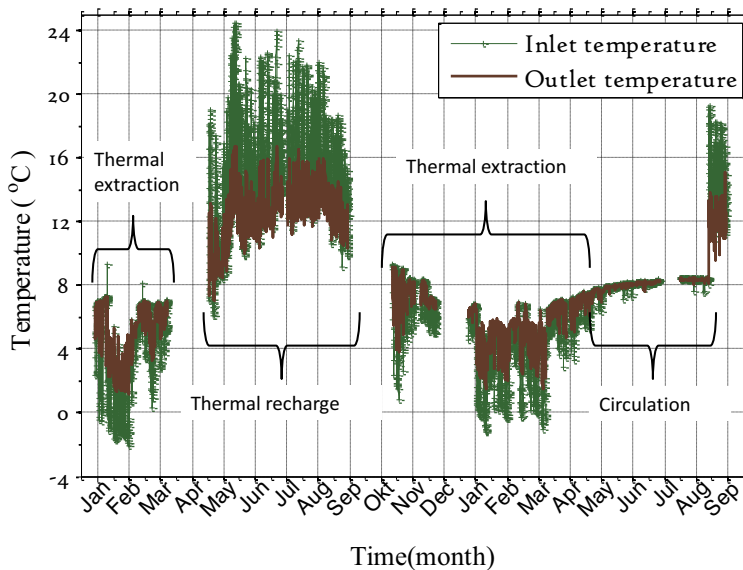


Figure I-18 BTES inlet and outlet temperatures for 2012 and 2013.

In the circulation part, the temperature of the heat carrier increases. This is mostly related to the thermal recovery of the boreholes, but also frictional losses due to fluid circulation increase the temperature. In the intermediate season, between the extraction period and the recharge period, the solar collector provides energy to the heat pump while the boreholes are disconnected. Between December 2012 and January 2013, there is a one month gap in the data where the data-logging system has failed. Several shorter gaps can as well be found in the data. This is unfortunate as it reduces the possibilities to use the data directly as a reference for modeling results.

In this study, it was decided to focus on the operational data for the first year while the data from the circulation part during the second year were not analysed.

I-5.4 METHODOLOGY

The specific system studied is constructed and operated in such a way that it cannot be accurately described by methods that are conventionally used to design and calculate the performance of BHEs, i.e. the BTES consists of two independent circuits that can be operated separately.

The boreholes are 200 m deep, and they are non-grouted in the lower part (46- 200 m) and therefore, water-filled. In water filled boreholes the heat transfer between the borehole wall and the collector occurs by thermal conduction and by natural convection; this was studied in detail

in Section I-4 and in Papers 1 and 2, where a Nusselt correlation for the convective heat transport was derived and implemented in a numerical model of a BHE. The correlation has been applied as well in the present system to determine an effective thermal conductivity for the water in the non-grouted part of the boreholes.

Regardless of the simple geometric features of a BHE, a numerical model of a BHE requires a large grid due the high aspect ratio. Transient simulation with several interacting boreholes does, therefore, require a considerable computational load. Alternatively, analytical or numerical solutions can be used to describe the performance of a BHE on a local scale and spatial superposition can then be used to account for the thermal interaction between several BHEs.

The finite line source solution, as presented in Section 2.1.1.2 is considered to be the most appropriate analytical solution for a BHE, and it is applied in this study. The assumption of a line source limits the accuracy of the solution for short time steps; therefore, the short time response from the analytical solution used in the present study is modified in accordance with a numerical model representing a more accurate description of a BHE. Temporal and spatial superposition is applied to handle the transient and changing heat load and the interaction between the boreholes.

A common assumption when simulating interacting BHEs is to assume that the heat load is equal for each BHE (Fossa et al. 2011). With this assumption, the thermal response from any evenly distributed heat load can be given instantaneously using pre-calculated response factors from analytical solutions such as applied e.g. in Javed (2012).

In the system studied, the heat load is clearly different between the inner and outer circuit since they are operated separately. As the BHEs are operated in parallel, it is logical to assume that the inlet temperature is equal to all the BHEs in operation. With this assumption (which has been applied in this study) the distribution of the thermal load between the BHEs can be determined based on an iterative scheme for each time step.

I-5.5 DISCUSSION

The developed model assumes that the inlet fluid temperature is equal for all the BHEs, i.e. the BHEs are connected in parallel. The heat load is then allowed to vary in-between the BHEs. As an alternative, it can be assumed that the heat load is uniformly distributed, which is the commonly used assumption. For most cases, these two assumptions will give the same answers. The presented model is, however, flexible in the sense that it is possible to simulate the thermal interaction between BHEs with distinctly different thermal loads. This is difficult to do with the assumption of a uniform thermal load.

Other scenarios that can be simulated with this approach are e.g. systems where there is an interaction between previously installed BHEs and new installations. This can be feasible when extending an existing BHE installation or when there is interaction between neighbouring BHE systems with distinctly different operation conditions.

I-5.6 PAPER 3: SOLAR ASSISTED BOREHOLE THERMAL ENERGY STORAGE
FOR GROUND SOURCE HEAT PUMP SYSTEM.

Holmberg, H., Ramstad, R.K., Næss, E., Sønju, O. K. (2016)

Submitted to Energy and Buildings

Solar Assisted Borehole Thermal Energy Storage for Ground Source Heat Pump System

Henrik Holmberg¹, Randi K. Ramstad^{2,4}, Erling Næss¹ Otto K. Sønju³

¹Department of Energy and Process Engineering, Norwegian University of Science and Technology

²Department of Geology and Mineral Engineering, Norwegian University of Science and Technology

³Rock Energy AS, ⁴Asplan Viak AS

Abstract

In this paper, a solar assisted borehole thermal energy storage (BTES) is presented. The operational data from the first 2 years of operation is analyzed and discussed. The BTES is constructed with two individual circuits consisting of each 10 respective 14 boreholes that are placed in a star configuration. The solar panel consists of a school yard area in which a heat carrier is being circulated through tubes approximately 10 cm below the surface. The heat is injected in the center of the BTES through the inner circuit during the summer, and extracted from both circuits in the winter. The thermal performance of the BTES is simulated with an analytical model which is presented in this paper. The results of the simulations are compared to measured data from the installation and are found to agree well. The model is used to analyze and determine the long term performance of the BTES. It is found that the thermal recharge strategy deployed at the studied installation increases the borehole fluid temperature mostly during the thermal recharge period. The potential for thermal recharge can, thereby, be increased by altering the strategy to recharge both circuits.

*Corresponding author

E-mail address: henrik.holmberg@ntnu.no

Keywords: Borehole heat exchanger, Simulation, Energy storage, Ground source heat pump system.

Nomenclature

Symbol

C	Specific heat capacity [J/kg K]
D_h	Hydraulic diameter [m]
f	Analytical function
g	Gravitational acceleration [m/ s ²]
H	Borehole depth [m]
k	Thermal conductivity [W / m·K]
L	Characteristic length scale [m]
\dot{m}	Mass flow rate [kg /s]
q'	Specific heat load [W /m]
q''	Heat flux [W /m ²]
Q	Thermal load [W]
r	Radius [m]
R_b^*	Effective borehole thermal resistance [K·m/ W]
T	Temperature [K]
t	Time [s]

Greek symbols

α	Thermal diffusivity, $k/\rho C$ [m ² /s]
ΔT	Temperature difference [K]
ρ	Density [kg /m ³]
ν	Kinematic viscosity [m ² /s]
β	Coefficient of thermal expansion [1/K]

Index

g	Ground
w	Water
f	Heat carrier
b	Borehole
i	Inner

Dimensionless numbers

Fo	Fourier number, $\frac{\alpha t}{r^2}$ [-]
K	Radius ratio r_b / r_i [-]
Ra*	Modified Rayleigh number $g\beta L^4 q'' / \alpha \nu k$ [-]

1. Introduction

Ground source heat pump systems have received a lot of attention during recent years and they constitute a way of reducing the high value energy usage for heating and cooling of buildings. The installations range from small scale systems for domestic heating to larger installations the size of smaller district heating networks. The heat pump in these systems might use the ground, the groundwater or the bedrock as a source and sink for heat. Also larger water-domains and rivers can be used with advantage.

In this paper, the novel borehole thermal energy storage (BTES) at Ljan elementary school in Norway is described and simulated. The BTES is a result of an idea competition for heating systems arranged by Undervisningsbygg, the school owner in Oslo municipality. As a part of the phasing out of fuel oil from the schools in Oslo, the main goal for Undervisningsbygg was to stimulate for innovative and green heating systems for the future.

Since Norwegian school buildings have no cooling demands, and since the accessible area for the schools in Oslo often are limited, the borehole pattern must be compact and therefore must be recharged during the summer. At Ljan school, the recharge is achieved by thermal energy from a solar collector imbedded in the schoolyard.

The performance of the BTES is simulated and analyzed using an analytical model which is presented in the paper. The studied BTES is constructed with two separate BHE circuits (one outer and one inner) which are operated independently of each other. In the summer, only the inner circuit is used for thermal recharge, it is, therefore, crucial that the simulation model is able to handle decoupled boreholes with individual heat loads and temperatures. In addition, the BHEs are non-grouted (water filled) and are therefore affected by natural convection, which reduces the internal resistance of the BHEs.

Several models exists (numerical, analytical and hybrid) that can be used to simulate borehole heat exchangers (BHEs) and the interaction between individual BHEs with different level of accuracy. In general, detailed numerical models of BHE fields become computationally heavy and are therefore, unpractical, and as a consequence, numerical models are usually used, either to study a specific phenomenon, or as a preprocessor to generate heat transfer response factors, so called g- functions that can be used in more rapid calculation schemes.

The superposition borehole model (SBM) of Eskilson [1] uses an intricate superposition of numerical solutions to account for the thermal influence between BHEs. The model is implemented in TRNSYS [2], and can be used to simulate the interaction between groups of boreholes with different thermal loads [3]. Due to the long computational time required for the model it is used mostly indirectly, through g-functions that have been precalculated and implemented in the more rapid and easier to access software such as, EED [4] and GLHEPro [5].

These g-functions are precalculated for specific layouts of BHEs and, when used, it is not possible to determine the distribution of the thermal load between the BHEs in the layout.

In the design of a BTES such as the one described in the present paper, with both a specific (and non-standard) borehole layout and a specific thermal load distribution, the user is forced to make qualified guesses regarding the performance of the system.

There are several publications on the topic of BHEs which strive to find accurate and fast methods to generate dimensionless BHE thermal response functions (g- functions) for arbitrary configurations of interacting boreholes. In general, models for interacting BHEs assume either a constant BHE wall temperature (for all BHEs), or a constant thermal load (for all BHEs) An extensive discussion on the common boundary conditions used in BHE models can be found in Cimmino and Bernier [6].

In addition to the SBM model, some well known models are the duct storage (DST) model [7] and the EWS model [8], both implemented in TRNSYS. Although these models are suitable for simulation of parallel coupled BHEs, neither of them can be used to simulate the interaction between decoupled boreholes, as needed in the present study.

There are only few analytical models available that can be used to simulate the interaction between decoupled boreholes. The authors are only aware of two publications, Lazzarotto [9] and Marcotte and Pasquier [10], in which analytical models are presented that might have the flexibility needed for simulation of the studied BTES. In these models, spectral methods (Laplace transformation and FFT transformation) are used to provide a fast evaluation of the convoluting analytical solution for temporal superposition. It is, however, noted that neither of these works provide verification with experimental data and only in [10] is a comparison with an additional model provided.

In the present paper, operational data is presented from a novel BTES which uses two separated, but thermally interacting BHE circuits. Due to the lack of appropriate models for this type of system, an analytical model has been developed and is presented. The model is suitable for simulation of the thermal interaction between several boreholes with individual thermal loads and borehole wall temperatures. The analytical model is also supplemented with a Nusselt –correlation to account for the effect of natural convection on the internal borehole resistance. The model is used to simulate the thermal performance of the studied BTES, and its performance is verified through comparison with experimental data. In addition, the effect of different ways to thermally recharge the BTES is studied.

2. Description of the BTES installation and the operation data

The three main parts of the heating system at Ljan school are the 24 boreholes, the solar collector in the 1400 m²-large asphalt paved schoolyard, and the heat pump. The purpose of the solar collector is to charge the boreholes during the summer season. The BTES consists of two separate circuits with 10 inner, respective 14 outer boreholes connected in parallel. The boreholes are placed in a pattern based on equilateral triangles where the sides are 7 meters long (Figure 1.a). The 10 inner boreholes are charged during summer, while all 24 boreholes are used for energy extraction during the heating season. The system layout is shown in Figure 1.b.

The bedrock at Ljan is Precambrian gneiss. The pre-investigations consisted of the drilling of a test borehole, temperature measurements prior to and after the thermal response test and a thermal response test. Due to a steeping terrain, the groundwater level was low, about 46 meters below the terrain surface. To utilize the length from the groundwater level to the surface, all boreholes were filled with a thermally conducting material (grout) from the groundwater level and to the top of the borehole. Beyond that, the boreholes have traditional Norwegian design with a single-U tube collector

[11] surrounded by groundwater and crystalline bedrock. The main properties of the BTES are summarized in Table 1.

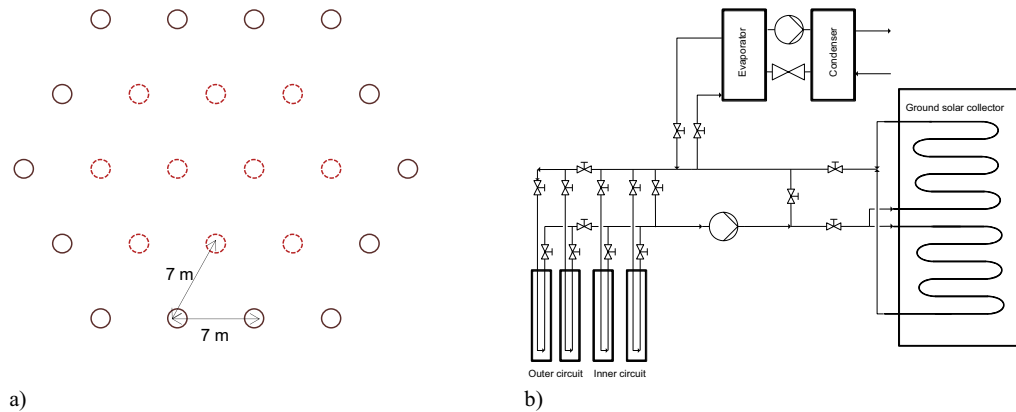


Figure 1. BTES borehole pattern and b) system layout. Boreholes in the inner circuit are dashed. The system is constructed in such way that the heat pump can take energy from either the boreholes or from the solar collector, the solar collector can also be used to recharge the boreholes.

Table 1. System parameters

Number of boreholes	24, (10+14)
H [m]	200
Water level below surface [m]	-46
r_b [mm]	59.5
U-Collector [mm]	PEM 40 x 2.4
k_g [W/(m·K)]	3.6
R_b^* [(m·K)/W]	0.08
Borehole initial average temperature [°C]	7.95
Thermal grout, k [W/(m·K)]	2

The BTES at Ljan was put into operation in December 2011. Figure 2 and Figure 3 show examples of operational data from the system. The data represent typical periods for heating load during the winter, and charging load in the spring/summer.

The operation period shown in Figure 2 represents a quite cold climate period from the 15th of January to the 31th of January 2013. The corresponding response between the specific heat load per meter borehole and the hourly variation in the collector fluid temperature from and into the boreholes is clearly observed. The daily minimum air temperature also corresponds to days where the heating load is highest, up to 35 W/m. Note that the two periods, 19th-20th, and 26th-27th are weekends, during these periods, the school building require less heating which is clearly seen in the figure. The collector fluid temperature from the boreholes (BTES T-in) is approximately 1.5 °C at its minimum.

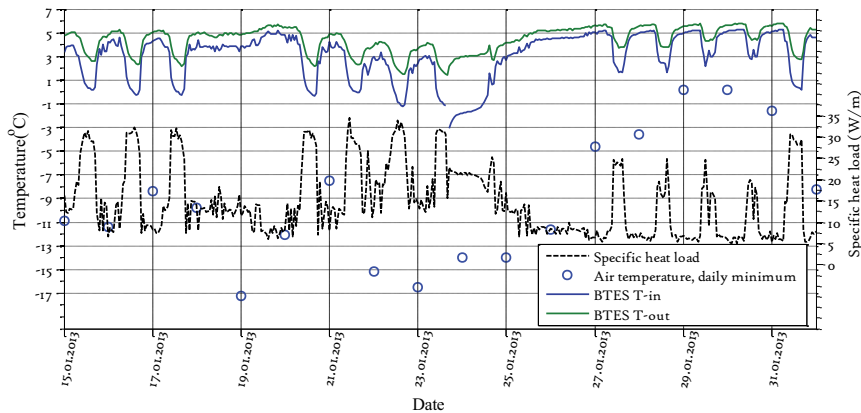


Figure 2. Example of typical operational data in heating mode for the BTES-plant at Ljan school in Oslo, Norway. The operation period represents a quite cold climate period from the 15th of January to the 31th of January 2013.

The operation period shown in Figure 3 represents a warm climate period from the 15th of May to the 31th of May 2013. The corresponding response between the specific heat charging per meter borehole and the hourly variation in the collector fluid temperature from and into the boreholes is clearly seen. The daily maximum air temperature also corresponds to days where the charging load is highest, up to 75 W/m as peak value. The collector fluid temperature from the boreholes (BTES T-out) is approximately 17 °C at its maximum.

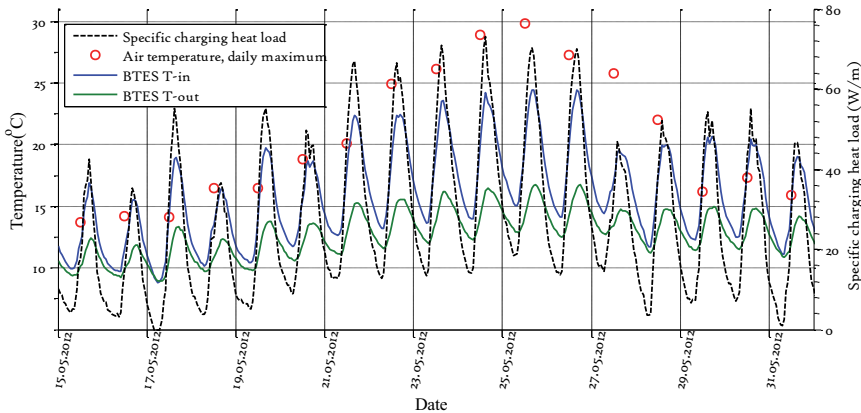


Figure 3. Example of typical operational data in charging mode for the BTES-plant at Ljan school in Oslo, Norway. The operation period represents a warm climate period from the 15th of May to the 31th of May 2013.

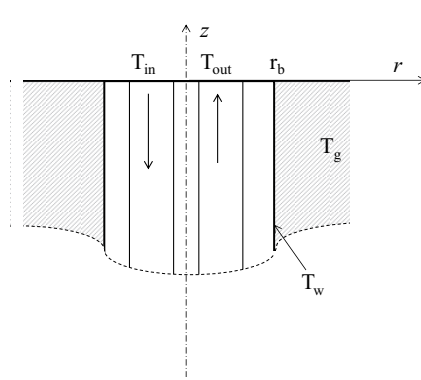
Note that the charging in this installation is limited to the 10 inner boreholes, while, if all the 24 boreholes were utilized, the potential for thermal recharge would be significantly larger.

3. BHE system model

The performance of the BTES is simulated using an analytical model, presented in the following. The model simulates the characteristics of the system and its long term performance. The model consists of an algebraic framework in which the response from an analytical solution is used to simulate the behavior of a single or multiple BHEs that may interact. The thermal load is allowed to vary in-between the boreholes, that is, a thermal load distribution is determined based on the individual borehole temperatures as determined based on previous and present loads and the interaction with surrounding boreholes, which is accounted for through spatial superposition. The complete model is implemented in Matlab® [12].

3.1. BHE thermal response model

With reference to Figure 4, the mean fluid temperature (T_f) between the inlet and outlet temperatures from the BHE can be calculated as:



$$T_f = T_g - q' R_b^* + q'(t) f(t, r_0), \quad 1$$

where

$$T_f = \frac{T_{in} + T_{out}}{2}, \text{ and} \quad 2$$

$$R_b^* = \frac{T_f - T_{wall}}{q'} \quad 3$$

Figure 4. BHE configuration with single U-tube.

q' is the heat extraction rate (W/m borehole) and R_b^* is the effective borehole thermal resistance as defined by Hellström [13], and the function f represents the temperature change due to the thermal history of the borehole which can be evaluated by several means such as numerical methods or using analytical solutions (e.g. Infinite Line Source (ILS) [14], Infinite Cylindrical Source (ICS) [15] or the Finite Line Source (FLS) [16],[17]). The differences, and applicability between these analytical solutions has been discussed in several publications [18],[19],[20].

The FLS-solution uses mirroring technique to account for the temperature at the ground's surface, and this is considered as the most appropriate analytical solution as discussed by Lamarche and Beauchamp [20].

The FLS method has been applied in the present work. While the FLS-solution is an accurate representation of the BHE on a longer time scale, it is inaccurate on a shorter time scale due to the line source assumption, which implicitly means that the interior of the borehole is assumed to have the physical properties of the surrounding ground, while the thermal load is placed in the center of the borehole. Ingersoll and Plass [14] recommended using the FLS-solution only for cases having Fourier numbers (Fo) larger than 20, which translates to 12 hours using the thermal properties and dimensions for the BHE under consideration. In spite of this, the FLS solution is applied to shorter time spans in

the present work. This is justified by the low frequency of the load variations, which are captured by the model. In addition, a method for improving the prediction accuracy for short time periods of the analytical model is presented in paragraph 3.2.5.

Following Lamarche and Beauchamp [20], $\Delta T = q'(t)f(t^*, \beta)$, where $t^* = t/(H^2/9\alpha)$, $\beta = r_b/H$, and $\gamma = 3/2\sqrt{t^*}$ the FLS -solution can be expressed as:

$$f(t^*, \beta) = A - B, \text{ where} \quad 4$$

$$A = \int_{\beta}^{\sqrt{\beta^2+1}} \frac{\operatorname{erfc}(\gamma z)}{\sqrt{z^2-\beta^2}} dz - \int_{\beta}^{\sqrt{\beta^2+1}} \operatorname{erfc}(\gamma z) dz \quad 5$$

$$B = \int_{\sqrt{\beta^2+1}}^{\sqrt{\beta^2+4}} \frac{\operatorname{erfc}(\gamma z)}{\sqrt{z^2-\beta^2}} dz + \frac{1}{2} \left(\int_{\beta}^{\sqrt{\beta^2+1}} \operatorname{erfc}(\gamma z) dz + \int_{\beta}^{\sqrt{\beta^2+4}} \operatorname{erfc}(\gamma z) dz \right) \quad 6$$

The integrals in equation 5 and 6 are evaluated numerically using global adaptive quadrature through the Integral function available in the Matlab® environment.

3.2. Analytical model

A common assumption when modeling multiple BHEs with analytical solutions (as based on e.g. the FLS solution) is that of a constant heat rate to all BHEs [21]. This assumption simplifies the solution, and reduces the required simulation time, while a reasonable accuracy is retained for most cases. The assumption does, however, result in inaccurate results for larger borehole fields and longer simulation times as pointed out by Malayappan and Spittler [22].

In the present case, the BHEs are relatively closely spaced, and the different BHEs will experience different temperature histories, resulting in different heat loads for each unique BHE. Moreover, the boreholes in the center of the BTES will experience a larger heat load after thermal recharge as they are warmer than the peripheral BHEs. In this case, the load variation between the BHEs is an important thermal characteristic of the system.

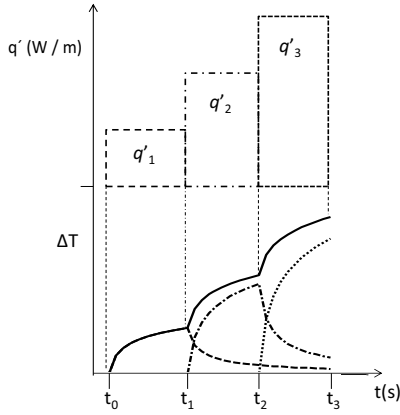
It is, therefore, important that the applied model can handle decoupled boreholes with individual heat loads and temperatures. In the proposed model for the BHE system it is assumed that the inlet temperature to all active BHEs is equal (which is logical since the BHEs are supplied in parallel from the same coolant circuit), the distribution of the thermal load is determined using an iterative scheme based on the individual temperatures of the boreholes.

The symmetry of the BTES arrangement is utilized to determine the number of individual BHEs having individual temperature and heat rate histories. For the specific case considered, the described BTES is represented by eight individual BHEs, of which four represent the inner circuit and four the outer circuit.

To account for the changes in thermal load and thermal interaction between the boreholes, the model relies highly on both temporal and spatial superposition, which is outlined in the following sections.

3.2.1. Temporal superposition.

To account for time-varying loads, temporal superposition is used. This is possible due to the temporal linearity of the heat conduction equation describing the temperature development in the ground surrounding the BHEs. Thereby, the temperature response from a series of piecewise constant heat loads can be determined by a summation of the individual responses. This is illustrated in Figure 5 where the responses from three loads are superimposed. The figure shows the incremental and total increase in borehole wall temperature due to a stepwise increase in thermal load.



Using superposition, it is possible to discretize the thermal load into short time intervals, for example hourly values, and calculate the thermal response of a BHE. It requires, however, a summation of the response for each discrete load. For a long time series of hourly load variations, this becomes a significant computational problem. To reduce the size of the problem, an aggregation scheme can be used to lump previous loads into larger periods [23], [19]. This reduces the number of individual loads to be handled and thereby the size of the computational problem. The aggregated solution is an approximation to the analytical solution and the accuracy of the aggregated solution is controlled by comparison with the non-aggregated solution.

Figure 5. Illustration of temporal superposition of three discrete loads

With reference to Figure 5 the thermal response (change in borehole wall temperature) can be determined from Equation 7 in which f is the analytical solution (Equation 4) and n is the total number of discrete loads, in this example $n=3$.

$$\Delta T = \sum_{i=1}^n q'_i [f(t^*_{t_n-t_{i-1}}, \beta) - f(t^*_{t_n-t_i}, \beta)] \quad 7$$

The aggregation principle is illustrated in Figure 6, where the discrete loads ($q'_1 - q'_3$) are replaced by a uniform load. As seen, with time the thermal response from the aggregated loads (dotted line) approaches that of the discrete loads (solid lines). Hence, historical load histories may be replaced by an aggregated load, reducing the computational complexity without losing accuracy.

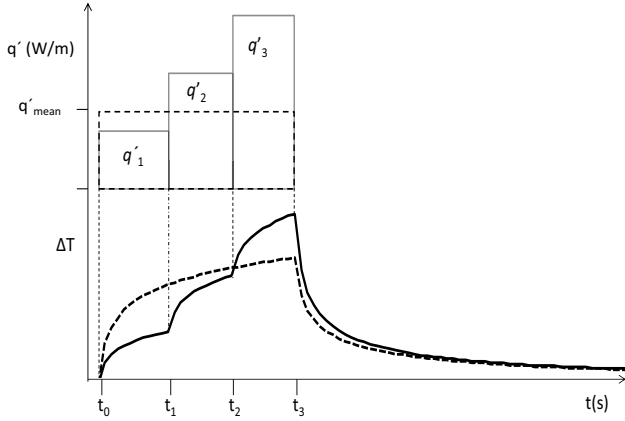


Figure 6. Thermal response from aggregated loads (dotted line) as compared to discrete loads (solid line).

The purpose of the aggregation scheme is to limit the number of individual loads that need be accounted for in the computation of the thermal response. In the present work, the scheme has been constructed so that the size of the aggregated time periods follow an exponential growth, starting with an aggregation time span of 6 hours and a minimum of 6 non-aggregated loads. This is found to be computational effective with no significant loss of accuracy.

The temporal superposition can as well be solved by spectral methods, as demonstrated e.g. in [6], [9] and [10]. This provides a faster way to evaluate the convoluting equation (Equation 7).

3.2.2. Spatial superposition

In addition to temporal linearity, the spatial linearity of the heat conduction equation also allows for superposition of the thermal response from spatially distributed heat sources. The underlying assumption is that the domain surrounding the borehole is isotropic in the radial direction.

According to Bernier [23] the mean fluid temperature for a BHE can be calculated from Equation 8:

$$T_f = T_g - q'R_b^* - q'f(t) + T_p \quad 8$$

T_p represents the temperature influence from neighboring boreholes, and in the case of uniformly distributed loads it can be evaluated as a mean value for the entire BTES (also referred to as the temperature penalty). In this work, however, T_p represents the sum of all thermal influences that are superimposed on the individual BHE being evaluated. In order to determine T_p , the analytical solution has to be evaluated for each unique distance in the borehole field, in this case, there are 24 individual distances, as illustrated in Figure 7 for some distances. There are 8 individual boreholes (4 each from the inner respective outer circuit) for which the thermal interaction and load will be unique, these boreholes are shown inside the dashed line in Figure 7.

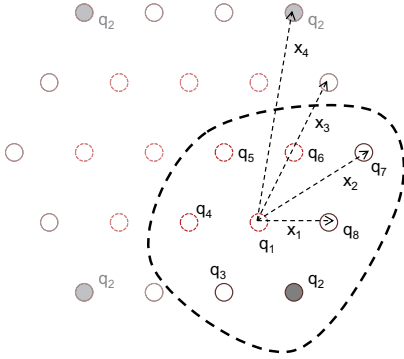


Figure 7. Spatial superposition, the symmetry of the borehole field is used to minimize the number of boreholes that has to be calculated. Boreholes with unique thermal load are shown within the dashed line. Distances to the other boreholes are denoted x , there are in total 24 unique distances of which 4 are shown in the figure.

If the individual boreholes are denoted M , and the total number of boreholes is N , the mean fluid temperature for each individual borehole can be determined as:

$$T_{f(M,t)} = T_g - q'_{(M,t)} R_b^* - \mathbf{q}'_{(M,t)} f(\mathbf{t}^*, \beta) + T_{p(M,t)} \quad 9$$

The first three parts of Equation 9 represents the local temperature change due to past ($\mathbf{q}'_{(M,t)}$) and present ($q'_{(M,t)}$) thermal loads. The last part ($T_{p(M,t)}$) represents the thermal influence from the other BHEs and is determined by Equation 10.

$$T_{p(M,t)} = \sum_{i=1}^N \mathbf{q}'_{(i,t)} f(\mathbf{t}^*, \beta_{(i)}) \quad 10$$

$\beta = x_{(i)}/H$, x is the distance to neighboring boreholes, the thermal load history for each borehole in the system is used to determine the total thermal influence (T_p). It is, however, only necessary to determine T_p for each individual group of BHEs, i.e. each corner BHE that have the unique thermal load history q_2 (filled circles in Figure 7) experiences the same thermal influence from the neighboring BHEs.

When solving for the mean fluid temperature in Equation 9, it is required both that the total thermal load is consistent with the input to the BTES, and that the inlet fluid temperature is equal for all BHEs. This is expressed through Equations 11 and 12:

$$\mathbf{Q}(t) = H \sum_{i=1}^N \mathbf{q}'_{(i,t)} \quad 11$$

$$T_{in(1:N,t)} = \frac{1}{N} \sum_{i=1}^N T_{in(i,t)} \quad 12$$

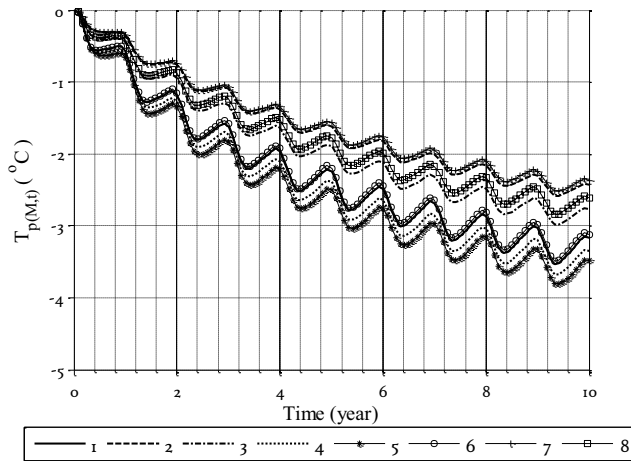
The inlet fluid temperature is determined as:

$$T_{in(M,t)} = T_{f(M,t)} - q'_{(M,t)} / (2\dot{m}C) \quad 13$$

The mean fluid temperature for each individual group is solved through an iterative procedure in which the residuals of successive calculations of Equations 11 and 12 are minimized. The average mean fluid temperature for the BTES is then determined from Equation 14:

$$T_f = \frac{1}{N} \sum_{i=1}^N T_{f(i)} \quad 14$$

It should be mentioned that the iterative procedure does not have any larger influence on the computational load which is essentially governed by the temporal superposition.



It is most illustrative to show the results from Equations 9- 14 for a case where the thermal load is negatively balanced, i.e. more energy is being extracted from the boreholes than recharged. Figure 8 show the total thermal influence experienced by each individual group of BHEs as determined by Equation 10. For single borehole placed far away from each other, $T_p=0$.

Figure 8. Thermal influence experienced by each group of BHEs in Figure 7

The curves are numbered according to Figure 7, as observed; BHEs nr 5, in the center of the system experiences the largest thermal influence. The distribution of the thermal load in-between the BHEs is shown in Figure 9, where the maximum load for each year is shown as normalized by the initial load (year 1). It is seen that rather large difference in thermal load between the BHEs in the center of the BTES (e.g. group 5) and in the periphery, (e.g. group 7).

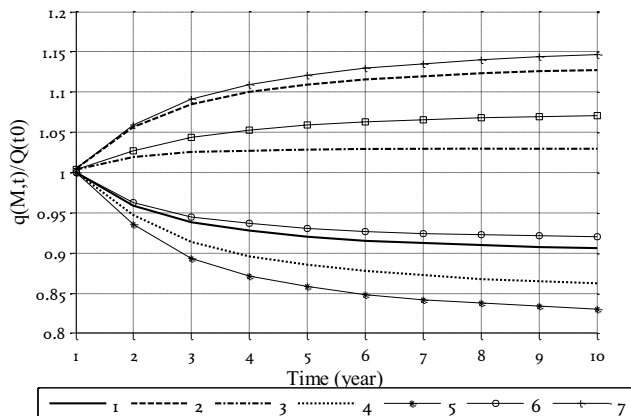


Figure 9. Thermal load experienced by each group of BHEs in Figure 7, the figure is based on the maximum thermal load for each BHE group each year.

The load distribution is proportional to the thermal influence and is reflected by the local temperature change as shown in Figure 10.a. Note that BHEs nr 5 experiences the least temperature drop. Figure 10.b show the mean fluid temperatures as determined by Equation 9, this is then the sum of the local temperature changes (Figure 10.a) and the thermal influence (Figure 8).

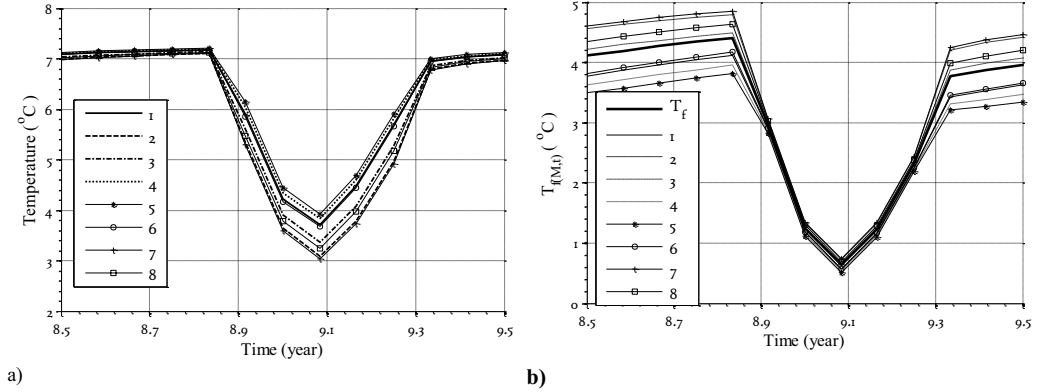


Figure 10. a) Mean fluid temperatures from the BHEs without considering T_p . b) Mean fluid temperatures from the BHEs.

While energy is being extracted the mean fluid temperature is almost uniform in-between the BHEs. The average mean fluid temperature T_f as determined by Equation 14 is as well seen in Figure 10.b.

3.2.3. Superposition of peak load

The mean fluid temperature can be determined either on a rather short time scale, in the order of hours, or it can be determined with larger time scales, such as monthly values. The large time scales provide results for average temperature variations; peak values can be determined on a shorter time scale and then superpositioned onto the average values, as shown in Equation 15 and 16 with reference to Figure 11. Such superposition is used e.g. in the commercial software EED [4].

$$T_f = T_f + \Delta T_{peak} \quad 15$$

Where,

$$\Delta T_{peak} = \left(q'_{p(M,t)} - q'_{mean(M,t)} \right) R_b^* - q'_{p(M,t)} f(t_p^*, \beta) \quad 16$$

t_p is the duration of the peak load.

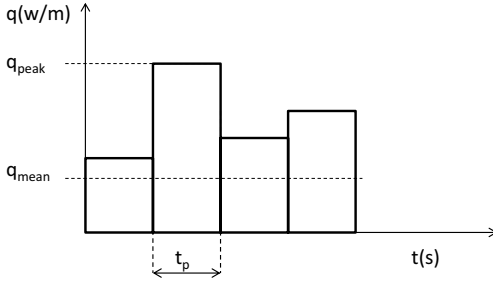


Figure 11. Superposition of thermal response from peak load and from mean load values

3.2.4. Borehole thermal resistance.

The effective borehole thermal resistance R_b^* , as defined in Equation 3, can be determined in a number of ways. For grouted boreholes, the heat transfer between the collector pipe and the ground is primary by thermal conduction, and in such cases the appropriate method is well documented by e.g. Lamarche et al. [24]. For non-grouted (water filled) BHEs, the heat transfer is enhanced by natural convection caused by temperature differences in the borehole during BHE operation. This has been noticed by several authors during thermal response tests, e.g. Kjellsson [25] and Gehlin [26]. The phenomenon has been studied in more detail by Gustafsson [27] and by Holmberg et al. [28]. For such situations, R_b^* is a function of the water temperature in the borehole and the wall-to-fluid temperature difference.

For the BTES considered in this paper, the evaluation of R_b^* is further complicated by the upper 46 m section of the boreholes being filled with grout. In this section the thermal resistance can be considered constant (for constant mass flow rates), while the thermal resistance varies according to the operating conditions of the system in the water filled part.

A thermal response test was performed prior to the grouting of the upper part of the borehole. The effective borehole thermal resistance R_b^* , was determined to 0.08 (m·K)/W. The applicability of this result is, however, limited since the measurement was disturbed by ground water inflow in the upper part of the borehole.

Holmberg et al. [28] derived a correlation to describe the influence of natural convection on the heat transfer in water filled boreholes, Equation 17. The correlation was applied in a numerical model to determine the heat transfer on a local scale. The results from the model were found to agree well with experimental data [29].

$$Nu = 0.1743Ra^{*(0.233-0.009K)}K^{0.442}, \quad 17$$

In Equation 17, Ra^* is the modified Rayleigh number and K is the radius ratio. The characteristic length scale used in the Rayleigh number and the radius ratio are based on the hydraulic diameter of the BHE.

$$L = D_h/2 \quad 18$$

$$K = r_b/(r_b - D_h/2) \quad 19$$

In the present work, Equation 17 is used to account for the influence of natural convection on a global scale, that is, the average heat flux and water temperatures in the BHEs are used. The physical properties of water are evaluated from NIST [30]. Equation 17 is used to determine an effective thermal conductivity of the water in the boreholes by Equation 20.

$$k_{w\text{effective}} = k_w N_u. \quad 20$$

The multipole method of Bennet et al. [31], as described in Lamarche et al. [24] is used to determine the effective borehole thermal resistance. Since the upper part of the borehole is grouted, the effective borehole resistance is also determined assuming a thermal conductivity of 2 W / m K for the thermal grout [32]. The total effective borehole resistance for the BHEs is then determined by weighting the effective resistances with their respective share of the borehole length.

For the monthly simulations, R_b^* has been varied between two fixed average values depending on whether energy is being injected or extracted.

3.2.5. Improving the short-term accuracy

Improvements on the short term accuracy of the solution can be achieved by using a more accurate representation of the BHE for the short time intervals. Javed [19] proposed to use a more accurate analytical solution for time spans less than 100 hours. Here, a similar approach has been adopted, where the thermal response solution from a numerical model is applied for the first hours. The numerical model is a simple axisymmetric representation of the BHE (Figure 12), which serves the purpose of preserving the thermal characteristics to an acceptable degree. The numerical model is implemented in the commercial finite element software Comsol Multiphysics [33].

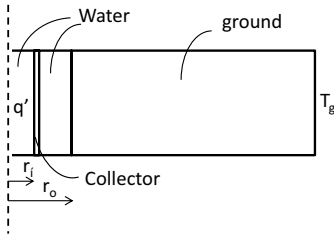


Figure 12. Layout of numerical model used to evaluate the thermal characteristics of the BHE.

In the numerical model the thermal load is applied as an internal heat source to the fluid in the center pipe, which has the same internal cross-sectional area as the U-tube collector. The thermal response from the numerical model is evaluated for a time period until it approaches the FLS- solution, which for the specific configuration simulated here occurs at about 140 hours.

As the distribution of the thermal load is determined successively for each time step in the model, it is not directly possible to skip forward to the last time step, and thereby limit the computational time required. The model is used on a standard laptop (dual core 2.53 GHz with 8 GB RAM), the simulation time (CPU – time) required to solve 240 time steps (20 years x 12 months) for different configurations, is shown in Table 2

Table 2. CPU time for 240 time steps

Configuration	Total time (s)	Precalculation of g-function (s)
3x4	30	8
6x4	65	15
6x6	78	17
8x8	243	30
10x 10	836	44

4. Results from modeling

Selected results from the modeling part are shown hereunder. The BTES is simulated using measured input data both on an hourly time scale and using averaged monthly values. The measured data is missing for some time periods, making the comparison between measured data and simulation results difficult. These ‘blind spots’ where data are missing have been accounted for as operation stops in the simulations (i.e. no heat extraction or charging). No attempts have been made to assume load profiles for these ‘blind spots’ for the hourly simulations, but for the simulations using averaged monthly values assumptions have been made regarding the load in the largest data gaps.

4.1. Simulation results using hourly variations

Simulations using input data having one-hour resolution are performed using the presented model. Measured BHE inlet and outlet temperature and mass flow rate are used to determine the thermal load to the BTES. This is then used on an hourly basis together with the mass flow rate in the simulation. The initial temperature of the ground and the thermal properties are in accordance with the performed thermal response test. The effective borehole thermal resistance varies with the temperature of the water in the boreholes and the applied thermal load. Selected parts of the results from the hourly simulation are shown hereunder. The results were selected to demonstrate the simulation during thermal extraction and thermal recharge. The results are also compared with simulations based on averaged monthly values in the next section.

In Figure 13 the mean BHES fluid temperature, as determined from the simulations and from the measurements is shown for the first 14 months of operation.

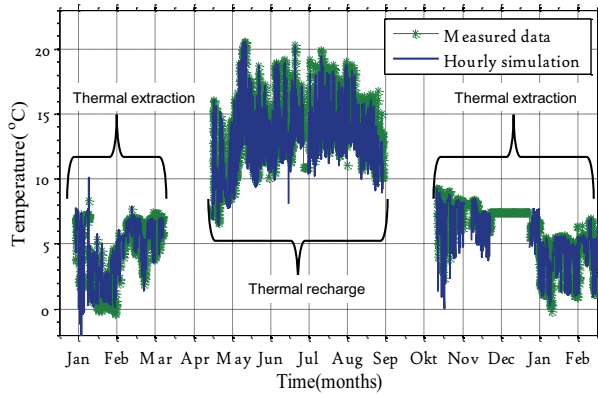
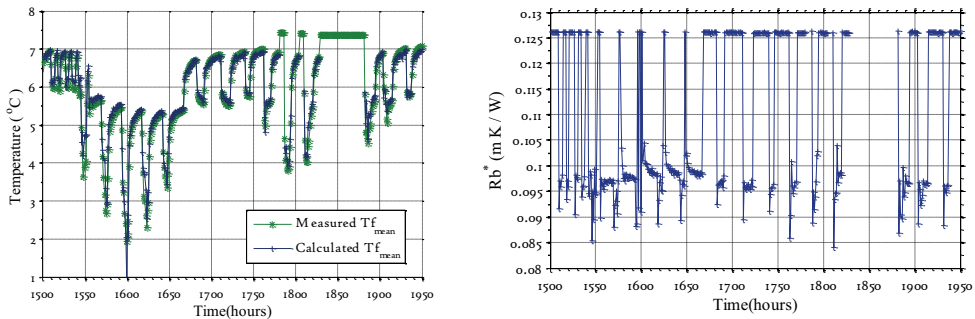


Figure 13. Measured and calculated mean fluid temperatures based on hourly input data.

In general, the predictions are observed to agree well with the measurements. It is, however, observed that minor discrepancies occur after periods where measurement data are missing, as is to be expected. In Figure 14.a the mean BHES fluid temperature for a 450 hr thermal extraction period is shown, corresponding to the end of March period in Figure 13. Also, the effective borehole thermal resistance is shown for the equivalent period.



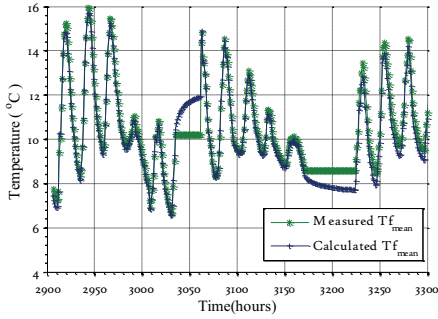
a)

b)

Figure 14. a) Measured and calculated mean fluid temperature during thermal extraction. b) Effective borehole thermal resistance.

The figure illustrates the mean fluid temperature variation during thermal extraction, and the heat pump operates in the periods seen as downward peaks, while the smooth curves correspond to the periods where no thermal energy is being extracted and where the temperature in the BTES recovers. The simulations are seen to correspond well with the measurements. R_b^* varies between 0.085 (m·K)/W and 0.126 (m·K)/W.

Figure 15 shows the mean fluid temperature during a 400 hr long thermal recharge period, corresponding to the startup of the thermal recharge in the middle of May Figure 13. Also, the effective borehole thermal resistance is shown for the equivalent period.



a)

b)

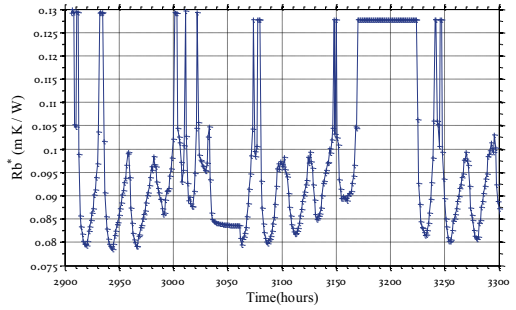


Figure 15.a) Measured and calculated mean fluid temperature during thermal recharge. b) Effective borehole thermal resistance.

The fluid temperature from the solar collector is sufficiently high to provide thermal recharge also during nighttime. For the two periods where logging data is missing (starting at around 3040 hrs and 3170 hrs) thermal extraction is assumed halted in the simulations, this influences the results, and it is observed that after the second period, the simulated temperature underpredicts the measured values slightly. This is expected, as the system in reality also receives energy during these periods. R_b^* varies between 0.078 (m·K)/W and 0.13 (m·K)/W.

Lower values of R_b^* in Figure 14.b and Figure 15.b correspond to periods where the thermal load is high. The temperature differences in the boreholes then triggers natural convection which reduces the heat transfer. The changes in R_b^* due to the influence of natural convection is somewhat lower than expected in a non-grouted BHE, this is because the upper part of the boreholes are grouted.

4.2. Conclusions from hourly simulations.

Simulation of the BTES on an hourly scale can be used to accurately determine the temperatures and operation conditions of the system. Despite the gaps in the input data, the model is able to replicate most of the variations in fluid temperatures accurately. The implementation of a Nusselt correlation to account for the effects of natural convection proved to be successful. In the present case it is, however, seen that the hourly simulations are susceptible to noise in the measured temperatures and mass flow. These fluctuations can be reduced by time-averaging the measurements. In the following section, results from simulations with monthly values are presented.

4.3. Simulation results using monthly values

While the hourly simulations provide detailed insight of the variations in mean fluid temperature on a time scale relevant for the operation of the system, the simulations based on monthly averaged input values can be used to study the long-term performance of the system. In this section, it is primarily the long term influence of different recharge strategies that is analyzed. For the considered BTES the thermal recharge is only applied to the center boreholes, and the influence of this strategy is compared to a recharge strategy where all boreholes are recharged. Also, the changes in mean fluid temperature with different magnitudes of thermal recharge are compared. To illustrate the connection between

simulations based on hourly and monthly values, the mean BTES fluid temperature for the first 14 months is shown based on hourly simulations, measurements, and on monthly simulations in Figure 16. The monthly simulation is based on the values shown in Table 3.

Table 3. Monthly load values

	Base load	Peak load	R_b^*
	MWh	W/m	(m·K)/W
Jan	40.12	30	0.11
Feb	31.35	30	0.11
Mar	31.46	30	0.11
Apr	-0.49	--	0.085
May	-26.71	-60	0.085
Jun	-30.05	-60	0.085
Jul	-30.41	-60	0.085
Aug	-29.59	-60	0.085
Sep	-6.84	--	0.085
Oct	0	--	--
Nov	15.16	30	0.11
Dec	40.80	30	0.11
Sum	34.7		

The thermal response from a peak load of 30 W/m (thermal extraction) respective 60 W/m (thermal recharge) with duration of 12 hours has been superpositioned to the mean fluid values. The effective borehole thermal resistance is kept at constant values determined from the hourly-based simulations. Qualified assumptions have been made to correct for the parts where data is missing.

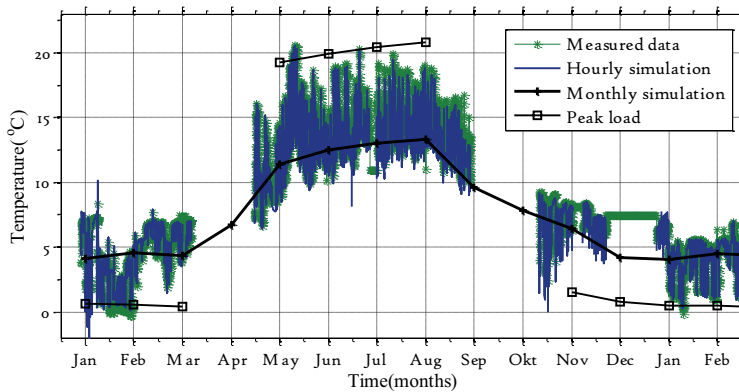


Figure 16. Measured and calculated mean fluid temperatures on hourly basis together with temperatures calculated on a monthly average. (Peak load values have been calculated by superposition of the mean value and peak values of 30 W/m (thermal extraction) respective 60 W/m (thermal recharge) for 12 hours.)

It is seen from Figure 16 that the results from the simulation using monthly averaged values correspond well with both the hourly simulations and the measurements. The peak load values were chosen based on the measured data, most of the measurements are within the range of the peak loads, although the thermal extraction period does have some load peaks in the range of 40 W/m, and the

recharge period in the range of 70 - 75 W/m, these are also observed to exceed the simulated peak load.

4.4. Recharge strategy

The objective of the thermal recharge is to replenish the thermal energy that has been extracted from the BTES during the cold period. Thereby the temperature of the BTES can be kept at a near constant temperature for many years.

To illustrate the effect of different thermal recharge loads, the three cases in Table 4 are simulated. Case 1 is equivalent to the case that is shown in Table 3 and Figure 16. Case 2 is with half the thermal recharge of Case 1 and Case 3 is with double the thermal recharge of Case 1.

Table 4. Cases with different recharge load, case 1 is equivalent to the case in table 1.

	Case 1	Case 2	Case 3	R_b' (m·K)/W
	Base load MWh			
Jan	40.12	40.12	40.12	0.11
Feb	31.35	31.35	31.35	0.11
Mar	31.46	31.46	31.46	0.11
Apr	-0.49	-0.245	-0.98	0.085
May	-26.71	-13.35	-53.42	0.085
Jun	-30.05	-15.02	-60.1	0.085
Jul	-30.41	-15.2	-60.82	0.085
Aug	-29.59	-14.79	-59.18	0.085
Sep	-6.84	-3.42	13.68	0.085
Oct	0	0	0	--
Nov	15.16	15.16	15.16	0.11
Dec	40.80	40.80	40.80	0.11
Sum:	34.7	96.8	-89.4	

Peak load, 30 W/m for 12 hours.

The resulting calculated minimum temperatures during thermal extraction are shown based on monthly averaged values in Figure 17 and with a super-positioned peak load of 30 W/m for 12 hours in Figure 18 The peak load is constant for all three cases and it shifts the curves downwards.

It is seen that for Case 1, the temperature decreases with less than one degree during 20 years, and this is because the system is nearly balanced in this case. In Case 2, the temperature decreases further and is approximately 1.7 K lower than for Case 1 after 20 years. In Case 3, the thermal recharge is higher, and as a result the temperature increases.

The COP of the heat pump is directly related to the evaporator temperature, and a change of 1 K can affect the COP with 2- 3 % [34]. For Case 3 the minimum temperature after 20 years is 3. 5 degrees, this can therefore be translated into a increase of coefficient of performance (COP) for the heat pump on the order of 9 % relative to Case 1, and 13 % relative to Case 2.

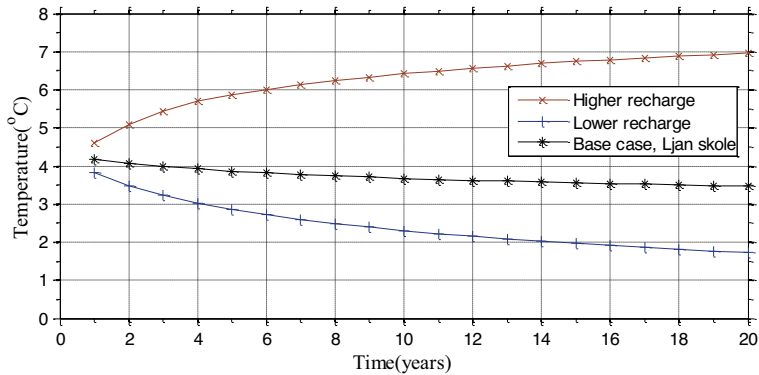


Figure 17. Minimum mean fluid temperature based on monthly average

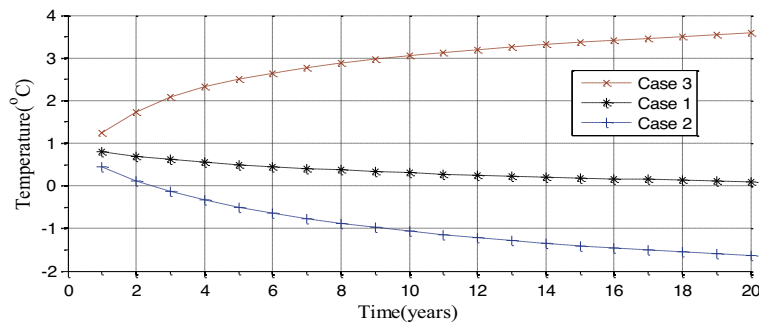


Figure 18. Minimum mean fluid temperature based on monthly average, with superposition of a peak load of 30 w/ m with duration of 12 h

It is apparent that thermal recharge is needed for the BTES to keep a stable temperature. Increasing the thermal recharge has a positive effect on the performance of the heat pump. It is, however, the overall system performance that has to be evaluated as increased thermal recharge might come at the price of increased use of high value energy.

In the following, two thermal recharge strategies are compared. Firstly, the strategy applied in the presented BTES (recharge to center boreholes) and secondly, recharge to all boreholes. In Figure 19 the mean fluid temperatures during year 24 and 25 are shown for the two strategies.

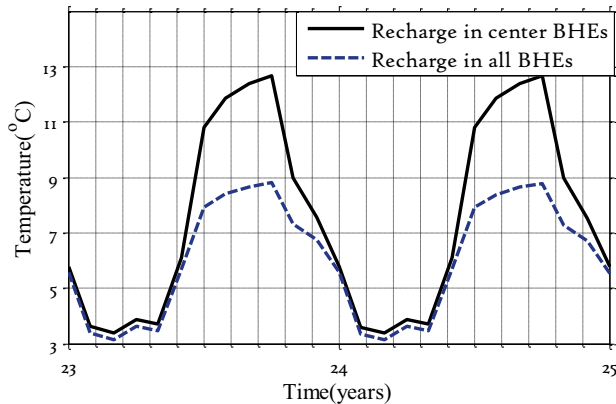


Figure 19. Thermal recharge in center BHEs and in all BHEs

The load profile is equal for both cases and the peak load has been neglected. It is seen that there is a small difference in the temperature during heat extraction, indicating that the BTES is able to reach a higher temperature when the energy is being injected in the center boreholes. It is, however, also clear that the temperature needed for thermal recharge is higher when recharging only the center boreholes.

The potential for thermal recharge depends on the temperature and nature of the energy source as well as the temperature and size of the BTES. With thermal recharge in all boreholes it is possible to either increase the thermal recharge or reduce the temperature level during recharge. This would then require an increased use of high value energy for circulation of the heat carrier. The optimal solution is therefore a function of the type of energy source used for thermal recharge, the requirements for high value energy, and in the end, the influence on the heat pump performance. In the cases compared in Figure 19, the difference in mean fluid temperature during thermal recharge is less than 4 K, with an increase in thermal recharge load this difference increases, and with an assumed double thermal recharge load the difference is more than 8 K.

5. Conclusions

Operational data from the first year of operation of a novel solar assisted BTES have been presented. The BTES consists of two independent but thermally interacting BHE circuits and it is operated in such a way that the performance of the system cannot be accurately determined using conventional dimensioning software's, e.g. EED.

There is a lot of knowledge and understanding that can be gained just from analyzing the operational data; unfortunately there are some gaps in the measurements which introduces uncertainties in the interpretation.

To analyze and predict the long term behavior of the BTES an analytical model has been constructed. The model is based on the finite line source solution and it is constructed and presented in such a way that it can be used to simulate and evaluate the performance of arbitrary configurations of BHEs with arbitrary heat load distributions. Since the BHEs in the specific case are non-grouted, the model has

been complemented with a Nusselt- correlation to account for the influence of natural convection on the effective thermal resistance of the BHEs.

Results from simulations made on an hourly and a monthly basis are presented; this can be seen as an upper and lower limit to what might be practical with the model.

The model is found to agree well with measurements for the first year of operation, further evaluation will have to be made to measurements for longer time periods once available.

The flexibility gained from the modeling approach is worth commenting on since it makes it possible not only to simulate arbitrary layouts of BHEs on a short time-scale, it also makes it possible to control the behavior by varying the thermal load distribution in the system, as shown in the presented results. This is feasible e.g. in the case of expanding an existing BTES.

Acknowledgments

The authors are grateful to Asplan Viak AS for making the measurements available and for assisting with information on the system. The paper was written with funding from the Norwegian centre for renewable energy (SFFE).

References

- [1] Eskilson. P.,(1986) Superposition borehole model. Manual for computer code. Lund Sweden: University of Lund
- [2] TRNSYS <http://www.trnsys.com/>
- [3] The Superposition Borehole Model for TRNSYS 16 or 17 (TRNSBM) <http://repository.supsi.ch/2839/1/143-Pahud-2012-TRNSBM.pdf> accessed: 22-09-2014
- [4] EED- Earth Energy Designer, version 3.16 (2010) www.Buildingphysics.com
- [5] GLHEPro 4.1 for Windows, Users' Guide, School of Mechanical and Aerospace Engineering, Oklahoma State University.
- [6] Cimmino M., M. Bernier (2014) A semi-analytical method to generate g-functions for geothermal bore fields. *Int Journal of Heat and Mass Transfer*, v 70, pp. 641- 650.
- [7] Hellström. G., (1989) Duct ground storage model. Manual for computer code. Lund Sweden: University of Lund
- [8] Wetter M., Huberg. A (1997) Vertical Borehole Heat Exchanger EWS model .
- [9] Lazzarotto A. (2014) A network-based methodology for the simulation of borehole heat storage systems.*Renewable Energy*, v 62, pp. 265- 275
- [10] Marcotte. D., P. Pasquier (2014) Unit-response function for ground heat exchanger with parallel, series or mixed borehole arrangement. *Renewable Energy* v 68, pp. 14- 24
- [11] Muovitech, <http://www.muovitech.com/pdf/turbo.pdf>, access data: 07.06.2014
- [12] Matlab R2013a, The MathWorks Inc., Natick, Massachusetts, United States.
- [13] Hellström. G., (1991) Ground Heat Storage, Thermal analyses of Duct Storage Systems, Theory. Department of Mathematical physics , University of Lund, Sweden
- [14] Ingersoll. L.R., H.J. Plass., (1948) Theory of the ground pipe heat-source for the heat pump, *Heating, Piping, Air Conditioning Journal* v 20, Nr 7, pp. 119-122
- [15] Carslaw, H.S., J.C. Jaeger., (1959) *Conduction of heat in solids*, second ed, Oxford University press, Oxford.
- [16] Claesson. J., P. Eskilson, *Conductive heat extraction by a deep borehole, analytical studies*, Tech. Rep., Lund University, Sweden, 1987.

- [17] Zeng, H., N. Diao., Z. Fang., (2002) A finite line-source model for boreholes in geothermal heat exchangers, *Heat Transfer Asian Research*, v 31, pp. 558–567.
- [18] Marcotte, D., P. Pasquier., F. Sheriff., M. Bernier (2010) The importance of axial effects for borehole design of geothermal heat-pump systems. *Renewable Energy* v 35, pp. 763- 770
- [19] Javed, S., (2012) *Thermal Modelling and Evaluation of Borehole Heat Transfer*, Doctoral Thesis, Department of Energy and Environment. Chalmers University of Technology
- [20] Lamarche, L., B. Beauchamp., (2007) A new contribution to the finite line-source model for geothermal boreholes, *Energy and buildings*, pp. 188-189
- [21] Fossa, M., (2011) The temperature penalty approach to the design of borehole heat exchangers for heat pump applications. *Energy and Buildings*, v 43, pp. 1473-1479.
- [22] Malayappan, V., J.D. Spitler (2013). Limitations of using uniform heat flux assumptions in sizing vertical borehole heat exchanger fields. *Proceedings of Clima 2013*, Prague, Czech Republic.
- [23] Bernier, M., P.Pinel, R. Labib and R.Paillet., (2004), A multiple load aggregation for annular hourly simulations of GCHP systems, *HVAC&R Research* v 10, Nr4, pp. 471-87
- [24] Lamarche, L., S. Kaji., B. Beauchamp., (2010) A review of methods to evaluate borehole thermal resistance in geothermal heat-pump systems. *Geothermics*, v 39 pp. 187-200
- [25] Kjellsson, E., (2009) *Solar Collectors Combined with Ground-Source Heat Pumps in Dwellings, Analyses of System Performance*. Doctoral thesis, Building Physics. University of Lund, Sweden.
- [26] Gehlin, S., (2002) *Thermal Response Test Method Development and Evaluation*, Doctoral Thesis, Department of Environmental Engineering. Luleå University of Technology. Sweden.
- [27] Gustafsson, A.-M., (2010) *Thermal Response Test, influence of convective flow in groundwater filled borehole heat exchangers*. Doctoral Thesis, Department of Civil, Mining and Environmental Engineering. Luleå University of Technology. Sweden.
- [28] Holmberg, H., Næss, E., Sønju, K. O, (2016) Numerical model for non- grouted borehole heat exchangers, Part 1- Development. Submitted to *Geothermics*
- [29] Holmberg, H., Acuña, J., Næss, E., Sønju, K. O, (2016) Numerical model for non- grouted borehole heat exchangers, Part 2-Evaluation. *Geothermics* v 59 pp. 134-144
- [30] Lemmon, E.W., M.O. McLinden and D.G. Friend, (2012) "Thermophysical Properties of Fluid Systems" in *NIST Chemistry WebBook, NIST Standard Reference Database Number 69*, Eds. P.J. Linstrom and W.G. Mallard, National Institute of Standards and Technology, Gaithersburg MD, 20899, <http://webbook.nist.gov>, (retrieved December 4, 2012).
- [31] Bennet, J., Claesson, J., Hellstrom, G., 1987. Multipole Method to Compute the Conductive Heat Transfer to and between Pipes in a Composite Cylinder. *Notes on Heat Transfer 3-1987*. Department of Building Physics, Lund Institute of Technology, Lund, Sweden.
- [32] Mikolit-Thermoseal (2014) Technical data, <http://www.mgs.co.uk/data/pdf/203.pdf>, (retrieved February 24, 2014).
- [33] Comsol multiphysics 4.3a, (2014) Comsol Inc, Stockholm, Sweden.
- [34] Acuña J. Distributed thermal response tests- new insights on u-tube and coaxial heat exchangers in groundwater-filled boreholes. Doctoral Thesis, KTH, Stockholm 2013.

I-6 Deep coaxial borehole heat exchangers

I-6.1 INTRODUCTION

In places where there is a scarcity of available construction area, the number of required boreholes for a given application for a ground source heat pump systems can be reduced by increasing the borehole depth. The temperature of the ground generally increases with depth and creates the potential to increase the amount of energy that can be extracted; therefore, a deep borehole heat exchanger can provide a larger heat source and thereby require a smaller construction area.

Drilling is cost intensive; therefore, it is desired that the borehole heat exchangers are as effective as possible. This can be achieved by using a larger mass flow rate as compared to conventional borehole heat exchangers where U-tube collectors are used. A coaxial BHE can operate with a higher mass flow rates than a conventional U-tube without causing excessively high pressure drops, and are, therefore, better suited for deeper boreholes.

In this study, a numerical model for a coaxial pipe-in-pipe borehole heat exchanger is presented. The model is compared against experimental data and is found to accurately predict the experimental results. The model is, thereafter, used to study the performance of coaxial BHEs. Especially the influence of borehole depth on the performance of the BHE is studied.

The essence of the study is presented in Paper 4: *Thermal evaluation of deep borehole heat exchangers*, and at the end of this section some additional results are discussed (0).

I-6.2 OBJECTIVES

The main objectives of the present study are:

- Develop and verify a transient model for the coaxial pipe-in-pipe BHE.
- Study the performance of the coaxial BHE as a function of borehole depth.
- Provide improvements for the design of deep coaxial BHE systems

I-6.3 BACKGROUND

Borehole heat exchangers are often used as both a source and sink for thermal energy, and if the positive and negative thermal loads are balanced the temperature level in the boreholes can be kept at a near constant level. However, in this section, the focus is on larger systems where the thermal loads are negatively unbalanced, i.e. more energy is being extracted than are recharged. This can be energy systems that are used only in the winter e.g. heating systems for school buildings that are closed in the summer season, or heating systems for deicing of pavements.

A ground source heat pump system can still provide thermal energy for such an installation. The unbalanced load does, however, require that the boreholes are separated by a relatively large

distance (≈ 15 -30 m). For larger installations with multiple boreholes this can require a large construction area which might not be available. An alternative solution is then to increase the depth of the boreholes.

With increasing borehole depth, also the average temperature in the borehole increases. Therefore, the deep BHE can either provide a higher mean fluid temperature, or it can provide a higher thermal load at the temperature level of a conventional BHE. If the BHE is operated as an open system, i.e. with water as the heat carrier, the freezing point of water is a further constraint which limits the amount of energy that can be extracted.

Increased borehole depth also makes it more beneficial to use a coaxial BHE. Different types of coaxial BHEs are studied experimentally by Acuña (2013). Acuña shows that a pipe-in-pipe coaxial collector has a better thermal performance and allows for a larger flow area than the U-tube BHE and can give a smaller pressure drop or a higher mass flow.

In this subsection the thermal performance of the coaxial BHE is studied. The coaxial BHE has been simulated as a pipe-in-pipe configuration where the outer pipe is a thin and flexible pipe which fits close to the borehole wall. The layout for a section of the coaxial BHE is shown in Figure I-19.

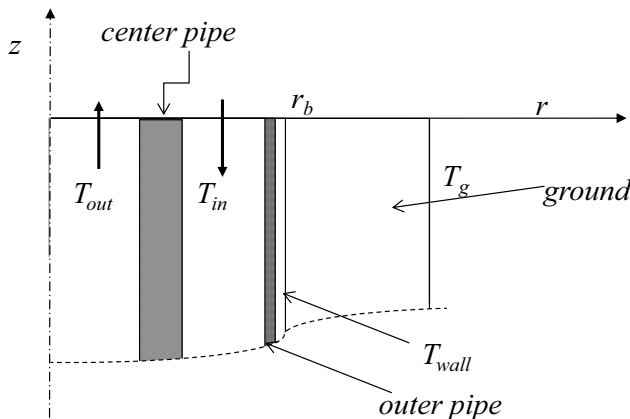


Figure I-19. Cross sectional layout of the coaxial BHE. The labels center pipe and outer pipe refers to the walls of the respective pipes.

Heat extraction that is the primary focus for this study, but heat injection is also considered. Heat injection is more beneficial for boreholes with depths of less than about 500 m (depending on the temperature in the borehole and the type of heat injection). For heat injection, the heat carrier enters the BHE through the center pipe, and for heat extraction the fluid enters through the annular space.

The fluids in the center pipe and in the annular space are separated by the wall of the center pipe. In general the fluid flow is turbulent, such that most of the thermal resistance between the fluid streams is in the material of the center pipe. Heat transfer between the fluid in the center pipe and in the annular space directly affect the thermal performance of the coaxial BHE and

should be minimized. The heat transfer can be reduced either by increasing the thermal resistance of the center pipe or by reducing the temperature difference between the fluid streams by increasing the mass flow rate.

Coaxial BHEs constructed in areas with higher temperature gradients might benefit from more complex center pipes, e.g vacuum insulated pipes, as demonstrated in Kohl et al. (2002). With the moderate temperature levels considered in this study, it is more beneficial to consider the second option as it allows for a higher heat load while the center pipe can be made simple and less expensive.

I-6.4 PAPER 4: THERMAL EVALUATION OF COAXIAL DEEP BOREHOLE
HEAT EXCHANGERS

Holmberg, H., Acuña J., Næss. E., Sønju. O. K. (2016)

Submitted to Renewable Energy

Thermal Evaluation of Coaxial Deep Borehole Heat Exchangers

Henrik Holmberg^{1*}, José Acuña², Erling Næss¹ Otto K. Sønju³

¹Department of Energy and Process Engineering, Norwegian University of Science and Technology

²Department of Energy Technology, KTH Royal Institute of Technology

³Rock Energy AS

Abstract

This paper presents a performance study of deep borehole heat exchangers. The coaxial borehole heat exchanger (BHE) has been selected because for the present conditions it has a better performance than the conventional U-tube BHE. A numerical model has been developed to study the coaxial BHE. The model predictions are compared to detailed distributed temperature measurements obtained during a thermal response test. The model is found to accurately predict the behavior of a coaxial BHE. The influence of the flow direction of the mass flow is studied for BHEs in the range 200 m to 500 m. A parametric performance study is then carried out for the coaxial case with different borehole depths, flow rates and collector properties. The results clearly show a significant increase in the system performance with depth. In addition, it is shown that with increasing borehole depth, the heat load that can be sustained by the BHE is significantly increased. An overall performance chart for coaxial BHEs for the depths of 300 to 1000 m is presented. The chart can be used as a guide when sizing deep BHE installations.

*Corresponding author

E-mail address: henrik.holmberg@ntnu.no

Keywords: Borehole heat exchanger, Numerical, Coaxial, Ground source heat pump system.

Nomenclature

Symbol

C	Specific heat capacity [J/kg·K]
D_h	Hydraulic diameter [m]
f	Friction factor [-]
h	Heat transfer coefficient [W / m ² ·K]
k	Thermal conductivity [W / m·K]
\dot{m}	Mass flow [kg / s]
ΔP	Pressure drop [Pa]
Q	Heat load [W]
T_{mean}	Mean fluid temperature, $(T_{\text{inlet}} + T_{\text{outlet}})/2$ [K]
\dot{q}	Specific heat load [W / m]
q''	Heat flux [W / m ²]
r_1	Collector inner radius [m]
r_2	Collector outer radius [m]
r	Radius [m]
r^*	Radius ratio [-]
R	Thermal resistance [K·m / W]
S	Source term [W / m]
s	Wall thickness [mm]
T	Temperature [K]
t	Time [s]
u	Internal energy [J / kg]
V	Velocity [m/s]
L	Borehole depth [m]
W	Electric effect [W]
GG	Geothermal gradient [K/km]

Greek letters

α	Thermal diffusivity, $\frac{k}{\rho C}$ [m ² / s]
Δ	Finite increment in a variable
ρ	Density [kg / m ³]
ν	Kinematic viscosity [m ² / s]
η	Pump Efficiency [%]
Dimensionless numbers	
Pr	Prandtl number, ν/α [-]
Nu	Nusselt number, hL/k [-]
COP	Coefficient of performance, $\frac{Q+W_{hp}}{W_{hp}}$ [-]
$\text{COP}_{\text{total}}$	Total COP, $\frac{Q+W_{hp}}{W_{hp}+W_p}$ [-]

Index

a	Annular
c	Center pipe
g	Ground
w	Water
f	Heat carrier fluid
o	Outer
b	Borehole
n	Index , temporal discretization
i	Index , spatial discretization (radial)
j	Index , spatial discretization (vertical)
p	Pump
hp	Heat pump
inlet	BHE inlet properties
outlet	BHE outlet properties

1. Introduction

Ground source heat pump systems usually utilize borehole heat exchangers (BHEs) 100 to 300 m deep as a source and sink for thermal energy. For smaller systems, this type of installations can be made space effective and have a small or negligible visual footprint. Still, larger systems require a certain amount of space (drilling area) which might be hard to find in densely populated urban areas, such as city centers.

As discussed in Rybach et al. 1992, there are two ways of upscaling BHE installations, either by increasing the number of boreholes or by increasing the depths of the boreholes. Although, the first alternative stands for the majority of the installations today, installations with BHEs based on 400-500 m boreholes are now being constructed on a commercial basis in Norway. The increased depth is in these cases largely motivated by scarcity of space.

In Scandinavia, the temperature in the undisturbed ground increases with about 1.0- 3 K / 100 m, thus the thermal potential for heat extraction increases with increasing depth while the potential for cooling purposes decreases. Therefore, the prospects of using BHE based on deep boreholes are most feasible (but not limited too) for buildings with large heating loads and either small or negligible cooling loads.

With increasing depth, the flow rate of the heat carrier has to be increased for the BHE to be effective (i.e. decrease the thermal contact between down and up-going fluid, thermal shunt). Therefore, also the flow area of the collector has to be increased in order to avoid excessively high pressure drops. In comparison with the conventional U-tube collector, the coaxial BHE utilizes a larger fraction of the borehole cross sectional area as flow area. It is, therefore, more appropriate for deeper boreholes since a larger mass flow rate can be used.

The coaxial BHE has also been shown to have a better thermal performance than the conventional U-tube collector (Acuna 2013). In addition, changes in the physical dimensions and properties of the center pipe can be applied to reduce the thermal shunt between down and up-going fluid. The present paper focuses on the coaxial BHE and its performance in boreholes in the depth range 200 m – 1000 m.

The boreholes are cost intensive, and it is, therefore, important to have a sound knowledge of the heat extraction rates that can be expected. The thermal performance of the coaxial BHE can be determined using either analytical or numerical simulation models. The analytical models can be made computationally cost effective, but they are in general not capable of describing all the involved phenomena, and therefore, lack some of the accuracy, flexibility and transparency gained from numerical methods.

Efficient numerical models can be implemented by applying the analogy to electric networks when describing the thermal resistances within the borehole; thus representing a geometrical simplification where the different parts of the borehole are described by single nodes. A numerical grid is then used to describe the bedrock around the borehole in two or three dimensions, while the borehole, the collector and the heat carrier are simulated as one-dimensional features. Numerical models based on this methodology have earlier been referred to as thermal resistance and capacity models (TRCM), Bauer et al. (2011^a). TRCM models for coaxial BHEs have been published by De Carli et al. (2010), Bauer et al. (2011^a and 2011^b), Diersch et al. (2011^a and 2011^b), Mottaghy and Dijkshoorn (2012).

Although, comparisons were made with experimental measurements of outlet and inlet fluid temperatures in De Carli et al. (2010), Bauer et al. 2011^b and in Mottaghy and Dijkshoorn (2012), neither of these models were compared with detailed experimental data from distributed temperature measurements during operation of the BHE.

In the present paper, the coaxial BHE is analyzed using a new numerical model. The model is validated through comparison with detailed distributed temperature measurements performed by Acuña (2013).

The model is then used to study the performance of coaxial BHEs as a function of the total borehole depth, the mass flow rates and the collector properties.

It is shown that with increasing borehole depth, the heat load that can be sustained by the BHE is significantly increased as compared with conventional 200- 300 m BHEs. With increasing borehole depth, the required circulation pump effect increases; it is, however, clearly shown, that the increase is manageable and small comparative with the gain in thermal effect. In addition, it is possible to compensate for an increased pressure drop using a larger borehole diameter.

2. Objectives and Methodology

2.1 Introduction

The objective of the paper is to analyze and establish the performance of coaxial BHEs for boreholes deeper than the conventional 200 m to 300 m.

It is assumed that the BHE is constructed as a coaxial pipe-in-pipe BHE which uses water as the heat carrier. The water in the annular space is separated from the borehole wall by a thin membrane. This type of installation has been demonstrated by Acuña (2013), and it can be categorized as a closed or near closed system

The benefits of having a closed, or a near closed system is that the water or heat carrier fluid is kept clean from contaminants that can deposit in, for example, the heat exchangers. Using water as the heat carrier also reflects the intention of using a slightly higher operation temperature, as compared to conventional BHE installations which often operate with fluid temperatures below 0°C during peak load.

A new numerical model for the coaxial BHE is developed and implemented in Matlab® and is validated against measurement data from a distributed thermal response test (DTRT). The model is used to further analyze the test and to study the performance of the coaxial BHE for different operating conditions.

Furthermore, the influence of flow direction during heat injection and heat extraction are studied using a 490 m deep coaxial BHE which is simulated based on the undisturbed temperature profile that were measured during the construction of a BHE installation.

The performance of coaxial BHEs is then further analyzed based on the results from an extensive parametric study in which the geothermal gradient, the borehole depth, the borehole diameter, the center pipe diameter and the heat carrier mass flow rate have been varied.

To study the overall performance of deep coaxial BHEs it has been assumed that the extracted energy will be upgraded to a constant output temperature using a heat pump. The heat pump then forms the coupling between the thermal performance of the BHE and the required use of high grade energy (i.e. electricity). The layout is shown in Figure 1. The flow direction indicated in Figure 1 can be changed as convenient.

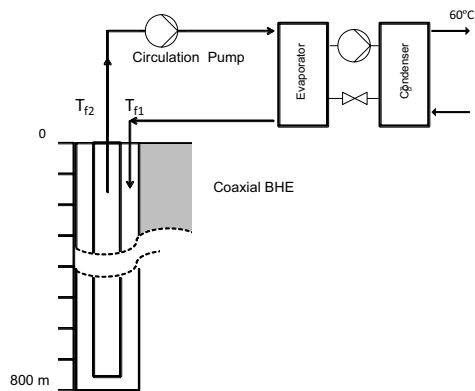


Figure 1. Layout for parametric study.

The overall performance is determined based on the amount of energy delivered from the heat pump and the total use of high value energy. Since it is assumed that the BHE operates with water as the heat carrier, the inlet temperature (T_{f1}) of the fluid sets a limitation to the amount of energy that can be extracted from the BHE, for a given ground temperature.

2.2 Center pipe material

Conventional U-tube collectors are made of polyethylene (PE), with a thermal conductivity of around $0.42 \text{ W / m}\cdot\text{K}$. These collectors have a relatively low thermal resistance and are, therefore, not optimal as center pipe in the Coaxial BHE. To increase the thermal resistance (i.e. reduce the thermal shunt), either the thermal conductivity has to be reduced, or the wall thickness of the center pipe has to be increased. In Kohl et al. 2002, the performance of a coaxial BHE based on a 2302 m deep borehole is investigated. The BHE uses a double walled vacuum insulated steel pipe for the upper 1780 meters of the center pipe. According to Kohl the equivalent thermal conductivity for the pipe is $0.09 \text{ W / m}\cdot\text{K}$ and the total wall thickness of the pipe is 1.6 cm. Zanchini et al. (2010) proposed to use center pipes made of the polypropylene (PP) with $k= 0.24 \text{ W / m}\cdot\text{K}$. Another material having lower thermal conductivity than PE can be PVC ($k=0.14$ to $0.28 \text{ W / m}\cdot\text{K}$). The choice of material for the center pipe has to be made based on thermal properties, structural strength, buoyancy forces, economical aspects, and not least the practical aspects related to transport and installation. PP and PE are lighter than water and require weights to balance the buoyancy forces while PVC is heavier and has to be lifted. In this paper, the center pipe has been assumed to have the properties of PP.

3. Experimental setup and measurements

The developed numerical model has been used to simulate the thermal response data from a heat injection distributed thermal response test (DTRT) performed in a 190 m deep borehole. The groundwater table was 3 m below the surface and the center pipe of the BHE ends at 182 meters; therefore, the total active length of the BHE is 179 meter. The first temperature measurements start at 17 m depth, and has been used as the inlet and outlet temperatures of the BHE. Therefore, the total simulated active length is 165 m.

Water is used as the heat carrier fluid and is being circulated down through the center pipe and up through the annular space (opposite the direction indicated in Figure 1). The BHE uses a PE (polyethylene) $40 \times 2.4 \text{ mm}$ collector that is inserted into a thin walled polyethylene membrane which

is pressed close to the wall of the borehole. The membrane is 0.4 mm thick and has a diameter of 114 mm. This coaxial BHE was found to have a significantly better performance than the conventional U-tube BHE, having a borehole resistance of about 0.02 Km/W.

When carrying out the DTRT, a fiber optic cable was placed inside the central pipe as well as in the annulus. Temperatures of the circulating fluid along the flow paths of the BHE were measured using this cable by sending laser light pulses which travel through the optic fiber. As part of the light is backscattered, the temperature and the position of any measured borehole segment are identified by analyzing the signal intensities over a time span corresponding to the delay time for the light to travel to the measured section and back. The instrument used for these measurements is of type HALO produced by Sensornet. The heat carrier temperatures (measured at 17 m depth) in the BHE are presented in Figure 2.

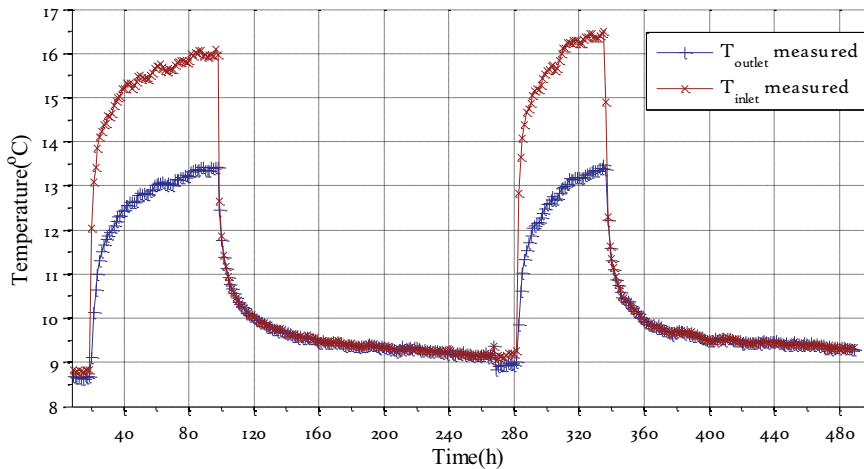


Figure 2. Inlet and outlet fluid temperatures during DTRT.

The DTRT was performed with two heat injection periods during which on average 6.4 kW of heat is injected to the BHE, the first heat injection period lasted for 78 hours during which the average volumetric flow rate was 0.58 l/s. Prior to the heat injection periods, the heat carrier fluid was circulated, but with no heat injection. This is common practice during conventional TRTs, and it is used to predict the average undisturbed temperature in the BHE. The first heating period is followed by a recovery period during which there is no fluid flow. The temperature changes during the recovery period were used to determine the thermal conductivity of the ground (k_g).

Local measurements were made every 10 meters along the flow path. These were carried out by integrating and averaging the temperature along the 10 meter segments over 2.5 minute intervals. The estimated accuracy of the measured temperatures is ± 0.1 K. The experimental setup and the data reduction are described in detail in Acuna (2013). Parameters for the experimental setup are listed in Table 1. Further data are shown and compared with numerical simulations in Section 5.

Table 1. Parameters for experimental setup.

Parameter	Value
k_g [W /m K]	3.53
Active length BHE [m]	165
Borehole diameter [mm]	115
Collector (center pipe)[mm]	40 x 2.4

Collector (outer membrane) [mm]	114 x 0.4
k_c [W/ m K]	0.42
Heat carrier	Water
Mass flow rate [kg/ s]	0.44-0.7
Heating effect [kW]	6.2 - 6.5 kW

4. Simulation method

4.1 Introduction

The developed numerical model uses a geometrical simplification where the analogy to electric networks is used to describe the thermal resistances within the borehole. A two-dimensional numerical grid is used to resolve the bedrock around the borehole, while the borehole, the collector and the heat carrier fluid are simulated as one-dimensional features. In the model, the heat capacity of the collector pipes has been neglected. This affects primarily the accuracy of the model for short time steps (< 60 s).

With the current material properties ($k_c = 0.42$ W/ m·K to $k_c = 0.24$ W/ m·K) it takes between 20 s to 40 s for a near constant temperature profile to develop through a pipe with a 4 mm wall thickness and between 2 min and 3 min for a pipe with a 10 mm wall thickness. The introduced error is, however, negligible for most cases since the total thermal mass of the collector is small relative to the thermal mass of the water in the borehole.

The model of the coaxial BHE has been setup based on the thermal network shown in Figure 3.

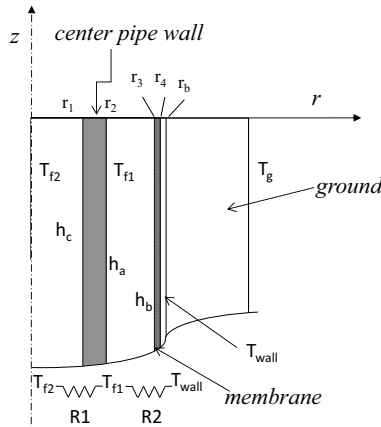


Figure 3. Thermal resistance network describing the coaxial BHE.

With reference to Figure 3 the thermal resistance between the fluid in the center pipe and the fluid in the annular space can be expressed as:

$$R_1 = \frac{1}{2\pi r_1 h_c} + \frac{\ln(r_2/r_1)}{2\pi k_c} + \frac{1}{2\pi r_2 h_a}, \quad \mathbf{1}$$

where h_c and h_a are the convective heat transfer coefficients on the inner and outer surface of the center pipe. k_c is the thermal conductivity of the central pipe material. With turbulent flow R_1 is primarily influenced by the wall-thickness and the thermal conductivity of this pipe.

The thermal resistance between the water in the annular space and the borehole surface can be expressed as:

$$R_2 = \frac{1}{2\pi r_3 h_b} + \frac{\ln(r_4/r_3)}{2\pi k_m} + \frac{\ln(r_b/r_4)}{2\pi k_{water}}, \quad 2$$

where h_b is the convective heat transfer coefficient on the inside of the outer membrane, and k_m is the thermal conductivity of the membrane. The space between the membrane and the borehole surface is treated as a thermal resistance where heat is transported through water by thermal conduction. This can also be thought of as a contact resistance between the outer surface of the membrane and the borehole wall surface.

For the thermal performance of the coaxial BHE it is desired that the thermal resistance R_1 is as high as possible while R_2 is as low as possible.

4.2 Description of the Numerical model

The coaxial BHE creates a heat source or sink in the ground which gives the potential for heat transport. Thermal conduction is the main heat transfer mechanism in the ground although heat can also be transported through advection (transport through movement of groundwater). Heat is also generated in the ground due to nuclear fission; this contribution is, however, negligible on the timescale of interest. In the present study, only conductive heat transport has been accounted for in the ground.

Assuming that the heat transfer is symmetric around the circumference of the borehole, the thermal conduction in the rock surrounding the borehole can be expressed by Fourier's law using cylindrical coordinates as follows:

$$\frac{1}{r} \frac{\partial}{\partial r} \left(kr \frac{\partial T}{\partial r} \right) + \frac{1}{z} \frac{\partial}{\partial z} \left(k \frac{\partial T}{\partial z} \right) = \rho C \frac{\partial T}{\partial t} + S_1, \quad 3$$

where S_1 is a heat source term.

Equation 3 can be discretized based on appropriate numerical schemes using, for example, finite element or finite difference methods. The ground surrounding the borehole is, in the present work, discretized using an axisymmetric cylindrical grid.

The convective heat transfer in the borehole depends primarily on the heat carrier fluid flow conditions and can readily be determined by analytical or empirical correlations. For the performance of the pipe-in-pipe coaxial BHE, it is desirable that the flow in the annular part is turbulent while the flow in the center pipe could be laminar (as it reduces the heat transfer coefficient). This is, however, difficult to achieve due to geometrical constraints.

Results for laminar and turbulent heat transfer coefficients in annular pipes were presented by Kays et al. (2005) for different radius ratios (r^*), Prandtl numbers and Reynolds numbers. With $Pr = 10$, $Re = 10^4$ and $r^* = 0.35$ (equivalent to a borehole of 115 mm, with a PEM40 collector as the center pipe) the difference is less than 5 % between the heat transfer coefficient on the inner and the outer surfaces of the annular space. This difference decreases with increasing radius ratio and is negligible when considering the total thermal resistances R_1 and R_2 . Therefore, for simplification it has been chosen to determine the heat transfer coefficient on both the inside and the outside surface of the annular space based on the hydraulic diameter. The convective heat transfer coefficient for turbulent flow is determined from the Petukhov Equation as modified by Gnielinski (1976), which is valid also in the transitional range between laminar and turbulent flow, as follows:

$$\text{Nu}_{D_h} = \frac{(f/8)(\text{Re}_{D_h} - 1000) \text{Pr}}{1 + 12.7(f/8)^{0.5}(\text{Pr}^{2/3} - 1)}, \quad 4$$

where f is the Darcy friction factor.

Equation 4 is used to determine the heat transfer coefficient both in the center pipe and in the annular space.

The Darcy friction factor is given by

$$f = (0.790 \ln(\text{Re}_{D_h}) - 1.64)^{-2}. \quad 5$$

Re_{D_h} is the Reynolds number based on the hydraulic diameter defined as:

$$D_h = \frac{4A}{P}, \quad 6$$

where A is the flow area and P is the wetted perimeter.

The energy equation for fluid flowing in a pipe, e.g. the center pipe, can be expressed as:

$$\pi r^2 \rho \frac{\partial u}{\partial t} + \pi r^2 \rho V \frac{\partial u}{\partial z} = S_2. \quad 7$$

S_2 is a source term that is used to couple the convective heat transfer in the pipe to an external source or sink, (see Equation 12). Assuming that the heat carrier fluid is incompressible, the energy equation can be solved independent of the momentum equation.

4.3 Numerical discretization of the equations

Starting with the energy equation for axisymmetric conduction in the ground in two dimensions, as derived from Equation 3, the equation is discretized using an implicit finite difference scheme as follows:

$$\frac{\partial T}{\partial t} = \frac{1}{r} \left[\frac{\partial}{\partial r} \left(\alpha r \frac{\partial T}{\partial r} \right) \right] + \alpha \frac{\partial^2 T}{\partial z^2} + S_1 \quad 8$$

$$\frac{T_i^{n+1} - T_i^n}{\Delta t} = \frac{2}{r_i \Delta r_i} [G1 * T_{i+1}^{n+1} - (G1 + G2) * T_i^{n+1} - G2 * T_{i-1}^{n+1}] \quad 9$$

$$+ \frac{\alpha}{\Delta z^2} [T_{j+1}^{n+1} - 2T_j^{n+1} + T_{j-1}^{n+1}] + S_1.$$

$G1$ and $G2$ are expressed as:

$$G1 = \frac{(r_i + \frac{1}{2} \Delta r_i)(\alpha_{i+1} \Delta r_{i+1} + \alpha_i \Delta r_i)}{(\Delta r_i + \Delta r_{i+1})^2}, \quad 10$$

$$G2 = \frac{(r_i - \frac{1}{2} \Delta r_i)(\alpha_i \Delta r_i + \alpha_{i-1} \Delta r_{i-1})}{(\Delta r_i + \Delta r_{i-1})^2}, \quad 11$$

where α is the thermal diffusivity of the rock.

The heat transfer and flow in a pipe are represented by the one-dimensional energy equation (Equation 7). Assuming that the change in internal energy only depends on the change in temperature of the fluid, the energy equation can be rewritten as:

$$\pi r^2 \rho C \frac{\partial T}{\partial t} + \pi r^2 \rho V C \frac{\partial T}{\partial z} = S_2 = 2\pi r h \Delta T. \quad 12$$

The source term, S_2 , represents convective heat transfer between an external source and the fluid in the pipe. ΔT represents the temperature difference between the mixing-cup fluid temperature in the pipe and the temperature of the source, while h is the convective heat transfer coefficient between the fluid and the heat source / heat sink. Equation 12 is further rearranged and discretized as follows:

$$\frac{T_j^{n+1} - T_j^n}{\Delta t} = \frac{2h(T_s - T_j^{n+1})}{r\rho C} - V \frac{T_{j+1}^{n+1} - T_j^{n+1}}{\Delta z}. \quad 13$$

T_s is the temperature of the heat source (e.g. the pipe wall), r is the inner radius of the pipe, V and C are the bulk velocity and the specific heat capacity of the fluid, respectively.

In Figure 4 the nodes used in the discretization scheme are illustrated. In order to couple the thermal processes in the borehole with the thermal conduction in the rock, a flux boundary on the wall of the borehole is introduced. In the conduction equation this is done through central finite differencing and the use of a fictitious node (T_0) in the pipe center as shown in Figure 4.

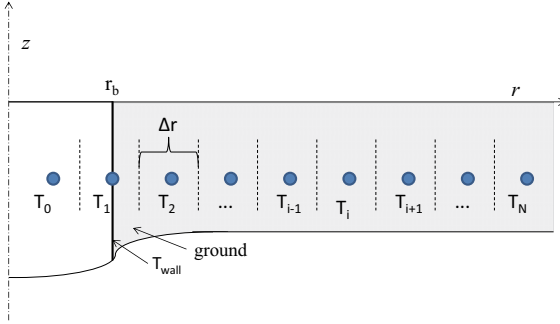


Figure 4. Illustration for coupling of conductive and convective model. T_0 is a fictitious node in the pipe center, used in the implementation of the boundary condition.

Using the fictive node, the flux boundary is implemented using central difference as follows:

$$q'' = -k \frac{dT}{dr} \approx k_g \frac{T_2 - T_0}{\frac{1}{2}\Delta r_0 + \Delta r_1 + \frac{1}{2}\Delta r_2}, \quad 14$$

$$T_0 = T_2 - \frac{q''}{k_g} \left(\frac{1}{2}\Delta r_0 + \Delta r_1 + \frac{1}{2}\Delta r_2 \right). \quad 15$$

Equation 15 is then used to represent the fictive node when applying Equation 9 to the boundary node in Figure 4. The equation can then be written as:

$$T_1^{n+1} = T_1^n + \frac{2\Delta t}{r_1 \Delta r_1} \left[(G1 + G2) * T_2^{n+1} - (G1 + G2) * T_1^{n+1} - G2 * \frac{q''}{k_g} \left(\frac{1}{2}\Delta r_0 + \Delta r_1 + \frac{1}{2}\Delta r_2 \right) \right] + \frac{\alpha}{\Delta z^2} [T_{j+1}^{n+1} - 2T_j^{n+1} + T_{j-1}^{n+1}]. \quad 16$$

$$\text{Further, with } B = \frac{G2}{k_g} \left(\frac{1}{2}\Delta r_0 + \Delta r_1 + \frac{1}{2}\Delta r_2 \right), \text{ it is possible to write:} \quad 17$$

$$T_1^{n+1} = T_1^n + \frac{2\Delta t}{r_1 \Delta r_1} [(G1 + G2) * T_2^{n+1} - (G1 + G2) * T_1^{n+1} - B * q''] + \frac{\alpha}{\Delta z^2} [T_{j+1}^{n+1} - 2T_j^{n+1} + T_{j-1}^{n+1}], \quad 18$$

With reference to Figure 3 and Figure 4 the heat flux (q'') in Equation 18 is expressed as:

$$q'' = \frac{1}{R_2 2\pi r_b} (T_1 - T_{f1}), \quad 19$$

where $T_1 = T_{\text{wall}}$.

The discretized conduction equation in the rock is, thereby, coupled to the heat transfer in the borehole. The complete equation system describing the coaxial BHE is summarized below. Notice that the fluid with temperature T_{f1} in the annular space exchanges heat through two surface areas which has been accounted for in the source term.

The thermal conduction in the ground around the borehole can be expressed as:

$$T_1^{n+1} = T_1^n + \frac{2\Delta t}{r_1 \Delta r_1} \left[(G1 + G2) * T_2^{n+1} - (G1 + G2) * T_1^{n+1} - B * \frac{1}{R_2 2\pi r_b} (T_1^{n+1} - T_j^{n+1}) \right] + \frac{\alpha}{\Delta z^2} [T_{j+1}^{n+1} - 2T_j^{n+1} + T_{j-1}^{n+1}]. \quad 20$$

The thermal convection in the annular fluid can be expresses as:

$$T_{f1j}^{n+1} = T_{f1j}^n + \Delta t \left(\frac{(T_1^{n+1} - T_{f1j}^{n+1})}{R_2 \pi (r_3^2 - r_2^2) \rho_f C_f} + \frac{(T_{f2j}^{n+1} - T_{f1j}^{n+1})}{R_1 \pi (r_3^2 - r_2^2) \rho_f C_f} - V_{f1} \frac{T_{f1j+1}^{n+1} - T_{f1j}^{n+1}}{\Delta z} \right). \quad 21$$

The thermal convection in center pipe can be expresses as:

$$T_{f2j}^{n+1} = T_{f2j}^n + \Delta t \left(\frac{(T_{f1j}^{n+1} - T_{f2j}^{n+1})}{R_1 \pi r_1^2 \rho_f C_f} - V_{f2} \frac{T_{f2j+1}^{n+1} - T_{f2j}^{n+1}}{\Delta z} \right). \quad 22$$

Equations 20 to 22 describe an implicit scheme which is implemented and solved simultaneously in Matlab using matrix division.

4.5 Heat pump COP - Pressure drop and pumping power.

The pressure drop in the BHE is an important factor in the parametric performance study of this paper as the electricity used by the circulation pump is added to the electricity usage of the heat pump compressor when determining the total performance ($\text{COP}_{\text{total}}$) of the system.

Acuña (2010) has shown that the pressure drop in a U-tube collector can be accurately determined based on the assumption of a smooth pipe, i.e. using the friction factor of Equation 6 in the Darcy-Weisbach equation. The equation used here is based on the hydraulic diameter, as applied to both the center pipe and the annular space of a coaxial BHE. The pressure drop can be written as:

$$\Delta P = f \frac{L}{D_h} \frac{\rho V^2}{2}. \quad 23$$

The effect required by the circulation pump can be determined based on the mass flow rate and pressure drop as:

$$W_{\text{Pump}} = \frac{\Delta P * \dot{m}}{\rho \eta / 100}, \quad 24$$

where η is the pump efficiency.

The influence of the circulation pump effect on the total performance of the coaxial BHE ($\text{COP}_{\text{total}}$) can then be determined.

$$\text{COP}_{\text{total}} = \frac{Q_{\text{BHE}} + W_{\text{HP}}}{W_{\text{HP}} + W_{\text{Pump}}}, \quad 25$$

5. Results

The developed numerical model is first used to simulate and replicate the measurements from the experimental DTRT. In addition, the influence of flow direction is studied for both heat injection and heat extraction using the parameters from the experimental setup. After verifying the model, the same parameter variations are then applied to a deeper BHE, which is simulated based on the undisturbed temperature profile (down to 490 m) measured from an installation in southern Norway.

Thereafter, simulation results are presented from a parametric study where the borehole depth is varied between 300 m and 1000 m. The thermal performance of the BHE is studied for each borehole depth using fixed surface conditions, i.e. BHE fluid temperatures. The size of the borehole and the center pipe are adjusted to compensate for an increase in mass flow rates with borehole depth.

5.1 Validation of numerical model

As described in Section 3, the numerical model is compared with the DTRT-measurements. The model uses implicit temporal discretization with a maximum time step of 100 seconds. The parameters used for the simulations are according to the description of the field installation in Section 3, as summarized in Table 1.

In Figure 5, the measured mean fluid temperature $T_{f,mean}$ are presented together with the arithmetic mean of the temperature in the annular space and the wall temperature. These temperature measurements are compared with the calculated values based on the numerical simulations.

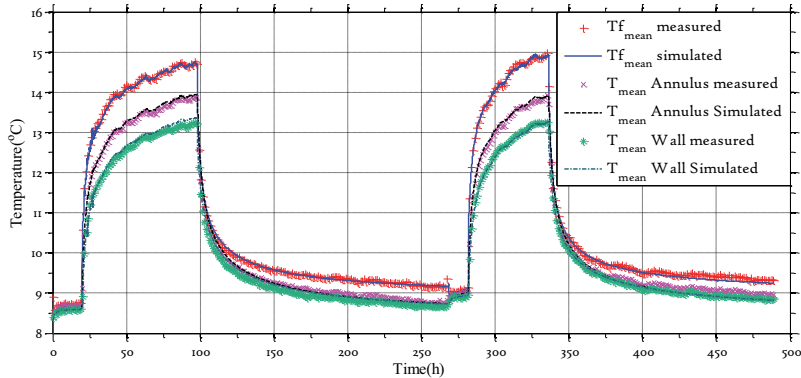


Figure 5. Comparison between results from the numerical model and from measurements.

It is established that the simulated values from the numerical model agree well with the measured temperatures. The temperatures in the borehole increase when heat is being injected. As both the fluid circulation and the heat injection is stopped at 100 hours, the fluid temperatures recover to their natural level. Fluid circulation starts somewhat before heat again is being injected in the second period after about 285 hours.

The vertical temperature profiles in the borehole are shown in Figure 6 both from the measurements and from the numerical simulations. The profiles are from both the early stage and from the late stage of the first DTRT period. It is seen that the temperatures increase with time and that the change is faster in the early period.

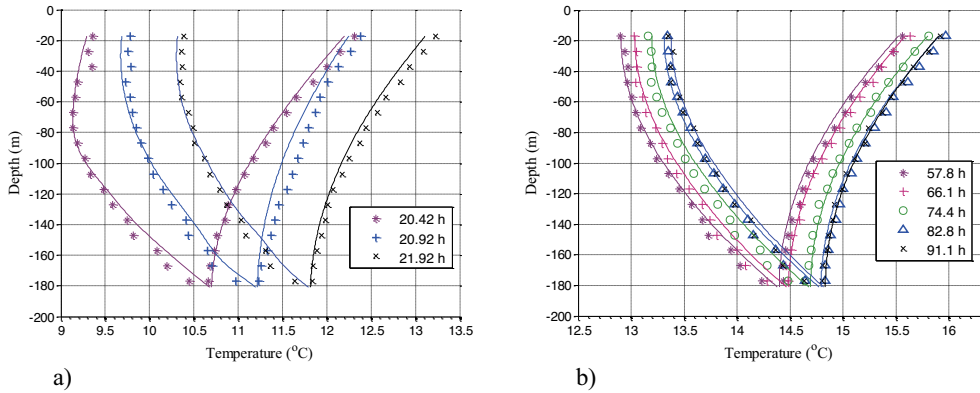


Figure 6. Vertical fluid temperature profiles in the early period of the DTRT (a.) and in the late period of the DTRT (b). The figures show measured temperatures (markers) and simulated temperatures (solid lines)

The simulated values agree well with the measurements also for the vertical temperature profiles. It can be concluded that the numerical model accurately predict the behavior of the coaxial BHE.

5.2 Influence of flow direction (case of a 190 m BHE)

In this section, the influence of flow direction is studied for both heat injection and heat extraction, using the same model parameters as discussed in Sections 3 and 5.1.

Heat injection

The temperature profile for 91.1 h shown in Figure 6 has been compared with a hypothetical case using the opposite flow direction (also heat injection). As shown in Figure 7 the temperature profiles and the distribution of the specific heat load in the borehole are substantially different for the two cases. It is also seen that for this configuration, changing the flow direction of the heat carrier fluid would not influence the overall thermal performance of the BHE during a DTRT. In the experimental setup, the lower part of the borehole is heated up as the warmer water is injected through the center pipe. If the flow direction is reversed so that the hot water enters the annular space, the upper part of the borehole will be heated up as shown in the figure.

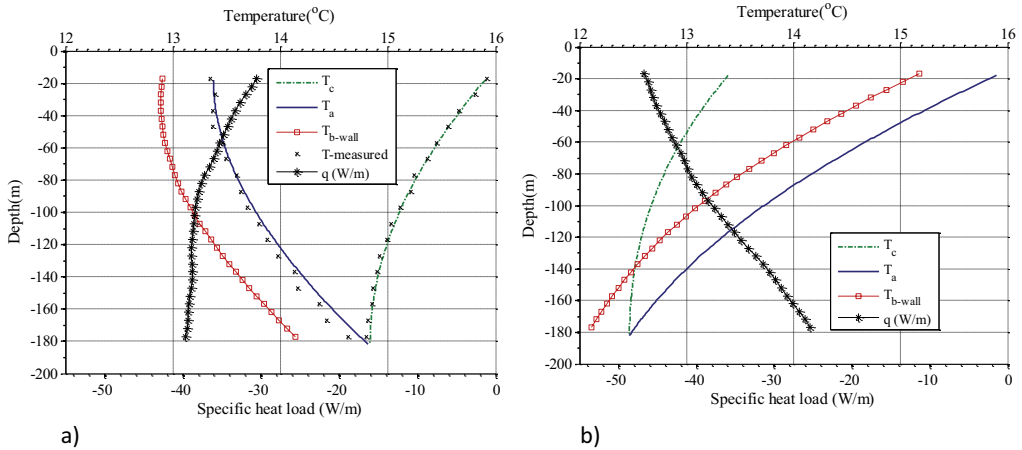


Figure 7. Vertical temperature profiles in the coaxial BHE with heat injection: a) fluid inlet through the center pipe and b) fluid inlet through the annular space. Operating parameters according to Table 1.

Heat extraction

The influence of flow direction on the temperature profiles and the distribution of the local specific heat load during heat extraction are visualized in Figure 8. The simulations are performed using the same parameters as for the DTRT shown in Figure 5, but instead of injecting heat, an equivalent thermal load is extracted from the borehole.

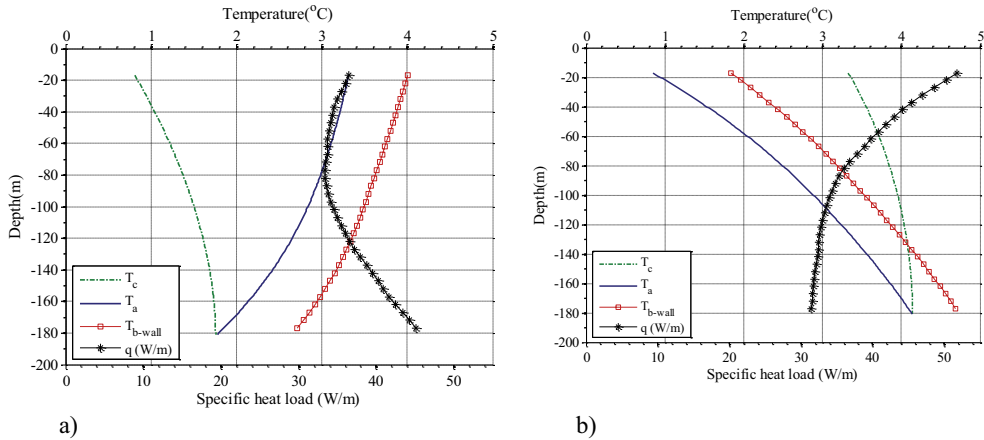


Figure 8. Vertical temperature profiles in the coaxial BHE during heat extraction: a) fluid inlet through the center pipe and b) fluid inlet through the annular space. Model parameters according to Table 1.

It is seen from the inlet and outlet temperatures that also for heat extraction, the thermal performance of the coaxial BHE is not affected by the flow direction. The temperature profiles in the borehole are different, though. Noticeable is also the difference in borehole wall temperature between the cases and the resulting distribution of the thermal load which is substantially different for the two cases. It is observed that with fluid inlet through the center pipe, the thermal load is largest at the bottom of the borehole while with inlet in the annular space, the load is largest in the upper part.

Although the flow direction does not directly affect the performance of the coaxial BHE in this setup, larger differences are expected for larger depths. With increasing depth, the coaxial BHE with inlet through the annular space is superior for heat extraction for two distinct reasons. Firstly, it mimics the

behavior of a counter-current heat exchanger (which has the highest theoretical thermal efficiency), and secondly, it can easily be improved through improving the insulation of the center pipe.

5.3 Flow direction (case of a 490 m deep BHE)

To further demonstrate the influence of flow direction the type of simulations performed in the previous section are repeated for a 490 m deep BHE. The initial temperature profile in the rock used in the simulation is based on measurements obtained during the construction of a U-tube BHE installation in southern Norway. The simulation parameters are summarized in Table 2. A higher mass flow rate is used as compared to the previous cases, and therefore, also larger collector and borehole dimensions. The coaxial BHE is assumed to use an outer membrane which has been up-scaled according to the borehole diameter (140 mm instead of 115 mm used in the previous case) while still having a membrane wall thickness of 0.4 mm.

Table 2. Parameters for 490 m deep BHE

Parameter	Value
k_g [W /m·K]	3.53
Active length BHE [m]	490
Borehole diameter [mm]	140
Collector (center pipe) [mm]	50 x 4.6
Collector (outer membrane) [mm]	139 x 0.4
k_c [W /m K]	0.42
Heat carrier	Water
Mass flow rate [kg / s]	1
Thermal load [W /m]	40

Results from both heat injection and heat extraction are presented, the results from the simulations are shown as temperature profiles taken after 50 hours of continuous operation in the following sub - sections. The mass flow rate, the applied thermal load and the undisturbed temperature profile are constant for all cases; the performance can, therefore, be compared based on the outlet temperature of the heat carrier.

Heat injection

The influence of the flow direction on the temperature profiles and the distribution of the specific heat load during heat injection are visualized in Figure 9. It is seen that for heat injection it is more feasible to inject the heat carrier through the center pipe since it results in lower outlet and inlet temperatures. In both cases, the highest heat load is in the upper part of the borehole where the undisturbed temperature is lowest. In case (b) where the inlet is through the annular space, the lower part of the borehole is poorly utilized, in fact, from 375 m and below, the heat transfer is positive, meaning that heat is being extracted from the borehole in this part instead of injected.

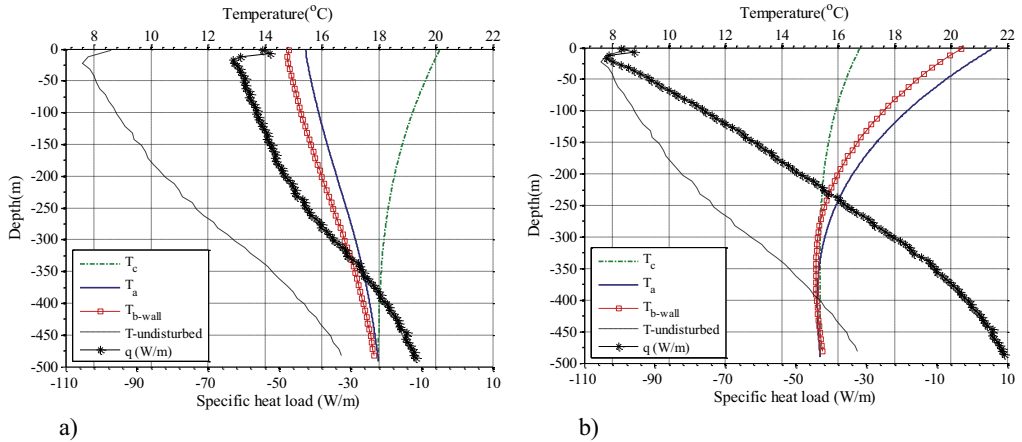


Figure 9. Temperature profiles for continuous heat injection 40 W/m for 50 hours, from a 490 m deep borehole: a) Coaxial BHE, inlet through center pipe and b) Coaxial BHE, inlet through annular space.

Heat extraction

The influence of the flow direction on the temperature profiles and the distribution of the specific heat load during heat extraction are visualized in Figure 10. As shown the best performance is in case b), where the fluid inlet is in the annular space. In this case the outlet fluid temperature is 1.2 K higher than in case (a). For both cases, the heat load is largest in the bottom of the borehole, thus, reflecting the undisturbed temperature profile. As shown, the heat load is more unevenly distributed in case a), where the fluid inlet is through the center pipe. In case b) it can be seen that the temperature of the fluid in the center pipe decreases upwards. This indicates that there is a potential for further improvements. The temperature losses can be reduced by increasing the thermal resistance, R_1 , between fluid in the center pipe and the annular space, this can be achieved either by using a pipe with a lower thermal conductivity or by increasing the center pipe wall thickness. Alternatively, the mass flow rate can be increased; this would then also increase the pressure drop in the BHE.

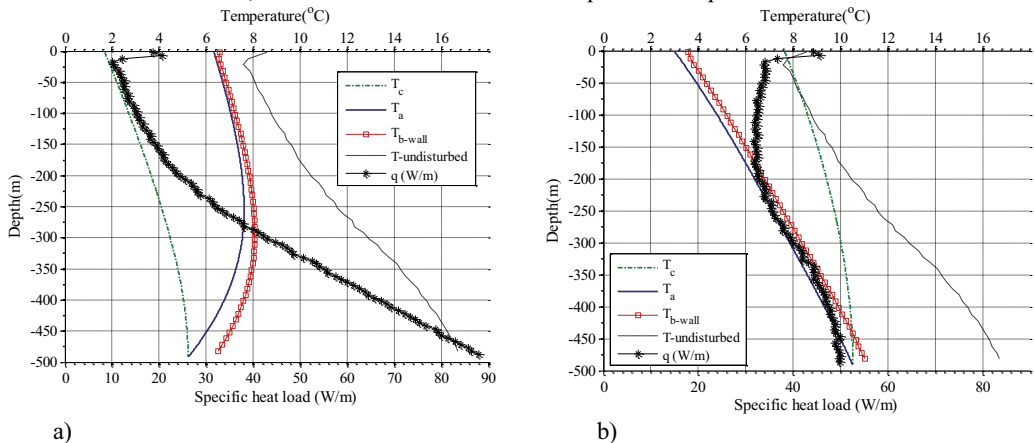


Figure 10. Temperature profiles for continuous heat extraction 40 W/m for 50 hours, from a 490 m deep borehole. a) Coaxial BHE, inlet through center pipe. b) Coaxial BHE, inlet through annular space.

In summary, while there clearly is a potential to use boreholes in the range of 500 m for cooling, for deeper boreholes, the lower part of the borehole becomes poorly utilized for cooling. Deeper boreholes are, therefore, most suitable for heat extraction. In the following section the results from a parametric study is presented. The borehole depth is varied in the range 300 – 1000 m.

5.4 Parametric study of the Coaxial BHE, borehole depth down to 1000 m

The performance of a deep coaxial BHE can be improved either by increasing the thermal resistance through the center pipe using e.g. thermal insulation, or by increasing the mass flow rate.

Since the main motivation to increase the borehole depth is to increase the heat extraction rate, it is most beneficial to use a higher mass flow rate while keeping the circulation fluid in the temperature range of a conventional BHE. This favors high heat extraction rates and reduces the importance of the thermal resistance between the annular space and the center pipe. The center pipe can, therefore, be dimensioned based on hydraulic and economical criteria rather than thermal. Also with a higher mass flow rate, the temperature change in the surface process is less, in the case of the pipe-in-pipe coaxial BHE this means that more energy can be extracted without risking freezing of the water.

In this section the simulated results from a parametric study are presented. The main parameters studied are:

- borehole depth
- mass flow rate
- borehole and center pipe dimensions
- geothermal gradient

The thermal conductivity of the center pipe has been set to $0.24 \text{ W/m}\cdot\text{K}$ which is equivalent to the material polypropylene, this gives a higher heat load (in the range of 4 %) compared with polyethylene pipes with a thermal conductivity of $0.42 \text{ W/m}\cdot\text{K}$.

In order to make the results comparative between each configuration in the study, the mass flow rate has been adjusted so that a constant ΔT is kept between the inlet fluid temperature and the time average outlet fluid temperature of the BHE.

The performance of the BHEs is evaluated after 5000 hours of simulation. The BHEs are operated with an on/off interval representing the operating cycles of the heat pump, a constant inlet temperature of 1°C is used, and the mass flow is adjusted so that the average outlet temperature in the end of the simulation is 4°C . This is illustrated in Figure 11 for a 800 m deep BHE. A rather long operation cycle of 24 hour is used since it reduces the computational time required in the parametric study. The mass flow rate used in this specific case is 4 kg/s and the average heat load after 5000 h is 50 kW .

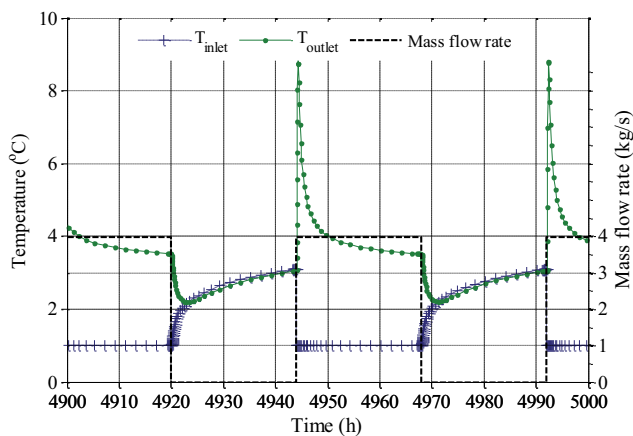


Figure 11. Illustration of cyclic operation scheme used in the simulations, simulation time 5000 h, $GG=20 \text{ K/km}$, 800 m depth.

As shown, a constant mass flow rate and inlet fluid temperature is used when the BHE is in operation; the outlet temperature has a peak in the beginning of each operation cycle representing the warmer fluid in the lower part of the BHE which is transported up. When the mass flow is turned off, the fluid temperatures in the top of the borehole increases with about 1 K being heated up by the surrounding rock.

The parameters used in the study are summarized in Table 3. The dimensions of the center pipe are chosen using commercially available pipe dimensions while minimizing the total pressure drop in the BHE.

Table 3. Parameters for parametric study

Parameter	Value
Depth [m]	300- 1000
D_0 [mm]	140, 165, 185
GG [K/km]	15, 20, 25
k_c [W/ m·K]	0.24
Center pipe dimensions [mm]	90 x 5.1, 110 x 6.3, 125 x 7.1
Inlet temperature [°C]	1
Average outlet temperature [°C]	4
k_g [W/ m·K]	3
Operation interval [hours]	24
Simulation time [hours]	5000

Figure 12 shows the heat load as a function of the borehole depth and the geothermal gradient (GG) while the borehole diameter is fixed at 140 mm. It is seen that doubling the borehole depth from 300 m to 600 m results in an increase in thermal effect of about 3.5 times, a further increase to 900 m borehole depth results in an increase of almost 8 times.

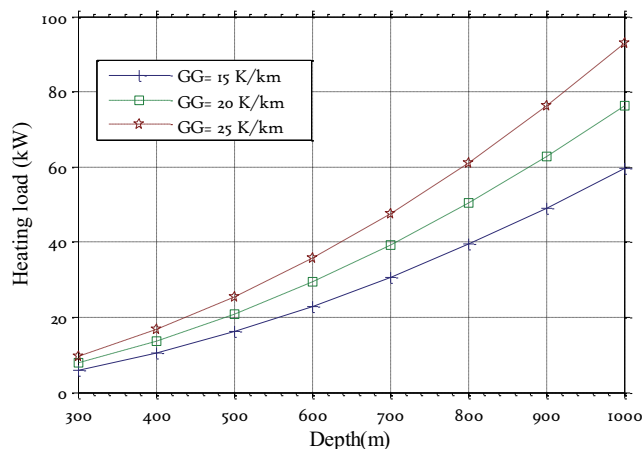


Figure 12 Heat load as function of depth and geothermal gradient, simulation time 5000 h, $d_0= 140$ mm.

The geothermal gradient has a rather large influence on the heating load i.e. with a gradient of 25 K/ km the heating load is 55 % larger than for a gradient of 15 K / km at 1000 m depth.

A larger thermal effect is equivalent to a larger mass flow rate; therefore, a larger borehole diameter is required for large geothermal gradients and/ or large borehole depths. While the main gain with a larger borehole and center pipe diameter is a reduced pressure drop, there is also a somewhat larger increase in thermal heat load for larger borehole diameters.

The pressure drops corresponding to the case with a geothermal gradient of 20 K / km are shown in Figure 13.a together with the results for a larger borehole diameter and center pipe. In comparison, the pressure drop in a single 40 x 2.4 mm U-tube collector in a 300m borehole is about 1.2 bar.

The influence of the pressure drop on the total performance can be determined by assuming that the energy supplied by the coaxial BHE is upgraded to a higher temperature level with a heat pump, having a constant average COP at the specified temperature levels. The power requirements for the circulation pump can then be determined and added to the compressor work of the heat pump. The results from this are shown in Figure 13.b where a constant COP of 4 and a circulation pump efficiency of 75 % have been assumed.

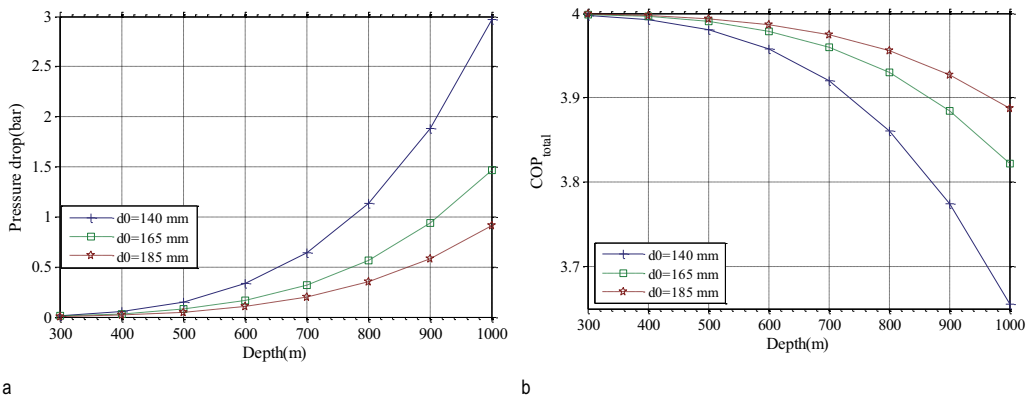


Figure 13. a) Pressure drop (bar) as function of borehole depth and diameter, simulation time 5000 h, GG=20 K / km b) COP_{total} , as function of borehole depth and diameter, simulation time 5000 h, GG=20 K / km

As seen, COP_{total} decreases with increasing borehole depth when the power requirements for fluid circulation are included. It is seen that for larger borehole diameters the pressure drop and the decrease in COP_{total} is significantly reduced.

The power requirements for fluid circulation are for most cases less than 5 % relative to the heat pump compressor. This is acceptable and comparable with a conventional GSHP system using 200 – 300 m boreholes.

It is important to point out that the decrease in COP_{total} with depth presupposes the criteria of a constant temperature level. Reducing both mass flow rate and the heat extraction rate increases the fluid temperature and reduces the pressure drop; as a result the COP_{total} increases. This does, however, reduce the total heat output somewhat.

The simulated time period of 5000 h is an approximation to the cold season (October to April) when heating is needed in Scandinavia. While in general, BHEs only operate at peak load for a shorter part of the operation time, the simulated deep BHEs are operated with a high heat load and a long operation cycle; this makes the results conservative and representative also for longer operation times.

As shown, there is a clear potential to extract significant amounts of energy from deep BHEs. These deep BHEs can be used as an option to shallow BHEs, for example to cover large heating loads in areas where there is scarcity of space. As an example, an 800 m deep coaxial BHE can provide the equivalent heat load of more than 6 conventional 300 m U-tube BHEs, thus dramatically reducing the total borehole length and the required surface area, thereby, making GSHP systems an option also in e.g. urban areas. The benefits of having a system that is space efficient, and that can sustain a higher specific heat load has to be weighted to the possible additional costs associated with drilling at larger borehole depths.

6. Discussion / Conclusion

The aim of this paper was to perform a study on the performance of deep coaxial borehole heat exchangers. This has been done through the means of a new numerical model representing a coaxial BHE, which has been presented and validated against measurements from an experimental setup. The coaxial BHE was chosen as it can have a better thermal performance than a conventional U-tube BHE and is more suitable for deeper boreholes.

While for boreholes in the range of (≈ 200 m) it is seen that there is little or none obvious effects related to the flow direction of the heat carrier, larger effects are seen for deeper boreholes. In general the coaxial BHE is best utilized if the fluid inlet is through the annular space during heat extraction and through the center pipe during heat injection. The thermal performance can be increased by reducing the heat transfer between the fluids in the center pipe and the annular space. For a given heat load, this can be achieved either by increasing the thermal resistance through the center pipe, and/or by increasing the mass flow rate.

The freezing temperature of water is an obvious limit for an open loop system, it is, however, demonstrated that even with this limitation, the deep coaxial BHE can support a significantly higher heat load than conventional U-tube BHEs.

The mass flow rate has a large influence on the thermal and hydraulic performance of the coaxial BHE, a large mass flow rate give a high thermal extraction rate while reducing the need for a thermally insulated center pipe. This comes at the cost of increased pressure losses; these can, however, be reduced by increasing the size of the borehole and the center pipe. The results from the parametric performance study show that the increase in system performance with increasing borehole depth outweighs the increase in pressure losses and pumping power.

Acknowledgments

The paper was written with funding from the Norwegian centre for renewable energy (SFFE).

References:

- Acuña J. Distributed thermal response tests- new insights on u-tube and coaxial heat exchangers in groundwater-filled boreholes. Doctoral Thesis, KTH, Stockholm 2013.
- Bauer. D., Heidemann. W., H. Müller-Steinhagen., H.-J.G. Diersch (2011) Thermal resistance and capacity models for borehole heat exchangers. *Int. J. Energy Res*, v 35, pp. 312-320
- De Carli. M., M. Tonon., A. Zarrella., R. Zecchin, (2010) A computational capacity resistance model (CaRM) for vertical ground-coupled heat exchangers. *Renewable Energy*, v 35, pp. 1537-1550

- Diersch. H.-J.G., D. Bauer., W. Heidemann., W. Rühaak., P Schätzl, (2011^a) Finite element modeling of borehole heat exchanger systems Part 1. Fundamentals. Computers & Geosciences, v 37, pp. 1122-1135
- Diersch. H.-J.G., D. Bauer., W. Heidemann., W. Rühaak., P Schätzl, (2011^b) Finite element modeling of borehole heat exchanger systems Part 1. Numerical simulation. Computers & Geosciences, v 37, pp. 1136-1147
- Kohl. T., Brenni. R. , Eugster. Walter, (2002) System performance of a deep borehole heat exchanger. Geothermics 31 p 687 - 708
- Kays. William., M. Crawford., B. Weigand, (2005) Convective Heat and Mass Transfer
- Mottaghy D., L. Dijkshoorn, (2012) Implementing an effective finite difference formulation for borehole heat exchangers into a heat and mass transport code, Renewable energy, v 45, pp. 59-71
- Rybach. L., R. Hopkirk., Shallow and deep borehole heat exchangers- Achievements and prospects. World Geothermal Congress 1995.
- Rybach. L., Eugster. W. J., Hopkirk. R. J., Kaelin. B., (1992), Borehole Heat Exchangers: Longterm Operational Characteristics of a Decentral Geothermal System
- Zanchini. E., S. Lazzari., A. Priarone, (2010) Improving the thermal performance of coaxial borehole heat exchangers. Energy V 35, N2, pp 657-666.

I-6.5 ADDITIONAL RESULTS AND DISCUSSION

In the following subsections, additional results are presented. These results are valuable complements to the results presented in Paper 4 and are meant to give further information, which could not be presented within the scope of the paper. Results are presented regarding the use of coaxial BHEs for both shallow and deep boreholes.

The results are divided into three parts of which the first (subsection I-6.5.1) is a direct extension of the results presented in Paper 4 for a 190 m deep borehole with a coaxial collector. In this part the transient heat transfer during heat extraction and heat injection is studied in detail using the numerical model. The results (from heat injection) are also further compared with the measurement data from Acuña (2013).

In the second part (subsection I-6.5.2) results are presented from simulations of heat extraction and heat injection in a 800 m deep coaxial BHE. The results focus on the transient heat transfer and the distribution of the specific heat load in the borehole. The results further show the suitability of the deeper boreholes as a heat source and sink.

In the third part (subsection I-6.5.3) the results from a parametric study are presented. This is also an extension to the results presented in Paper 4, although a slightly different approach is used. In Paper 4, the changes in thermal performance (heat extraction rate) with depth are evaluated using a constant heat carrier inlet temperature to the BHE and a constant time average of the heat carrier outlet temperature from the BHE. In this part the performance is instead evaluated using the total COP (COP_{total}) for a system where the heat extracted from the BHE is assumed upgraded to a higher and constant temperature level using a heat pump. The performance of the system is then evaluated based on the use of high value energy (electricity) for the circulation of the heat carrier and for the compressor in the heat pump. Since the COP of the heat pump increases with the temperature level of the extracted heat carrier, the value of having a higher heat carrier temperature level using a deeper BHE is assessed. The result from this study is important as it is shown that the increase in heat pump performance with depth outweighs the associated increase in pump work for circulation of the heat carrier.

I-6.5.1 SIMULATION OF 190 M COAXIAL BHE

In the following, the numerical model is used to study the influence of mass flow and flow direction for heat extraction and recharge using the BHE configuration presented in Paper 4. The parameters for the BHE are summarized in Table I-2.

Table I-2. Parameters for experimental setup.

Parameter	Value
k_g [W /m·K]	3.53
Active length BHE [m]	165
Borehole diameter [mm]	115
Collector (center pipe)[mm]	40 x 2.4
Collector (outer membrane) [mm]	114 x 0.4
k_c [W/ m·K]	0.42
Heat carrier	Water
Mass flow rate [kg/ s]	0.44-0.7
Heat load [kW]	6.2 - 6.5 kW

The numerical model is used to simulate the measured data obtained in the DTRT performed by Acuna (2013). The distributed temperature measurements are used to calculate the applied thermal load during the DTRT. The specific heat capacity of water is evaluated from NIST(2013) based on the arithmetic mean value of the inlet and outlet temperatures. Note that the temperature measurements and the simulated results presented start at 17 m depth in the borehole. heat transfer in the upper part of the borehole as well as in the surface equipment (piping and circulation pump) is not accounted for. The applied heat load during the DTRT is shown in Figure I-20. This section focuses on the first heating period and the first part of the recovery period.

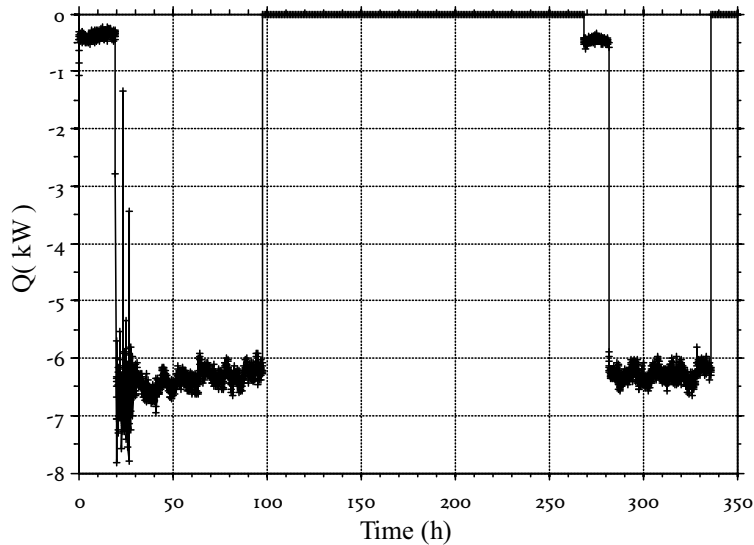


Figure I-20. Calculated heat load during DTRT.

I-6.5.1.1 HEAT INJECTION TO 190 M COAXIAL BHE

In this subsection results from simulation of heat injection to a 190 m deep coaxial BHE is presented.

Temperature profiles during the start of the first heat load period (19.76 h to 20.92 h) are shown in Figure I-21. The left (colder) part of each profile corresponds to the annular space and the right (warmer) part to the center pipe. The first profile (19.76 h) is taken before the heat load is applied.

The mass flow rate is about 0.58 kg / s during the test. The flow velocities in the annular space and in the center pipe are approximately 0.065 m/ s and 0.6 m/s, respectively. Therefore, it takes the fluid about 4.6 minutes to travel down through the simulated center pipe and 42.5 minutes to return up through annular space of the BHE. This difference in flow velocity is the reason why the curve representing the annular space in the second profile has barely changed from the first profile while the curve corresponding to the center pipe has moved to the right in the figure.

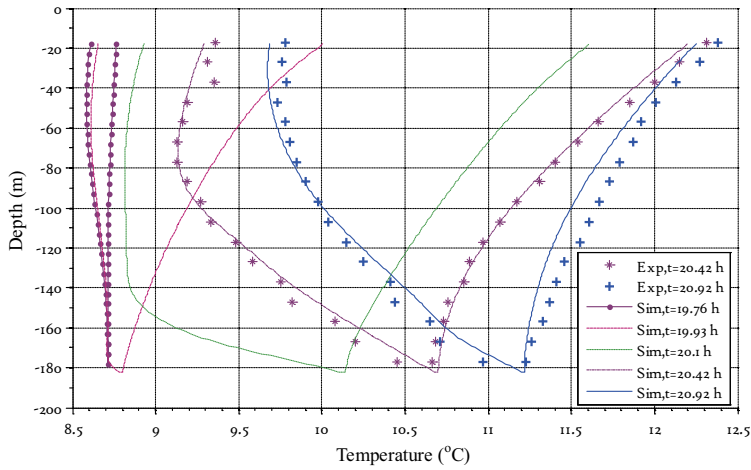


Figure I-21. Fluid temperature profiles, temperature in coaxial BHE, heat injection with inlet through center pipe

In Figure I-22 the borehole wall temperature is shown for the times corresponding to the profiles in Figure I-21. Note that the second profile (19.93 h) is nearly identical to the first. This is because the warm water is circulated down through the center pipe, and it is separated from direct contact with the borehole since it has not yet reached the annular space. The third, fourth and fifth profiles clearly show that the lower part of the borehole is heated up first as the fluid travels slowly up the annular space.

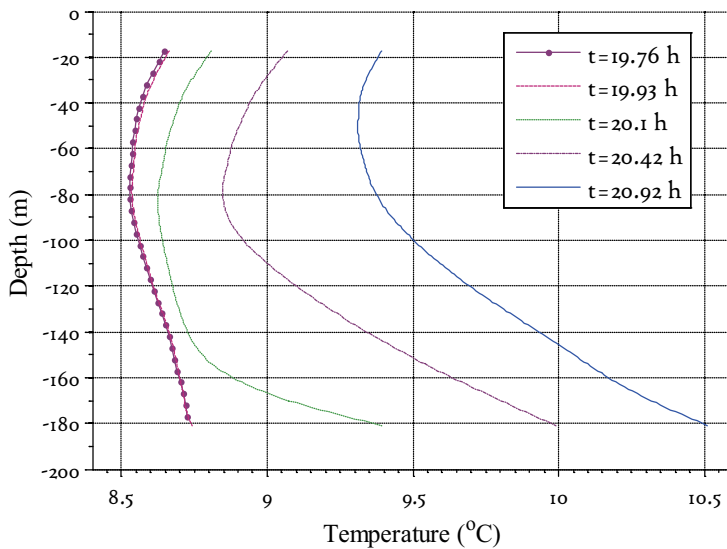


Figure I-22. Borehole wall temperature in coaxial BHE, corresponding to Figure I-21.

In Figure I-23, the specific heat load in the borehole is seen. The heat load is determined based on the conductive heat transfer in the rock. As expected the later profiles show a heat load that is largest in the lower part of the borehole; moreover, it is clearly shown on the second profile that the fluid has just entered the annular space. On the third profile (20.1 h) the fluid in the annular space has moved slightly less than 40 meters which is in accordance with the flow velocity.

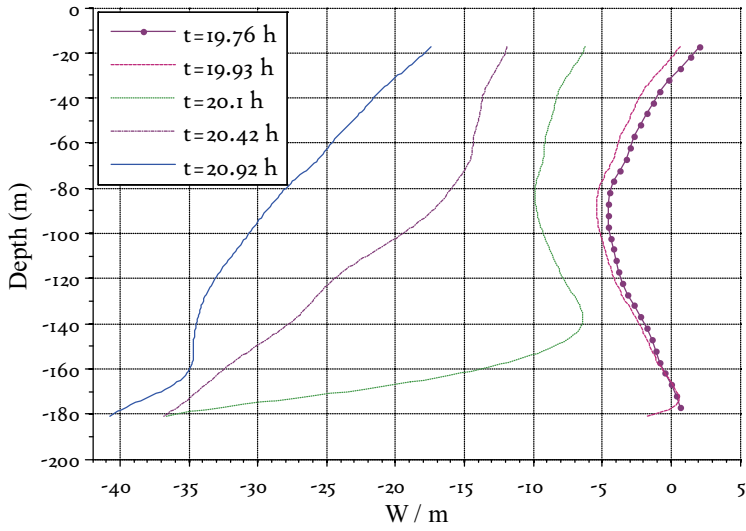


Figure I-23. Specific heat load in coaxial BHE, corresponding to Figure I-21.

Although the mass flow is stopped at 97.9 hours after the first heating period, the fluid in the annular space is initially not stagnant. While energy is still being transferred from the borehole, natural convection is initiated in the annular space. In the numerical model, this has been accounted for through a Nusselt- correlation derived in Paper 1. As seen in Figure I-24 this gives a better fit to the experimental data than assuming stagnant water.

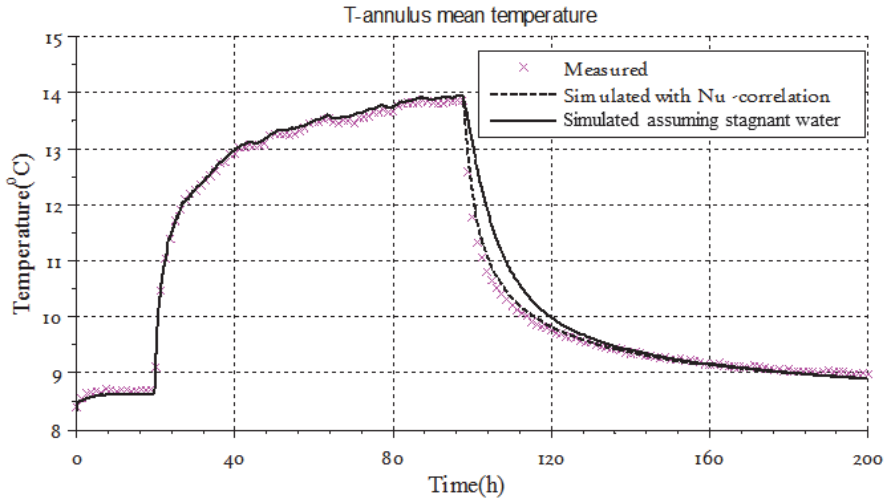
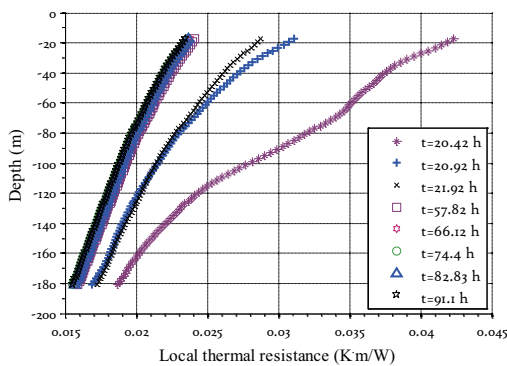


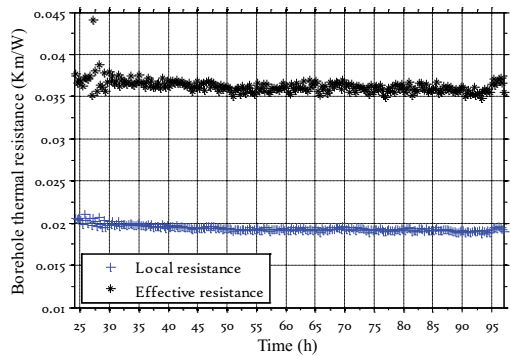
Figure I-24. Comparison between arithmetic mean values of the temperature in the annular space as determined with and without the influence of natural convection.

As shown, there is clearly a difference which remains for about 40 hours (between 97 and 137 hours). In the case of the studied DTRT experiment, this difference does not significantly affect the calculated results during the second heating period. During simulation of normal and continuous heat pump operation (shorter time periods), it is, however, likely that it will have some influence on the results.

In Figure I-25 a) the vertical distribution of the local thermal resistance is shown for the different times during the heat injection phase of the DTRT. The vertical averages of the local thermal resistance and the effective resistance are shown in Figure I-25 b).



a)



b)

Figure I-25. a) vertical distribution of local borehole thermal resistance. b) Variation over time of the vertical mean value of the local resistance and effective resistance.

The thermal resistances are low in comparison with the corresponding values for a U-tube collector as shown in Figure I-11. The values are also nearly constant in time as they are independent on the changes in water temperature. As seen in Figure I-25 a) the local thermal resistance is higher in the upper part of borehole, indicating that the overall heat transfer in this section of the borehole is less effective.

I-6.5.1.2 HEAT EXTRACTION FROM 190 M COAXIAL BHE

In the following figures, both the flow direction and the heat load is reversed as compared to the previously presented case (I-6.5.1.1). The left (colder) part of each profile corresponds to the annular space and the right (warmer) part to the center pipe. As seen in Figure I-26 the resulting temperature profiles are distinctly different from that of Figure I-21.

The first profile (19.76 h) still show the profile before the extracted heat load is applied. In the second profile, the cold water travels down in the annular space. Note that the top of the part of the second profile that corresponds to the center pipe is as well cooled down, this is more obvious in the third and fourth profiles. As the injected cold fluid has not yet reached the bottom of annular space, and therefore, not entered the center pipe, this is clearly due to heat transfer between the fluid in the center pipe and the annular space. This heat transfer can be thought of as a thermal short circuit, and it is undesired as it reduces the thermal performance of the BHE. In the last profile (20.92 h), this gives a negative curvature of the profile for the center pipe. By either reducing the temperature difference between the fluid in the annular space and the center pipe, or by increasing the thermal resistance in the center pipe, the short-circuit can be reduced.

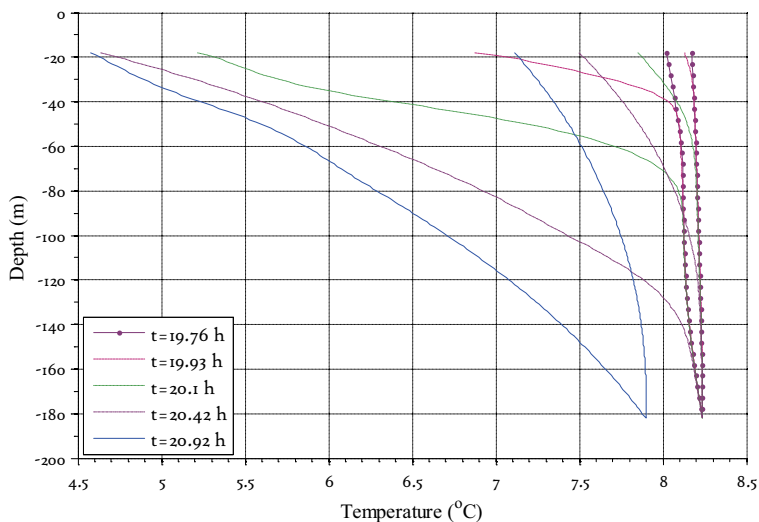


Figure I-26. Fluid temperature profiles, temperature in coaxial BHE, heat extraction with inlet through annular pipe.

In Figure I-27 the borehole wall temperature is shown. The decrease in wall temperature starts in the upper part of the borehole and spreads downward with the velocity of the flow in the

annual space. The temperature change is largest in the upper part of the borehole and consequently also the specific heat load as seen in Figure I-28.

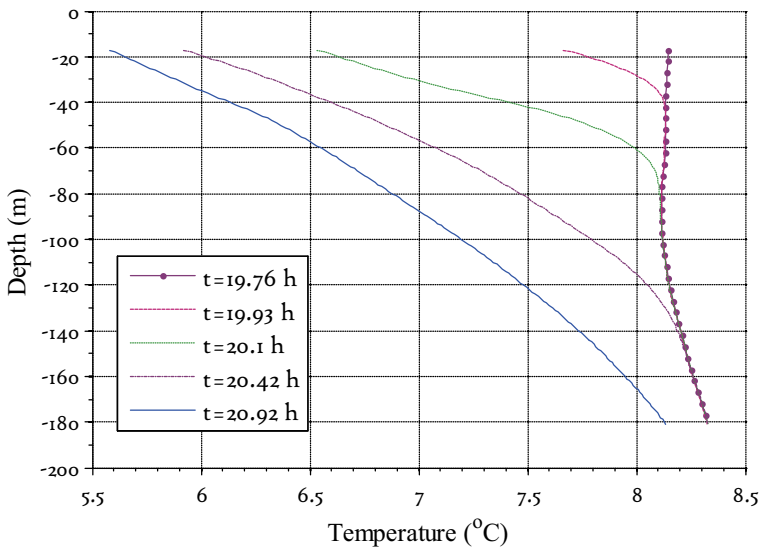


Figure I-27. Borehole wall temperature in coaxial BHE during heat extraction, corresponding to Figure I-26

The specific heat load is largest in the upper part of the borehole. And the heat transfer spreads downward with the rate of the temperature profiles in Figure I-27.

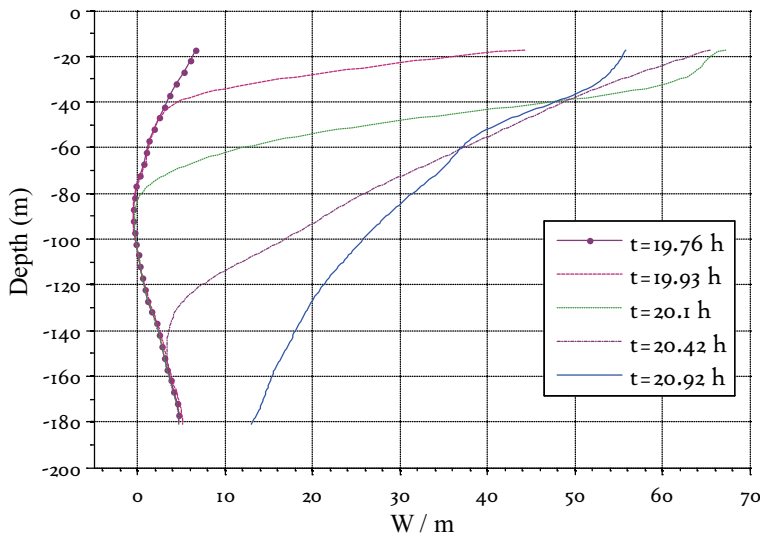


Figure I-28. Specific heat load in coaxial BHE during heat extraction, corresponding to Figure I-26.

In Figure I-29 a) the vertical distribution of the local thermal resistance is shown for the different times during the heat extraction phase. The vertical averages of the local thermal resistance and the effective resistance are shown in Figure I-29 b).

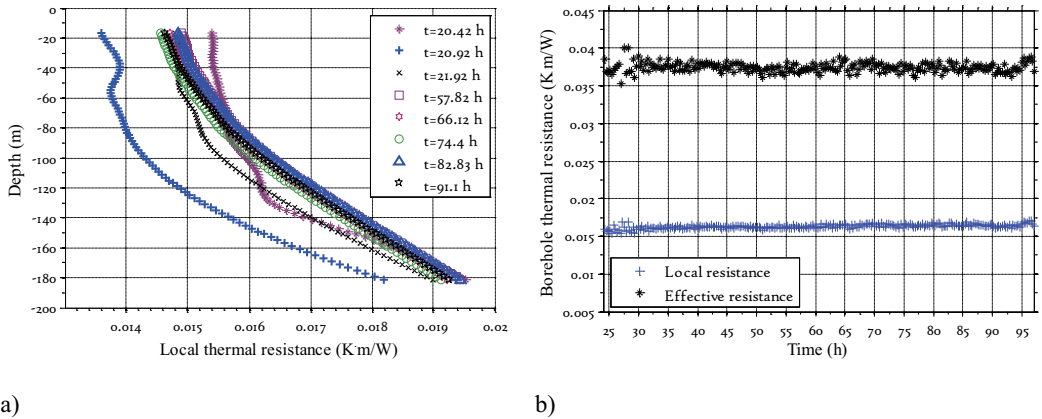


Figure I-29. a) Vertical distribution of local borehole thermal resistance during heat extraction. b) Variation over time of the vertical mean value of the local resistance and effective resistance during heat extraction.

In Figure I-29 it is seen that the local thermal resistance is slightly higher than during heat injection (Figure I-25), and that there is also a small (negligible) difference in the effective thermal resistance between heat extraction and heat injection.

I-6.5.1.3 SUMMARY

The heat transfer during heat injection and heat extraction from a 190 m deep coaxial BHE (active depth 165 m) has been studied. It is seen that the coaxial BHE perform equally well for both heat extraction and heat injection and that it has a better thermal performance than a conventional U-tube BHE (shown by the low thermal resistance). The temperature drop shown for the return fluid in Figure I-26 indicates that the collector would gain from having a thermally insulated center pipe. Alternatively, the mass flow rate could be increased, this would then require an upscaling of the center pipe.

I-6.5.2 SIMULATION OF 800 M COAXIAL BHE

In the following subsection, the numerical model is applied to cases where the borehole depth is increased. Results from a 800 m borehole is presented. The configuration studied is based on the parametric performance study in Paper 4. The borehole diameter is 140 mm, the center pipe has a wall thickness of 5.1 mm and an outer diameter of 90 mm, this is standard dimension for PE(polyethylene) pipes with 10 bars pressure rating. A relatively high mass flow rate (4 kg / s) is used to reduce the need for thermal insulation between the fluid in the center pipe and the fluid in the annular space.

While the potential for heat extraction increases with borehole depth, the potential for thermal recharge decreases. To illustrate this, temperature profiles for both heat injection and extraction are presented. In the case with heat extraction the fluid inlet is in the annular space and in the case with heat injection the fluid inlet is in the center pipe.

A linear fluid temperature profile is assumed as the starting condition for the simulations and the applied thermal load is specified as constant.

I-6.5.2.1 HEAT EXTRACTION FROM 800 M COAXIAL BHE

The fluid temperature profiles for a case with heat extraction versus time and the initial temperature profile of the ground is shown in Figure I-30.

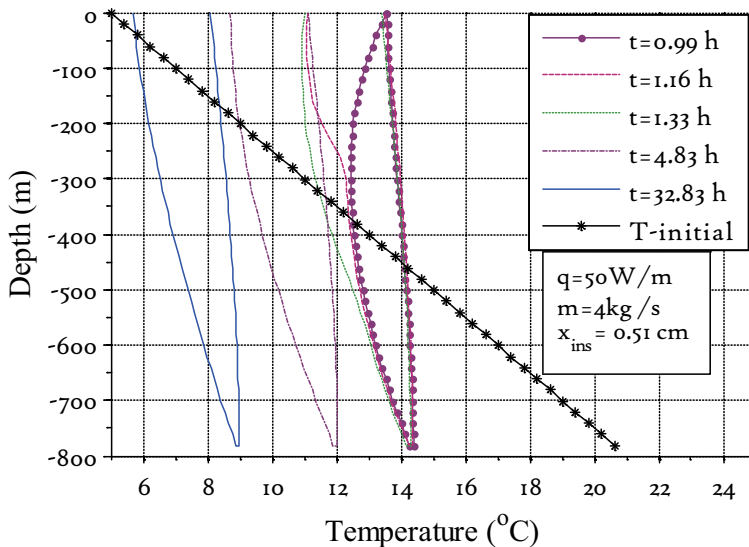


Figure I-30. Temperatur profiles. Specific heat load, 50 W / m

The first profile is taken after 1 hour of fluid circulation without heat extraction. Thereafter, a constant and average specific heat load of 50 W / m is extracted from the BHE. The mass flow rate is 4 kg / s and the flow velocities in the annular space and in the center pipe are 0.44 m/ s and 0.8 m/s, respectively. It takes the fluid 1800 s to travel down on the annular side and 1000 s to return through the center pipe. The first profile is taken just before the heat load is applied. The circulation transports energy between the lower part and the upper part of the borehole, as is evident in Figure I-32. It is first in the fourth profile (4.38 h) in Figure I-30 that the fluid has circulated through the entire BHE and a temperature profile is established. In the fifth profile (32.83 h) the temperature has decreased while the shape of the profile is almost constant.

In Figure I-31 the borehole wall temperature is shown for the instances corresponding to the profiles in Figure I-30. It is seen that the borehole wall temperature for the first profile (0.99 h) reflects the fluid temperature in the annular space. In the following two profiles (1.16 h and 1.33 h) it is seen that the borehole wall is cooled down as the colder fluid travels down in the annular space.

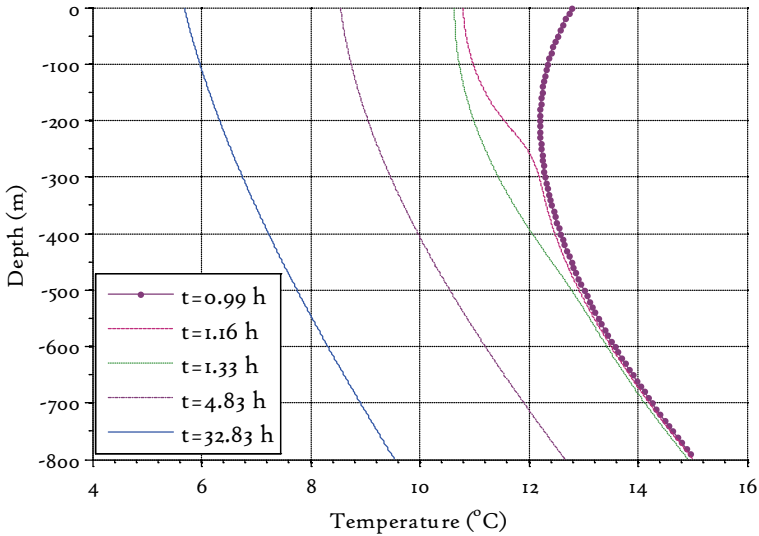


Figure I-31. Borehole wall temperature, profiles corresponding to Figure I-30

In Figure I-32 the specific heat load is shown for the times corresponding to the profiles in Figure I-30. Note that it is only for the last profile (32.8 h) that the heat load is positive also in the upper part of the borehole; that is, heat in being extracted from the entire borehole. As the fluid enters through the annular space, this can as well be seen from Figure I-30 where the temperature of the inlet fluid is close to the initial ground temperature in the last profile.

Instead of applying a constant thermal load, a constant inlet temperature can be used. Given that this temperature is less than the ground temperature, the heat load will be positive all along the borehole. It is primarily the transient behavior as reflected by the first profiles (1.16 h to 4.83 h) that differs between a constant thermal load and a constant inlet temperature. The results from a simulation of heat extraction with a constant inlet temperature and with the same model parameters as used in this section are described in Appendix B.

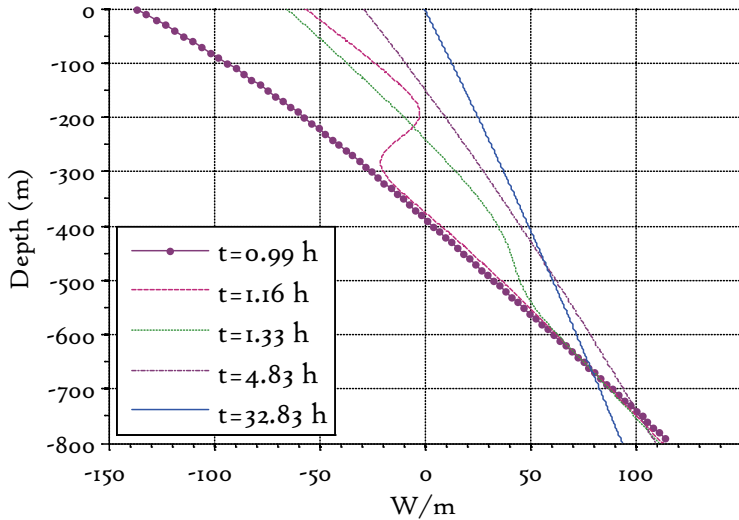


Figure I-32. Distribution of specific heat load in the borehole, profiles corresponding to Figure I-30

The distribution of the specific thermal load in the BHE (Figure I-32) becomes nearly constant after only a few hours of operation (fifth profile (32.83 h)) and clearly reflects the initial temperature gradient in the ground. It is not possible to sustain a constant and high thermal load from the BHE over longer times as the temperature decline becomes too large. This is evident when comparing the relative large load in the lower part of the borehole with Figure 2-7 in Section 2.1.4 where the temperature decline of the borehole wall is seen as a function of time and specific heat load.

Therefore, simulations over time have been made with an operation strategy where the BHE operates for a distinct period, followed by a recovery period. This is similar to the operation of conventional BHE installations. In Figure I-33 the distribution of the specific thermal load is shown for a case where an 800 m deep coaxial BHE has been simulated for 20 years. The simulation is based on the same parameters as the simulation presented in Figure I-30 - Figure I-32.

The BHE has been operated with a period of 24 hours. In addition, a seasonal recovery period of 4 months is applied. The choice of a relatively large operation period of 24 hours is arbitrary and has little influence on the results (see Figure 2-7 in Section 0). A longer period does, however, reduce the amount of transient changes in the simulation and is, therefore, faster to calculate.

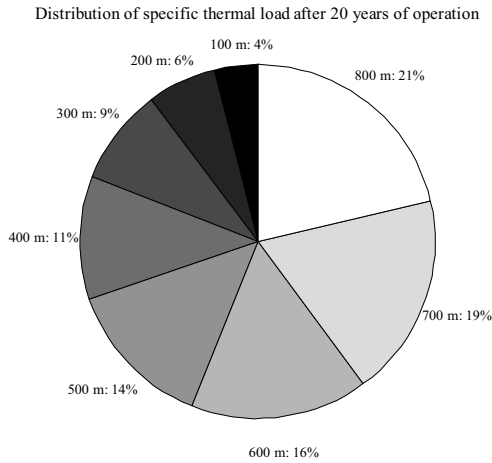


Figure I-33 Distribution of the thermal load in a 800 m deep coaxial BHE after 20 years of operation, the fluid inlet is in the annular space.

It is seen that most of the energy is extracted from the lower part of the borehole, e.g. 40 % of the extracted energy comes from the lowest 200 m while only 10 % comes from the upper 200 m of the borehole.

The distribution of the specific heat load is important as it directly affects the way a deep BHE should be designed and constructed. Since only a small share of the energy is extracted from the top of the borehole, the sensitivity to thermal influence between several deep BHEs is small in the upper part. If the borehole for the BHEs can be drilled with a small deviation, this means that deep BHEs can be placed closely together on the surface and then deviate from each other to create sufficiently large distances between the boreholes near the bottom. The spatial temperature influence from a deep BHE can be determined using Figure 2-5 - Figure 2-6. An illustration of how a number of deep boreholes can be placed together is shown in Figure I-34.

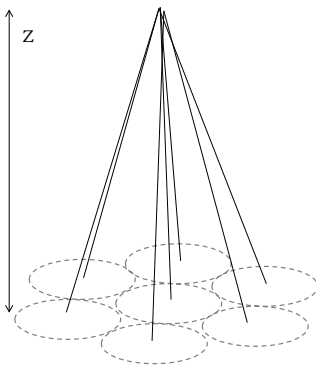


Figure I-34. Illustration of how a number of deep boreholes can be placed together.

I-6.5.2.2 HEAT INJECTION TO 800 M COAXIAL BHE

Conventional borehole heat exchangers can be used for cooling purposes. The potential for cooling decreases with depth as the temperature of the ground increases. In this subsection, the simulation presented in Figure I-30 to Figure I-32 is repeated, but with a reversed flow direction. In this case the warm fluid enters the center pipe and is cooled down as it returns through the annular section.

The temperature profiles are shown in Figure I-35. As seen from the second profile (4.8 h) and last (32.8 h) profiles, it is primary the upper part of the borehole that is used while less energy is being recharged to the lower part. Results from a simulation with the fluid inlet through the annular space can be found in Appendix B, but this is not advisable for thermal recharge as it gives a lower thermal performance (higher mean fluid temperature).

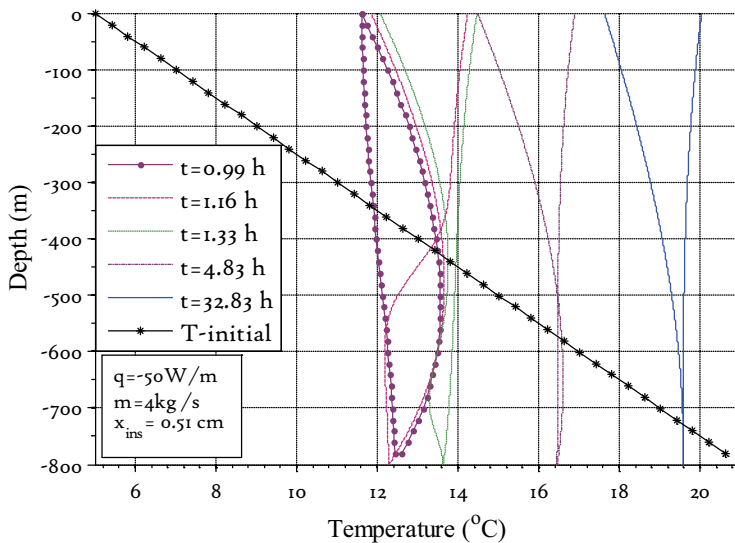


Figure I-35. Temperature profiles during thermal recharge.

When the fluid has reached the bottom of the BHE and entered the annular space, the borehole wall starts to heat up. This can be seen from the third (1.33 h) profile in Figure I-36 (showing the borehole wall temperature) and Figure I-37 (showing the distribution of the specific heat load along the borehole). The later temperature profiles (4.83 h and 32.83 h) show that there is little temperature decrease of the fluid in the lower part of the borehole (from about 500 -600 m depth).

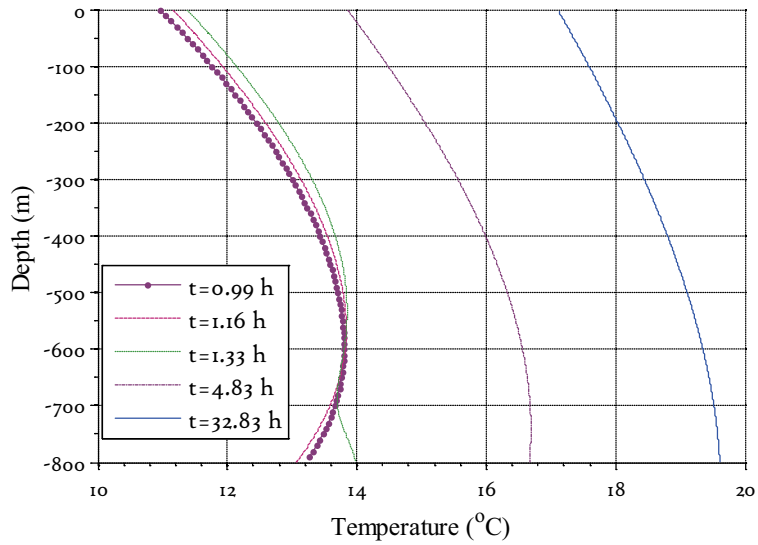


Figure I-36. Borehole wall temperature during thermal recharge, profiles corresponding to Figure I-35

In the lower part of the borehole, the borehole wall is initially warmer than the entering warm fluid; therefore, energy is first being extracted in the lower part, this is most clearly seen in Figure I-37. In the last profile (32.8 h) the temperature of the fluid has increased so that energy is being transferred to the wall in most of the borehole (Figure I-37).

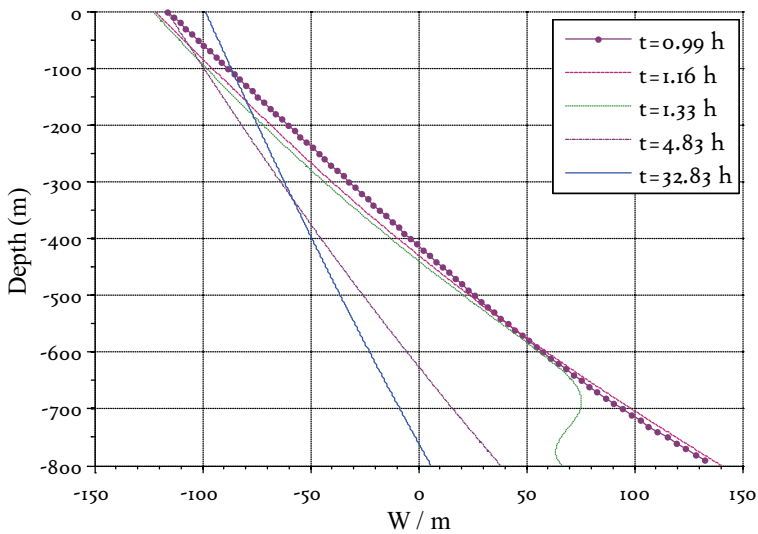


Figure I-37. Distribution of specific heat load during thermal recharge, profiles corresponding to Figure I-35

I-6.5.2.3 SUMMARY

Heat extraction and heat injection is simulated in a 800 m deep coaxial BHE. It is seen that for heat extraction the majority of the heat transfer is located to the lower part of the borehole. This indicates that the separation distance between several deep BHEs should be increased as compared to the distances used for conventional 200 to 300 m BHEs.

The figures show that the presented 800 m deep coaxial BHE can be used also for cooling. It is, however, seen that not the entire borehole is utilized. A shallower borehole could, therefore, have a similar performance for cooling. Also, most of the energy is being recharged to the upper part of the borehole while the lower part, which is most affected during heat extraction is relatively unaffected.

The figures presented have focused on the transient behavior of the deep coaxial BHE, since it takes the heat carrier about 45 minutes to circulate through the entire BHE and at least a few hours before a stable temperature profile is established in the borehole, a relatively large part of the BHEs operation time in connection with a heat pump can be transient.

I-6.5.3 PARAMETRIC STUDY OF COAXIAL BHE

In this subsection, a parametric study of the coaxial BHE is presented. In the study, the performance of the coaxial BHE, as measured by the optimized COP_{total} for each borehole depth as function of the mass flow rate and the physical dimensions of the collector pipe is investigated

I-6.5.3.1 HEAT PUMP AND SYSTEM PERFORMANCE

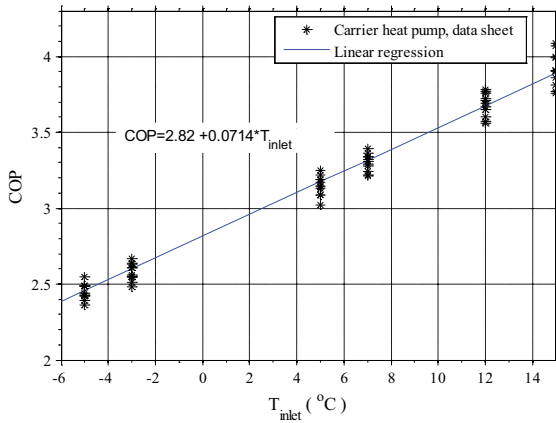
The thermal performance of the coaxial BHE during heat extraction was presented in Paper 4 and is further explored through a parametric study in this subsection. In the parametric study the thermal performance of the coaxial BHE is studied as a function of primarily the borehole depth.

For deep BHEs there is the option to either extract a high amount of thermal energy at a lower temperature level, or to extract less energy but at a higher temperature level. In Paper 4, the study focuses on the first option. In this subsection the focus is on the total performance of the system; that is, the total COP of the system (including the pump work required for circulation of the heat carrier) is used to evaluate the performance.

The maximum total COP is determined as a function of the center pipe wall thickness for different mass flow rates, borehole depths and thermal loads.

The heat pump has not been explicitly modeled; instead it is represented by a correlation as a function of the source temperature. This is then used together with the pump effect of the circulation pump for the heat carrier to determine the overall coefficient of performance (COP_{total}) of the heat pump and the BHE.

For a water to water heat pump, it can be shown that for a constant condenser temperature, there is usually a linear relationship between the heating capacity of the heat pump and the required compressor power as a function of the source temperature. In Figure I-38, a linear regression is fitted (Equation I-5) to data from a range of heat pumps from the producer Carrier (2014). The equation describes COP as a function of the source temperature. The heat pumps use the refrigerant R-410, and the condenser temperature is kept constant at 60 °C. The data has been scaled so that the inlet temperature to the borehole can be used to represent the source temperature.



$$\text{COP} = 2.82 + 0.0714 * T_{\text{inlet}}, \quad \text{I-5}$$

where T_{inlet} is the inlet fluid temperature to the BHE.

Figure I-38. COP as a function of the BHE inlet fluid temperature. Linear regression based on data sheet for Carrier heat pumps.

Increasing or reducing the condenser temperature shifts the trend vertically in the figure while the slope of the linear regression remains constant. It was chosen to keep the condenser temperature constant at 60 °C as it is sufficient for hot water production, the COP values would, however, be higher if lower (between 30 and 45°C) condenser temperatures are used (as those used in modern distribution systems such as floor heating and compact radiators). The overall system performance is then determined as:

$$\text{COP}_{\text{total}} = \frac{Q_{\text{BHE}} + W_{\text{hp}}}{W_{\text{hp}} + W_{\text{p}}}, \quad \text{I-6}$$

$$\text{where } W_{\text{hp}} = \frac{Q_{\text{BHE}}}{\text{COP} - 1}, \quad \text{I-7}$$

and W_{p} is the pump effect of the circulation pump.

I-6.5.3.2 RESULTS FROM PARAMETRIC STUDY

The performance of the coaxial BHE can be improved either by increasing the thermal resistance through the center pipe or by reducing the thermal potential through an increase in mass flow rate. Hereunder, the results from a parametric study are presented in which primarily the influence of wall thickness of the center pipe and the influence of the mass flow rate are studied. The thermal conductivity of the center pipe has been set to 0.24 W/m K which is equivalent to the material polypropylene.

The borehole depth has been varied between 600 m and 1000 m; for each depth, the optimum combination of mass flow rate and physical dimension of the center pipe has been determined. The performance of the BHEs is evaluated after 1000 hours of simulation. The BHEs are operated with an on/off interval representing the operating cycles of the heat pump and assuming that a constant heat load is extracted when the BHE is in operation. This is illustrated in Figure I-39 for an 800 m deep BHE with a constant heat extraction rate of 40 kW; the first two cycles after startup are shown. A rather long operation cycle (of 24 hours) has been used since it reduces the computational time required in the parametric study.

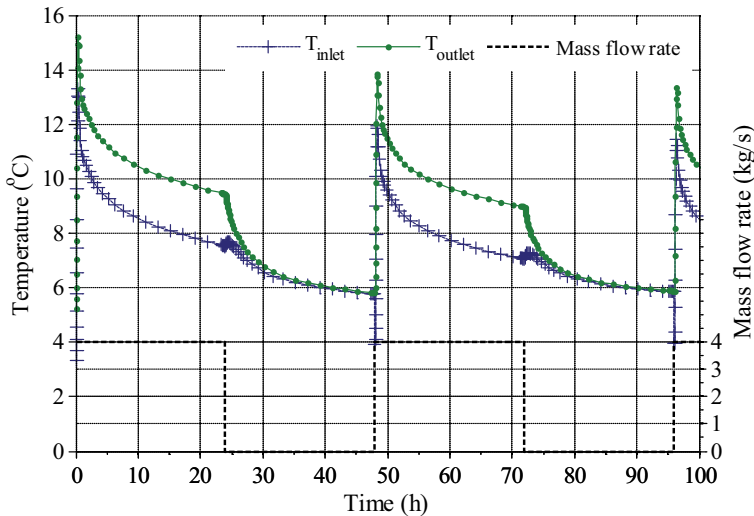


Figure I-39. Illustration of cyclic operation scheme for coaxial BHEs.

The figure shows the inlet and the outlet fluid temperatures from the deep coaxial BHE, for each operation cycle, the mass flow rate is kept at a constant value.

The parameters used in the study are summarized in Table I-3. The flow area of the annular space and the center pipe are chosen so that the pressure drop is kept equal in both parts while the wall thickness of the center pipe is varied. As an alternative, the two flow areas could be kept equal; this will, however, result in a somewhat higher overall pressure drop.

Table I-3. Parameters for parametric study

Parameter	Value
Depth [m]	600- 1000
d_b [mm]	140
Thermal gradient [K / m]	0.02
k_c [W/ m·K]	0.24
Center pipe wall thickness (s) [mm]	1- 20
Heat duty (q) [W /m]	40
Mass flow rate [kg/ s]	1.5 - 5
k_g [W/ m·K]	3

Operation interval [hours]	24
Simulation time [hours]	1000
Pump efficiency, η [%]	75

The correlation for the heat pump (Equation I-5) is used to relate the thermal performance of the BHE to the use of high value energy (electricity) through the COP. The overall performance (COP_{total}) is determined for different flow rates as a function of the center pipe wall thickness (s). To illustrate this, the performance (COP_{total}) of a 800 m deep BHE is presented in Figure I-40. The values in the figure have been normalized to the highest COP_{total} .

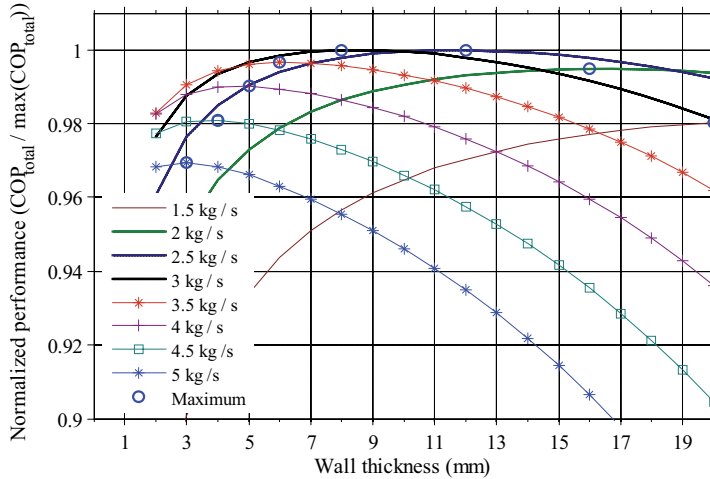


Figure I-40. 800 m coaxial BHE with 40 W/m heat extraction, $D_0 = 140$ mm. The figure shows normalized overall performance for different mass flow rates and center pipe wall thickness. Simulated time 1000 hours.

The maximum value for each mass flow rate is shown in the figure. It is seen that while the maximum performance in this case is found for a mass flow rates of 2.5 and 3 kg/s and a corresponding center pipe wall thickness of 8 and 12 mm, respectively. Other combinations yield a similar maximum performance. As expected, with increasing mass flow rate, the importance of the thermal resistance between the annular space and the center pipe decreases. The figure is based on a borehole with a fixed diameter of 140 mm; however, with a larger diameter, the optimum values would move further to the right in the figure.

The results shown in Figure I-40 are taken after 1000 hours of operation, which is a rather short time period, considering the expected life time of a BHE. The figure is, however, representative, since the changes in optimum wall thickness with time is small, and the rate of change will decrease with longer operating time. The increase in optimum center pipe wall thickness is shown in Figure I-41.

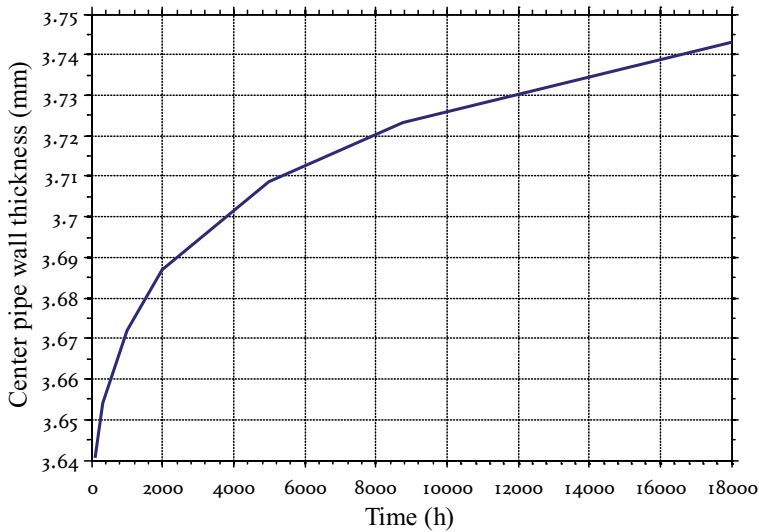


Figure I-41. Change in optimum wall thickness of the center pipe as function of operation time.

E.g. increasing the operation time from 1000 hours to 5000 hours increases the optimum wall thickness with 0.1 mm ($\approx 1.7\%$ of the value for a mass flow rate of 4 kg / s) and has almost no effect on the performance of the BHE. Figure I-40 is, therefore, a robust and accurate representation of the performance of an 800 m coaxial BHE given the parameters in Table I-3.

For different borehole depths, the maximum values of the COP_{total} for each mass flow rate as shown in Figure I-40 have been used to create a chart for the optimum performance of the BHE as a function of center pipe wall thickness and mass flow rate. The borehole diameter and the average thermal extraction rate (W/m) have been kept constant. The chart is presented in Figure I-42 for mass flow rates varying between 2.5 kg/s and 5 kg/s.

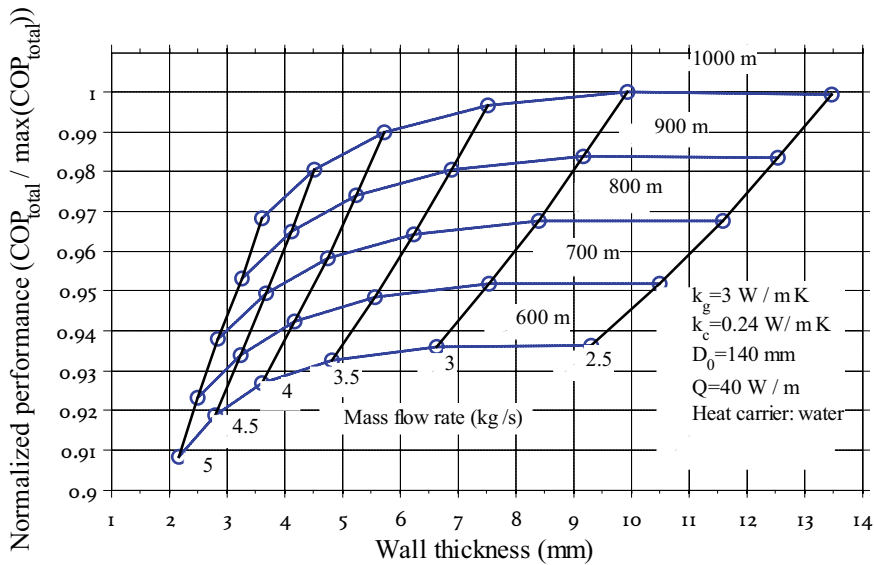


Figure I-42. Performance chart for pipe-in-pipe BHEs. The figure shows normalized COP_{total} as a function of center pipe wall thickness, borehole depth and mass flow rate. Lines for constant borehole depths and constant mass flow rates are shown in the figure. Simulated operating time is 1000 hours.

Figure I-42 shows the optimum performance of the BHE based on COP_{total} , the lines correspond to both constant borehole depths and mass flow rates. It is seen that the overall performance increases with depth and that the maximum COP_{total} is found for a mass flow rate of about 3 kg/s and a center pipe wall thickness between 6.6 mm and 10 mm. There are, however, several combinations of mass flow rate and wall thickness that can give an almost similar performance.

These results assume a constant heat pump condenser temperature of 60 °C, and as a result a rather low COP. If the heat pump COP is increased the power consumption of the circulation pump becomes relatively larger and has more influence on the total COP. As a consequence, the optimum wall thickness corresponding to each mass flow rates decreases.

Also, the thermal conductivity of the center pipe has been kept fixed at 0.24 W/m K in the study. Increasing the thermal conductivity to 0.42 W/m K, (corresponding to polyethylene pipes) results in similar center pipe dimensions for larger mass flow rates while a larger center pipe wall thickness is required for lower mass flow ranges.

The price of the center pipe is linearly proportional to its weight which increases with an increasing wall thickness, i.e. increasing the wall thickness from 4 mm to 10 mm increases the price about 2.5 times. If economical aspects would be weighted in, it is, therefore, expected that the optimum would move further to the left side of the figure, favoring a larger mass flow rate and a thinner wall thickness.

Another way of showing the increasing potential with borehole depth is to keep COP_{total} constant while determining the resulting heat load. This would imply that the temperature lift by the heat pump, and the return temperature from the heat pump both are kept constant and

invariant with borehole depth. Further, means that the ratio between the power used by the circulation pump (W_p) and the heat pump compressor (W_{hp}) is kept constant.

The parameters from the previously modelled case (Table I-3) are used, but instead of using a constant heat load, a constant inlet fluid temperature is used. The center pipe dimensions determined in Figure I-42 are used while the mass flow rate is adjusted accordingly to the average heat load and the requirement of a constant COP_{total} . The parameters used in addition to Table I-3 are summarized in Table I-4.

Table I-4. Parameters for parametric study

Parameter	Value
COP_{total} [-]	3.8
T_{inlet} [°C]	2
W_p / W_{hp} [%]	5

It is found that for each borehole depth, the variation in the results is small. It is, therefore, sufficient to show only the values for pipe dimensions corresponding to a mass flow rate of 4 kg/s in Figure I-42. The results for the total heat loads are presented in Figure I-43.a and the temperatures and the heat loads in the end of the simulation are shown for the 800 m BHE in Figure I-43.b.

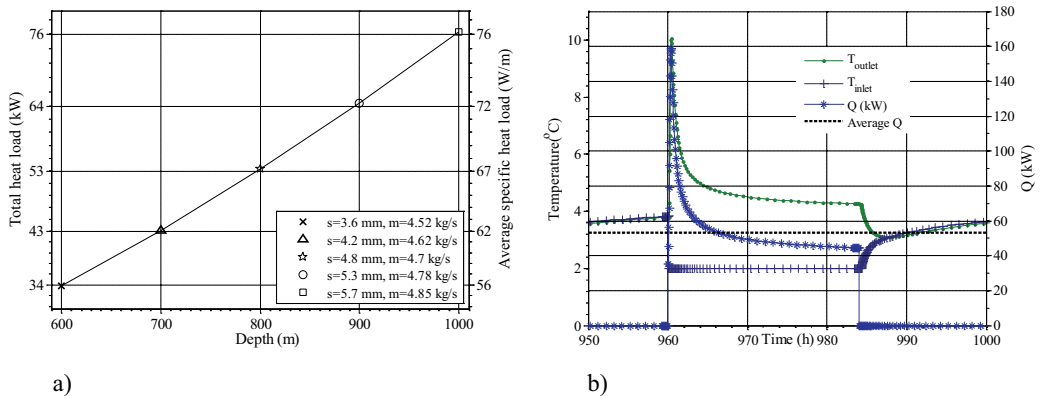


Figure I-43. a) Total and average specific heat load as function of borehole depth. b) Temperatures and heat load in the end of the simulation for 800 m BHE, $s= 4.8$ mm, $\dot{m}=4.7$ kg/s. Simulated time 1000 hours.

The average specific heat load increases with depth; the change is 35 % between 600 m and 1000 m. A rather large mass flow is used in all cases, which reduces the thermal potential between the inlet and outlet fluid, and the need for thermal insulation. Also, with a higher mass flow rate, the temperature change in the surface process is less which in the case of the pipe-in-pipe coaxial BHE means that more energy can be extracted without risking freezing of the water.

It should be emphasized that the heat load declines over time, after 1 year it has declined with 5% and after 5 years the decline is in total 30 % but thereafter, the decline is almost negligible.

As shown, there is a clear potential to extract significant amounts of energy from deep BHEs. Deep BHEs can be used as an option to shallow BHEs, especially for large heating loads in areas where there is a scarcity of space. As an example, an 800 m deep coaxial BHE can provide the equivalent heat load of more than 6 conventional 200 m U-tube BHEs thus dramatically reduce the required surface area and thereby, make GSHP systems an option also in e.g urban areas where there often is a scarcity of space. The benefits of having a system that is space efficient, and that can sustain a higher specific heat load has to be weighted to possible additional costs associated with increased borehole depth

I-6.6 CONCLUSIONS

The thermal performance of the coaxial BHE has been studied for different borehole depths and with water as the heat carrier. The deep BHE is most efficient for heat extraction, and the potential for cooling decreases as the ground temperature increases with borehole depth. Relative to conventional BHEs, the deep BHE can sustain a higher thermal load during heat extraction which significantly reduces the total drilling length required to cover a given heat load.

The flow direction of the heat carrier affects the thermal performance of the coaxial BHE. During heat extraction, the heat carrier should be injected through the annular space. If used for heat injection, the fluid should enter through the center pipe. This is most important for deeper boreholes, for a shallow borehole with a single and uninsulated center pipe, the flow direction has little importance, as seen in Paper 4.

During heat extraction, the vertical distribution of the thermal load in the borehole follows the thermal gradient; therefore, most of the energy is extracted from the lower part of the borehole. During heat injection, the distribution of the thermal load is reversed such that the upper part of the borehole will be heated up while the lower part is poorly utilized.

The distribution of the thermal load also influences the way deep BHEs should be constructed. The thermal influence is proportional to the thermal load, which during heat extraction is small in the upper part of the boreholes. Several boreholes can, therefore, be placed near each other on the surface, but should have a deviating pattern to create a sufficient distance between the boreholes in the deeper parts of the boreholes.

For a deep BHE with water as the heat carrier, there is a bottleneck problem connected to the thermal output from the borehole. In order to get the heat out from the borehole without lowering the inlet temperature below 0 °C, the mass flow has to be rather high. A high mass flow also increases the thermal performance of the deep coaxial BHE since it reduces the internal heat losses and increases the heat transfer for the surrounding rock. The drawback with a high mass flow rate is that it can cause excessive pressure losses if the internal flow area in the coaxial BHE is too small. It is, however, shown in the parametric study that the increase in system performance with increasing borehole depth significantly outweighs the effect of the increase in pressure losses and pumping power. This indicates that the optimum configuration for a deep coaxial BHE used for heat pump applications is a combination of a thin walled center pipe and a rather high mass flow rate.

PART II

II CLOSED LOOP ENGINEERED GEOTHERMAL SYSTEMS

II-1 Introduction

In this part of the thesis the focus is on the geothermal resources that are made up by the thermal energy stored in the upper few kilometers of the earth 's crust; that is outside the tectonically active areas with naturally occurring hydrothermal resources. The aim with the development of Engineered geothermal systems (EGS) is to access and extract this vast energy resource.

EGS has so far mainly been developed through a series of research and pilot projects where the target has been to use the thermal energy for production of electricity, which requires a rather high production temperature. These projects have as well been initiated in geological locations that have more favorable conditions, i.e. higher temperature levels than what can be found in Norway (which is the main focus and origin for this work).

An EGS installation in Norway would, however, most likely be used directly in district heating systems, (due to the country's high heating demands and large hydropower resources) thus eliminating the rather low efficiency associated with binary cycles used for electricity production. The most commonly known approach to an EGS is a system where the connectivity between the production and injection well is established using artificially created networks of fractures. In such system the heat transfer is less dependent on the thermal conduction in the rock (as a large heat transfer area can be created). In the EGS concept studied here the connectivity between the production and injection well is created by drilling a number of wellbores. This limits the heat transfer area (which means that the heat transfer is more dependent on thermal conduction). And thus, generally a larger temperature difference is required between the working fluid and the initial temperature of the rock surrounding the wellbores. Interaction with existing fractures, and resident fluids in the rock is not wanted, and the system can, therefore, be referred to as a closed loop EGS.

The concept enables production of hot water in the temperature range required for district heating (60 °C – 90 °C) given what is considered accessible depth (say 5 to 6 km) and a geothermal temperature gradient of about 20 K/km to 30 K/km.

Presently there are no boreholes in the depth range sought onshore in Norway; therefore, the temperature levels at the target depth for an EGS have to be estimated using measurements of temperature and thermal properties from shallower boreholes (< 1000 m).

II-2 Section structure

This section starts with a summary of related previous works. Thereafter follows three parts, the first part is a brief presentation of the closed loop EGS and serves the purpose of demonstrating the performance of the system. This part is summarized in Paper 5, “*A novel concept to engineered geothermal systems*”.

The second part is about the thermal structure of the ground. In Norway there is a lack of deep boreholes (> 1000 m) onshore. As a consequence there are no direct temperature measurements showing the thermal structure in the depths of interest for EGS. An indirect method to estimate the temperatures is presented, where a numerical steady state thermal model is applied to a geophysical model of the Oslo graben. This part is presented in Paper 6 “*Thermal modeling in the Oslo rift, Norway*”.

The third part contains a more detailed study of the closed loop EGS presented in Paper 5. A transient numerical model is developed and presented for the system. The model is then used to study the thermal characteristics of the system. To further explore the usefulness of the EGS as a provider of thermal energy, the model is used in conjunction with measurements from a district heating network.

II-3 Previous works

Geothermal energy is one of the energy resources that has attracted attention as the search for alternatives to fossil fuels has increased. In the MIT report “Future of Geothermal Energy”, Tester et al. (2006) estimated that 100 GW_e could be produced from geothermal systems in the USA within the next 50 years after a moderate R&D investment. The interest for geothermal energy has increased worldwide, and assessments of geothermal potential are made for many parts of the world, e.g. during the World Geothermal Congress 2010 in total 111 papers were presented in the categories “country updates” and “resource assessments”. Also in Norway, heat flow measurements have been conducted in recent years, indicating an average thermal gradient slightly less than the world average of (30 K/km) Slagstad et al. (2009), Pascal (2010).

II-3.1. ENGINEERED GEOTHERMAL SYSTEMS (EGS)

In the past, deep geothermal energy has been closely associated with the geographically constricted and naturally occurring hydrothermal systems in active volcanic regions. In recent years it has been pointed out that Engineered Geothermal Systems (EGS) can provide a way for geothermal energy as an energy resource to grow independently of the geographical constraints of hydrothermal systems and, thereby, to reach a significant share of its huge global potential.

The research on EGS or hot dry rock (HDR) systems as it was first named started in the early nineteen seventies at the Los Alamos National Laboratory and with Fenton Hill as the first field

project. The aim of the project was to develop methods for heat extraction from hot dry crystalline rock. The project which started in 1974 targeted resources in the vicinity of a hydrothermal system, the deepest well reached a depth of 4390 m and reached a temperature of 327 °C. Hydraulic fracturing was successfully used to create permeability between production and injection wells and flow testing showed that it is possible to extract heat from dry crystalline rock at reasonable rates (around 10 MW_{th} and with a production temperature of 180 – 190 °C). The produced fluids were used to generate electricity with a binary turbine cycle, producing 2- 3 times the amount of energy required to operate the system (Brown and Duchane 1999). The Fenton Hill project generated a substantial amount of novel experience and knowledge regarding EGS.

The Fenton Hill project has been followed by several subsequent projects that have been placed primarily in sedimentary basins and in the periphery of hydrothermal regions. A good review of the major R&D field projects is given in Tester et al. (2006).

A milestone was reached in 2006 when electricity production could be started from a research project in Soultz, France (Cuenot et al. 2008), (Genter et al. 2009). Since then, commercial companies have been joining the field, and amongst others, USA and Australia have invested significant resources into the research and development of geothermal energy. The 3rd of May 2014 electricity production started at the commercial EGS power plant in Habanero, Australia where heat is extracted from a sedimentary basin. Although these pilot-plants have a relatively low power output in the range of 1 MW_e, they are important proofs to the validity of the concept with artificially created geothermal systems.

For EGS to reach a significant portion of its vast potential, it must be proven that the concept can be applied largely independent of site conditions. Since the geological and thermal structure of the uppermost kilometers of the earth crust varies geographically, the designs are site dependent. This makes EGS a conceptual name for a wide range of ways to utilize deep geothermal energy, ranging from single well concepts using the natural permeability of sedimentary basins to systems with multiple wells and artificially constructed fractures in crystalline rock. A variety of concepts should be expected since the aim is to create the possibility to use geothermal energy regardless of site specific geology.

Australia and Germany are examples of countries that are active in the development of EGS systems as illustrated by the work of Long et al. (2010) and Schellschmidt et al. (2010). Their priorities and aims are to produce electricity and their geological conditions are more favorable than what are found in Norway. However, an EGS system constructed in Norway would supply hot water e.g. for district heating purposes, without the low efficiency associated with binary power cycles. In comparison to an EGS for power production which would typically target areas with the highest geothermal potential, a geothermal plant for district heating would be restricted to areas where infrastructure and demand for hot water exists. In addition, the temperature level requirements of the heat consumer will have a significant impact on the amount of thermal energy that can be extracted from the EGS.

A key benefit of EGS is that it can provide a stable energy source that is local and environmentally friendly. Thus it can be used as a base load for both heat and electricity

production. Since it is a local resource it also has socioeconomical benefits such as improved energy security.

With only a few EGS plants operative today the technology is still in a development phase. Although reports such as Tester et al. (2006) predict a bright future for the technology, there are some obstacles ahead, e.g.

- Reservoir stimulation induces seismicity. In 2006 the stimulation of a reservoir in Basel resulted in an earthquake that caused damage to buildings, Häring et al. (2010). This subsequently caused a major drop in popularity and acceptance of EGS.
- Large quantities of water are required both for the construction phase and for operation of the plants, Driscoll (2010). This can prevent the development of EGS using fractures in areas where there is a scarcity of water.

II-3.2. EGS- CONCEPTS

In an EGS with several wells or with fracturing, the idea is to create connectivity between the wells. The basement rock is by nature intersected by fractures. By applying hydraulic pressure in the first well, existing fractures are widened, this enables existing shear forces acting on the fractures to cause slip, which creates permeability after the pressure is released. The propagation and location of fractures can be monitored through seismic measurements and can then be targeted by a second well, Rothert and Baisch (2010). This is the most established method to create an EGS and has been applied in several projects, Genter et al.(2010), Quick et al. (2010), Kaieda et al. (2010). An schematic illustration of a EGS based on fracturing is shown in Figure II-1.

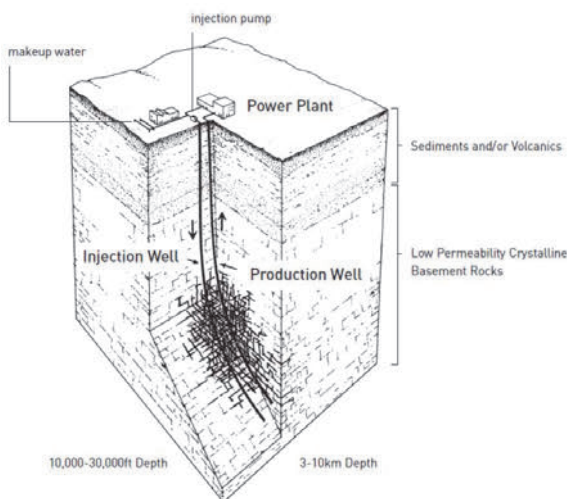


Figure II-1. Schematic illustration of an EGS based on fracturing (Tester et al. 2006).

The fundamental idea is that the fluid heats up as it is circulated with a lower mass flow rate as compared to the fractured based EGS. Another concept which bears some similarities has also been published by a geothermal consulting firm operating in the US, Sanyal et al. (2005). These systems require significantly more drilling than EGS based on fracturing. It is also implicit in the scheme to leave the connecting wells without casing, thus relying on the integrity of the bedrock.

The main benefits of these systems would be that it can:

- reduce problems with fluid losses
- enhance the reservoir control and reduce risk for thermal drawdown.
- manage problems with short-circuiting
- eliminate risks for induced seismicity
- be designed for a long operation time

Short-circuiting in relation to EGS based on fracturing means that the injected fluid finds the “easiest” way between two wells without capturing sufficient heat. Theoretically the EGS concept proposed by Rock Energy AS avoids this since the flow paths are controlled by the drilled heat exchanger part having the lowest hydraulic resistance.

There are some fundamental differences between this type of concept and the fracturing concept. Firstly, the priority would be to target structurally stable bedrock with little fractures, secondly the heat transfer area would be limited to the surface area of the boreholes, the dominating heat transfer mechanism would, therefore, be thermal conduction in the rock surrounding the boreholes. The heat transfer to boreholes is often called wellbore heat transmission and is a known concept e.g. in relation to the petroleum industry where controlled wellbore temperatures during injection and production are desired. The usual assumption when calculating the transfer is that the thermal resistance is in the bedrock and that the fluid and the wellbore are at or near thermal equilibrium. Most of the practical calculation methods used relate to the classical semi analytic approach by Ramey (1962). The heat transfer problem is in many aspects similar to the heat transfer in shallow boreholes for ground source heat pump systems, and estimates of heat extraction rates and temperatures can be made using the heat transfer examples in Section 2.1.4 in the present work. More detailed studies can be performed using numerical methods.

II-3.3. NUMERICAL SIMULATION

In relation to EGS, numerical models can be used for two separate, but closely connected reasons. The first is a resource assessment in which the thermal structure, properties and temperatures in the ground are predicted. This can be performed based on geophysical data and observations, examples of this can be found in Gibson et al. 2010 and Backé et al. 2010. The

second reason is to determine the performance of an EGS, and to give a prediction of the extractable resource.

The performance of an EGS is governed by many interacting and coupled processes; therefore, a realistic model might have to handle thermal, hydraulic, chemical and mechanical processes, in addition the processes behave with very different time scales. The modeling is further complicated by the combination of high temperature and pressure and by the chemical composition of the fluid in the system.

E.g. to accurately model and predict the performance of an EGS based on artificially created fractures it is necessary to estimate the effective heat transfer volume that is accessed by the fractures, and the distribution of the fractures (fluid flow paths) in the heat transfer volume (Xing et al, 2010). This is further complicated since the permeability of the created reservoir is a function of the induced pressure, and might change over time as a result of e.g. chemical precipitation and dissolution processes and differential reservoir cooling, which can cause fractures and thus changes in permeability (McDermott et al. 2006), (Koh et al 2011).

Although models exist that can account for all modes, it is in most cases feasible to simplify the problem by focusing on the phenomena having the largest influence on the performance.

In the present study of the closed loop EGS it is chosen to focus primarily on the fluid flow and heat transfer in the EGS, this is motivated by specific characteristics of the system studied. That is, the importance of rock mechanics is reduced since the system is constructed through drilled boreholes rather than fractures, and the potential for chemical precipitation and dissolution processes is limited due to the combination of a controlled and limited heat transfer area (contact area between the rock and the heat carrier) and the relatively low operation temperatures (in the range of district heating).

In the present work a numerical model has been developed specifically for the closed loop EGS concept. The model is used to study the transient behaviour and performance of the EGS concept on both short time scales (minutes to hours) and on longer time scales (multiple years). To the authors knowledge, this is the first work in which such a closed loop EGS concept has been studied on a detailed level.

II-4 A novel concept to engineered geothermal systems

II-4.1. INTRODUCTION

The target for the development of Engineered Geothermal Systems (EGS) is concepts which can be used to extract heat from the ground independent of geological conditions and in areas with what would earlier be regarded as an area with low geothermal potential.

In this section of the thesis, an EGS concept which is based on thermal conduction as the primary heat transfer process is presented. The concept utilizes a subsurface heat exchanger consisting of drilled wellbores. This gives a well defined, but limited heat transfer surface area. The system is, therefore, highly dependent on the heat transport through the rock by thermal conduction.

From a thermal perspective, it is seen that if managed correctly, the proposed system can provide thermal energy for a virtually unlimited time.

II-4.2. OBJECTIVES

The main objectives for the present study are to :

- Develop a transient numerical model for the proposed EGS system.
- Study the thermal performance of the system over time and as a function of physical dimensions, thermal properties and operation parameters.

II-4.3. BACKGROUND

The novel EGS concept presented and studied is based on the US-patent (2001) and is being commercialized by the Norwegian company Rock Energy AS. The concept is illustrated in Figure II-3.

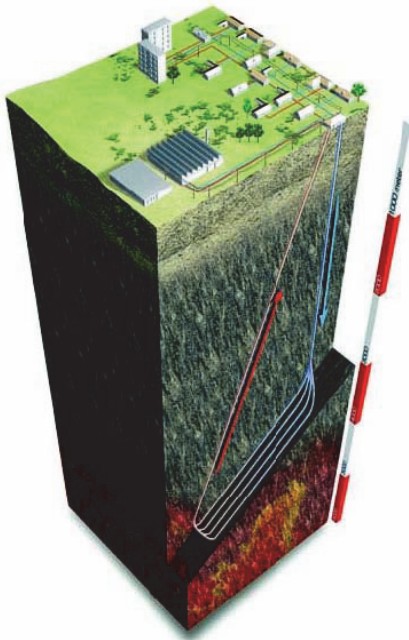


Figure II-3. Conceptual illustration showing the closed loop EGS for extraction of geothermal energy (Rock Energy AS).

The figure shows heat being extracted from parallel and inclined boreholes that are placed at a depth of about 5 km. Since drilling is at present cost intensive, it is crucial that the EGS can provide heat over long operation times, e.g as a base load heat provider in a district heating network. The thermal output and operation temperatures required together with the thermal properties and temperature of the rock determines the main system layout.

The focus for this study is on thermal performance of the system. The overall thermal performance of the system is studied as a function of the operation time, the thermal properties of the rock (primarily the thermal conductivity) and the physical dimensions (diameter of the boreholes).

The aim is, thereby, to provide essential information on the performance that can be expected for this type of system.

II-4.4. PAPER 5 : A NOVEL CONCEPT TO ENGINEERED GEOTHERMAL
SYSTEMS

Holmberg H., E. Næss., Sønju. O. K. (2012)

Proceedings, Thirty-Seventh Workshop on Geothermal Reservoir Engineering Stanford
University, Stanford, California, January 30- February 1, 2012, SGP-TR-194

A NOVEL CONCEPT TO ENGINEERED GEOTHERMAL SYSTEMS

Henrik Holmberg¹, Otto, K. Sønju² and Erling Næss¹

¹Norwegian University of Science and Technology
Department of Energy and process Engineering
NO-7491, Trondheim, Norway

²Rock Energy AS, N-1327 Lysaker, Norway
e-mail: henrik.holmberg@ntnu.no

ABSTRACT

Geothermal energy has emerged as one of the viable options in a future clean energy based society. It poses a nearly inexhaustible resource with a worldwide potential. As pointed out in several recent publications, engineered geothermal systems (EGS) represent the future development of geothermal energy. These systems are still in the development stage while commercialization is lurching in the near future.

The common concept representing an EGS relies on engineered fractures for permeability and heat transfer area. This paper elaborates on a different and novel approach to the EGS concept, where wellbores instead of fractures are used. The system consists of a production well and an injection well interconnected by drilled wellbores. The wellbores act as a subsurface heat exchanger with a limited, but well defined heat transfer area. The result is a system that can be controlled and adapted to the specific thermal and geological structure of the site and that reduces the uncertainties regarding reservoir lifetime, thermal breakthrough, connectivity and short-circuiting. Since there is no fracturing involved, the construction of the system does not cause seismic events, the system can, therefore, be built directly within populated areas to provide heat and power where it is needed.

The thermal performance of this type of system is characterized by an initial decline in thermal effect which reaches a semi-steady state after a few years. Thus the system has to be dimensioned for its performance at year 20 or 30 of operation. Interestingly, the performance between 30 and 50 years degrades with only 1 %, thus showing the long term sustainability of the concept. This paper presents the concept and demonstrates its performance based on geological prerequisites.

INTRODUCTION

Geothermal energy has unique features as it is one of few renewable resources that can be used for continuous base load production of clean heat and power. Thus it has a given role in a future energy system. The starting point for this article is in Norway, a country with vast hydropower resources and a cold climate, this together with a moderate geothermal gradient makes production of heat the obvious choice.

System outline

The system outline would consist of a production well and an injection well interconnected by drilled wellbores. These wellbores would thus act as a subsurface heat exchanger with a limited, but well defined heat transfer area. This creates a system that in theory can be controlled and adapted to the specific thermal and geological structure of the site. A principle sketch of the system is shown in Figure 1.

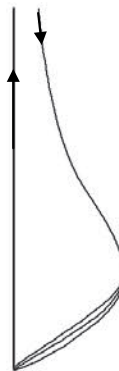


Figure 1: The system consists of an inlet and an outlet well that are connected through deviated wellbores.

The concept has previously been presented in a US-patent (2001) and was mentioned in Sanyal et al. (2005). Rock Energy AS is presently developing this concept further. The aim with this article is to elaborate on the thermal aspects of this type of concept.

The vertical extent of the system depends on the thermal structure and properties of the rock together with the designated production temperature and thermal effect. Today, accessible depths are considered in the range of 5000 m (Tester, 2006), (IGA Roadmap, 2011).

The process in which such system would extract heat is best described as mining of heat, as a heat sink will develop around the wellbores. By adopting the system to the limits of heat conduction, the process can be continuous for a significant amount of time.

This type of geothermal concept involves much more drilling than creating a heat exchanger through fracturing the rock; it would also have a restricted heat exchange area, directly linked to the amount of drilling and thus the costs. The cost of drilling is very important, and the use of modern drilling technology is essential. On the other side, the concept would directly cut away uncertainties involved with EGS regarding reservoir lifetime, thermal breakthrough, connectivity and short-circuiting (Workshop, 2007). Since there is no fracturing involved, the system would not cause seismic events and could thus be built directly within populated areas to provide heat and power where it is needed.

Heat transfer

The primarily heat transport mechanism in such system would be heat conduction within the rock and convection between the flowing water and the surface of the wellbore. Since the thermal resistance in the rock is orders of magnitude higher than the resistance between the fluid and the wellbore, it will be governing for the heat transfer process. Thus for such conduction based concepts it is important to have a sound estimate of the thermal properties of the rock.

Short circuiting means that the fluid takes the path with the least resistance. For a fractured based EGS this means that instead of spreading through the whole fractured network, the fluid will take the easiest path and thus capture less heat than it otherwise would. With wellbores constituting the heat exchanger the flow resistance can be controlled to avoid short circuiting.

Thermal breakthrough will here be defined as the point when the wellbores start to have thermal interaction. Through engineering the heat exchanger with drilled pathways the risks for thermal

breakthrough can in theory be controlled and avoided.

Wellbore heat transmission

To assess such a system it is important to consider the heat transfer around the wellbore, this is commonly referred to as the wellbore heat transmission. It has been treated by authors like Ramey (1962), Horne and Shinohara (1979) and Pruess and Zhang (2005). Pruess and Zhang (2005) mentions that it can have importance as the heat transfer in the wellbore is of the same order of magnitude as a major fracture in the system. However, it is often neglected in conventional hydrothermal systems. There are two primary reasons for this, hydrothermal systems are targeted at relatively shallow depths of around 2-2.5 km and the circulation flow rates are high.

Wellbore heat transmission is a well known concept in relation to the petroleum industry where controlled wellbore temperatures during injection and production are desired. The usual assumption when calculating the heat transfer, is that the thermal resistance is in the bedrock and that the fluid and the wellbore surface are at thermal equilibrium, thus the Biot number is large. Most practical methods relate to the classical semi-analytic approach by Ramey (1962) that uses the line source from Carslaw and Jaeger (1959). The problem can as well be treated with the analytical solution for a cylindrical geometry within an infinite domain (Carslaw and Jaeger, 1959). These solutions are also frequently used for simulation of shallow ground source heat pump systems (Bernier, 2000). However, with numerical methods it is possible to study the heat transfer in more detail, (Pruess and Zhang, 2005). This also allows for variation in physical properties and simplifies for time dependent variation of heat extraction rates.

Discretization of the concept

To analyze the system one can start with neglecting the heat transfer in the injection and production wells. With sufficiently good insulation in the upper part of these wellbores this can be a viable choice. If then the wellbores in the subsurface heat exchanger are placed sufficiently far from each other to avoid thermal breakthrough within the desired operation time, and the fluid flow will be evenly distributed, the performance of one single wellbore can be representative for the whole system. This wellbore can be discretized along its axial length into sections of unit length, thereby neglecting axial conduction. Figure 2 describes the discretization of the system.

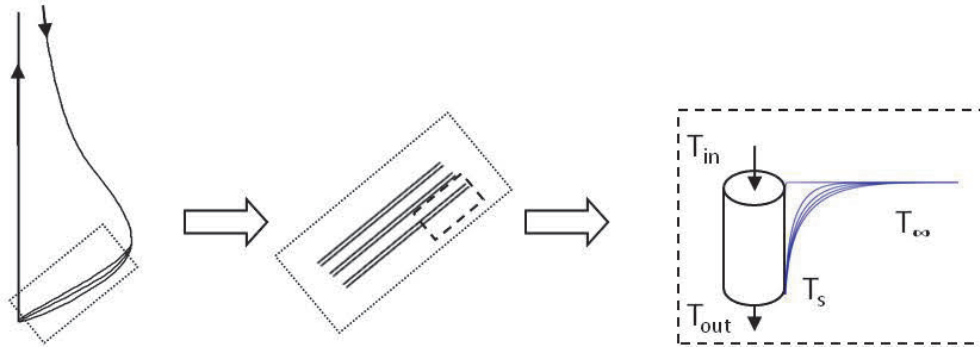


Figure 2: Discretisation of the EGS concept from full system down to unit length segment of the wellbore.

Within a section of the wellbore a heat carrier fluid will flow with turbulent conditions leading to a high heat transfer coefficient between the fluid and the wall of the segment. Depending on the structure and integrity of the rock there might be a casing between the rock and the fluid. Assuming that there is good thermal contact between the casing and the bedrock, the overall thermal resistance between the turbulent fluid and the wall can be lumped together with the resistance of the casing and the higher resistance of the bedrock. See Figure 3 and Equation (1.1, 1.2)

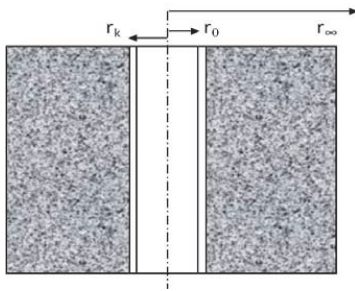


Figure 3: Cross section of wellbore segment. r_0 is the radius of the wellbore, r_k is the radius of the casing and r_∞ aims at the infinite undisturbed rock around the wellbore.

$$\frac{1}{2\pi r_0 h_\infty} = \frac{1}{2\pi r_0 h_0} + \frac{\ln(r_k / r_0)}{2\pi k_c} + \frac{1}{2\pi r 2h_\infty} \quad (1.1)$$

$$(1.2)$$

$$\frac{1}{2\pi r 2h_\infty} \gg \frac{1}{2\pi r_0 h_0} + \frac{\ln(r_k / r_0)}{2\pi k_c}$$

h_∞ is the equivalent heat transfer coefficient for the thermal resistance in the rock, h_0 is the convective resistance and k_c is the thermal conductivity of the casing material.

This gives a heat transfer coefficient h ($\text{W/m}^2 \text{K}$) between the wellbore and the surrounding bedrock which is a function of primarily the thermal diffusivity and time.

A heat flux per unit length (Q^*) of wellbore can be considered, this will then be dependent on the heat transfer coefficient and the temperature difference between the rock and the fluid, as follows:

$$Q^* = h D \pi (T_\infty - T_s) \quad (1.3)$$

Where T_∞ is the undisturbed temperature far from the wellbore, T_s is the temperature at the surface of the wellbore and D is the diameter of the wellbore.

If the temperatures T_∞ and T_s are being held as constants, the unit length heat flux will be proportional to the heat transfer coefficient, which is dependent on the properties of the rock and the heat extraction history.

Numerical evaluation

Numerical evaluation of the concept has been performed based on the finite-difference method with the use of Matlab. This has been done by representing the wellbores with 1-d models that are then coupled with 2-d radial models for the surrounding rock domains. This enables transient simulation with sufficiently small time-steps to study the system with hourly load variations, while still performing simulations of the full life-length of the system.

The thermal properties of the simulated rock domain are allowed to vary with temperature. The dependencies are according to the empirical equation by Sass et al. (1992) and Vosteen and Schellschmidt,

(2003) for thermal conductivity (k), see Equation (1.4).

$$k(T) = k_0 / \left(a + T (b - c / k_0) \right) \quad (1.4)$$

The coefficients a , b and c have been based on Vosteen and Schellschmidt (2003) for basement rocks.

For specific heat capacity the normalized empirical equation of Waples and Waples (2004) for nonporous rock has been used, see Equation (1.5).

$$Cp_{nT} = 8.95 * 10^{-10} T^3 - 2.13 * 10^{-6} T^2 + 0.00172 T + 0.716 \quad (1.5)$$

See Waples and Waples (2004) for further details. The temperature dependencies are visualized in Figure 4.

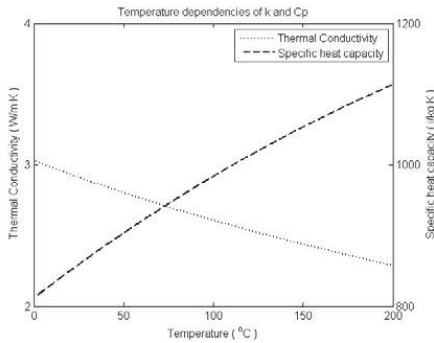


Figure 4: Temperature dependency of thermal conductivity and specific heat capacity.

Thermal conductivity is temperature dependent mostly due to the effect of phonon scattering. This causes the conductivity around the wellbore to increase as energy is being extracted. The specific heat capacity increases with temperature and will thus decrease as the temperature around the wellbore decreases. This means that the heat transfer coefficient defined in Equation (1.3) is a function of the temperature field around the wellbore.

Thermal conductivity of crystalline rocks also depends on porosity. Porosity is a function of pressure, and for the considerable depth considered for the heat exchanger wellbores, the pressure should be high enough to close any intrinsic porosity in the rock. The influence of porosity has, therefore, been neglected within this paper. However, it should be mentioned that results from deep drilling projects have shown that there can be zones with increased porosity and migrating fluids even at considerable depths (Huenges et al. 1997).

The aim with the numerical model has been to further explore this type of concept beyond the limitations of simpler analytical solutions. And to exploit how the system reacts for different operating strategies. Some characteristic results will hereunder be presented.

These results are presented based on continuous heat extraction. This is sufficient to describe the main characteristics of the system. In reality the system would likely operate with a variable load. This can be done either by changing the mass flow or through bypassing the heat carrier fluid and thus changing the inlet temperature. A change in mass flow is directly felt by the system and thus has a direct impact on the produced energy. Bypassing causes the inlet temperature to increase, the response in change of production temperature will then be delayed with the time it takes the fluid to travel through the system. In addition, both methods cause a lagging thermal response in the bedrock.

RESULTS

It is of interest to explore the long term sustainability of this type of concept. As mentioned the process whereby heat is being extracted can be called mining of heat. Heat is thus being transported away from the wellbore faster than it can be replenished. This causes a rapid drop in temperature around the wellbore. The thermal effect of the system will thus decline rapidly in the beginning until it reaches a semi-steady state. If the system is dimensioned based on this semi-steady extraction process it is possible to create a process which can be continuous for a significant amount of time. This can be visualized either by the change in thermal performance or the heat transfer coefficient over time. Given that the wellbores are placed with a sufficient distance in-between to avoid thermal breakthrough, the curve in Figure 5 will be representative for the thermal performance of the entire system.

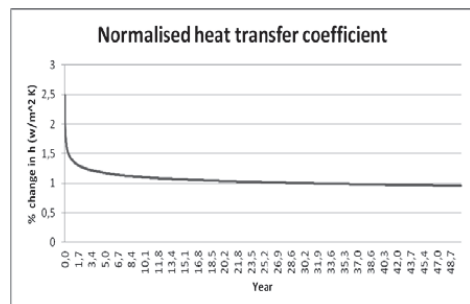


Figure 5: The graph shows the heat transfer coefficient as a function of time, the values have been normalized by the value of year 30. As can be seen the decline after year 30 is small.

The thermal properties govern how quickly heat diffuses through the rock, this is important as it determines the distance the heat diffuses during the lifetime of the system and thus the required distance between the wellbores. As mentioned both the specific heat capacity and the thermal conductivity have strong temperature dependencies. This can be visualized by plotting the conductivity and specific heat capacity around the wellbore. See Figure 6.

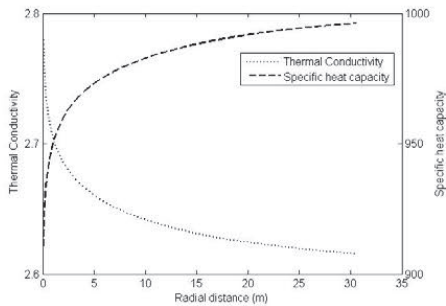


Figure 6: Thermal conductivity and specific heat capacity varies in radial distance from the wellbore due to their temperature dependencies.

As seen in Equation (1.3) the heat flux is dependent on the diameter of the wellbore, and thus on the heat transfer area. However, by decreasing the diameter of the wellbore, the thermal performance of the system is only slightly affected. This means that if it is possible, a smaller diameter would probably reduce the drilling costs for the system. This would then be bounded by the subsequent pressure drop and the available drilling technology. This dependency can be visualized by plotting the product of the heat transfer coefficient and the surface area of the segment, as shown in Figure 7.

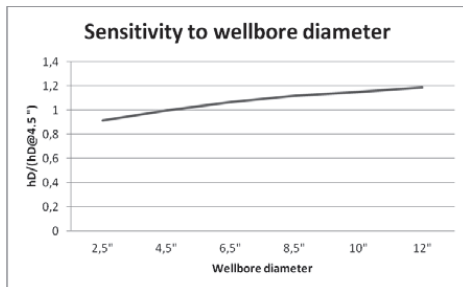


Figure 7: Normalized plot of the product between the heat transfer coefficient and the wellbore diameter for different diameters. The figure shows that the heat extraction only increases slightly with increased diameter.

A typical temperature profile through the system is visualized in Figure 8. In this figure the water enters the system at 60 °C and returns at 90 °C.

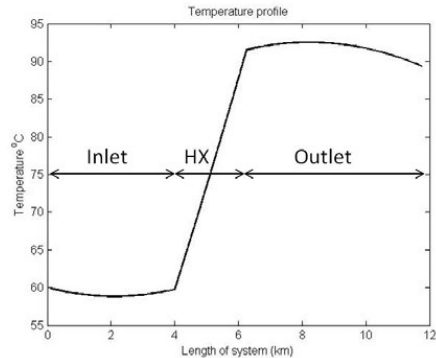


Figure 8: Typical temperature profiles through the geothermal system. This is simulated without insulation in the upper wellbores. HX refers to the heat exchanger wellbores.

And as can be seen, the temperature decreases in the production wellbore. Thus there are some heat losses that could be prevented by adding insulation to the wellbores. These are most prominent during the first years of operation, and are mostly important for smaller systems.

Sensitivity to thermal conductivity

The heat transfer coefficient is strongly dependent on the thermal conductivity. In Figure 9 the thermal conductivity around one segment has been varied between 2 and 4 W/m K. This shows the importance of accurate conductivity estimates when sizing the wellbore heat exchanger. In this case the temperature dependency of the conductivity has been neglected to simplify the figure.

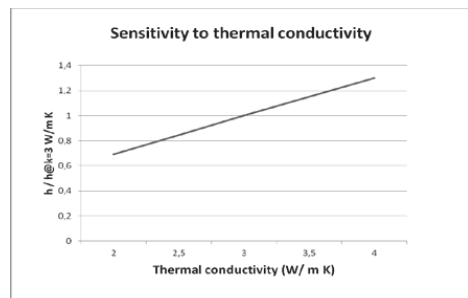


Figure 9: Normalized plot of the heat transfer coefficient and the variation with thermal conductivity of the rock.

DISCUSSION:

The aim with this paper has been to present some characteristics of a novel EGS concept based on wellbores instead of fractures. The thermal aspect of the system has been in focus. The primary features of the concept are the predictability and the long lifetime.

The motive has been to provide heat at moderate temperatures for district heating, this is a limitation imposed by the geological conditions in Norway and not a characteristic for the concept. Nevertheless it affects the way the system has been analyzed and thus the results.

Thermal conductivity is one key-factor that has to be considered for this type of concept. There are many factors that govern the thermal conductivity of rocks, of which some have been mentioned in this paper. Accurate dimensioning of the system requires accurate determination of in-situ thermal conductivity. There are several different empirical equations in the literature that describes the temperature dependency of thermal conductivity. The general trend is, however, the same and the difference between them have little influence on the results in this paper.

There are several factors that could affect the result. For example, it has been assumed that the rock is an impermeable medium where conduction is the sole heat transfer mechanism. Thus the impact of advection has not been considered in this paper.

To eliminate losses and improve the performance of the system it is advisable that some type of insulation is placed in the upper parts of the inlet and outlet wells. This is of course dependent on the actual operation conditions for the system.

The geometry of the system and the operation conditions govern the overall pressure drop and the energy required to circulate water in the system. In general this energy consumption amounts to less than 1 % of the thermal effect of the system.

Heat transfer surface is often a key factor in EGS, it should, therefore, be noted that for this type of concept the performance is not very sensitive to the diameter of the wellbore, but more related to the axial extent of the wellbores and the temperature difference as the driving force. In Figure 7, the product between the heat transfer coefficient and the wellbore diameter increases with 43% as the surface area increases 4.8 times.

CONCLUSION:

Some thermal perspectives of a novel EGS concept based on wellbores instead of fractures has been presented. The concept poses an alternative way of considering EGS.

The thermal properties of the rock are essential for this type of concept as it relies only on conductive heat transfer for the extraction of energy.

Predictability and simplicity are the major strengths of the concept, while increased requirement for drilling is the most obvious weakness.

The long term sustainability of the concept has been demonstrated in the results. Accurate dimensioning of the system requires measurements of in-situ thermal properties. Once operative, the system can provide heat at a near constant rate for a significant time, (50 + years), with low energy requirements for circulation.

To eliminate thermal losses in the inlet and outlet wells, insulation of the upper wellbores should be considered.

The optimal diameter of the wellbores in the heat exchanger part is a function of, heat extraction rate, pressure drop and available drilling technology.

REFERENCES

- Bernier. M. (2000), "A Review of the Cylindrical Heat Source Method for the Design and Analysis of Vertical Ground-Coupled Heat Pump Systems". 4th International Conference on Heat Pumps in Cold Climate, Aylmer, Québec.
- Carslaw. H.S., J.C. Jaeger. (1959), *Conduction of heat in solids*, second ed., Oxford University press, Oxford.
- Horne. R.N. and Shinohara. K. (1979), "Wellbore Heat Loss in Production and Injection Wells," *Journal of Petroleum Technology*, **31**, 116-118.
- Huenges. E., J. Erzinger., J. Kück., B. Engeser., W.Kessels. (1997), "The permeable crust: Geohydraulic properties down to 9101 m depth," *Journal of Geophysical research*, **102**, 18 255-18 265
- IEA (2011) "Technology Roadmap, Geothermal heat and Power," Available at http://www.iea.org/papers/2011/Geothermal_Roadmap.pdf
- Pruess. K. and Y. Zhang. (2005) A Hybrid Semi-Analytical Numerical Method for Modeling Wellbore Heat Transmission, Proceedings, 30th Workshop on Geothermal Reservoir Engineering Stanford University
- Ramey. H.J. (1962), "Wellbore Heat Transmission," *SPE* **9**, 465-474.
- Sass. J. H., A. Lachenbruch. and T. H. Moses. (1992), "Heat Flow From a Scientific Research Well at Cajon Pass, California," *Journal of Geophysical research*," **97**, 5017- 5030
- Tester. J.W. et al. (2006). "The Future of Geothermal Energy – Impact of Enhanced Geothermal Systems (EGS) on the United States in the 21st Century," MIT - Massachusetts Institute of Technology, Cambridge, MA. 358 p. Available at http://www1.eere.energy.gov/geothermal/future_geothermal.html.
- Vosteen. H-D. and R. Schellschmidt. (2003), "Influence of temperature on thermal conductivity, thermal capacity and thermal diffusivity for different types of rock", *Physics and Chemistry of the Earth* **28**, 499-509.
- Waples. D.W. and J.S. Waples (2004), "A Review and Evaluation of Specific Heat Capacities of Rocks, Minerals, and Subsurface Fluids, Part 1," *Minerals and Nonporous Rocks Natural Resources Research*, Vol. **13**, No. **2**.
- Workshop. (2007), Enhanced Geothermal Systems Reservoir Management and Operations Workshop, San Francisco CA, September 17, 2007, Available at http://www1.eere.energy.gov/geothermal/pdfs/reservoir_management.pdf
- U.S. Patent, #6,247,313B1, 19 June 2001

II-5 Thermal modeling in the Oslo rift

II-5.1. INTRODUCTION

The aim with the EGS concept presented in Section II-4 is to extract heat from about 5 to 6 km depth in geologically stable continental areas where there is no naturally occurring hydrothermal systems and where thermal conduction is the dominant heat transfer mechanism in the ground.

The thermal performance that can be expected from the EGS is highly dependent on the thermal properties of the rock and the temperatures at the target depth. In absence of direct measurements from the target depth, the properties and temperatures have to be predicted based on measurements of temperature and thermal properties from shallower boreholes. In case of onshore Norway, this means boreholes with depths less than 1000 to 1600 m.

In Paper 6: *Thermal modeling in the oslo rift, Norway*, a steady state thermal model is presented. The model is using heat flow data together with a geophysical model. The aim with this study is to provide information on the temperature distribution in the upper crust.

II-5.2. OBJECTIVES

The main objectives are to:

- Study the heat flow and thermal structure of the Oslo graben
- Construct a steady state thermal model for a section of the Oslo graben.

II-5.3. BACKGROUND

Outside tectonically active areas, variations in the geothermal heat flow is strongly related to variations in the concentration of radioactive heat producing elements in rocks of the surface crust. Heat is generated primary by radiogenic decay of ^{238}U , ^{232}Th and ^{40}K , (Turcotte and Schubert (2002)). High concentrations of heat producing elements can result in favourable conditions for EGS, especially if the produced heat is accumulated under an insulating sedimentary layer, such as in sedimentary basins.

In this study, the focus is on the Oslo rift in Norway where relatively high heat flow values have been determined, which represent an increased potential for geothermal energy. The rift is, however, either lacking or having a negligible sedimentary cover.

Since there are no boreholes in the depth range of EGS in the region, the temperatures and thermal properties at the target depth (≈ 5 to 6 km) have to be predicted using measurements of temperature and rock thermal conductivity from shallow boreholes (< 1000 to 1600 m). The

temperature distribution down to the target depth can then be extrapolated using models for the variation in radiogenic heat production and the thermal conductivity of the rock.

In Norway this is complicated by paleoclimatic disturbances of the temperature in the ground, i.e. the temperature of the rock has been cooled down by previous ice ages. This is a transient effect which influences the upper 1-2 km of the ground. As a result the heat flow as determined from direct measurements in shallow boreholes is lower than it otherwise would be and cannot be used directly to determine the temperatures at further depth. Therefore, when determining the geothermal heat flow the temperature measurements have to be corrected for palaeoclimatic disturbances. In addition, the exploration boreholes needs to be deeper than what is usually required in order to reduce the uncertainty, Slagstad et al (2009).

II-5.4. PAPER 6: THERMAL MODELING IN THE OSLO RIFT, NORWAY

Holmberg H., E. Næss., Evensen. J.E. (2012)

Proceedings, Thirty-Seventh Workshop on Geothermal Reservoir Engineering Stanford University, Stanford, California, January 30- February 1, 2012, SGP-TR-194

THEMAL MODELING IN THE OSLO RIFT, NORWAY

Henrik Holmberg¹, Erling Næss¹ and Jan E. Evensen²

¹Norwegian University of Science and Technology
Department of Energy and process Engineering
NO-7491, Trondheim, Norway

²Rock Energy AS, N-1327 Lysaker, Norway
e-mail: henrik.holmberg@ntnu.no

ABSTRACT

In stable continental regions, local variations of heat flow are usually related to variations in radiogenic heat production. Depending on the location of the heat source and the geological structure, areas with high heat flow might be suitable for geothermal prospecting. Given that transient effects can be neglected, the thermal structure of the continental basement can be modeled with a steady state conductive model based on primarily the radiogenic heat production and the variation of thermal conductivity.

The Oslo rift is situated on the Fennoscandian Shield and comprises a complex lithology. It has been subjected to extensive geological and geophysical studies; however, there are no boreholes exceeding 1000m within the region. Therefore, temperature and properties at depths relevant for geothermal energy have to be extrapolated from shallow measurements. This is further complicated by palaeoclimatic effects. In this study a published geophysical model of the Oslo rift developed by the Geological Survey of Norway has been used. The model is based on integration of geophysical data such as magnetic and gravity data with geological models, and has been used as basis for thermal modeling. The results from the thermal modeling can be used both to evaluate geothermal potential and as a further constraint for the geophysical model.

INTRODUCTION

Geothermal heat flow can be used as an indicator to suitable areas for exploitation of geothermal energy.

The majority of the continental heat flow originates from decay of radioactive isotopes in the crust, thus finding areas with a high heat flow can be equal to finding areas with high isotope concentration.

Scandinavia has, with exception of Iceland long been considered to have a lower than average heat flow, and thus to less suitable for deep geothermal energy. In 2009 the Geological Survey of Norway presented heat flow data from a series of scientific wells drilled across the country. The wells ranged in depth between 500 and 900 m and the results showed that the heat flow was on average higher than earlier measurements had indicated. The discrepancy can partly be explained by corrections for paleoclimatic influence, (Slagstad et al. 2009).

These heat flow data can be considered as a first step in a characterization of the geothermal potential of Norway. Some locations have shown higher than average geothermal heat flow, which points to more favorable conditions for geothermal exploration. However, the data is to scarce for any general conclusions to be drawn.

The highest heat flow values were found in Hurdal (73 mW/m²) and in Fredrikstad (73 mW/m²). Hurdal is situated 65 km North of Oslo while still in the Oslo rift. Fredrikstad is situated southeast of Oslo. Significantly lower values were also determinate east of the rift in Berger (49 mW/m²). The locations including their heat flow values can be seen in Figure 1.

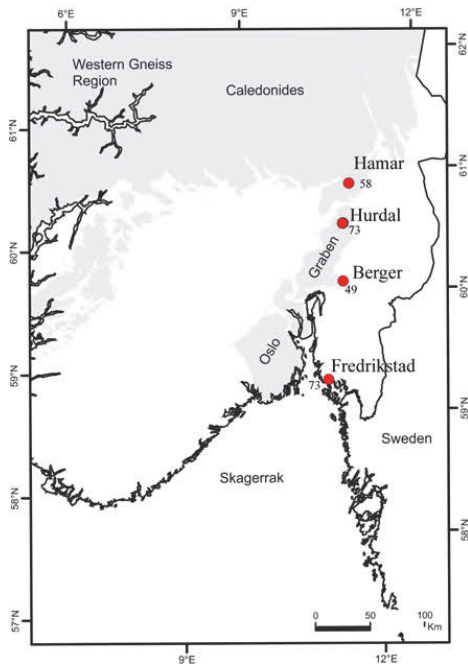


Figure 1: Locations for heat flow determination, the average heat flow for each location is displayed in mW/m^2 . The figure is modified from Slagstad (2005).

This paper will focus on the region around the Oslo rift; thermal modeling has been used in an attempt to explain the variation in thermal heat flow that has been determined in and around the rift.

One particular aim with the study has been to explore whether the higher heat flow in the northern part of the Oslo rift is a common feature of the rift or a local anomaly. This is motivated by the high population density in the southern part of the rift, which could make the region a possible target for geothermal developments.

The Oslo rift is an intercontinental rift situated on the Fennoscandian Shield as an incision within the Sveconorwegian geological province. The rift comprises a complex lithology which is outside the scope of this paper.

The rift has been subject to extensive geological and geophysical studies; however, there are no boreholes exceeding 1000 m within the region. Therefore, temperature and thermal properties at depths relevant for deep geothermal energy (5000m) have to be extrapolated from shallow measurements. This is further complicated by palaeoclimatic transients.

As a basis for thermal modeling a published geophysical model of the Oslo rift developed by the Geological Survey of Norway has been used. The model is based on integration of geophysical data such as magnetic and gravity data with geological models, (Ebbing et al. 2007). The model consists of a series of 2-D geological profiles that are placed perpendicular to the rift. For further information on the geophysical model the reader is referred to the work of Ebbing et al. (2007).

The commercial finite element software Comsol 4.2a has been used to construct thermal models based on the geological profiles.

The thermal structure of the ground in stable continental areas is governed principally by the heat flux from the mantle, the radiogenic heat generation and the thermal conductivity of the crust. These parameters also constitute the primary input parameters to the thermal model.

Thermal conductivity and heat production

Due to the absence of deep boreholes (> 1000 m) within the study area, there are no prior data available on the distribution of heat sources, or variability of thermal conductivity with depth. Therefore, surface measurements have been used as the main information source. There is an extensive coverage of surface data within and in the vicinity of the rift. Conductivity and heat production data has been retrieved primarily from the LITO-project at the Geological Survey of Norway, and yields more than 1400 measurements. Radiogenic heat production data is based on XRF and LA-ICP-MS analysis of core samples from surface rocks. The methodology and the results from this project are well summarized in Slagstad (2008). Thermal conductivity measurements were performed on dry samples based on the approach by Middleton (1993), the methodology is further described in (Ramstad et al. 2008). The conductivity data has as well been presented in Liebel et al. (2010).

Heat generation

Radiogenic heat production, H ($\mu W/m^3$), is related to the decay of primarily the radioactive isotopes ^{232}Th , ^{238}U and ^{40}K and can be estimated based the concentration of the respective elements through Equation 1 (Rybach, 1988).

$$H = \delta(9.52C_U + 2.56C_{Th} + 3.48C_K)10^{-5} \quad (1.1)$$

Where δ is the density of the rock. High isotope concentrations are associated with enriched felsic rocks like granite, while depleted mafic rocks have the lowest concentration and thus lower heat

production. The average heat production of the Precambrian shield has been estimated to $0.77 \pm 0.08 \mu\text{W}/\text{m}^3$ by Jaupart and Mareschal (2003), however, they also stressed that on a local scale the variation can be significant. Published data from the KTB deep borehole in Germany show high vertical variations down to 9 km (Jaupart and Mareschal, 2003).

Heat production data have been combined with lithology maps from the Geological survey of Norway, to produce a heat production map over the rift region. Figure 2 displays arithmetic mean values of heat production based on the measurements in each geological domain.

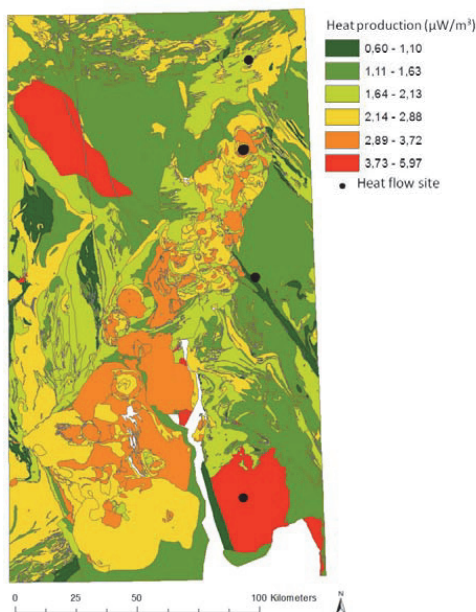


Figure 2: Heat production in the rift region. The map is based on the arithmetic mean values of the measurements in each geological domain.

In general the heat producing rate of the Permian rock within the Oslo rift is higher than in the surrounding Precambrian rock. According to Slagstad (2008) the area weighted mean value of the Oslo rift is $2.93 \mu\text{W}/\text{m}^3$ and for the Precambrian $1.76 \mu\text{W}/\text{m}^3$. The two red domains with noticeable higher heat production are the Precambrian Flå granite to the west and Iddefjord granite to the east.

Thermal conductivity

Thermal conductivity together with specific heat capacity and density constitute the thermal diffusivity which governs how quickly heat diffuses through a medium. This is important when considering

transient effects; steady state heat flow on the other side, is only dependent on the thermal conductivity of the medium.

As with the heat production data, the thermal conductivity data has been combined with lithology maps to display the variation of thermal conductivity in the rift region, see Figure 3. The figure displays arithmetic mean values of heat production based on the measurements in each geological domain.

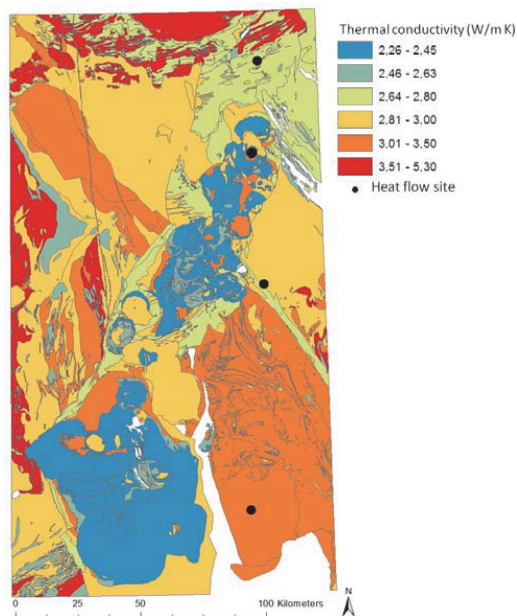


Figure 3: Thermal conductivity in the rift region. The map is based on the arithmetic mean value of the measurements in each geological domain.

It is clear from Figure 3, that the granitic rock within the rift has a lower thermal conductivity than the surrounding domain.

Thermal conductivity of crystalline rocks is known to have a strong dependency on temperature and decreases with increasing temperature. This behavior is dominated by the effect of phonon scattering, (Clauser, 2006), it is also related to changes in contact resistance and porosity due to thermal expansion of the mineral constituents of the rock, (Clauser, 2006), (Pridnow et al. 1996). This effect is less pronounced if the rock is saturated with water (Walsh and Decker, 1966); however, most measurements of the temperature dependency have

been done with dry samples, (Abdulagatov et al. 2006), (Mottaghy et al. 2008), (Vosteen and Schellschmidt, 2003). Pressure has a counter effect and acts to decrease the porosity (Walsh and Decker 1966). Several authors have published empirical laws for how thermal conductivity varies with temperature. A summary of empirical equations for the thermal dependency of conductivity can be found in Lee and Deming (1998) and in Vosteen and Schellschmidt (2003). The perhaps most common empirical equation was first published by Sass et al. (1992) in the form:

$$k(T) = \frac{k_0}{a + T(b - c/k_0)} \quad (1.2)$$

Where $k(T)$ is the thermal conductivity in (W/m K) at a given temperature $T(^{\circ}\text{C})$ and k_0 is the thermal conductivity at 0°C , the coefficients **a**, **b** and **c** where adapted to data from Birch and Clark (1940) and could predict the temperature relationship within experimental error of the measurements. Equation 1.2 has then been used and cited in several publications (Clauser and Huenges, 1995), (Vosteen and Schellschmidt, 2003) and (Clauser, 2006), (Hartman, 2008). Seipold (1998) also derived a general equation for the temperature dependency of thermal conductivity for different rock types. In the present study, Equation 1.2 has been used in the thermal model, with the coefficients from Vosteen and Schellschmidt (2003) for magmatic and metamorphic rock.

Heat flow measurements.

There is in general scarce data on the thermal heat flow in Norway. In 2009 the Geological Survey of Norway presented results from a study in which measurements of thermal gradients and thermal conductivity from 9 sites in Norway were used to determine the heat flow. The values were corrected for topography and paleoclimatic disturbances and the average values ranged between 50-60 mW/m², while locally higher values were found. The results were in general higher than what had been earlier measured (Slagstad et al. 2009). This can to some extent be attributed to paleoclimatic corrections that were applied and which constituted between 10- 20 % of the final values.

The highest values were obtained in Hurdal and in Fredrikstad (see Figure 1). The data from Hurdal were derived from 4 wells of which the deepest reaches 900 m, Hurdal is situated 65 km North of Oslo while still in the Olso rift. The average corrected heat flow based on the four wells was 73 mW/m². The same value was determined at Fredrikstad where only one well, 733m deep was

used. In Berger, which is on the east side of the rift, 49 mW/m² was determined from a well extending to 640 m (Slagstad et al. 2009).

There was no core available from the borehole in Berger. Therefore, the thermal conductivity was based on surface lithology and interpretation of televiwer recordings down to 480 m (Slagstad et al. 2009). The result from Berger might thus contain a larger uncertainty than the other data used in this paper. The results from the heat flow study are summarized in table 1.

Table 1: Reproduced heat flow data from Slagstad et al. (2009)

	Corrected heat flow (mW/ m ²)	
	Avg	Range
Berger	49	48-51
Hamar	58	53-63
Fredrikstad	73	72-75
Hurdal	73	66-82

Slagstad et al. (2009) determined the heat flow for major geological provinces in Norway based on both the new heat flow data and earlier works. Some of the earlier measurements were performed as lake heat flow measurement, these can have a higher uncertainty than measurements performed in deeper wells (Haenel, 1979).

Excluding these measurements, the average corrected heat flow was determined to be 57.4 ± 4.6 mW/m² for the Sveconorwegian province (Slagstad et al. 2009).

Geothermal heat flow is an indirect property, and as such it can be subject to several uncertainties through both temperature logs and thermal conductivity measurements. There are also uncertainties involved with the applied corrections for topography and paleoclimatic influence. According to personal communication with Slagstad, T at the Geological Survey of Norway (2011) the largest uncertainty is likely within the paleoclimatic corrections.

It is difficult to estimate the uncertainty of these corrections; however, recent studies by Kukkonen on the Outokumpu deep borehole in Finland points to similar magnitude of corrections (Kukkonen et al. 2011).

Geophysical model.

Ebbing et al. (2007) presented a geophysical model over the Oslo rift. The model is based on integration of geophysical data such as magnetic and gravity data with geological models. The geophysical model explains the rift as a differentiation of Granite-Diorite and Gabbro intrusions that extend down to

roughly 10-15 km. This differentiation series is in line with recent results from Stratford and Thybo (2011) based on seismic velocities and Poisson's ratio.

Without going in to detail on the model, the general geological trend that is described has been used and combined with data over heat production and thermal conductivities to construct a thermal model.

While the geophysical model covers the whole extent of the rift, this paper presents the results based on only one profile. The reason for this is the lack of heat flow data. The profile is placed in the vicinity of the heat flow locations from Slagstad et al. (2009). See Figure 4.

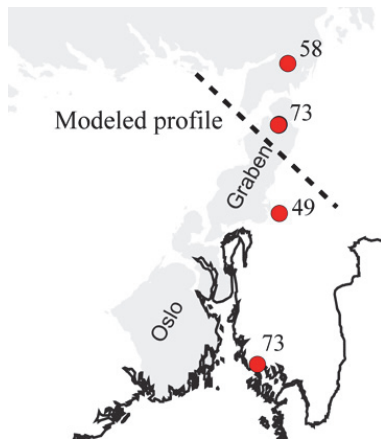


Figure 4: The modeled profile is placed perpendicular to the rift, between Hurdal and Berger. The average heat flow for each location is displayed in mW/m^2 .

Thermal modeling

Thermal models were constructed with Comsol multiphysics 4.2a, which is a commercial multipurpose finite element software. The profiles have been modeled essentially as 2-d profiles that extend down to the Moho.

The Oslo rift was formed during the Permian and is around 250 million years old. This time-span should be sufficient to eliminate any transient thermal effect in the crust (Jaupart and Mareschal, 2011), hence, steady state models have been constructed. Thermal transients induced by climatic disturbances are neglected, this is implicit as the corrected heat flow values have been used.

According to Jaupart and Mareschal (2011) and Kukkonen and Peltonen (1999), the heat flux at the Moho is around 7- 15 mW/m^2 for the Fennoscandian shield. Based on this the heat flux at the Moho has been assumed constant at 15 mW/m^2 .

The average depth of the crust in southern Norway is 38 km (Stratford and Thybo, 2011), with an assumed heat flux of 15 mW/m^2 at the Moho and a surface heat flux of $57.4 \pm 4.6 mW/m^2$, the average heat production for the crust would be $1.11 \pm 0.12 \mu W/m^3$.

In regions of extension, the heat flux is normally increased by the induced heat from an up-warping hot mantle. This is a transient effect, and after return to steady state the heat flow might actually have decreased. Since the majority of the heat flow originates from decay of radioactive isotopes in the crust, thinning the crust through extensional rifting decreases the amount of isotopes and thereby the heat flow (Jaupart and Mareschal, 2011).

According to the geophysical model (Ebbing et al. 2007) there is an up-warping of the Moho underneath the rift, this is also in accordance with seismic refraction of the southern part of the rift (Stratford and Thybo, 2011) which shows a thinning of the crust of about 2 kilometers under the rift. The magnitude of this up-warp varies through the rift and according to the geophysical model; the crust is 35 km thick for the section considered in this paper.

With an average heat production of $1.1 \mu W/m^3$ the thinning of the crust with 3 kilometers for the modeled profile would reduce the surface heat flow in the rift with around $3.3 mW/m^2$.

The geophysical model explains the rift as a differentiation series from felsic rocks at the surface to mafic rocks. Heat production would, therefore, decrease with depth as mafic rocks are virtually depleted of radiogenic isotopes.

A value of $2.93 \mu W/m^3$ has been used for the heat production of the felsic top-layer in accordance with Slagstad et al. (2008). The intermediate rocks (diorite) and mafic rocks (gabbro) have been given $1.08 \mu W/m^3$ respective $0.3 \mu W/m^3$ with reference to Haenel et al. (1988). The differentiation series in the rift has also been assigned a lower thermal conductivity (2.5 W/m K) than the Sveconorwegian region (2.87 W/m K) based on Figure (3).

The principle outline of the model for the rift can be seen in Figure 5.

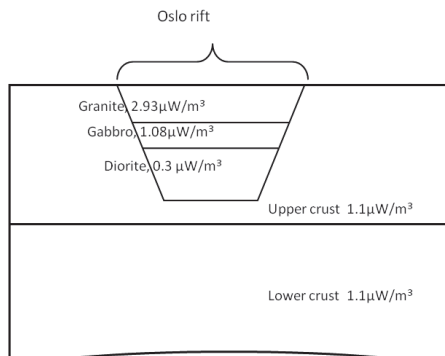


Figure 5: Principle outline of the geology used in the thermal model.

Hurdal is situated 36 km from Hamar and 52 km from Berger, heat flow variations within such short distances are usually related to variations in concentration of heat producing elements in the upper crust, (Jaupart and Mareschal, 2011), (Perry et al. 2004), and cannot be explained by changes in heat-flux from the Moho or by deep seated heat sources.

RESULTS

In Fredrikstad the high heat flow can easily be explained by the presence of Iddefjord granites with high heat production. The heat production of these granites is on average $6 \mu\text{W}/\text{m}^3$ (Slagstad et al. 2009), (Landström et al. 1979) and the thermal conductivity is $3.2 \text{ W}/\text{m K}$ with reference to Figure 3. To explain the high heat flow, these granites have to extend down to around 3.5-5 kilometers. This is in accordance with earlier gravimetric studies, (Ramberg and Scott, 1971), which estimated the Iddefjord-granite to have a thickness ranging between 3 and 5 kilometers. Figure 6 shows a simplified model of the structure in Fredrikstad. It has been assumed here that the surrounding surface heat flow is $57 \text{ mW}/\text{m}^2$. Figure 7 shows the heat flow profile as a result of the geological structure in Figure 6.

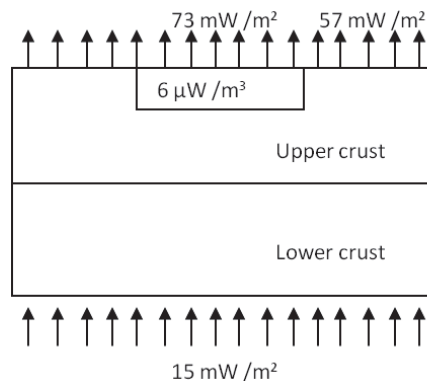


Figure 6: Simplified model for the structure in Fredrikstad, with a domain of high heat producing granites. The upper crust and the lower crust have been assigned a heat production of $1.1 \mu\text{W}/\text{m}^3$.

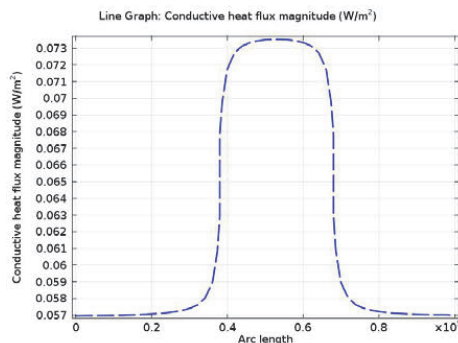


Figure 7: Surface heat flow profile as a result of the Iddefjord granite in Fredrikstad.

The vertical thickness of the Iddefjord granite required to generate the heat flow anomaly is dependent on the contrast to the surrounding rock. If the extent of this granite could be determined in more detail through, for example, geophysical modeling, this could provide information on the variation of heat sources in the upper crust.

The thermal state of the Oslo rift is a function of several factors. The thinning of the crust causes a decrease in heat flow, which is then compensated for by the geological structure of the rift. Thermal modeling does, however, show that an additional heat source is required to reach the elevated heat flow in Hurdal. The structure used in the simulation can be seen in Figure 8.

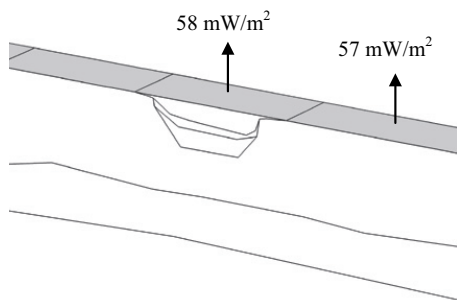


Figure 8: Layout for the model of the model for the Oslo rift.

The next step is to introduce a slab of granite with similar properties and thickness to the Iddefjord granite into the felsic top layer of the model. See Figure 9.

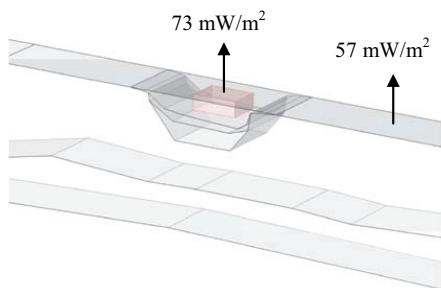


Figure 9: Shallow heat source introduced in the top layer of the rift.

This creates a situation which is fairly similar to the heat flow in Fredrikstad with a confined heat flow peak. The Iddefjord granite has similar density and magnetic susceptibility as the granite in the top layer of the geophysical model, and would therefore not cause any difference to the model. Measurements in the drilled wells in Hurdal did not indicate elevated heat production, thus this body would have to be placed at least 900 m below the surface, personal communication with Slagstad. T at the Geological Survey of Norway (2011).

A shallow heat source such as introduced in Figure 10 can cause the elevation in heat flow. For geothermal purposes it does not have any significant impact, the temperature increase at 5000 m depth is only a few degrees. Since a confined heat source is considered, the size required to generate the elevated heat flow increases rapidly if the granitic block

would be moved downwards in the model. This is because heat diffuses out on the sides of the heat source. Heat flow contour lines in the horizontal plane for such case can be seen in Figure 11 where a 10 km block of high heat producing granite ($6 \mu\text{W}/\text{m}^3$) has been placed underneath the rift. This would as well be inconsistent with the geophysical model.

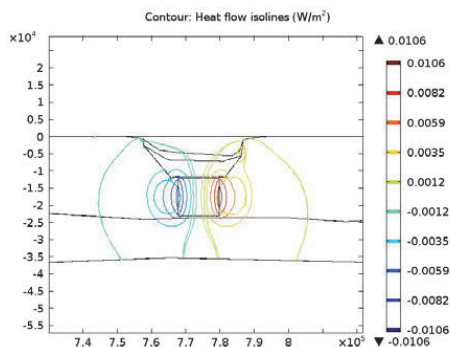


Figure 10: Heat flow contour lines in the horizontal plane for a deep seated heat source.

DISCUSSION

The results presented in this paper are based on a uniform heat production in the lower and upper crust of the Sveconorwegian province. In Slagstad et al. (2009) the heat production rate for this region was determined to be on average $1.76 \mu\text{W}/\text{m}^3$. Without further information on the variation of heat production in the crust, an average of $1.1 \mu\text{W}/\text{m}^3$ has been assumed. This has implications for the result since the contrast between the Oslo rift and the upper crust of the Sveconorwegian region is dependent on this assumption. This also affects the thermal structure of the crust which is a function of both the distribution of the heat sources and of the variability of thermal conductivity. Increasing the heat production in the upper crust implies a decrease of either heat production in the lower crust or heat flux at the lower boundary (Moho), which in turn decreases the temperature in the upper crust.

The result from this paper indicates that the high heat flow in Hurdal is most likely a local phenomenon. It is thus, not a feature of the Oslo rift, and extrapolation based on these heat flow measurements should be made with caution.

Although it has been assumed for the thermal modeling, there is nothing that states that the heat flow anomaly in Hurdal is the peak heat flow in the region. The location for the measurements might just as well be placed on the side of a larger heat source.

The extent of the high producing granite cannot be determined based on the available heat flow data today. Whether a body of high heat producing granites extend outside the rift, might be possible to resolve through geophysical modeling based on gravity and magnetic data.

Likewise there might be other locations in the Oslo rift region that can have elevated heat flow due to buried heat sources.

A shallow heat source such in Figure 9 can cause local heat flow anomalies, it does, however, not have any significant impact on subsurface temperatures. To elevate the temperatures at reachable depths for geothermal energy, the heat sources need to be placed at greater depths.

It should be noted that the thermal conductivity data used in this paper are based on dry measurements. It is, therefore, likely that the actual in-situ thermal conductivity is slightly higher. This does not affect the results with respect to heat flow, but could change the interpretation of the thermal structure of the crust. Also the actual temperature dependency of the type of rocks considered in this paper has not been evaluated, the error involved with this is difficult to assess.

The geophysical model does not contain the level of detail required to further evaluate the structure within the rift. Likewise the thermal model presented is coarse. The general trends are, however, captured.

In absent of local data, the differentiation series in the rift has been assigned heat production values from literature, there is indeed a significant uncertainty involved with this assumption.

Thermal modeling can provide additional constrictions to geophysical models. Currently the heat flow data is scarce in Norway and limited to some few boreholes that are deep enough to become insensitive to the thermal transients induced by palaeoclimatic disturbances.

To produce reliable heat flow data, either further exploration through deep boreholes, or improved reliability of correction methods for shallow boreholes are needed.

Recently, shallow ground source heat pump systems have been constructed in the vicinity of Oslo based on 500 m deep boreholes. The increased depth compared to normal systems (200 m) is explained by limited construction area. This is an interesting development as it can create an opportunity for an increased heat flow data base.

CONCLUSION

Thermal modeling has been used with the aim to explain some recent heat flow data in the vicinity of the Oslo rift in Norway. Thermal modeling shows that a shallow heat source, with the same properties as the Iddefjord granite, could explain the higher heat flow in Hurdal. This points to a local heat flow anomaly, and should therefore not be considered as a feature of the Oslo rift.

Shallow heat sources do not necessarily increase the temperature at depths reachable for geothermal energy. The thermal modeling shows that the heat source only increases the temperature with a few degrees at 5000 m depth.

The best estimate for the heat flow in the Oslo rift is around 58 mW / m² from Slagstad et al. (2009), it is, however, possible that there might be elevated heat flow also in other parts of the rift region.

A larger heat flow database could resolve the variations in heat flow and be used to explore the geothermal potential in the region.

REFERENCES:

- Abdulagatov. I.M., S.N., Emirov., Z.Z. Abdulagatova., S.Y. Askerov. (2006), "Effect of Pressure and Temperature on the Thermal Conductivity," *Journal of Chemical Engineering*, **51**, 22-23.
- Birch. F., H. Clark. (1940), "The thermal conductivity of rocks and its dependence upon temperature and composition," *American Journal of Science*, **238**, 529-558.
- Clauser. C. (2006), "Geothermal Energy", In: K. Heinloth (ed), Landolt-Börnstein, Group VIII: Advanced Materials and Technologies, Vol. 3: Energy Technologies, Subvol. C: Renewable Energies, Springer Verlag, Heidelberg-Berlin, pp. 493-604.
- Ebbing. J., J. R. Skilbrei, and O. Olesen. (2007), "Insights into the magmatic architecture of the Oslo Graben by petrophysically constrained analysis of the gravity and magnetic field," *Journal of Geophysical Research*. **112**, B04404, doi:10.1029/2006JB004694.
- Haenel. R. (1979), "A critical review of heat flow measurements in sea and lake bottoms sediments," In: Cermák, V., Rybach, L. (Eds.), *Terrestrial Heat Flow in Europe*, Berlin, pp. 49-73.
- Huenges. E., J. Erzinger., J. Kück., B. Engeser., W. Kessels. (1997), "The permeable crust: Geohydraulic properties down to 9101 m depth," *Journal of Geophysical research*, **102**, 18,255-18,265.
- Jaupart. C., Mareschal, J.-C. (2003), "Constraints on crustal heat production from heat flow data," *Treatise of Geochemistry, Volume 3: The Crust*, edited by Rudnick, R.L., 65-84, Elsevier Science Publishers, Amsterdam.
- Jaupart. C. and Mareschal. J.-C. (2011), "Heat Generation and Transport in the Earth," University Press, Cambridge.
- Kukkonen. I.T., P. Peltonen. (1999), "Xenolith-controlled geotherm for the central Fennoscandian Shield: implications for the lithosphere-asthenosphere relations," *Tectonophysics*, **304**, 301-315.
- Landström. O., S.Å. Larson., G. Lind., D. Malmqvist. (1979), "Geothermal Investigation in the Bohus Granite Area in Southwestern Sweden," *Tectonophysics*, **64**, 131-162.
- Lee. Y., D. Deming. (1998), "Evaluation of thermal conductivity temperature corrections applied in terrestrial heat flow studies," *Journal of Geophysical Research*, **103**, 2447-2454.
- Liebel. H.T., K. Huber., B.S. Frengstad., R. Kalskin Ramstad and B. Brattli. (2010), "Rock Core Samples Cannot Replace Thermal Response Tests - A Statistical Comparison Based On Thermal Conductivity Data From The Oslo Region (Norway)," *zero emission buildings - proceedings of Renewable Energy Conference 2010*, Trondheim, Norway.
- Middleton. M.F. (1993), "A transient method of measuring the thermal properties of rocks," *Geophysics*, **58**, 357-365.
- Mottaghy. D., H-D. Vosteen., R. Schellschmidt. (2008), "Temperature dependency of the relationship of thermal diffusivity versus thermal conductivity for crystalline rocks," *Int J Earth Sci*, **97**, 435-442.
- Pridnow. D., C.F., Williams., J.H. Sass., R. Keating. (1996), "Thermal conductivity of water-saturated rocks from the KTB pilot hole at temperatures of 25 to 300°C," *Geophysical Research letters*, **23**, 391-394.
- Ramberg. Ivar., S.B. Smithson. (1971), "Gravity Interpretation of the Southern Oslo Graben and Adjacent Precambrian Rocks, Norway," *Tectonophysics*, **11**, 419-431.
- Ramstad. R.K., de Beer, H., Midttomme, K., Koziel, J., Wissing. (2008), "Thermal diffusivity measurement at NGU – Status and method development 2005-2008," Geological Survey. Of Norway., rep. 2008.050, p 41.
- Rybach, L. (1988), "Determination of heat production rate," In Hanel, R., Rybach, L. & Stegena, L. (eds.), *Handbook of Terrestrial Heat-Flow Determination*, 125-142. Kluwer Academic Publishers, Dordrecht.

- Seipold. U. and E. Huenges. (1998), "Thermal properties of gneisses and amphibolites – high pressure and temperature investigations of KTB-rock samples," *Tectonophysics*, **291**, 173-178.
- Slagstad. T. (2005), "Did hot, high heat-producing granites determine the location of the Oslo rift?," *Tectonophysics*, **412**, 105-119.
- Slagstad T., N. Balling., H. Elvebakk., K. Midttømme., O. Olesen., L. Olsen., C. Pascal. (2009), "Heat-flow measurements in Late Palaeoproterozoic to Permian geological provinces in south and central Norway and a new heat-flow map of Fennoscandia and the Norwegian–Greenland Sea," *Tectonophysics*, **473**, 341–361.
- Slagstad.T. (2008), "Radiogenic heat production of Archean to Permian geological provinces in Norway," *Norwegian Journal of Geology*, **88**, 149-166.
- Slagstad. T. (2011), Researcher at the Geological Survey of Norway.
- Stratford. W., H. Thybo. (2011), "Crustal structure and composition of the Oslo Graben, Norway," *Earth and Planetary Science Letters*, **304**, 431-442.
- Vosteen. H-D., R. Schellschmidt. (2003), "Influence of temperature on thermal conductivity, thermal capacity and thermal diffusivity for different types of rock," *Physics and Chemistry of the Earth*, **28**, 499-509.
- Walsh. J.B. and E.R. Decker. (1966), "Effect of Pressure and Saturation Fluid on the Thermal Conductivity of Compact Rock," *Journal of Geophysical Research*, **71**, 3053- 3061.
- Waples. D.W. (2001), "A new model for heat flow in extensional basins: radiogenic heat, asthenospheric heat, and the McKenzie model," *Natural Resources research*, **10**, 3.
- Zimmerman. R.W. (1989), "Thermal conductivity of Fluid-saturated Rocks," *Journal of Petroleum science and Engineering*, **3**, 219-227.

II-6 Numerical model for simulation of the novel closed loop engineered geothermal system- as applied to district heating systems.

II-6.1. INTRODUCTION

A numerical model for heat transfer analysis of wellbores is presented; the model has been developed with the aim to simulate the heat transfer characteristics of the novel Engineered Geothermal System (EGS) concept presented in Paper 5. The aim with the model is to develop a method that can be used for transient analysis on relatively short time scales, (on the order of hours), while still being accurate on a longer time scale. The structure of the numerical model is presented hereunder and is validated against analytical solutions. The model is used to study the performance of the EGS concept for different variations of operating parameters and to explore the usefulness of the EGS concept as a provider of hot water to a District Heating (DH) network. The novel EGS concept is a so-called closed loop system. In principle, the EGS system consists of a production well and an injection well interconnected by drilled wellbores. The wellbores act as a subsurface heat exchanger with a limited, but well defined heat transfer area. This system relies solely on the conductive heat transfer around the wellbores to extract heat from the geothermal reservoir. The thermal performance of the system is closely related to the thermal properties of the bedrock, the temperature at the geothermal reservoir and the operating conditions i.e. temperature range of the heat carrier.

To explore the usefulness of a closed loop EGS as a provider for a DH -network, transient modeling of the system is performed with a numerical model and in conjunction with DH data. This offers a way to both characterize the way the system operates and to determine optimal operation conditions.

Nomenclature

Symbol

C	Specific heat capacity [J/kg·K]	u	Axial velocity component [m/s]
C_v	Specific heat capacity, constant volume [J/kg·K]	V	Velocity [m/s]
d	Diameter [m]	v_r	Radial velocity component [m/s]
e	Internal energy [J/kg]	W	Electric effect [W]
f	Friction factor [-]	z	Axial coordinate [m]
g	Gravitational acceleration [m/s^2]	Greek symbols	
GG	Geothermal gradient [K/km]	Δ	Finite increment in a variable
H	Depth [m]	α	Thermal diffusivity, $\frac{k}{\rho C}$ [m^2/s]
h	heat transfer coefficient [w/m^2]	v	Specific volume [m^3/kg]
h_0	Total enthalphy [J/kg]	ρ	density [kg/m^3]
k	Thermal conductivity [W/m·K]	ϕ	Porosity [%]
L	Length of crosswells [m]	μ	Dynamic viscosity [Pa·s]
\dot{m}	Mass flow [kg/s]	φ	Inclination [°]
N	Number of crosswells [-]	Subscripts	
P	Pressure [N/m^2]	n	Index, temporal discretization

Q	Heat load [W]	i	Index , spatial discretization (radial)
q''	Heat flux [W/m ²]	j	Index , spatial discretization (vertical)
r	Radius [m]	f	fluid
S	Thermal source term [W/m]	g	ground
T	Temperature [K]	b	borehole
t	Time [s]		

II-6.2. THE EGS CONCEPT

The EGS concept consists of a system where a production well and an injection well are interconnected by drilled wellbores. The wellbores does, therefore, act as a subsurface heat exchanger. The principle outline of the system can be seen in Figure II-4.

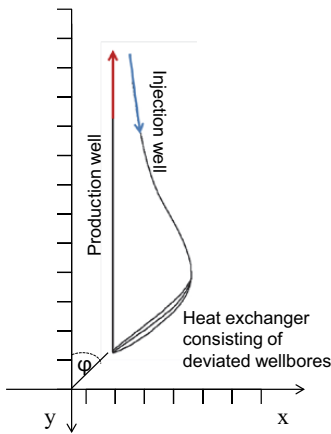


Figure II-4. The system consists of an inlet (injection) and an outlet (production) well that are connected through deviated wellbores.

The fundamental idea is that the fluid heats up as it is circulated through the system. Most of the temperature increase occurs in the deviated boreholes of the heat exchanger part where the mass flow is distributed and reduced accordingly. The characteristics and the dimensions of the system are highly dependent on the operating conditions and the site conditions; this will be discussed further in depth in this part of the thesis.

The system operation can be regulated by either changing the mass flow rate or through bypassing the heat carrier fluid in the process on the surface and thus changing the inlet fluid temperature. If the mass flow in the system is changed, the change will be directly correlated to the produced energy on a short timescale. As a secondary result the production temperature from the system will either increase or decrease.

Bypassing causes the inlet temperature to increase, the response in change of production temperature will then be delayed with the time it takes the fluid to travel through the system. Both methods cause a lagging thermal response in the bedrock.

If the fluid is bypassed (which might be required e.g. in the warm season when the heating demand is low) the temperature of the overall system will increase and thus thermal losses will occur in both the injection well and in the production well. This can to some extent be compensated by insulation in the upper part of both the injection and production wellbores. Other options are to use the excess heat also through the summer, for example for district cooling with absorption chillers. Alternatively, the system can also be operated with a seasonal recovery period where the fluid circulation is stopped during the warm season.

While the entire range of the heat demand (in a DH network) can in principle be covered with an EGS, it is logical to adapt the geothermal system to cover the base load and then use an additional heat source so cover the peak demand. This is also strongly affected by the fact that the thermal load that can be produced by the EGS is inversely proportional to the required temperature level of the heat carrier. The system can, therefore, produce more energy if it is used as a base load at a lower temperature.

The stable nature of geothermal energy makes it a suitable base load candidate in a DH network. However, existing district nets today often operate at excessively high temperatures. In Scandinavia it is common with production temperatures around 80-90 °C and return temperatures around 65 °C. In some systems even higher temperatures can be found. High temperatures are often related to requirements from industrial processes while domestic consumers in general need significantly lower temperatures. Future DH networks are likely to be operated at lower temperatures as the heating demand of buildings decrease; this also reduces transmission losses and promotes renewable energy resources such as solar and geothermal. As an example, the borehole thermal energy storage used for residential heating in Anneberg, Sweden (2014), is estimated to cover 80 % of the heating demand in the buildings with warm water at 32 °C from the energy storage.

II-6.3. HEAT TRANSFER AND THERMAL PROPERTIES

The two primary and dominant heat transfer mechanisms in the EGS are the thermal conduction through the rock and convective heat transfer in the boreholes. The thermal resistance in the rock is orders of magnitude higher than the thermal resistance between the fluid and the wall of the borehole (assuming turbulent flow), and will, therefore, be dominant for the heat transfer process. It is, therefore, important to have a sound estimate of the thermal properties of the rock, in particular the effective thermal conductivity and the specific heat capacity.

While the thermal storage capacity of the rock (product of the specific heat capacity and the density) is in general relatively stable, the effective thermal conductivity can show a larger variability depending on the mineral constituents of the rock as well as the porosity and the presence of fractures. In addition, the thermal conductivity and the specific heat capacity are temperature dependent. These properties are most often measured at ambient temperature and pressure and the measured values are then corrected with empirical laws (for the pressure and temperature dependency) to determine the properties off the reservoir with depth. There are different empirical correlations published for the temperature dependency of thermal conductivity and specific heat capacity as summarized in Section 2.2 of this thesis.

The heat transfer in a borehole can be treated either with numerical or analytical methods. It is usually assumed that the thermal resistance is in the bedrock and that the heat carrier and the wellbore surface are at or near thermal equilibrium. Most practical methods used for e.g. heat transfer calculations in petroleum wells are based on the classical semi-analytic approach by (Ramey, 1962) that uses the line source (Carslaw and Jaeger, 1959). The heat transfer can also be treated with the analytical solution for a cylindrical geometry bounded by an infinite domain (Carslaw and Jaeger, 1959). These analytical solutions are also used frequently for simulation of boreholes in shallow ground source heat pump systems. Using numerical methods it is, however, possible to study the heat transfer in more detail, (Pruess and Zhang, 2005). This also allows for spatial variation in physical properties, and further simplifies transient simulations with time dependent boundary conditions.

The model used in the present study is developed based on a numerical scheme using the finite difference method. This was motivated by the inherent flexibility and transparency offered by numerical methods which allow for detailed system simulation and evaluation.

II-6.4. NUMERICAL MODEL

The numerical model is based on the energy equation for conductive heat transport in the rock and further a one- dimensional energy equation is used to analyse the fluid flow through the different parts of the EGS concept i.e. the injection well, the production well and the heat exchanger part. The equations are discretized and solved simultaneously.

II-6.4.1. HEAT CONDUCTION IN THE ROCK

In this subsection, focus is on the conductive heat transfer in the ground surrounding the wellbore. The energy equation for thermal conduction in the rock surrounding the borehole can be expressed by Fourier's law using cylindrical coordinates as follows:

$$\frac{1}{r} \frac{\partial}{\partial r} \left(kr \frac{\partial T}{\partial r} \right) + \frac{1}{r^2} \frac{\partial}{\partial \phi} \left(kr \frac{\partial T}{\partial \phi} \right) + \frac{\partial}{\partial z} \left(k \frac{\partial T}{\partial z} \right) = \rho C \frac{\partial T}{\partial t} + S \quad \text{II-1}$$

where S is a heat source term. Assuming that the heat transfer is symmetric around the perimeter of the borehole and that the axial conduction can be neglected, the problem can be reduced to an axisymmetric 1-dimensional transient equation.

$$\frac{\partial T}{\partial t} = \frac{1}{r} \left[\frac{\partial}{\partial r} \left(\alpha r \frac{\partial T}{\partial r} \right) \right] + S \quad \text{II-2}$$

Equation II-2 can be discretized based on appropriate numerical schemes using, for example, finite element or finite difference methods. The ground surrounding the borehole is, in the present work, discretized using an axisymmetric cylindrical grid and results in the following equations:

$$\frac{T_i^{n+1} - T_i^n}{\Delta t} = \frac{2}{r_i \Delta r_i} \left[G1 * T_{i+1}^{n+1} - (G1 + G2) * T_i^{n+1} - G2 * T_{i-1}^{n+1} \right] \quad \text{II-3}$$

where G1 and G2 are given by

$$G1 = \frac{\left(r_i + \frac{1}{2}\Delta r_i\right)(\alpha_{i+1}\Delta r_{i+1} + \alpha_i\Delta r_i)}{(\Delta r_i + \Delta r_{i+1})^2} \quad \text{II-4}$$

$$G2 = \frac{\left(r_i - \frac{1}{2}\Delta r_i\right)(\alpha_i\Delta r_i + \alpha_{i-1}\Delta r_{i-1})}{(\Delta r_i + \Delta r_{i-1})^2}, \text{ and} \quad \text{II-5}$$

α is the thermal diffusivity of the ground, and

$$\alpha_i = \frac{\alpha_i\Delta r_i + \alpha_{i+1}\Delta r_{i+1}}{\Delta r_i + \Delta r_{i+1}} \quad \text{II-6}$$

II-6.4.2. MOMENTUM EQUATION FOR THE HEAT CARRIER FLUID

Since the heat carrier fluid (e.g. single phase water) is incompressible, the velocity field in the system is known based on the mass flow rate and the dimensions of the system; therefore, the momentum equation does not have to be solved. The pressure field is, however, required as the properties of the fluid are pressure dependent.

The momentum equation for single phase water is expressed in cylindrical coordinates as:

$$u \frac{\partial u}{\partial t} + \rho u \frac{\partial u}{\partial z} + \rho v_r \frac{\partial u}{\partial z} = -\frac{dP}{dz} + \frac{1}{r} \frac{\partial}{\partial r} \left(r \mu \frac{\partial u}{\partial r} \right) - g\rho \quad \text{II-7}$$

If it assumed that the pressure profile is invariant, and that the change in kinetic energy is negligible. The three first parts on the left side are equal to zero.

The viscous part of the right side of Equation II-7 relates to changes in pressure due to friction. Using the Darcy – Weisbach friction factor (f), the pressure equation can be expressed as:

$$0 = -\frac{dP}{dz} + \frac{fV^2\rho}{2d} - g\rho \quad \text{II-8}$$

The pressure gradient is evaluated based on the results of the energy equation (described below). The equation gives the required pressure to determine the local properties.

II-6.4.3. ENERGY EQUATION FOR THE HEAT CARRIER FLUID

The heat transfer in the wellbore can be represented by the one-dimensional energy equation.

The equation can be expressed based on the total enthalpy ($h_0 = e + \frac{p}{\rho} + gH$)

$$\rho \frac{\partial h_0}{\partial t} + \rho u \frac{\partial h_0}{\partial z} + \rho v_r \frac{\partial h_0}{\partial r} - \frac{1}{r} \frac{\partial}{\partial r} \left(rk \frac{\partial T_f}{\partial r} \right) - \mu \left(\frac{\partial u}{\partial r} \right)^2 - u \frac{dP}{dz} - S = 0, \quad \text{II-9}$$

where mass diffusion has been neglected. Equation II-9 is then simplified by neglecting radial changes in total enthalpy and radial heat conduction (considering 1-d fluid flow). Furthermore, the terms representing friction work and pressure work are neglected, being negligible

compared to the heat transfer from the surrounding borehole walls which is included as a heat source (S), Equation II-9 can, be rewritten as

$$\rho \frac{\partial h_0}{\partial t} + \rho u \frac{\partial h_0}{\partial z} - \frac{2h\Delta T}{r} = 0, \quad \text{II-10}$$

where ΔT represents the temperature difference between the fluid and the temperature of the wall of the wellbore, h is the heat transfer coefficient between the fluid and the wall of the wellbore.

The total enthalphy can be expressed as

$$h_0 = e + \frac{P}{\rho} + gH = T_f C_v + \frac{P}{\rho} + gH. \quad \text{II-11}$$

The derivatives of h_0 can be expressed as

$$\frac{\partial h_0}{\partial z} = C_v \frac{\partial T_f}{\partial z} + \frac{\partial P_v}{\partial z} + g \frac{\partial H}{\partial z}, \quad \text{II-12}$$

$$\frac{\partial h_0}{\partial t} = C_v \frac{\partial T_f}{\partial t} + \frac{\partial P_v}{\partial t} + g \frac{\partial H}{\partial t}, \quad \text{II-13}$$

where $v = \frac{1}{\rho}$.

Neglecting transient changes in gravitational potential and pressure-volume work in Equation II-13, Equation II-10 can be written as:

$$\rho C_v \frac{\partial T_f}{\partial t} + \rho u C_v \frac{\partial T_f}{\partial z} + \rho u \frac{\partial P_v}{\partial z} + \rho u g \frac{\partial H}{\partial z} - \frac{2h\Delta T}{r} = 0. \quad \text{II-14}$$

Equation II-14 can then be rearranged and discretized as shown in Equation II-15.

$$\frac{T_{f_j}^{n+1} - T_{f_j}^n}{\Delta t} = -u \left(\frac{T_{f_{j+1}}^n - T_{f_{j-1}}^n}{\Delta z} \right) - \frac{u}{C_v} \left(\frac{(Pv)_{j+1}^n - (Pv)_j^n}{\partial z} \right) - \frac{ug}{C_v} \left(\frac{H_{j+1}^n - H_j^n}{\partial z} \right) + \frac{2h\Delta T}{r\rho C_v}. \quad \text{II-15}$$

The second and third part of the right side of Equation II-15 balances each other by transferring energy between thermodynamic and gravitational potentials. When the static pressure gradient is dominant, these two parts are essentially of the same magnitude and can, therefore, be removed. The energy equation can, therefore, be further simplified as:

$$\frac{T_{f_j}^{n+1} - T_{f_j}^n}{\Delta t} = -u \left(\frac{T_{f_{j+1}}^n - T_{f_{j-1}}^n}{\Delta z} \right) + \frac{2h\Delta T}{r\rho C_v}. \quad \text{II-16}$$

It is, thereby, shown that the change in internal energy only depends on the change in temperature of the fluid.

Equation II-16 can then be rearranged and discretized based on a third order upwind scheme as follows:

$$\frac{T_{fj}^{n+1} - T_{fj}^n}{\Delta t} = \frac{2h(T_s - T_{fj}^{n+1})}{r\rho C_v} - V \frac{2T_{fj+1}^{n+1} + 3T_{fj}^{n+1} - 6T_{fj-1}^{n+1} + T_{fj-2}^{n+1}}{6\Delta z} \quad \text{II-17}$$

T_s is the temperature of the source (i.e. the borehole wall) and r is the radius of the borehole, V and C_v are the fluid bulk velocity and the specific heat capacity of the fluid, respectively.

II-6.4.4. COUPLING BETWEEN THE CONDUCTION AND CONVECTION MODELS.

To couple the thermal conduction in the rock with the borehole fluid flow models, a flux boundary on the wall of the borehole is introduced. In the conduction equation this is done through central finite difference and the use of a ghost node (T_0) as shown in Figure II-5.

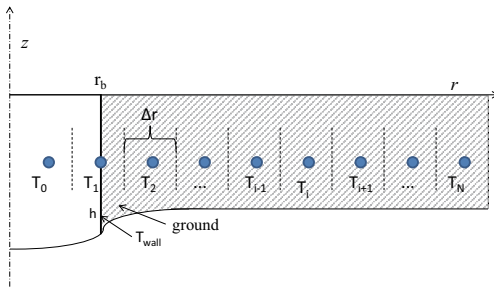


Figure II-5. Illustration for implementation of flux boundary

The heat flux on the boundary is discretized with central difference as shown in Equation II-18 (based on Fourier's equation). The temperature, T_0 , is then determined as shown in Equation II-19 below:

$$q'' = -k \frac{dT}{dx} \approx k \frac{T_2 - T_0}{\frac{1}{2}\Delta r_0 + \Delta r_1 + \frac{1}{2}\Delta r_2} \quad \text{II-18}$$

$$T_0 = T_2 - \frac{q''}{k} \left(\frac{1}{2}\Delta r_0 + \Delta r_1 + \frac{1}{2}\Delta r_2 \right) \quad \text{II-19}$$

Equation II-19 is then used when applying the discretization in Equation II-3 to the boundary node. The resulting equation can be rewritten and simplified as :

$$T_1^{n+1} = T_1^n + \frac{2\Delta t}{r_1 \Delta r_1} [(G1 + G2) * T_2^{n+1} - (G1 + G2) * T_1^{n+1} - q'' * G3] \quad \text{II-20}$$

where

$$G3 = \frac{G2}{k} \left(\frac{1}{2}\Delta r_0 + \Delta r_1 + \frac{1}{2}\Delta r_2 \right) \quad \text{II-21}$$

Thereby, the temperature of the borehole wall is expressed based on the heat flux. The heat flux can also be expressed as:

$$q'' = h_0(T_1 - T_f), \quad \text{II-22}$$

where T_f is the fluid temperature in the borehole. The discretized conduction equation is thereby coupled to the heat transfer in the borehole. The complete equation system is summarized as follows:

Convective equation:

$$T_{f_j}^{n+1} = T_{f_j}^n + \Delta t \left(\frac{2h_0(T_1^{n+1} - T_{f_j}^{n+1})}{r_0 \rho c_p} - V \frac{2T_{f_{j+1}}^{n+1} + 3T_{f_j}^{n+1} - 6T_{f_{j-1}}^{n+1} + T_{f_{j-2}}^{n+1}}{6\Delta z} \right) \quad \text{II-23}$$

Conductive equation:

$$T_1^{n+1} = T_1^n + \frac{2\Delta t}{r_1 \Delta r_1} \left[(G1 + G2) * T_2^{n+1} - (G1 + G2) * T_1^{n+1} - G3 * h_0(T_1^{n+1} - T_{f_j}^{n+1}) \right] \quad \text{II-24}$$

Equation II-23 and II-24 are then setup for the required domain and solved simultaneously through matrix division in Matlab.

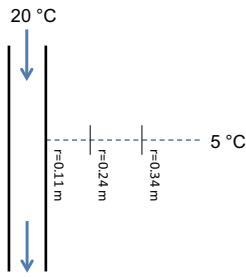
II-6.5. RESULTS AND DISCUSSION

In the following section, the accuracy of the described model is first evaluated in Section II-6.5.1. In Section II-6.5.2 the model is thereafter used to simulate the EGS system and to study the sensitivity to variations in fluid mass flow rate, inlet fluid temperature and ground thermal conductivity. In Section II-6.5.3 the model is used to simulate the performance of the EGS as a provider of heat to a district heating network.

II-6.5.1. VALIDATION OF THE NUMERICAL MODEL

II-6.5.1.1. CONDUCTIVE MODEL

In this part, the conductive heat transfer perpendicular to one section of a borehole is compared with the results from the corresponding analytical solution. The analytical solution for a cylindrical hole bounded by an infinite medium is presented in Carslaw and Jaeger (1959). The analytical solution has been numerically evaluated using the Matlab function `Integral`. Water with a temperature of 20 °C is injected through a borehole with a diameter of 0.2159 m , (8”), as shown in Figure II-6. The initial temperature of the surrounding rock is 5 °C. The change in temperature with time of the borehole wall and at two further positions are compared between the numerical model and the analytical solution.



The flux boundary condition that has been used in the analytical solution is determined from the numerical modeling results. In Figure II-7 the temperature changes at the three specific locations are shown as a function of time.

Figure II-6. Layout for validation of the conductive model.

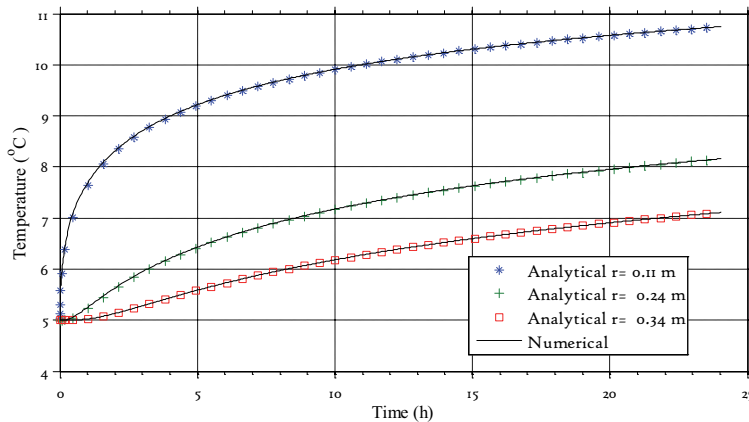


Figure II-7. Temperature profiles at radius $R=r_0 = 0.11\text{ m}$, $R=0.24\text{ m}$ and at 0.34 m , simulated at one section of the pipe.

It is seen that there is good agreement between the temperature profiles from the numerical modeling and the analytical solution.

II-6.5.1.2. CONVECTIVE MODEL

In the convective model, it is primarily the influence of larger temporal and spatial discretization on the accuracy of the solution that is of concern. Since the objective is to simulate convective flow in boreholes with a significantly high aspect ratio, it is important to establish that the simulation method is conservative, meaning that the quantities entering and leaving the pipe are equal. By nature, numerical methods are approximate and are bound to introduce some error. The magnitude depends on both the numerical discretization method and on the nature of the problem it is applied to. For example, a coarse discretization becomes an inaccurate approximation when the problem involves sharp gradients. For continuous heat extraction over long time, it is possible to perform the simulation with a coarse discretization. Refinements can then be made when needed, e.g. if the temperatures or flow conditions changes.

It is not the objective to explicitly simulate step changes in operation conditions. They do, however, pose a challenge for the model, as sharp gradients are introduced. Step changes can, therefore, be used when validating the model. In Figure II-8 a step change in inlet temperature to a 1000 m long pipe is simulated. The simulated time is 10 hours, and the temperature changes from 30 °C to 60 °C with a ramp function over 100 s. The initial temperature of the rock is 90 °C. This introduces sharp temperature gradients that are then attenuated as the fluid travels along the borehole. Since thermal diffusion is not accounted for in the convective model (see Equation II-10), the attenuation occurs by numerical diffusion and by the convective heat transfer to the surrounding rock. It is seen in Figure II-8 that a coarse spatial and temporal discretization gives the same result as the finer discretization. The difference in accumulated energy transfer between the two cases is on the order of 0.2 %. This is simulated with a variable time step that changes and becomes smaller when the gradients are high. For the applications of interest here, the heat transport between the rock and the fluid in the pipe is much larger than the effect of numerical diffusion.

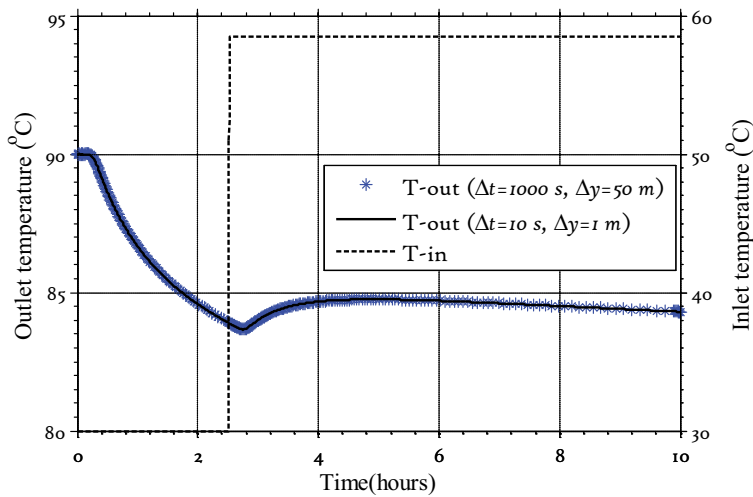


Figure II-8. The figure shows inlet and outlet temperatures from a 1000 m long pipe segment surrounded by an infinite solid domain. The results from two cases with different spatial and temporal discretization are shown. The change in accumulated energy transfer between the two cases is on the order of 0.2 % .

In Figure II-9 the change in thermal load is shown for a 5000 m long borehole with a step change in temperature. The initial temperature of the rock is 90 °C and the inlet temperature changes from 30°C to 60°C. It is seen that with a coarser discretization essentially the same thermal load is determined. The difference in accumulated energy transferred between the two cases in the figure is on the order of 0.35 %.

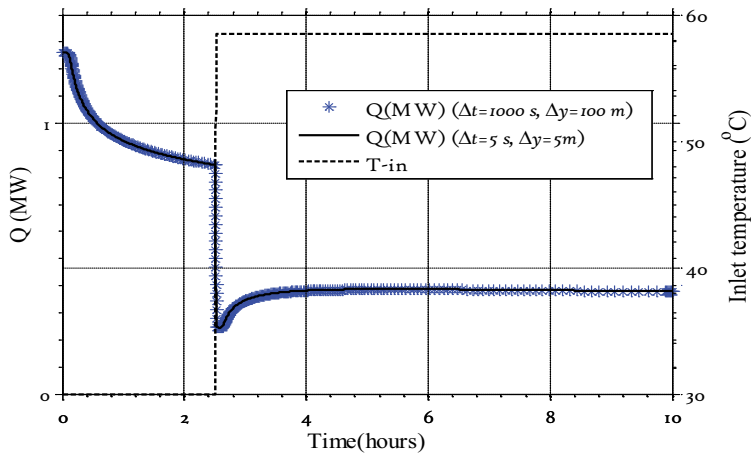


Figure II-9. The figure shows inlet temperature and thermal load from a 5000 m long pipe segment surrounded by an infinite solid domain. The results from two cases with different spatial and temporal discretization are shown. The change in accumulated energy transfer between the two cases is on the order of 0.35 %.

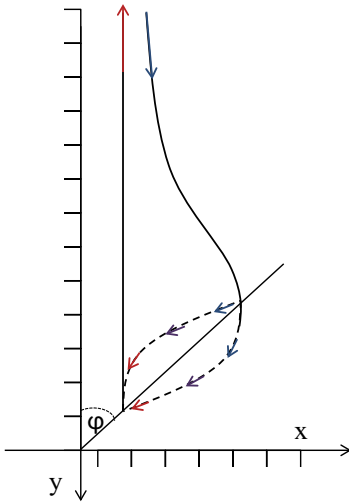
In conclusion, it has been shown that both the conductive and the convective parts of the model are sufficiently accurate. The model can, therefore, be used with confidence to simulate the performance of the EGS.

II-6.5.2. SIMULATION OF CLOSED LOOP EGS.

In this part, the numerical model is applied to the novel closed loop EGS concept. By assuming that the wellbores constituting the heat exchanger part of the EGS are placed sufficiently far apart from each other so that thermal influence between the boreholes can be considered negligible, the system can be segregated into a series of wellbores that are connected only through the transfer of energy by the fluid in each of the wellbores.

The required length of the wellbores, the inclination (ϕ) and the number of cross-wells with a specific length, depends on the temperature gradient in the ground, the thermal properties of the rock the, target fluid temperature range (injection and production temperatures) and the target thermal load value.

A specific system is designed and simulated with the aim to demonstrate the thermal performance for different operation parameters. The parameters describing the system are shown in Table II-1 with reference to Figure II-10. This system layout is then used as a base case when studying the influence of some of the important parameters.



These parameters are :

- mass flow rate
- inlet fluid temperature
- effective ground thermal conductivity
- operation time

The model is, thereafter, used to simulate the performance of the EGS as a provider of hot water to a DH-network.

Figure II-10 System layout for closed loop EGS

The EGS is simulated with three parallel boreholes, each with a length of 2000 m constituting the heat exchanger part. In the simulated case the undisturbed temperature at 5000 m is 105 °C.

Table II-1. Parameters defining the base case.

Geological	Value	System	Value
GG [°C / km]	20 °	H [m]	5000
* k _g [W/ m K]	3	L [m]	2000
ρ _g [kg / m ³]	2600	ṁ [kg / s]	25
C [J/ K·kg]	840	D [m] /	0.2159 (8")
Φ [%]	0	φ [°]	40 °
		N [-]	3

*Thermal properties of the rock are here assumed constant with respect to temperature and pressure.

The temperature profile in the system after 1000 hours of operation is presented in Figure II-11, the pressure and density profiles are shown in Figure II-12.

Since the fluid heats up along the borehole, the rising fluid in the production well will have a lower density than the fluid in the injection well. The fluid can, therefore, to some extent circulate in the system without assistance from a circulation pump. To meet certain criteria's of temperatures and flow rates, the flow has to be controlled by a circulation pump.

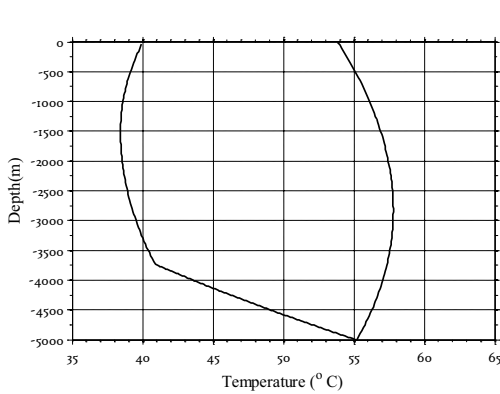


Figure II-11. temperature profile in the system. Water enters at 40 °C and leaves at 54 °C. simulation time: 1000 hours

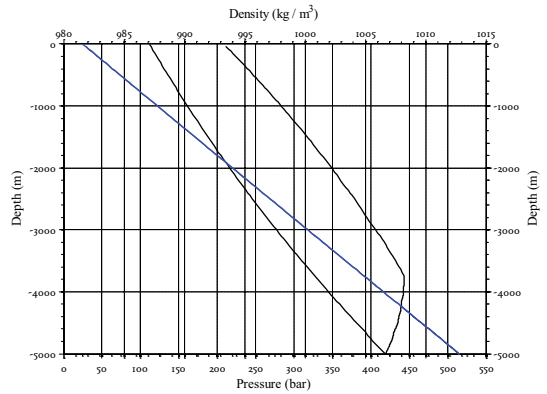


Figure II-12. Pressure and density profile in the system. simulation time: 1000 hours

For the simulated case, the total frictional pressure drop is 3.7 bar while the pressure difference due to the density differences between the fluid in the injection well and the production well is 3.5 bars, the fluid is, therefore, almost self circulating. The heat load from the simulated system after 1000 hours of continuous operation is 1.45 MW.

It is obvious from Figure II-11 that there are temperature losses in the upper part of the wells. To limit these losses, thermal insulation can be added in the wells. This also increases the frictional pressure drop as the flow area is reduced, alternatively the borehole diameter can be increased. In Figure II-13 and Figure II-14, 2 cm of thermal insulation with a thermal conductivity of 0.1 W / m K is used in the upper 2500 m of the production well and 2000 m of the injection well.

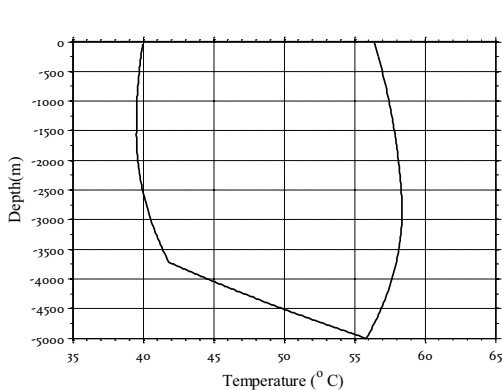


Figure II-13. temperature profile in the system with insulation. Water enters at 40 °C and leaves at 56 °C. Simulation time: 1000 hours.

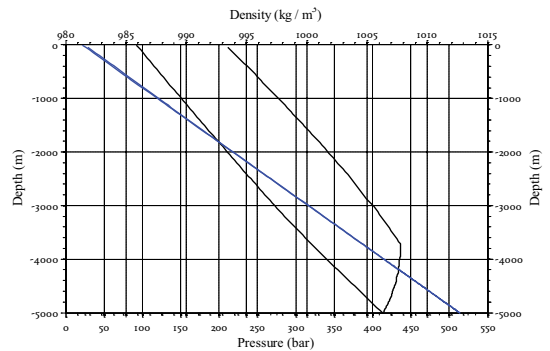


Figure II-14. Pressure and density profile in the system with insulation. Simulation time: 1000 hours.

The frictional pressure drop is in this case 6.9 bar which means that the real pressure difference required on the surface is 3.4 bars, or 12.1 KW, with an assumed pump efficiency of 0.7. The pressure drop can, however, be limited using a larger borehole diameter. The heat load from the system is 1.72 MW (18.5 % larger than for the uninsulated case).

In the following cases, the influence of mass flow rate, inlet temperature, ground thermal conductivity and operation time is studied. In all cases, the EGS is simulated without insulation in the production well and the injection well.

In Figure II-15 the mass flow is varied while the inlet temperature is kept constant. With an increasing mass flow rate, the temperature rise of the fluid through the system decreases. Therefore, a higher temperature difference is maintained to the surrounding rock. As a consequence, more thermal energy can be extracted.

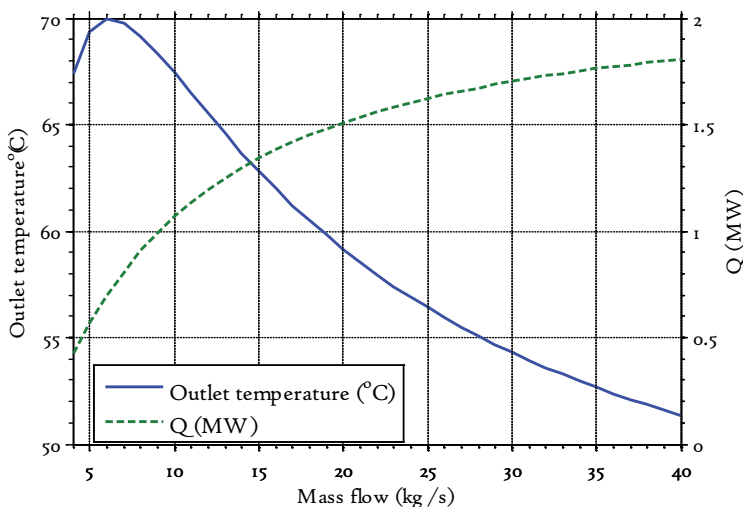


Figure II-15. Variation in mass flow. Water enters at 40 °C. Simulation time : 1000 hours,

A higher mass flow requires more pump work both because of the increased frictional pressure loss and because of lower density differences (driving potential for self-circulation). The required pump work is in the simulated cases at most 4.7 % of the produced heat load.

In Figure II-16 the inlet temperature is varied while the mass flow rate is kept constant.

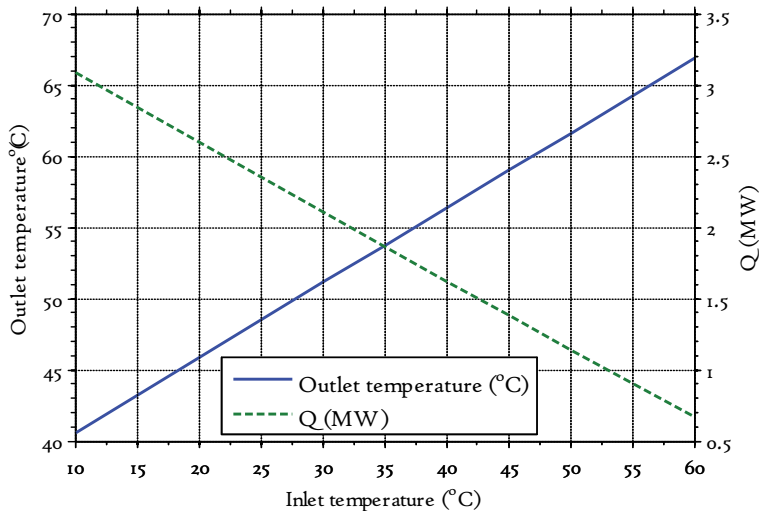


Figure II-16. Variation in Inlet temperature, simulation time : 1000 hours

It is seen that the heat load and the outlet temperature are both linearly proportional to the inlet temperature. Figure II-16 clearly shows that it is crucial that the geothermal installation provides energy in the lowest temperature range possible.

In Figure II-17 the thermal conductivity of the ground is varied while the mass flow rate and the inlet fluid temperature are kept at constant values. In the figure, the thermal load has been normalized with the value at a thermal conductivity of 3 W / m K.

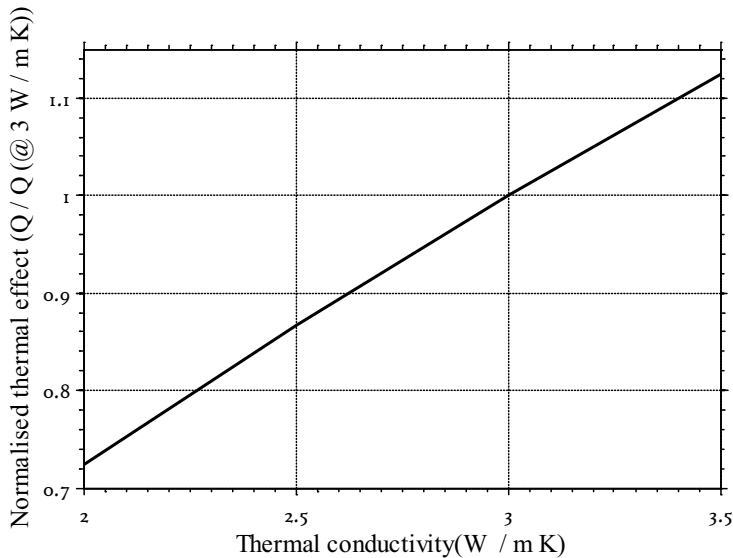


Figure II-17. Variation of thermal effect with ground thermal conductivity.

It is seen that the thermal conductivity has a significant influence on the performance of the system. This is expected since the system relies on thermal conduction as the sole heat transport mechanism.

There is a relatively large decline in thermal performance of the system during the first years of operation. As seen in Figure II-18, the heat load declines from 1.19 MW after the first year to 1 MW after 10 years, in the following 10 years the heat load decreases further 5 %. Interestingly, the decrease between year 30 and 50 is only on the order of 1 %. Thereafter, the performance can be said to be near constant.

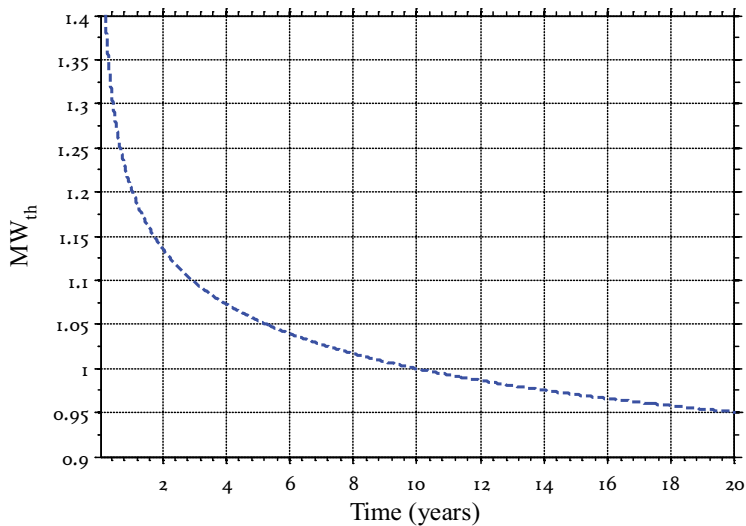


Figure II-18. Decline in thermal output over time

II-6.5.2.1. THERMAL INTERFERENCE BETWEEN WELLS.

The main part of the heat extraction occurs in the heat exchanger part of the system, and it is crucial for the performance of the system, (and for the validity of the numerical model) that thermal breakthrough (interference) between the wellbores is avoided in this part. Through engineering the heat exchanger with drilled wellbores the risks for thermal breakthrough can in theory be controlled and/or avoided. The required separation distance between the wellbores can be determined based on the rate at which heat diffuses through the ground and the designed life length of the system.

The thermal influence around a wellbore with a constant heat extraction rate is shown as a function of time and radial distance in Section 2.1.4 (Figure 2-6 b). It is seen that after 50 years, the influence at 100 m radius is almost negligible. This can, therefore, be considered as an appropriate distance between the wellbores in the heat exchanger part.

II-6.5.3. EGS SYSTEM COUPLED WITH DISTRICT HEATING

In this subsection, the closed loop EGS is assumed to provide heat for a DH network. To get a realistic behavior, operational data from a DH network is used; the data is sampled on daily basis over one year. An illustration of how the model is coupled with the DH network is shown in Figure II-19.

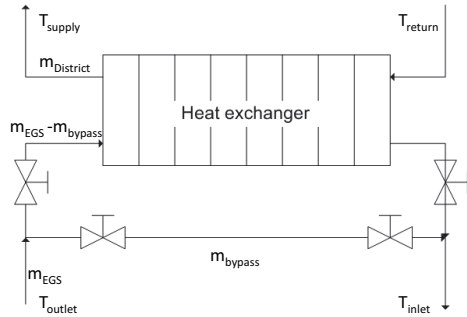


Figure II-19. Illustration of the EGS in connection with heat exchanger.

The amount of energy extracted from the geothermal loop is varied by adjusting the mass flow rate (m_{EGS}) and the amount of mass flow that is bypassed (m_{bypass}). The thermal load in the DH network varies between a minimum of 0.5 MW during the summer and a maximum of 8 MW during the winter. The return temperature from the DH network varies between 36 °C and 58 °C and the production temperature varies between 70 °C and 96 °C. In the simulation, the mass flow in the geothermal system is allowed to vary between 20 kg/s and 40 kg/s. To reduce the thermal output, the mass flow can be bypassed, e.g. when the system provides more heat than is required and the mass flow rate is at the minimum.

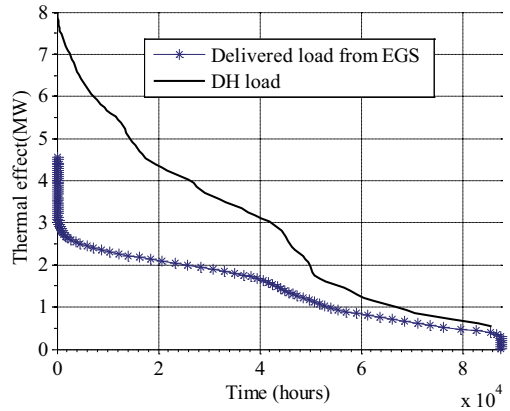
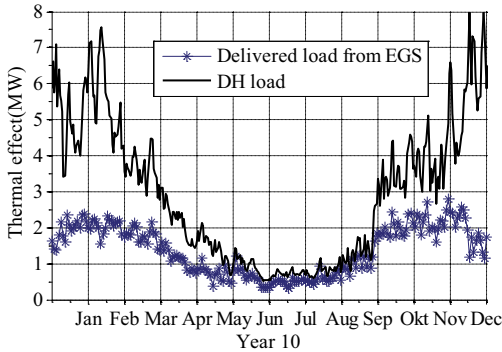
The parameters describing the simulated geothermal plant are summarized in Table II-2. The EGS is simulated with five parallel boreholes, each with a length of 2000 m constituting the heat exchanger part. The undisturbed temperature at 5000 m is 105 °C.

Table II-2. Parameters defining the base case.

Geological	Value	System	Value
GG [°C / km]	20	H [m]	5000
k_{g0} [W / m K]	3	L [m]	2000
ρ_g [kg / m ³]	2600	\dot{m} [kg / s]	20- 40
C [J / K·kg]	840	D [m] /	0.2159 (8°)
Φ [%]	0	φ [°]	40
		N [-]	5

The thermal conductivity of the ground is allowed to vary with temperature (see Section 2.2). The dependencies are according to the empirical equation by Sass et al. (1992) and Vosteen and Schellschmidt, (2003) for thermal conductivity, see Equation 2-13 and Equation 2-14. The pressure dependency of the thermal conductivity has been neglected as it is of minor

importance. The simulation is done for 10 years of operation, and the results are presented hereunder. The delivered heat load during year 10 is shown in Figure II-20.a, and the duration curve for the 10 years is shown in Figure II-20.b.



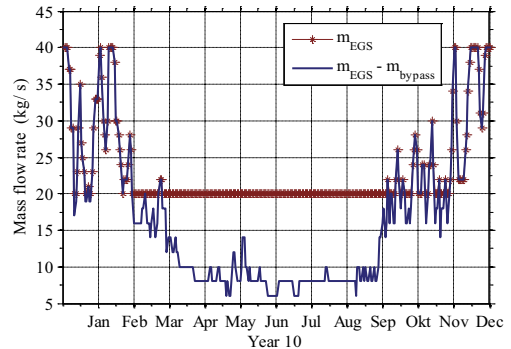
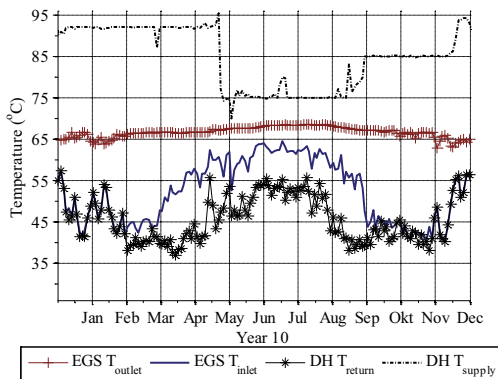
a

b

Figure II-20 a) Thermal effect delivered by EGS during year 10 . b) Duration curve for 10 years.

As can be seen from Figure II-20 a, the energy supply from the EGS can vary quite significantly (between about 0.4 MW and 3 MW heat load). The higher heat loads (> 3 MW) shown in Figure II-20 b represents the startup of the installation during the first year. A combination of mass flow regulation and bypassing is used to control the system. The return and production temperatures and the variation in mass flow rate are shown in Figure II-21.a and b.

The temperature increases when the load demand is low. In this specific case in total 40 % of the required energy for the DH network is provided by the geothermal system.



a

b

Figure II-21. a) Production and return temperatures in the EGS and in the DH network. b) Mass flow rates. The outlet temperature from the EGS increases due to bypassing when the load demand is low.

The required energy by the circulation pump is seen in Figure II-22. The energy requirement becomes negative when the mass flow is low, this indicates that the system is self circulating. As the mass flow increases, the frictional pressure losses increases and the circulation requires energy. In this case the pump work is somewhat idealized, using a constant efficiency of 0.7.

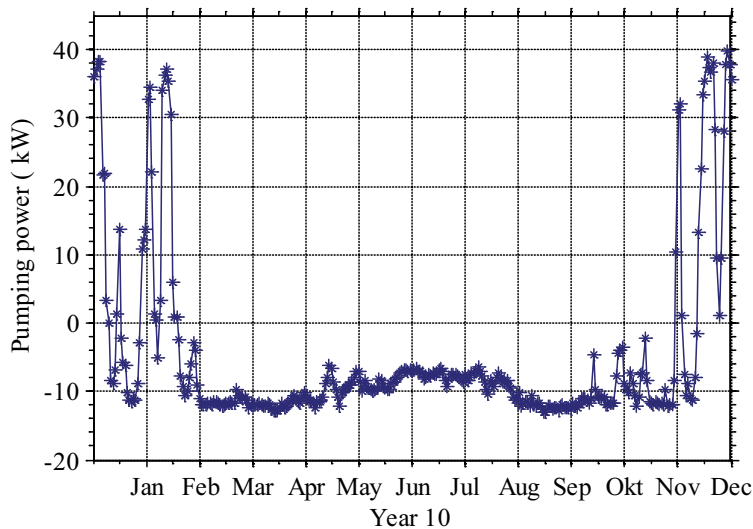


Figure II-22. Power required for fluid circulation in the system.

As shown in Figure II-16 the heat load delivered by the EGS is directly proportional to the inlet temperature. This can be illustrated by a reduction in the temperature level of the district heating network. If for example the temperature level of the DH network is reduced by 10 K, i.e. the minimum return temperature is 26 °C and the maximum supply temperature is 86°C. The amount of energy that the geothermal system can provide increases with about 30 %. Thereby, the share of geothermal energy in the DH-network increases from 40 % to 53 %. Complementary figures showing the performance of the EGS operating at these conditions can be found in Appendix C.

II-6.6. CONCLUSIONS

A numerical model is presented, the aim with the model is to simulate and study the transient behavior and thermal performance of a novel closed loop EGS. The model is found to be accurate in comparison with an analytical solution and by variation of spatial and temporal discretization. The model is used to simulate the closed loop EGS, and the performance is studied for different variations of the operating parameters. It is found that thermal conductivity of the ground has a large influence on the system performance and that the thermal output for

the system is directly related to the inlet fluid temperature; therefore, the lowest possible temperature range should be sought for a given system.

The model is used to simulate heat extraction with the purpose to supply hot water to a DH-network. It is seen that the system can sustain heat production while requiring little or no use of high value energy for fluid circulation. While the EGS is a stable heat source which is best utilized as a base load, transient simulation show that the system also can be operated dynamically to cover periods with higher or lower heat demands at different temperature levels. The simulated system provides thermal energy in the range of 1 to 3 MW, it can, however, be upscaled to meet significantly larger heating demands.

It is shown that the system can supply energy for a significant time. After the initial decline during the first years of operation, the thermal performance reaches a semi- steady state with very little change in performance over time. It can therefore, be concluded that if the system is designed and operated correctly it will, from a thermal perspective, have a virtually unlimited lifetime.

The operating conditions have a significant influence on the performance of the EGS. The presence of a suitable heat consumer that guarantees a high operation time at a rather low temperature range, can, therefore, be the most important factor when finding suitable locations for an EGS.

References

- Abdulagatov. I.M., S.N., Emirov., Z.Z. Abdulagatova., S.Y. Askerov. (2006), "Effect of Pressure and Temperature on the Thermal Conductivity," *Journal of Chemical Engineering*, 51, 22-23.
- Acuna J. Licentiate Thesis, (2010). KTH school of industrial Engineering and Management, Division of applied thermodynamic Refrigeration, SE-100 44 Stockholm
- Anneberg, (2014), <http://www.anneberg.org/generell-information/sol-och-bergvaermesystemet>, accessed 20 august 2014.
- Andersson. O., and L. Bjelm, (2013) Geothermal Energy use Country Update for Sweden. European Geothermal congress 2013, Pisa Italy 3-7 June 2013
- Al- Khoury. R., P.G. Bonnier., R.b.J. Brinkgreve, (2005) Efficient finite element formulation for geothermal heating systems. Part 1: Steady state, *International Journal of Numerical Methods in Engineering*, v 63, pp.988-1013
- Asplan viak, (2014). <http://www.asplanviak.no/index.asp?id=36478> Access data 30/06- 2014
- Bauer. D., Heidemann. W., H. Müller-Steinhagen., H.-J.G. Diersch, (2011) Thermal resistance and capacity models for borehole heat exchangers. *Int. J. Energy Res*, v 35, pp. 312-320
- Batchelor. T., R. Curtis., P. Ledingham, (2010) Country Update for the United Kingdom, Proceedings WGC2010
- Backe. G., D.Giles., G. Baines., K. Amos, (2010) 3D Geological Modeling of Potential Geothermal Energy Reservoirs in the Flinders Ranges, Australia. Proceedings WGC 2010, Bali, Indonesia, 25-29 April 2010
- Bernier. M., P.Pinel, R. Labib and R.Paillot, (2004), A multiple load aggregation for annular hourly simulations of GCHP systems, *HVAC&R Research* v 10, Nr4, pp. 471-87
- Birch. F., H. Clark, (1940), "The thermal conductivity of rocks and its dependence upon temperature and composition," *American Journal of Science*, 238, 529-558
- Bjelm. L., P-G. Alm., O. Andersson, (2010) Country Update for Sweden, Proceedings WGC2010
- Carslaw. H.S., J.C. Jaeger, (1959), *Conduction of heat in solids*, second ed., Oxford University press, Oxford.
- Carrier, (2014), data sheet, http://www.carrierab.se/media/69477/61wg__30wg__30wga_produkblad.pdf. Accessed: 10 january 2014.
- Clauser. C, (2006), "Geothermal Energy", In: K. Heinloth (ed), *Landolt-Börnstein, Group VIII: Advanced Materials and Technologies, Vol. 3: Energy Technologies, Subvol. C: Renewable Energies*, Springer Verlag, Heidelberg-Berlin, pp. 493-604.
- Clauser and Huenges, (1995) *Thermal conductivity of Rocks and Minerals. Rock Physics and Phase Relations A Handbook of Physical Constants*.
- Comsol multiphysics (version 4.3.a) Comsol Inc.
- Cuenot. N., J-P Faucher., D. Fritsch., A. Genter., D. Szablinski,(2008) The European EGS project at Soultz-sous Forets: From extensive exploration to power production. IEEE Power and Energy Society 2008 General Meeting: conversion and delivery of electrical energy in the 21st century.
- Diersch. H.-J.G., D. Bauer., W. Heidemann., W. Rühak., P Schätzl, (2011) Finite element modeling of borehole heat exchanger systems Part I. Fundamentals. *Computers & Geosciences*, v 37, pp. 1122-1135
- Driscoll. J.P, (2010) Geothermal Systems Assessments and Their Use in Conductive Regimes, Proceedings WGC2010

- Eckert. E. R. G., R.M. Drake JR, (1972) Analysis of Heat and Mass Transfer, McGraw-Hill, New York.
- Fossa. M, (2011) The temperature penalty approach to the design of borehole heat exchangers for heat pump applications. Energy and Buildings, v 43, pp. 1473-1479.
- Genter. A., X. Goerke., J-J. Graff., N. Cuenot., G. Krall., M. Schindler., G. Ravier, (2010) Current Status of the EGS Soultz Geothermal Project (France), Proceedings WGC2010
- Geothermal Projects in Germany, Proceedings WGC2010
- Geodynamics, (2013) <http://www.geodynamics.com.au/home.aspx>, accessed 20-06-2013
- Genter. A., D. Fritsh., N. Cuenot., J. Baumgärtner., J-J. Graf,(2009) Overview of the current activities of the European EGS Soultz Project: from exploration to electricity production. 34th Workshop on geothermal reservoir engineering, Stanford university, Stanford, California, February 9- 11, 2009.
- Ghelin S, (2002) Thermal Response Test Method Development and Evaluation, Doctoral Thesis, Department of Environmental Engineering. Luleå University of Technology. Sweden.
- Gibson. H.J., K. Stüwe., R. Seikel., D., FitzGerald,(2010) Practical aspects of 3D temperature and heat flow modeling for EGS energy exploration including a high relief terrain case study. Proceedings WGC 2010, Bali, Indonesia, 25-29 April 2010.
- Gustafsson. A.-M., L. Westerlund, (2011) Heat extraction thermal response test in groundwater-filled borehole heat exchanger Investigation of the borehole thermal resistance, Renewable energy, v 36 pp. 2388-2394
- Gustafsson. A.-M., L. Westerlund., Hellström.G, (2010) CFD-modelling of natural convection in a groundwater-filled borehole heat exchanger. Applied thermal engineering, v 30, pp. 683-691
- Haenel. R., Rybach. L., Stegena. L, (1988) Handbook of Terrestrial Heat-Flow Density Determination. Kluwer Academic Publishers 1988.
- Hellström. G. (1991) Ground Heat Storage, Thermal analyses of Duct Storage Systems, Theory. Department of Mathematical physics , University of Lund, Sweden
- Häring. M.O., U. Schanz., F. Ladner., B.C. Dyer, (2010) Characterisation of the Basel 1 enhanced geothermal system, Proceedings WGC2010
- IEA 2011, http://www.iea.org/publications/freepublications/publication/Geothermal_Roadmap.pdf accessed 26-08-2014
- IEA 2010, Energy Technology Perspectives 2010 <http://www.iea.org/publications/freepublications/publication/etp2010.pdf>, accessed 26-08-2014
- Ingersoll, L.R. and H.J. Plass, (1948): Theory of the ground pipe heat-source for the heat pump, Heating, Piping, Air Conditioning Journal 20 (7) 119-122
- Javed. S., Thermal modeling and evaluation of borehole heat transfer, (2012). Doctoral thesis, Department of Building Technology, Building Services Engineering. Chalmers University of Technology.
- Kaieda. H., S Sasaki., D, Wyborn, (2010) Comparison of Characteristics of Micro-Earthquakes Observed During Hydraulic Stimulation Operations in Ogachi, Hijiori and Cooper Basin HDR Projects, Proceedings WGC2010
- Kelly. K, (1960) Contributions to the data on theoretical metallurgy. XIII. High-temperature, heat-content, heat-capacity and entropy data for elements and inorganic compounds: U.S. Bur. Mines Bull. No 584, 232 p.
- Keyhani. M., F.A. Kulacki, R.N. Christensen, (1983) Free convection in a vertical annulus with constant heat flux on the inner wall, Transactions of the ASME 105.
- Keyhani. M., F.A. Kulacki, R.N. Christensen, (1985) Experimental Investigation of free convection in a vertical rod bundle – A general correlation for Nusselt number, Journal of heat transfer, v 107, pp. 611-623

- Koh, J., H. Roshan., S. S. Rahman,(2011) A numerical study on the long term thermo-poroelastic effects of cold water injection into naturally fractured geothermal reservoirs. *Computers and geotechnics* (2011), v 38. Issue 5, pp. 669 -682
- Kjellsson. E. (2009) *Solar Collectors Combined with Ground-Source Heat Pumps in Dwellings, Analyses of System Performance*. Doctoral thesis, Building Physics. University of Lund, Sweden.
- Kjellsson E., Hellström G, (1999) *Laboratory study of the heat transfer in a water-filled borehole with a c-pipe – Preliminary report*. Lund University, Lund, Sweden.
- Krewitt, W., K. Nienhaus, C. Klessmann, C. Capone, E. Stricker, W. Graus, M. Hoogwijk, N. Supersberger, U.von Winterfeld and S. Samadi, (2009) *Role and Potential of Renewable Energy and*
- Lazzarotto A, (2014) *A network-based methodology for the simulation of borehole heat storage systems*.*Renewable Energy*, v 62, pp. 265- 275
- Lee. Y., S. Korpela, (1983) *Multicellular natural convection in a vertical slot*, *Journal of Fluid Mechanics*, v 126, pp. 91-121
- Lemmon. E.W., M.O. McLinden and D.G. Friend, (2012) "Thermophysical Properties of Fluid Systems" in *NIST Chemistry WebBook, NIST Standard Reference Database Number 69*, Eds. P.J. Linstrom and W.G. Mallard, National Institute of Standards and Technology, Gaithersburg MD, 20899, <http://webbook.nist.gov>, (retrieved December 4, 2012).
- Littlefield. D., P. Desai, (1986) *Buoyant Laminar convection in a vertical cylindrical annulus*, *Journal of heat transfer*, v 108, pp. 815-821
- Lund. W. J., D.H. Freeston., T.L.Boyd,(2010) *Direct utilization of geothermal energy 2010 worldwide review*, *Proceedings, WGC2010*.
- Long. A., B. A. Goldstein., T. Hill., A. Budd,(2010) *Review of Australian Geothermal Activities and Research*, *Proceedings WGC2010*
- Lund J.W., D. H. Freeston., T. L. Boyd, (2010) *Direct Utilization of Geothermal Energy 2010*. *Proceedings World Geothermal Congress 2010*
- Mahler. A., J. Magtengaard, (2010) *Country Update Report for Denmark*, *Proceedings WGC2010*
- Marcotte. D., P. Pasquier, (2014) *Unit-response function for ground heat exchanger with parallel, series or mixed borehole arrangement*. *Renewable Energy* v 68, pp. 14- 24
- Matlab 2012b, The MathWorks Inc., Natick, Massachusetts, United States.
- McDermott. C.I., A.R.L Randiamanjatosoa, H. Tenzer., O. Kolditz, (2006) *Simulation of heat extraction from crystalline rocks: The influence of coupled processes on differential reservoir cooling*. *Geothermics*, v 35, issue 3, pp 321-344
- Mottaghy. D., H-D. Vosteen., R. Schellschmidt, (2008) *Temperature dependency of the relationship of thermal diffusivity versus thermal conductivity for crystalline rocks*, *Int J Earth Sci*, 97, 435-442.
- Mottaghy D., L. Dijkshoorn, (2012) *Implementing an effective finite difference formulation for borehole heat exchangers into a heat and mass transport code*, *Renewable energy*, v 45, pp. 59-71
- Midttømme. K., J. Müller., H. Skarphagen., I. Berre., R. K. Ramstad., H. R. Sørheim, (2013) *Geothermal Energy Use, Country Update for Norway*. *European Geothermal congress 2013, Pisa Italy 3-7 June 2013*
- Pascal. C., H. Elvebakk., O. Olesen, (2010) *An Assessment of Deep Geothermal Resources in Norway*, *Proceedings WGC2010*
- Pruess. K., Y. Zhang, (2005) *A Hybrid Semi-Analytical Numerical Method for Modeling Wellbore Heat Transmission*, *Proceedings, 30th Workshop on Geothermal Reservoir Engineering*Stanford University
- Pruess. K., N. Spycher, (2010) *Enhanced Geothermal Systems (EGS) with CO2 as Heat Transmission Fluid - A Scheme for Combining Recovery of Renewable Energy with Geologic Storage of CO2*, *Proceedings WGC2010*

- Peng H.Y., H.D. Yeh., S.Y. Yang, (2002) Improved numerical evaluation of the radial groundwater flow equation, *Adv. Water Resour.* 25, pp. 663–667.
- Pridnow. D., C.F. Williams., J.H. Sass, and R. Keating, (1996) Thermal conductivity of water-saturated rocks from the KTB pilot borehole at temperatures of 25 to 300 °C. *Geophysical research letters.* Vol 23,, No. 4. pp. 391-394.
- Rybach, L. (1988), "Determination of heat production rate," In Hanel, R., Rybach, L. & Stegena, L. (eds.), *Handbook of Terrestrial Heat-Flow Determination*, 125-142. Kluwer Academic Publishers, Dordrecht.
- Quick. H., J. Michael., H. Huber., U. Arslan, (2010), *History of International Geothermal Power Plants and*
- Ramey. H.J, (1962) Wellbore Heat Transmission, *SPE* 9, 1962, No 4, pp 465-474
- Rothert. E., S. Baisch, (2010) *Passive Seismic Monitoring: Mapping Enhanced Fracture Permeability*, Proceedings WGC2010
- Eskilson. G, (1987) *Thermal Analysis of Heat Extraction Boreholes*. Doctoral Thesis, University of Lund, Department of Mathematical Physics. Lund, Sweden.
- Energy Efficiency for Global Energy Supply.
http://www.ecofys.com/files/report_role_potential_renewable_energy_efficiency_global_energy_supply.pdf accessed 26-08-2014'
- Sanyal. S. K. E.E. Granados., S. J. Butler., R.N. Horne, (2005) An alternative and modular approach to Enhanced Geothermal Systems. Proceedings WGC 2005, Antalya, Turkey 24-29 April 2005.
- Sass. J.H., Lachenbruch. A.H., Moses. T., Morgan, P, (1992). Heat flow from a scientific research well at Cajon Pass, California, *J. Geophys. Res.* 97, pp. 5017-5030
- Seipold. U, (1998) Temperature dependence of thermal properties of crystalline rocks- a general law. *Tectonophysics* 291 pp 161-171
- Seki. N., S. Fukusako., H. Inaba, (1978) Visual observation of natural convective flow in a narrow vertical cavity. *Journal of Fluid mechanics* v. 84, part 4, pp. 695-704
- Slagstad. T, (2008) Radiogenic heat production of Archaean to Permian geological provinces in Norway, *Norwegian Journal of Geology* vol 88, pp. 149-166.
- Stefansson. V,(2005) *World Geothermal Assessment*. Proceedings WGC2005
- Tester. J.W. et al, (2006). "The Future of Geothermal Energy – Impact of Enhanced Geothermal Systems (EGS) on the United States in the 21st Century," MIT - Massachusetts Institute of Technology, Cambridge, MA. 358 p. Available at http://www1.eere.energy.gov/geothermal/future_geothermal.html.
- Turcotte. D.L., G. Schubert, (2002) *Geodynamics 2*. Edition, Cambridge University press (2002), ISBN 0521 661862
- U.S. Patent, #6,247,313B1, 19 June 2001
- Vosteen. H.D., R. Schellschmidt, (2003) Influence of temperature on thermal conductivity, thermal capacity and thermal diffusivity for different types of rock. (2003) *Physics and Chemistry of the Earth* 28. pp 499–509
- Wright. J.L., H. Jin., K.G.T., Hollands., D. Naylor, (2006) Flow visualization of natural convection in a tall air-filled vertical cavity. *International Journal of Heat and Mass Transfer*, v 49, pp. 889-904
- Wang. Z., M.W. McClure., R. N Horne, (2009) A single-well EGS configuration using a thermosiphon 34th Workshop on geothermal reservoir engineering, Stanford university, Stanford, California, February 9- 11, 2009.
- Walsh. J.B., W.F. Brace, (1984) The effect of pressure on porosity and the transport properties of rock. *Journal of Geophysical Research* V 89, No B11, pp 9425-9431.

- Walsh. J.B., Decker. E.R, (1966) Effect of Pressure and Saturating fluid on the thermal conductivity of compact rock. *Journal of Geophysical Research* vol.71. No 12 pp 3053-3061
- Waples. D.W. and J.S. Waples, (2004) A Review and Evaluation of Specific Heat Capacities of Rocks, Minerals, and Subsurface Fluids, Part 1, Minerals and Nonporous Rocks *Natural Resources Research*, Vol. 13, No. 2.
- Wetter M., A. Huberg, (1997) Vertical Borehole Heat Exchanger EWS model , version 2.4. Model description and implementing into TRNSYS.
- Xing. H. L., J. Gao., J. Zhang., Y. Liu, (2010) Towards an Integrated Simulator for Enhanced Geothermal Reservoirs *Proceedings WGC 2010, Bali, Indonesia*, 25-29 April 2010.
- Yavuzturk, C., J.D. Spitler, (1999): A Short Time Step Response Factor Model for Vertical Ground Loop Heat Exchangers. *ASHRAE Transactions*. 105(2): 475-485.
- Zimmerman. R.W, (1989), "Thermal conductivity of Fluid-saturated Rocks," *Journal of Petroleum science and Engineering*, 3, 219-227.

APPENDIX

A. ANALYTICAL SOLUTIONS

INFINITE LINE SOURCE (ILS)

Equation A-1 describes the change in temperature of a line source (infinite line of point sources) at the radius r , as result of the constant heat load q and the duration of the heat load t .

$$T(r, t) - T_{\infty} = \frac{q}{4\pi\kappa} \int_y^{\infty} \frac{e^{-u}}{u} du, \quad \text{A-1}$$

$$\text{Where } y = \frac{r}{2\sqrt{\alpha t}}$$

FINITE LINE SOURCE (FLS)

Following Lamarche and Beauchamp (2007), with $q'f(t) = q'f(t^*, \beta)$. Where $t^* = t/(H^2/9\alpha)$ and $\beta = r_b/H$, the finite line source solution can be expressed as:

$$f(t^*, \beta) = A - B, \text{ where} \quad \text{A-2}$$

$$A = \int_{\beta}^{\sqrt{\beta^2+1}} \frac{\text{erfc}(\gamma z)}{\sqrt{z^2-\beta^2}} dz - \int_{\beta}^{\sqrt{\beta^2+1}} \text{erfc}(\gamma z) dz \quad \text{A-3}$$

$$B = \int_{\sqrt{\beta^2+1}}^{\sqrt{\beta^2+4}} \frac{\text{erfc}(\gamma z)}{\sqrt{z^2-\beta^2}} dz + \frac{1}{2} \left(\int_{\beta}^{\sqrt{\beta^2+1}} \text{erfc}(\gamma z) dz + \int_{\beta}^{\sqrt{\beta^2+4}} \text{erfc}(\gamma z) dz \right) \quad \text{A-4}$$

The finite line source solution is used in Section I-5 and in Paper 3.

INFINITE CYLINDRICAL SOURCE (ICS)

The infinite cylindrical source solutions, equations A-5 and A-6 describe the temperature change at a radius r , as result of a constant heat load q imposed on the radius r_b (equation A-5) and a constant temperature T_s imposed on the radius r_b (equation A-6), both with a duration of t .

With reference to Carslaw and Jaeger (1959), with $\tau = \frac{\alpha t}{r^2}$, and $p = \frac{r}{r_b}$

ICS WITH HEAT FLUX BOUNDARY

$$T(r, t) - T_{\infty} = \frac{q}{\kappa\pi^2} \int_0^{\infty} \frac{e^{-\tau\beta^2} - 1}{J_1^2(\beta) + Y_1^2(\beta)} [J_0(p\beta)Y_1(\beta) - J_1(\beta)Y_0(p\beta)] \frac{1}{\beta^2} d\beta \quad \text{A-5}$$

ICS WITH TEMPERATURE BOUNDARY

$$T(r, t) = T_s + (T_\infty - T_s) = \frac{2}{\pi} \int_0^\infty \exp\left(-\frac{\alpha t u^2}{r_0^2}\right) \frac{Y_0\left(\frac{ur}{r_0}\right) J_0(u) - J_0\left(\frac{ur}{r_0}\right) Y_0(u)}{J_0^2(u) + Y_0^2(u)} \frac{du}{u} \quad \text{A-6}$$

The solution given by Equation A-6 is not straightforward as it contains a singularity; a procedure to evaluate the intergral is described in Peng et al. (2002).

MULTIPOOL METHOD

The multipool method is used to determine the local borehole thermal resistnace (R_b) in Section I-4.3.2. The mehod is used with reference to Lamarche et al. (2010). To account for the influence of natural convection, the method is complemented with a Nusselt correlation to determine the effective thermal conductivity ($k_{w_effective}$) of the water in the borehole.

$$k_{w_effective} = k_w * Nu \quad \text{A-7}$$

$$\sigma = \frac{k_{w_effective} - k_g}{k_{w_effective} + k_g} \quad \text{A-8}$$

$$\lambda_1 = \frac{r_b}{r_p}, \quad \lambda_2 = \frac{r_b}{x_c}, \quad \lambda_3 = \frac{\lambda_2}{2\lambda_1}, \quad \text{A-9}$$

$$R_b = \frac{1}{4\pi k_w} \left[\ln\left(\frac{\lambda_1 \lambda_2^{1+4\sigma}}{2(\lambda_2^4 - 1)^\sigma}\right) - \frac{\lambda_3^2 \left(1 - (4\sigma / (\lambda_2^4 - 1))\right)^2}{1 + \lambda_3^2 \left(1 + (16\sigma / (\lambda_2^2 - 1 / \lambda_2^2))^2\right)} \right] \quad \text{A-10}$$

k_g is the ground thermal conductivity, x_c is the shank spacing (half the distance between center to center of the two collector pipes), r_b is the borehole radius and r_p is the collector pipe radius. k_w is the thermal conductivity of the water in the borehole.

B. DEEP COAXIAL BOREHOLE HEAT EXCHANGERS

CONSTANT INLET TEMPERATURE

The figures in this section complement the results presented in Section I-6.5.2 where heat extraction is simulated using a constant heat load. The simulation uses the same model parameters as described in Section I-6.5.2. Instead of applying a constant heat load, a constant inlet temperature of 5 °C is used. The heat extraction is preceded by 1 hour of fluid circulation during which the first temperature profile shown in Figure B-1 is established, this profile is the same as the first profile in Figure I-30.

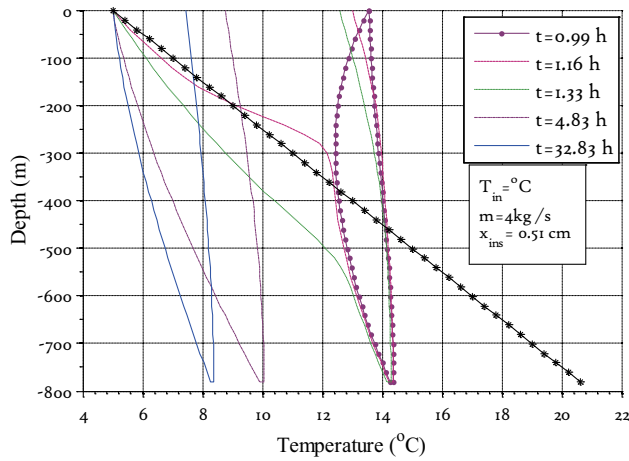


Figure B-1. Temperature profiles. Constant inlet temperature.

The temperature of the borehole wall is shown in Figure B-2, the temperature profiles correspond to the instances shown in Figure B-1. This figure can be compared with the results shown in Figure I-31 for a constant heat load.

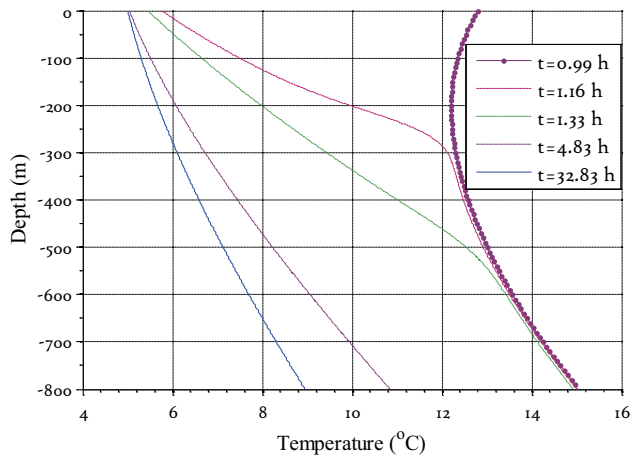


Figure B-2. Borehole wall temperatures, profiles corresponding to Figure B-1.

In Figure B-3 the specific heat load is shown for the times corresponding to the profiles in Figure B-1. This figure can be compared with the results shown in Figure I-32 for a constant heat load.

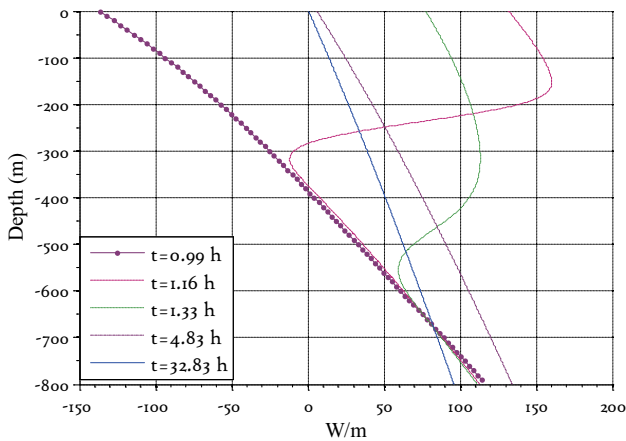


Figure B-3. Distribution of Specific heat load in the borehole, profiles corresponding to Figure B-1.

THERMAL RECHARGE WITH INLET THROUGH THE ANNULAR SPACE

The figures in this section complement the results presented in Section I-6.5.2.2 where heat injection to a 800 m deep coaxial BHE is simulated. The simulation uses the same model

parameters as described in Section I-6.5.2.2 but instead of having the fluid inlet through the center pipe, the fluid inlet is through the annular space.

In Figure B-4 thermal recharge is simulated with the fluid inlet through the annular space. The profiles can be compared with the profiles in Figure I-35.

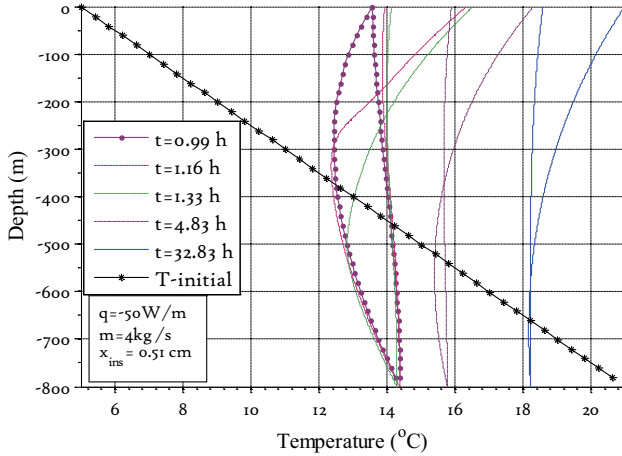


Figure B-4. Temperature profiles during thermal recharge. Fluid inlet through annular space.

The temperature of the borehole wall is shown in Figure B-5, the temperature profiles correspond to the instances shown in Figure B-4. This figure can be compared with the results shown in Figure I-36 where the temperature profiles is shown for a case with the fluid inlet through the center pipe.

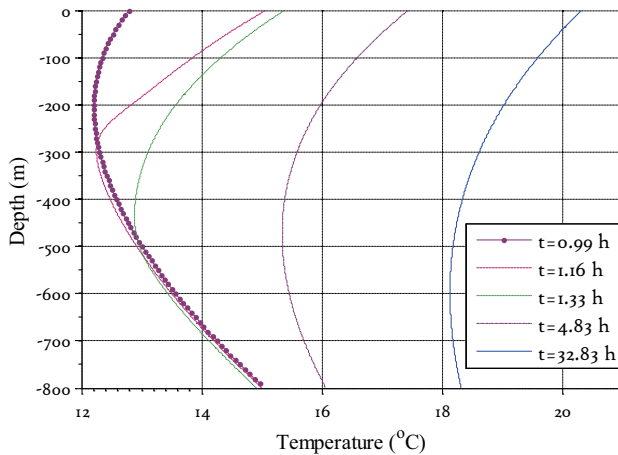


Figure B-5. Borehole wall temperature during thermal recharge, profiles corresponding to Figure B-4

In Figure B-6 the specific heat load is shown for the times corresponding to the profiles in Figure B-4. This figure can be compared with the results shown in Figure I-37 where the distribution of the specific heat load is shown for a case with the fluid inlet through the center pipe.

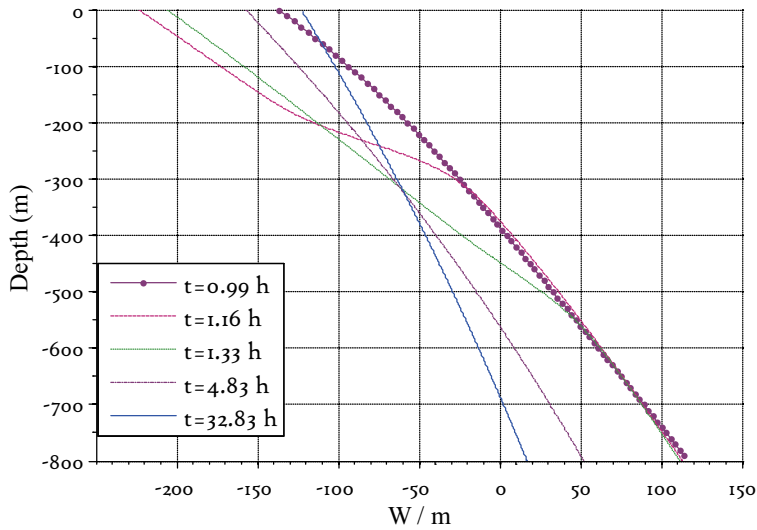


Figure B-6. Distribution of specific heat load during thermal recharge, profiles corresponding to Figure B-4

C. CLOSED LOOP ENGINEERED GEOTHERMAL SYSTEM

EGS COUPLED WITH DISTRICT HEATING.

In this section, additional results are shown to Section II-6.5.3. It is assumed that the temperature level in the district heating network is reduced with 10 K compared to the temperature level in II-6.5.3. The parameters describing the simulated geothermal plant are summarized in Table II-2.

Figure C-1 shows the thermal effect delivered by the EGS and the thermal effect in the district heating network during year 10. A comparison with Figure II-20.a reveals that the heat load supported by the EGS has increased. This is also seen in the duration curve for the heat load which is shown Figure C-2, the duration curve should be compared with Figure II-20.b. In total, a temperature reduction of 10 K in the district heating network increases the amount of energy that the geothermal system can provide with about 30 % and increases the share of geothermal energy in the DH-network from 40 % to 53 %.

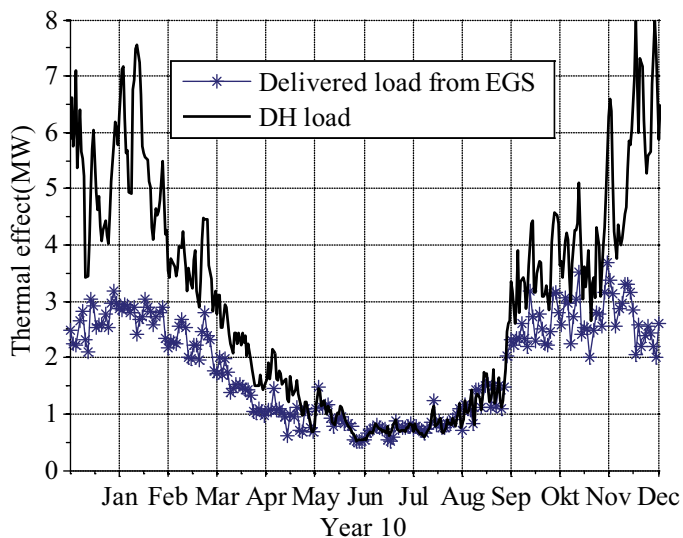


Figure C-1. Thermal effect delivered by EGS during year 10.

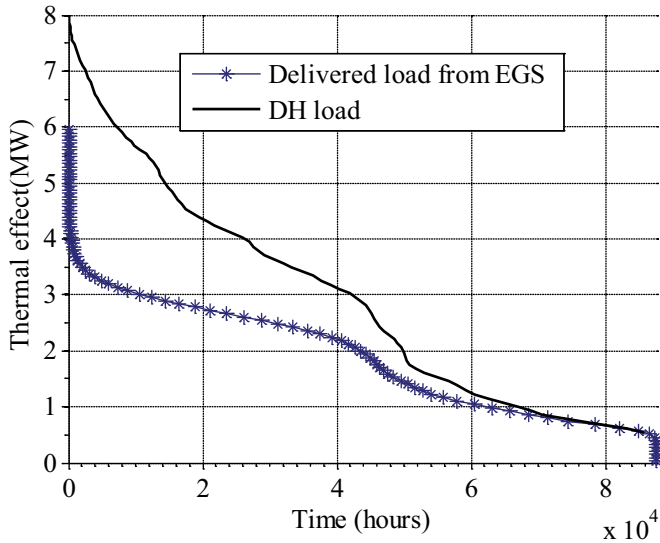


Figure C-2. Duration curve for the heat load for 10 years of simulated operation.

Figure C-3 shows the production and return temperatures in the EGS and in the DH network. The temperatures should be compared with Figure II-21.a. It is seen that the outlet temperature from the EGS is in this case high enough to cover the entire heat demand of the DH network in the summer.

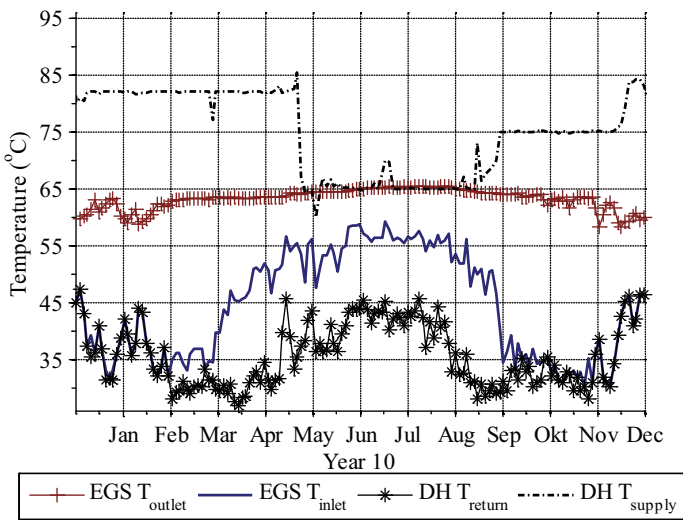


Figure C-3. Production and return temperatures in the EGS and in the district heating (DH) network

Figure C-4 shows the mass flow rates in the EGS, the figure should be compared with Figure II-21.b.

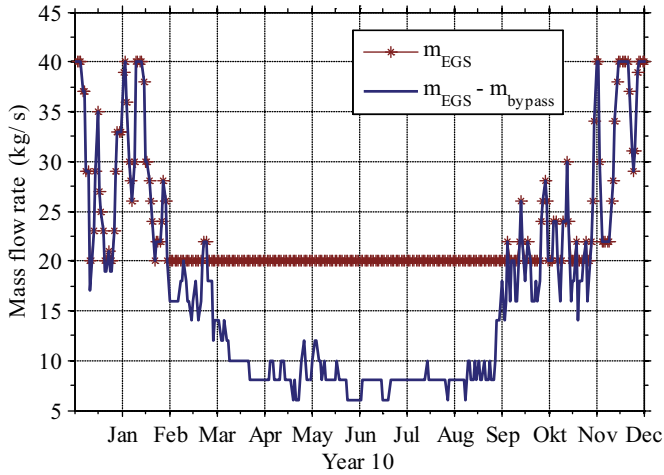


Figure C-4. Mass flow rates

Figure C-5 shows the required energy by the circulation pump, the figure should be compared with Figure II-22. It is seen that also in this case, the system is self circulating during a large part of the year as indicated by the negative pumping power.

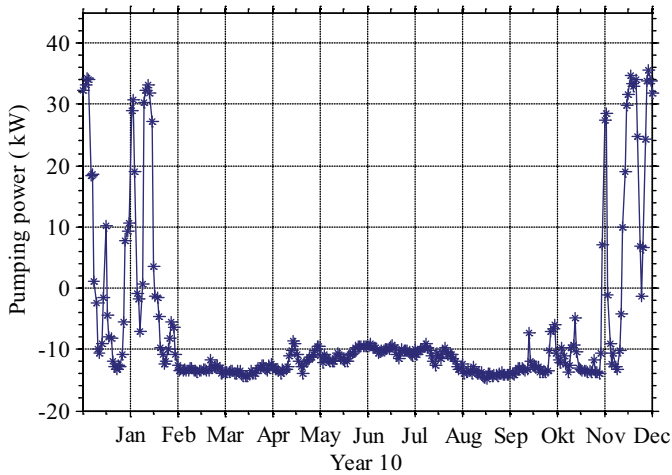


Figure C-5. Power required for fluid circulation in the system.

D. DEEP BOREHOLE HEAT EXCHANGERS, APPLICATION TO
GROUND SOURCE HEAT PUMP SYSTEMS –PROCEEDINGS
PRESENTED AT WORLD GEOTHERMAL CONGRESS 2015

Holmberg. H., Acuña J., Næss. E., Sønju. O. K. (2015)

Proceedings World Geothermal Congress 2015. Melbourne, Australia, 19- 25 April
2015

Deep Borehole Heat Exchangers, Application to Ground Source Heat Pump Systems

Henrik Holmberg¹, José Acuña², Erling Næss¹, Otto K. Sønju³

1. Department of Energy and Process Engineering, Norwegian University of Science and Technology

2. Department of Energy Technology, KTH Royal Institute of Technology

3. Rock Energy AS

E-mail, henrik.holmberg@ntnu.no

Keywords: Ground source, coaxial, BHE, numerical simulation, heat transfer.

ABSTRACT

Deep borehole heat exchangers (BHE) can be used as a complementary heat source in ground source heat pump (GSHP) installations with a negatively balanced thermal load, i.e. when more thermal energy is extracted than recharged. GSHP systems can be made space effective and with a small or negligible visual footprint. Larger installations may, however, require certain amount of available drilling area for the boreholes. This area can be reduced by placing the boreholes closely together. This creates a system susceptible to the load balance. If the possibilities for thermal recharge are limited, the temperature in the boreholes will decline, which also degrades the performance of the system. To balance the thermal load, deep BHEs have to sustain the required temperature level without the need for thermal recharge. A numerical model is applied to simulate the performance of deep BHEs over time, and to determine the average specific thermal load and amount of energy extraction that can be sustained. The results are used to propose an alternative solution for a GSHP installation having a limited construction area and a negatively balanced thermal load. It is seen that the deep BHEs can support a high (increasingly with depth) thermal load, and that the required temperature level can be sustained over the life time of the system. Deep BHEs reduce the required borehole length, and are a viable option for GSHP installations in areas with scarcity of space and/or with negatively balanced loads.

1. INTRODUCTION

GSHP systems are made space effective by placing the boreholes in a compact pattern. Such systems favors thermal interaction between the boreholes and can be designed to store energy. Thus, if the yearly thermal load is positively balanced (more energy is being recharged than extracted) the temperature in the boreholes will increase over time, which favors the performance of the heat pump. On the contrary, if the thermal load is negatively balanced, the temperature in the boreholes will decline. Thermal recharge can often be provided with free cooling or by use of other thermal sources such as solar collectors, building exhaust air, outdoor air, amongst others.

This paper discusses cases where it is desired to use a GSHP system to provide heating in an energy system where both the recharge possibilities and construction area are limited, e.g. buildings with a heating dominated thermal load in urban areas. The study considers to what extent boreholes deeper than the conventional 200 – 300 m can be used to provide either a complementary or a standalone thermal source in such energy systems.

As discussed in Rybach and Hopkirk (1995), for a deep BHE there is the choice to produce either a higher thermal load at a lower temperature, or a lower thermal load at a higher temperature. With the depths (600- 1000 m) and undisturbed temperature gradient (0.02 K / m) analyzed in this paper it is most profitable to pursue the first option. Therefore, the aim is to provide thermal energy in the temperature range of conventional BHE installations. The temperatures the deep BHEs can provide are determined given a predefined average specific heat load, and operation time.

The BHE is modeled as a coaxial, pipe-in-pipe BHE where the central pipe is made of polypropylene. The annular space is separated from the borehole wall by a thin polyethylene membrane. This type of coaxial BHE has been presented in Acuña (2013). An illustration of the coaxial BHE is shown in Figure 1, where the fluid inlet is in the annular space.

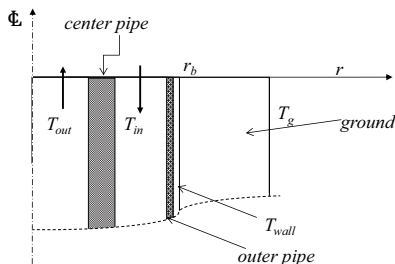


Figure 1: Coaxial BHE.

It is assumed that water is to be used as the heat carrier, which limits the possible minimum temperature. During heat extraction, the water temperature will be lowest at the inlet of the BHE and this temperature limits the amount of energy that can be transferred in the BHE. By increasing the mass flow rate, it is possible to transfer more heat. Increasing the mass flow rate reduces the requirements for thermal insulation between the fluid in the annular space and the center pipe. Therefore, the center pipe can be made thinner and thus less expensive. This also allows for higher mass flow rates without causing excessively high-pressure drops.

The results presented in this paper are based on a numerical model that has been described and verified in an earlier paper (Holmberg et al. 2014). The model is used to determine the thermal performance of coaxial BHEs for three different depths and average specific heat loads. It is assumed that the BHEs will provide energy as a complementary source in a GSHP system. The layout for a GSHP system with a complementary deep BHE is shown in Figure 2. The deep BHE is working in parallel with conventional BHEs. The inlet temperature of the heat carrier of the conventional BHEs is coupled through the heat exchanger with the inlet temperature of the deep BHE. Due to the higher ground temperature level of the deep BHEs, they can sustain a higher specific heat load than shallow BHEs without needing thermal recharge.

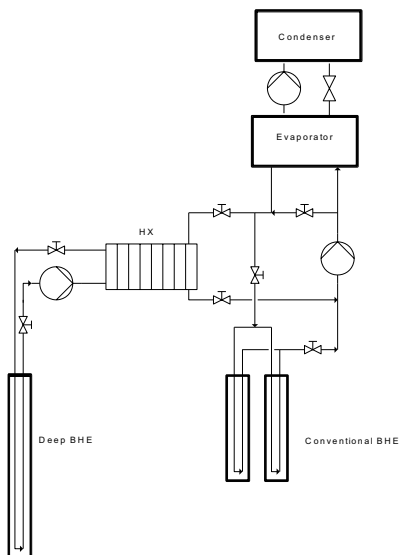


Figure 2: Layout for GSHP system with deep BHE.

2. MODELING

The coaxial BHE is simulated with a numerical model which uses an axisymmetric grid. The model uses a geometrical simplification where the analogy to electric networks is used to describe the thermal resistances within the borehole. A numerical grid is used to resolve the temperature profile in the bedrock surrounding the borehole in two dimensions, while the borehole, the collector and the heat carrier are simulated as one-dimensional features. The model is implemented in the Matlab® environment and it is compared with experimental data in the next section. Further details on the model and a more extensive comparison with experimental data can be found in (Holmberg et al. 2014).

It is assumed that the ground is homogenous and that the thermal properties of the ground are isotropic. The borehole diameter, the dimensions of the outer pipe, and the thermal properties of the center pipe and the outer pipe are assumed constant. The physical dimensions of the center pipe and the mass flow rate being used are determined from a parametric study and depend on the borehole depth. The values of the parameters held constant in the present study are shown in Table 1.

Table 1. Parameters that assumed constant.

Parameter	Value
Borehole diameter [mm]	140
Outer pipe [mm]	139 x 0.4
Ground thermal conductivity, k_g [W /m K]	3
Ground density, ρ_g [kg /m ³]	2600
Ground specific heat capacity, C_g [J/kg K]	840
Outer pipe, thermal conductivity, k_c [W /m K]	0.42
Center pipe, thermal conductivity k_{cp} [W /m K]	0.24
Heat carrier fluid	Water
Thermal gradient [K / m]	0.02

3. RESULT

3.1 Validation of numerical model

The results from the numerical model are validated with experimental data from Acuña (2013). The temperature measurements are from a distributed thermal response test (DTRT) with a coaxial pipe-in-pipe BHE operating with water in a 190 m deep borehole. Figure 3 show vertical temperature profiles that are measured in the early and late period of the DTRT. As seen the simulated values agree well with the experimental data.

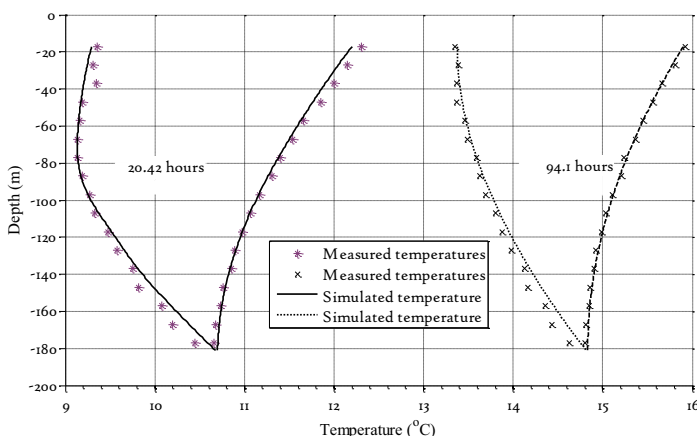


Figure 3: Vertical temperature profiles. Measured and simulated values are shown.

It should be noted that in the experimental setup, the BHE operates with the fluid inlet in the central pipe. For that specific setup, the flow direction does not affect the inlet and outlet temperatures. In the following sections the inlet is through the annular space since it is advantageous for heat extraction from deep BHEs.

3.2 Thermal performance for the deep BHE

The thermal performance of deep BHEs is studied using the numerical model. Three depths are simulated, namely 600, 800 and 1000 m. The parameters used are shown in Table 1 and Table 2. The dimensions of the center pipe was determined in a parametric study presented in Holmberg et al. (2014), where the influence of center pipe dimensions and the mass flow rate were studied for different borehole depths and heat loads. The simulations are performed assuming a continuous operation with an on/off interval of 24 hours and a seasonal recovery period of 4 months representing the warm season. The fluid temperatures for two cycles of the operation scheme are shown in Figure 4 for a 800 m BHE with an average specific heat load of 50 W /m.

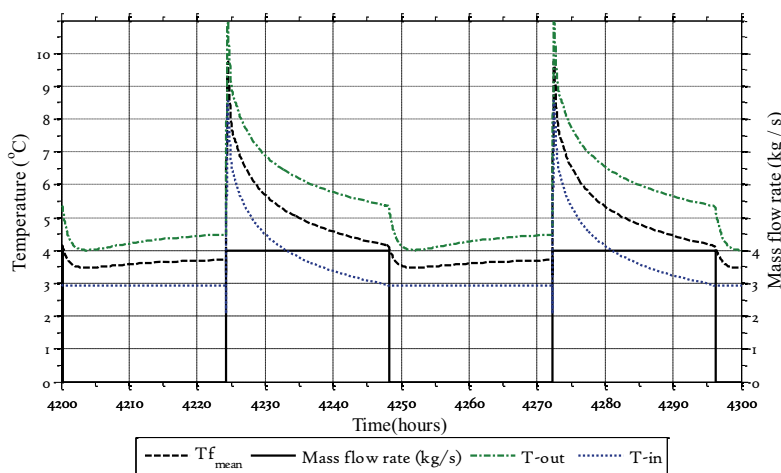


Figure 4: Inlet, outlet and mean fluid temperatures together with mass flow rate.

As shown in Figure 4 the fluid temperatures experiences a peak each time the mass flow is switched on followed by a monotonic decrease until the mass flow is switched off. The profiles shown are taken after nearly half a year of operation (4200 – 4300 h), the mass flow rate is 4 kg / s and the mean fluid temperature varies between 9.5 °C and 4.2 °C.

Table 2. Case specific parameters

Parameter	Value	Value	Value
Active length BHE [m]	600	800	1000
Collector (center pipe) [mm]	75 x 4.3	90 x 5.1	90 x 3.5
Mass flow rate [kg / s]	3.5	4.0	5
Thermal load [W / m]	40	50	60
Pressure drop ¹ [bar]	1.0	1.0	1.7
Pump power required ² [kW]	0.47	0.53	1.33

¹It is assumed that the annular space is confined within a smooth-walled outer pipe. ²Assuming $\eta_{\text{pump}}=0.75$.

The mean fluid temperatures ($T_{f,\text{mean}}$) are shown in Figure 5 for the cases described in Table 2. As seen, the minimum temperature decreases by approximately 1.5 K during 20 years operation. The values in Figure 5 are calculated by averaging each load cycle, i.e. the mean value of $T_{f,\text{mean}}$ shown in Figure 4 is determined for each period when the mass flow is on.

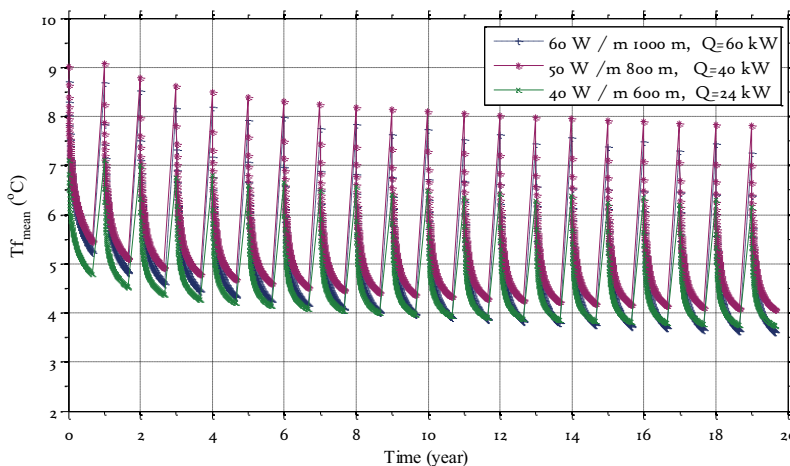


Figure 5: Mean fluid temperature ($T_{f,\text{mean}}$) for 1000 m, 800 m and 600 m deep BHEs, with an average specific heat load of 60, 50 and 40 W/m, respectively. The BHE operates with an on/ off interval of 24 hours and a seasonal recovery period of 4 months.

As seen from the figure, the decline in minimum mean temperature is relatively small. In these cases the total accumulated operation time is 4 months / year. Given this operation time, the 1000 m BHE can sustain 60 kW_{th} and can deliver 175 MWh_{th} / year, the 800 m BHE can sustain 40 kW_{th} and can deliver 117 MWh_{th} / year, and the 600 m BHE can sustain 24 kW_{th} and can deliver 70 MWh_{th} / year. The share of high value energy (electricity) required for fluid circulation is highest for the 1000 m BHE and amounts to 2.2% relative to the produced thermal energy. This could, however, be reduced using a somewhat larger borehole diameter.

The specific heat flux is proportional to the temperature difference between the BHE wall and the undisturbed temperature profile and increases with depth. Therefore, most energy is being extracted in the lower part of the borehole. In Figure 6, the change in the temperature of the borehole wall during the first 5 years of operation is shown along with its initial (undisturbed) profile for a 800 m BHE. It is seen that the temperature change is largest in the lower part of the borehole, indicating that most energy has been extracted in the deeper region.

The figure shows both the temperatures during heat extraction, (which takes place during the first 2/ 3 of the year) and recovery (last 1/ 3 of the year). As seen, the temperature of the upper part of the borehole wall is initially warmer than the undisturbed temperature, indicating that heat is being transported from the borehole. As more energy is being extracted, the temperature drops and in the extraction profile at 5000 h the temperature of the borehole wall is lower than the undisturbed temperature profile also in the upper part. The profiles for 6000 h and 8000 h show how the temperature recovers and approaches that of the initial undisturbed profile. The last profile shows the temperature profile at the end of the thermal extraction period during the fifth year.

The specific thermal load is calculated based on the conductive temperature profile and is shown in Figure 7 for the same cases as in Figure 6. The first temperature profile (100 h) show a negative specific thermal load in the upper 100 meters of the borehole while the energy extraction is higher in the lower part as compared to the later profiles. For 5000 hours, the thermal load is positive in the entire borehole.

As the operation time increases, the distribution of the specific thermal load becomes slightly more evenly distributed. Most of the energy is, however, extracted from the lower part of the borehole. The distribution of the thermal load at the end of the thermal extraction period during the fifth year is shown in Figure 8.

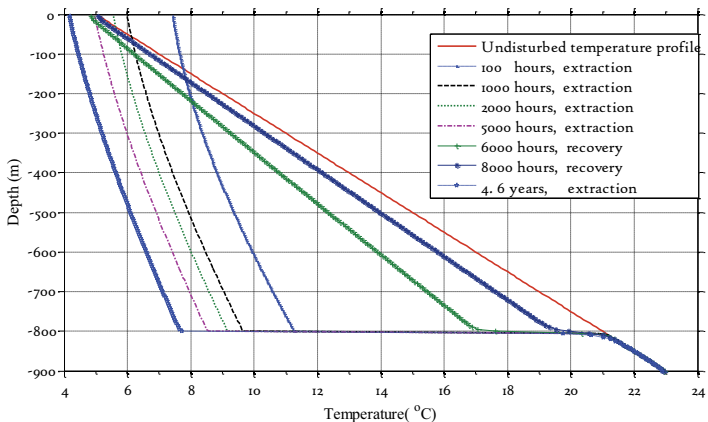


Figure 6: Vertical profiles showing the borehole wall temperature during the first 5 years of operation.

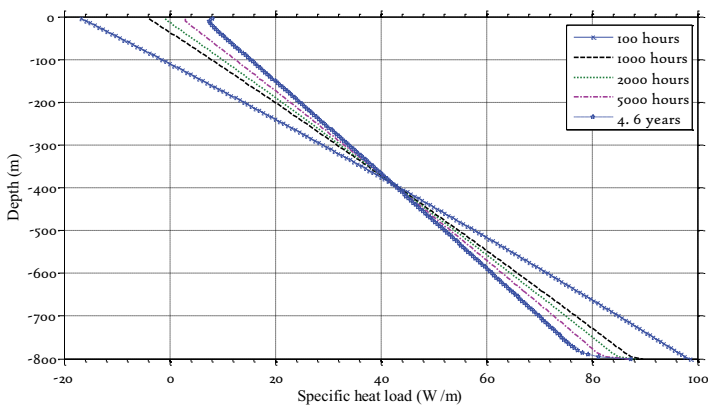


Figure 7: Vertical distribution of thermal load in 800 m deep coaxial BHE, total thermal load is 40 KW.

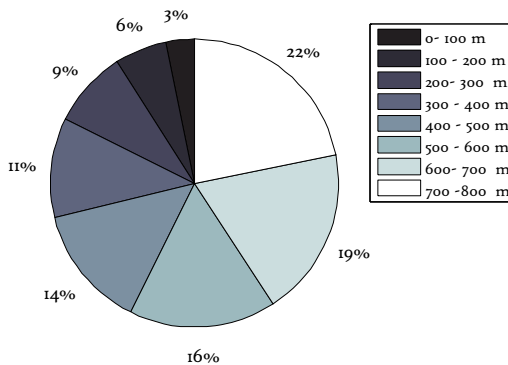


Figure 8: The distribution of the thermal load in the borehole after 4.6 years of operation.

It is noticeable that 71 % of the thermal energy is extracted from the lower half of the borehole, while less than 10 % is being extracted from the upper 200 meters. Although there is a slight change in the distribution as the borehole is further cooled down, the distribution in Figure 8 is characteristic for the this type of deep BHEs.

The distribution of the specific heat is important when considering thermal influence from neighboring boreholes. With a higher heat flux, a larger thermal volume is required. Deep BHEs can, therefore, be placed relatively close on the surface and then deviate a few degrees from vertical to create sufficient distance between the lower parts of the boreholes. The required distance between the wells can be determined based on the distribution of the specific heat flux. Figure 9 shows the thermal influence based on an infinite series of boreholes placed on a line. The figure is based on a simulation using Comsol Multiphysics (2014); the parameters in Table 1 are used in the simulation together with values representing the vertical distribution of the specific heat load in Figure 7.

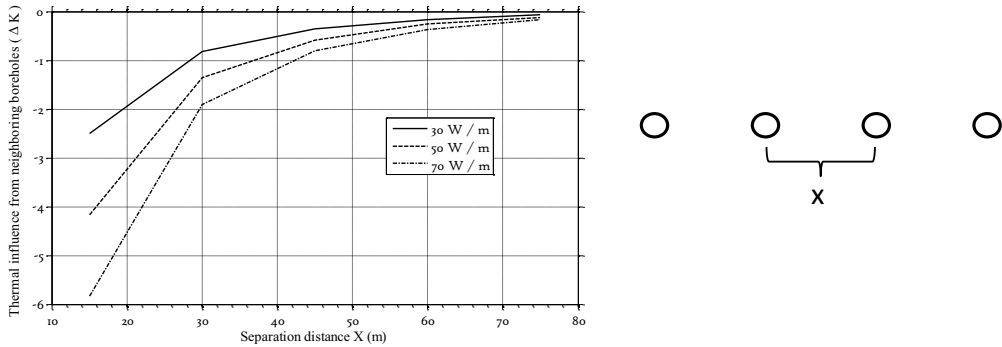


Figure 9: Thermal influence after 20 years of operation. X is the separation distance for a series of boreholes placed on a line as seen on the right side.

The additional temperature decrease due to the thermal influence from neighboring borehole is expressed by ΔK in the figure. The values are taken after 20 years of operation. It is seen in Figure 9 that the influence of the specific heat load is largest for short separation distances, and that a larger separation distance is required for higher specific heat loads. E.g. assuming two BHEs with a separation distance of 20 meters and a deviation from vertical of a few degrees creates a sufficient distance between the boreholes to avoid thermal influence in the lower part of the boreholes.

3.3 GSHP system with complementary deep BHEs

A GSHP installation is to be built. The specified thermal effect is 180 kW_{th} , the yearly heating load is 600 MWh and the cooling load is 200 MWh. With an average heat pump coefficient of performance (COP) of 3, the heating load (energy that is extracted from the BHEs) is twice the cooling load (amount of energy rejected to the BHEs). The site is large enough to fit twenty, 200 m deep boreholes with 6 m spacing (Figure 10, left). It is, however, expected that the temperature level will decrease in the BHEs due to the unbalanced thermal load. Simulations using the design software EED (2010) do indeed show a temperature decline on the order of 6-7 K during 20 years with a minimum $T_{f_{mean}}$ of $-4.8 \text{ }^\circ\text{C}$.

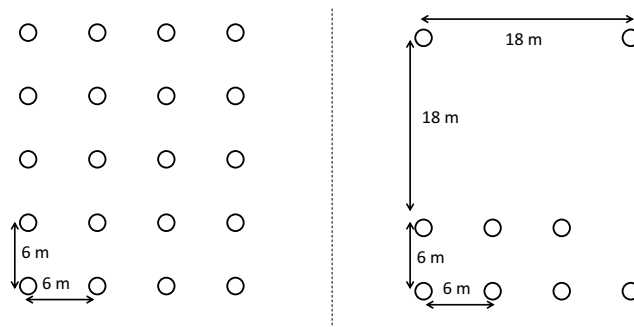


Figure 10: borehole pattern for 20 BHEs (left) and for pattern with complementary deep BHEs (right).

As an alternative, it is proposed to drill fewer boreholes and to complement these with some deep coaxial BHEs. As mentioned above a 800 m deep BHE could produce 40 kW_{th} and deliver 117 MWh / year of water in the temperature range needed by the heat pump. Therefore, the unbalanced heating load can be covered by two 800 m deep BHEs, which can deliver 2/3 of the required thermal effect. These would have to be drilled with a deviation of a few degrees away from each other to ensure that thermal interaction is limited in the lower part of the boreholes. Additionally, seven, 200 m BHEs can cover the rest of the thermal effect requirement (Figure 10, right), these are now thermally balanced and the minimum $T_{f_{mean}}$ is $-1.75 \text{ }^\circ\text{C}$ after 20 years. For the two 800 m deep BHEs the minimum $T_{f_{mean}}$ is $4 \text{ }^\circ\text{C}$ as shown in Figure 5. The total drilling length for this alternative solution is 3000 m, as compared to 4000 m for the twenty 200 m boreholes. The required power for fluid circulation in the deep BHEs is approximately 1.7 % of the power required for the heat pump.

4. CONCLUSIONS

It is seen that deep BHEs can sustain a higher average specific heat load than conventional BHEs; this is due to the higher temperature level in the borehole. The analysis performed favors high mass flow rates since it makes it possible both to keep the thermal extraction rate high and the installation cost low as the need for thermal insulation is reduced. The distribution of the thermal load is proportional to the thermal gradient, which in the simulated cases is linear. Most energy is extracted in the lower part of the borehole, making deep BHEs insensitive to thermal influence from neighboring BHEs (shallow or deep) in the upper part. Deviated deep BHEs can be closely spaced and provide a significant amount of thermal energy. Since the thermal influence in the upper part is small, deep BHEs can also be placed in the vicinity of conventional borehole fields. The required energy for circulation of the heat carrier fluid in the cases shown is on the order of 1-2 % of the produced thermal energy and can be reduced using a larger borehole diameter. Deep BHEs are, therefore, a viable option for GSHP installations in areas with scarcity of space and negatively balanced loads.

REFERENCES

- Acuña, J.: Distributed thermal response tests- new insights on u-tube and coaxial heat exchangers in groundwater-filled boreholes. *Doctoral Thesis*, KTH, Stockholm (2013).
- Comsol multiphysics 4.3a, (2014) Comsol Inc, Stockholm, Sweden.
- EED- Earth Energy Designer, version 3.16 (2010), www.Buildingphysics.com
- Holmberg, H., Acuña, J., Næss, E., Sønju, O.K.: Thermal evaluation of deep borehole heat exchangers. Submitted for publication. (2014).
- Matlab R2013a, The MathWorks Inc., Natick, Massachusetts, United States.
- Rybach, L., and Hopkirk, R.: Shallow and deep borehole heat exchangers- Achievements and prospects. *Proceedings*, World Geothermal Congress (1995).